Summer 7-12-2021

Filovirus and Coronavirus Modulation of Host Processes to Promote Immune Evasion and Replication

Caroline Williams
cwilliams334@student.gsu.edu

Filovirus and Coronavirus Modulation of Host Processes to Promote Immune Evasion and Replication

by

Caroline Gaston Williams

Under the Direction of Dr. Christopher F. Basler, PhD

A Dissertation Submitted in Partial Fulfillment of the Requirements for the Degree of

Doctor of Philosophy

in the Institute for Biomedical Sciences

Georgia State University

2021

ABSTRACT

Novel emerging zoonotic viruses are of significant public health concern due to a lack of treatment options and the required to achieve pharmaceutical development.

Coronaviruses, a family of positive-sense RNA viruses, have spilled over from their animal hosts into the human population. Most notably, is the recent emergence of SARS-CoV-2 that has caused a multi-year global pandemic, nearing a billion cases worldwide. Coronaviruses rely on host membranes for entry, establishment of replication centers, and egress. Compounds targeting cellular membrane biology and lipid biosynthetic pathways have previously shown promise as antivirals and are actively being pursued as treatments for other conditions. In chapter one we show that compounds targeting VPS34 and fatty-acid metabolism exhibit potent inhibition of SARS-CoV-2. Mechanistic studies with compounds targeting multiple steps up- and down-stream of fatty acid synthase (FASN) identified triacylglycerol production and protein palmitoylation as requirements for viral RNA synthesis and infectious virus production. Further, FASN knockout results in significantly impaired SARS-CoV-2 replication that can be rescued with fatty-acid supplementation. These observations identify fatty-acid metabolism as a promising target for novel SARS-CoV-2 therapeutic development.

Filoviruses are a family of zoonotic negative-sense RNA viruses known to cause severe and fatal disease in humans. The growing number of novel filoviruses being discovered have caused speculation over whether or not they are capable of causing productive human disease. A determining factor of virulence is the ability of viral proteins to antagonize host immune defenses to promote infection. Chapter two characterizes the VP35, VP40, and VP24 proteins of the newly identified Měnglà virus (MLAV) for their ability to regulate the interferon response in human and bat cells, as compared to their Ebola (EBOV) and Marburg (MARV) counterparts.

MLAV VP35 and VP40 inhibited type I IFN responses, consistent with the activity of their homologues. MLAV VP40 inhibited IFN production and signaling by unlinked mechanisms. MLAV VP24 did not inhibit IFN gene expression or activate an antioxidant response, functions of EBOV and MARV, respectively. These functional observations support placement of MLAV in a distinct genus and provide insight into potential novel host-interactions that provide value for future filovirus antiviral development.

INDEX WORDS: Coronaviruses, Membrane rearrangements, Fatty-acid metabolism, VPS34, Filoviruses, Innate immune antagonism

Filovirus and Coronavirus Modulation of Host Processes to Promote Immune Evasion and Replication

by

Caroline Gaston Williams

Committee Chair: Christopher F. Basler

Committee: Richard Plemper

Margo Brinton

Electronic Version Approved:

Office of Graduate Services

Institute for Biomedical Sciences

Georgia State University

July 2021

ACKNOWLEDGEMENTS

First and foremost, I'd like to thank my PhD mentor Dr. Christopher Basler for his continued support, guidance, and valuable scientific expertise. My years with you have provided me a valuable skill set and shaped me into a better scientist, and for that I am truly grateful. You have been an amazing mentor and I will look back on my time in your lab fondly.

Next, I would like to thank the members of the Basler Lab, both past and present. I have had the joy of working with so many amazing mentors who have each bestowed upon me a unique way of approaching scientific problems that will help me excel in my career. I'd like to give a special thank you to Dr. Alexander Jurkea, for all the time, energy, and patience that he put into training me and guiding me over the last year. Most importantly, I'd like to thank Dr. Joyce Sweeney Gibbons, without which I probably would not have survived this process. Your love and friendship and constant genuine support in and out of the lab means the world to me, you are so very special, and I will always be grateful that this lab brought us together.

I would also like to thank my committee, Dr. Richard Plemper and Dr. Margo Brinton, for their support and guidance on this journey. The scientific guidance I have received through the years in courses and seminars has been invaluable to me, and I truly appreciate you putting in the time to help me grow and succeed as a scientist.

Finally, to my parents Craig and Logan Williams, you always made sure I knew that I could do anything I wanted to in life if I put in the work, and that you would be there to support me through it no matter what. Without your encouragement and tough-love I would not be here today. Thank you for never letting me give up. And to Beau Wood, thank you for being there for me through the good, the bad, and the stressful. I cannot put into words how much I truly appreciate your love and support.

TABLE OF CONTENTS

LIST OF TABLES

LIST OF FIGURES

LIST OF ABBREVIATIONS

ACC – Acetyl-CoA Carboxylase
ACE2 – Angiotensin Converting Enzyme 2
ACS – Long chain Acyl-CoA Synthetase
ARE – Antioxidant Response Element
ATG – Autophagy related gene
BDBV – Bundinugyo virus
BOMV – Bombali virus
BSA – Bovine serum albumin
Caco2 – Colorectal adenocarcinoma cells (human intestinal epithelium)
Calu-3 – Lung adenocarcinoma cells (human lung epithelium)
CC50 – Cytotoxic concentration 50%
CHIKV – Chickungunya virus
CLR – C-type lectin receptor
CM – Convolutes membranes
CoV – Coronavirus
COVID-19 – Coronavirus disease 2019
CPT1A – Carnitine palmitoyl-transferase 1A
DAG – Diacylglycerol
DENV – Dengue virus
DGAT – Diglyceride acyltransferase
DMS – Double membrane spherule
DMSO – Dimethyl sulfoxide
DMV – Double membrane vesicle
DRC – Democratic Republic of Congo
dsRNA – Double stranded RNA
E – Envelope protein
EAU – Emergency use authorization
EBOV – Zaire Ebola virus
eIF4a – Eukaryotic initiation factor 4
EndoU – Endonuclease
ER – Endoplasmic reticulum
ERGIC – ER-Golgi intermediate compartment
ESCRT – Endosomal sorting complex required for transport
EVD – Ebolavirus disease
ExoN – Exoribonuclease
FAF – Fatty acid free
FASN – Fatty-acid Synthase
FBS – Fetal bovine serum
FDA – Food and Drug Administraton
GP – Glycoprotein
HCoV-229E – Human coronavirus-229E
HCoV-HKU1 – Human coronavirus-Hong Kong U1
HCoV-NL63 – Human coronavirus-Netherlands 63
HCoV-OC43 – Human coronavirus-Organ Culture 43

HCV – Hepatitis C virus
HEK293T – Human embryonic kidney cells
HeLa – Ovarian cancer cells
Hpi – hours post-infection
HUJV – Huángjiāo virus
IC50 – Inhibitory concentration 50%
IFN – Interferon
IFNAR – Interferon α/β receptor
IKKe – inhibitor of nuclear factor kappa-b kinase subunit e
IRF – Interferon stimulated gene factor
ISG – Interferon stimulated gene
ISGF3 – Interferon-stimulated gene factor-3 complex
ISRE – Interferon stimulated response element
Jak1– Janus kinase 1
Keap1 – Kelch-like ECH-associated protein
KO – Knockout
KPNA – Karyopherin alpha
LC3 – Microtubule-associated protein 1A/1B- light chain 3
LLOV – Lloviu virus
M – Matrix protein
MARV – Marburg virus
MAVS – Mitochondrial antiviral-signaling protein
MDA5 – Melanoma differentiation associated gene 5
MERS – Middle East Respiratory Syndrome
MHV – Mouse hepititis virus
MLAV – Měnglà virus
mM – micromolar
MOI – Multiplicity of infection
mRNA – messenger RNA
MTase – Methyltransferase
N – Nucleocapsid protein (Coronaviruses)
NC – Nucleocapsid complex
NLR – Nucleotide binding oligomerization domain-like receptor
NNS – Non-segmented negative-sense
NP – Nucleocapsid protein (Filoviruses)
Nrf2 – Nuclear erythroid-2 related factor 2
NS – Non-structural
NSP – Non-structural protein
NT – Non-targeting
ORF – Open reading frame
PACT – Protein activator on interferon induced protein
PAMP – Pathoden associated molecular pattern
PAT – Palmitoyl acetyltransferase
PI3 – Phosphoinositol-3
PI3K – Phosphoinositol-3 kinase
PI3P- Phosphoinositol-3 phosphate

PKR- Protein kinase R
pp1a- Polyprotein 1a
pp1ab- Polyprotein 1b
PRR- pattern recognition receptor
pY-STAT – Tyrosine phosphorylated STAT
RAB5 – Ras-Related protein
RAVV – Ravn virus
RdRp – RNA dependent RNA polymerase
RESTV – Reston virus
RIG-I – Retnoic acid inducible gene I
RLR – RIG-I like receptor
RO6E – *Rosettus egypticus* bat cells
RT-PCR – Reverse transcription polymerase chain reaction
RTC – Replication transcription complex
RV – Rota virus
S – Spike protein
SARS – Sever Acute Respiratory Syndrome
SARS-CoV-2 –
SeV – Sendaii virus
sgmRNA – Sub-genomic mRNA
sGP – soluble glycoprotein
sgRNA – Sub-genomic RNA
SIGMAR1 – sigma nonopiod recepter 1
ssGP – small soluble glycoprotein
ssRNA – sinlge-stranded RNA
STAT – signal transducer and activator of transcription
SUDV – Sudan virus
TAFV – Tai Forest virus
TAG – Triacylglycerol
TBK1 – Tank binding kinase 1
TBSV – tombusvirus
TGEV – Transmissible gastroenteritis virus
TLR – Toll-like receptor
Tyk2 – tyrosine kinase 2
UIFN – universal interferon
UVRAG
VLP – Virus like particle
VP – vesicle packet
VP24 – Viral protein 24 Kilodaltons
VP30 – Viral protein 30 Kilodaltons
VP35 – Viral protein 35 Kilodaltons
VP40 – Viral protein 40 Kilodaltons
VPS – Vacuolar protein sorting protein
WCL – Whole cell lysate
WT – Wildtype
XILV – Xīlǎng virus

1 INTRODUCTION

1.1 Coronaviruses

1.1.1 Coronavirus Taxonomy

Coronaviruses (CoVs) are positive sense single-stranded RNA viruses from the subfamily *Orthocoronavirinae* in the order *Nidovirales.* The subfamily is made of the *Alphacoronavirus*, *Betacoronavirus*, *Deltacoronavirus*, and *Gammacoronavirus* genera. Viruses in the *Alpha-* and *Betacoronavirus* genera all have mammalian hosts, while those of the *Delta-* and *Gammacoronavirus* genera mainly infect birds. Amongst the mammalian viruses, there are seven that cause human disease: Human Coronavirus (HCoV)-229E, HCoV-NL63, HCoV-OC43, and HCoV-HKU1, Severe Acute Respiratory Syndrome (SARS)-CoV, Middle East Respiratory Syndrome (MERS)-CoV, and the newly emerging SARS-CoV-2 (Arora et al. 2020; Knipe and Howley 2013).

1.1.2 Coronavirus Outbreaks

The 1960s marked the earliest instance of human coronaviruses with the identification and isolation of HCoV-229E and HCoV-OC43 in samples cultured from patients suffering with minor respiratory illness (Corman et al. 2018; Hamre and Procknow 1966; Tyrrell and Bynoe 1965). Shortly after, in the early 2000s, HCoV-NL63 and HCoV-HKU1 were discovered from a child with Bronchiolitis and an elderly man with pneumonia, respectively (Corman et al. 2018; van der Hoek et al. 2004; Woo et al. 2005). All four of these viruses typically cause mild disease in humans worldwide, with studies identifying coronaviruses in up to 26% of common cold cases sampled (Annan et al. 2016; Gaunt et al. 2010; Larson, Reed, and Tyrrell 1980; Walsh, Shin, and Falsey 2013).

In addition to the endemic common cold causing coronaviruses, three additional coronaviruses cause severe respiratory syndrome in humans. SARS was first identified in 2002 in Southern China where it is thought to have spilled over into the human population from an animal host. The outbreak spread quickly, affecting 8,098 people in 29 countries and causing 774 deaths in a span of seven months (Table 1) (Xu et al. 2004; WHO 2003; Gumel et al. 2004; CDC 2013; Al-Osail and Al-Wazzah 2017). Since the conclusion of the outbreak, there have been no identified cases of SARS infection. An absence of SARS, however, does not mean an absence of SARS-like disease. In June 2012, a 60-year-old man in Saudi Arabia presented with severe pneumonia and died two weeks later. Samples taken from the patient were analyzed for various respiratory viruses and confirmed positive for coronaviruses; sequencing later revealed this to be a new virus in the *betacoronavirus* lineage that would become known as MERS (Al-Omari et al. 2019; Peeri et al. 2020; Zaki et al. 2012). To date, 27 countries have experienced cases, all of which can be tracked back to initial exposure in the Middle East, and more specifically Saudi Arabia. Of the 2,494 total cases there have been 858 deaths, resulting in a case fatality rate of 34.4%, four-times higher than that of SARS (Table 1) (Al-Omari et al. 2019; Peeri et al. 2020; CDC 2019).

While SARS and MERS have caused outbreaks of importance, with significant impact on the affected communities, they have recently been rivaled by the newest outbreak causing member of the coronavirus family: SARS-CoV-2. In December 2019, clusters of a respiratory virus of unknown origin started appearing in Wuhan, Hubei Province, China. Using a surveillance system developed after the 2003 outbreak to identify pneumonia causing disease of unknown origin, the causative agent was determined to be a novel *betacoronavirus* closely related to SARS (Peeri et al. 2020; Wang, Horby, et al. 2020; Wu, Wu, et al. 2020). By the end

of January 2020, the World Health Organization had declared the outbreak a public health emergency of international concern. In the year and a half since the first identified cases, there have been over 181 million cases and almost 4 million deaths worldwide (WHO 2021b; Wu, Wu, et al. 2020).

Table 1. Outbreaks of severe respiratory syndrome causing coronaviruses including date, number of countries effected, number of cases, and case fatality rates since the first documented occurrence.

Virus	Year	Number of countries	Number of cases	Number of deaths	Case fatality (%)
SARS-CoV	2002-2003	29	8,098	774	9.6%
MERS-CoV	2012-2021	27	2,494	858	34.4%
SARS-CoV-2	2019 – June 30, 2021	192	181,344,224	3,934,252	2.2%

*Table is adapted from (CDC 2019; WHO 2003, 2021b)

Coronaviruses are considered zoonotic pathogens, originating in an animal host and spilling over into the human population (Banerjee et al. 2019; Plowright et al. 2017). During an investigation into the emergence of SARS-CoV in 2003, virus and antibodies were isolated from bats found in the animal market thought to be involved in the spread of the virus (Cui, Li, and Shi 2019; Guan et al. 2003; Song et al. 2005; Tu et al. 2004). In the proceeding years, surveillance studies of bats in the same region identified a SARS-like CoV whose sequence closely matched that of the human SARS-CoV. The unique bat virus was capable of replicating in human cells expressing the host-cell receptor for SARS-CoV, as well as cells derived from bats and pigs, further suggesting a spillover transmission event as the origin for SARS (Lau et al. 2005; Li et al. 2005). While MERS-CoV infection is known to originate from direct transmission from camels to humans, there is strong support for bats being one of the original reservoirs for MERS (Memish et al. 2013; Anthony et al. 2017; Widagdo et al. 2017). Following this pattern, sequencing data suggest a possible bat CoV origin for the newly characterized SARS-CoV-2; however, this has not been fully elucidated and remains an topic of controversy in the ongoing

outbreak (Li et al. 2020; Dabravolski and Kavalionak 2020; Forster et al. 2020). With the evolution of RNA sequencing technology and continued surveillance efforts to stay ahead of possible spillover events, over 200 CoV-like viruses have been identified in bats, justifying the sustained investigation into the evolution of human CoVs from bats (Banerjee et al. 2019).

1.1.3 Coronavirus Structure and Proteins

Coronaviruses are packaged as spherical viral particles containing a non-segmented, positive-sense, single stranded RNA genome roughly 30 kilobases long, with 8 – 15 open reading frames (ORFs) encoding 22 – 29 viral proteins (Figure 1). The viral particles encompass a lipid envelope derived from the host cell membranes containing virally encoded structural proteins (Artika, Dewantari, and Wiyatno 2020; Wang, Grunewald, and Perlman 2020). The membrane (M) protein plays a critical role in virion structure and promoting membrane curvature, as well as binding to the nucleocapsid (N) protein on the encapsidated viral genome for packaging (Chen, Liu, and Guo 2020; Kirtipal, Bharadwaj, and Kang 2020). The envelope (E) protein contributes to virus assembly and release, as well as viral pathogenesis through the formation of a pentameric structure that acts as an ion channel in the viral membrane; deletion of E or mutation abolishing ion channel activity results in attenuation of infection or mutagenic evolution to regain activity (Chen, Liu, and Guo 2020; DeDiego et al. 2007; Nieto-Torres et al. 2014). Additionally, the membrane is decorated with Spike (S) protein trimers. Spike recognizes and binds to the cellular receptor responsible for virus entry determining host range and tissue tropism (Chen, Liu, and Guo 2020; Huang et al. 2020; Kirtipal, Bharadwaj, and Kang 2020; Li 2016). Upon binding, the S protein mediates viral uptake and membrane fusion, allowing for the release of the viral genome and initiation of downstream viral processes (Huang et al. 2020; Li 2016).

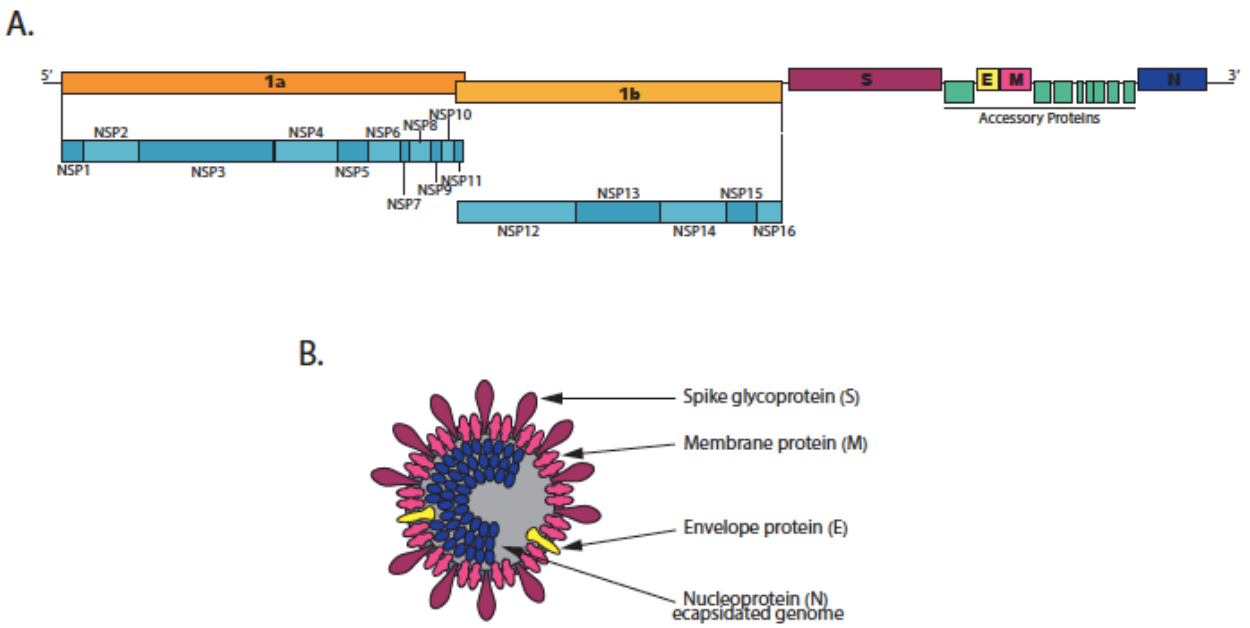

Figure 1 Genome organization and morphology of coronaviruses

Schematic representation of Coronavirus genome organization (A). Schematic representation of a Coronavirus virion and structural protein organization (B).

In addition to the main structural proteins, coronaviruses encode 16 non-structural proteins (NSPs) that get translated as two large polyproteins: polyprotein 1a (pp1a) containing NSP1-NSP11 and polyprotein (pp1ab) containing NSP1-NSP16. The polyproteins are cleaved into individual protein products that function together in forming the replication-transcription complex (RTC) and producing RNA templates for protein production and additional copies of the viral genome. NSP1 and NSP2, are not directly incorporated into the RTC or enzymatically involved in replication and transcription, but still play a critical role in progression of these processes. NSP1 enhances viral production by promoting host cell mRNA degradation and blocking host cell translation and gene expression (Kamitani et al. 2006; Rohaim et al. 2021; Schubert et al. 2020). Additionally, NSP1 is thought to be a virulence factor involved in pathogenicity of CoV infection by mediating inhibition of IFN-dependent signaling (Wathelet et al. 2007; Zust et al. 2007). The role of NSP2 in CoV replication has yet to be identified; the lack of impact on replication caused by preventing NSP1-NSP2 cleavage, and therefore production of

mature NSP2 proteins, suggests either it can function in its un-cleaved form or has a role that is dispensable to the viral life cycle (Denison et al. 2004; Rohaim et al. 2021). NSP3, the papain-like protease (PLpro) responsible for releasing itself, NSP1 and NSP2 from the polyproteins, is a multifunctional protein that functions in polyprotein processing and as a scaffold during the formation of the RTC by interacting with both viral and host proteins (Hagemeijer, Rottier, and de Haan 2012; Imbert et al. 2008; Rohaim et al. 2021). NSP3 and NSP4, in conjunction with NSP6, are necessary for the formation of double membrane replication centers that provide an isolated, protected environment in which replication occurs (Angelini et al. 2013; Knoops et al. 2008; Neuman 2016; Rohaim et al. 2021; Snijder et al. 2006).

The remaining NSPs, NSP5 and NSP7-16, come together to form complexes directly utilized in viral replication and transcription. NSP5 acts as the main protease (Mpro), and as such cleaves the polyproteins at 11 sites producing mature NSP4-NSP16 (Anand et al. 2003; Decroly et al. 2011; Ziebuhr, Snijder, and Gorbalenya 2000). NSP12 is the RNA-dependent RNA polymerase (RdRp) for coronaviruses. It has two main known domains bestowing its RdRp activity: the nidovirus RdRp-associated nucleotidyltransferase (NiRAN) domain and the canonical RdRp domain (Gorbalenya et al. 1989; Lehmann et al. 2015; Rohaim et al. 2021). NSP7 and NSP8 together form a complex that aids in the activation and processivity of NSP12 (Rohaim et al. 2021; Subissi et al. 2014; Zhai et al. 2005). There is evidence to suggest that NSP8 may be functionally related to DNA-dependent RNA polymerase primases and make short, six nucleotide or less, primers used by NSP12 to initiate RdRp activity (Imbert et al. 2006; Rohaim et al. 2021). NSP9 is a single stranded RNA-binding protein whose full functionality is still in question (Egloff et al. 2004; Rohaim et al. 2021; Sutton et al. 2004). The importance of NSP9 for viral replication, however, is not in question; mutations that disrupt NSP9 homo-

dimerization lead to severe defects in viral propagation (Chen, Fang, et al. 2009; Miknis et al. 2009). Another critical factor for replication is NSP10, which is required for activation NSP14 exoribonuclease activity, NSP16 methyltransferase activity, and NSP5 polyprotein processing activity (Bouvet et al. 2012; Bouvet et al. 2014). Mutation of NSP10 to disrupt the interactions required for the aforementioned activation results in a loss of negative strand viral RNA synthesis (Donaldson et al. 2007; Sawicki et al. 2005). Upon processing of polyprotein 1a, a small protein product comprising NSP11 should be made; however, data from infected cells suggests this processing may not occur and that an independent NSP11 protein may not be made. Instead, the NSP11 sequence is thought to function primarily in directing the translational frame shift responsible for dictating production of polyprotein 1a or polyprotein 1ab. As a result, parts of the NSP11 sequence get incorporated as a part of the C-terminus of NSP10 and the N-terminus of NSP12 (Rohaim et al. 2021).

In addition to the RdRp and the related cofactors, the RTC contains four more key enzymatic components. The helicase, NSP13, has multiple activities including hydrolysis of NTPs and dNTPs, 5’ to 3’ unwinding of RNA and DNA, and RNA 5′-triphosphatase activity that may be involved in the capping of viral RNA (Adedeji and Lazarus 2016; Adedeji et al. 2012; Ivanov et al. 2004; Ivanov and Ziebuhr 2004). NSP14 provides both exoribonuclease (ExoN) activity and cap N7-Methyltransferase (N7-MTase) activity through two separate domains found at the N- and C- termini, respectively (Chen, Cai, et al. 2009; Jin et al. 2013; Ma et al. 2015; Minskaia et al. 2006). Mutation of the ExoN domain results in increased mutations within the viral genome as well as decreased N7-MTase activity, while mutation of the N7-MTase domain affects only capping activity (Chen et al. 2013; Eckerle et al. 2007). NSP16 exhibits complementary cap 2’-O-Methyltransferase (2’-O-MTase) activity and requires the pre-existence

of N7-methylation of the guanosine cap for binding and methylation (von Grotthuss, Wyrwicz, and Rychlewski 2003; Decroly et al. 2008). Viruses lacking 2'-O-MTase activity were shown to be attenuated *in vitro* and *in vivo* due to recognition as "non-self" RNA by host immune sensors involved in type I interferon production and by ISGs that trigger sequestration of proteins to inhibit translation (Menachery et al. 2014). Lastly, the NSP15 protein impacts replication by two related mechanisms, its main endonuclease (EndoU) activity and the resulting ability to evade host-cell dsRNA sensors (Deng et al. 2017; Kindler et al. 2017; Snijder et al. 2003). It is thought that the localization and utilization of virally encoded EndoU activity may have evolved as a viral-specific RNA decay pathway that degrades dsRNA intermediates to avoid detection by host pattern recognition sensors that would activate the host innate immune response. Mutants with altered EndoU activity exhibit attenuated replication and early and robust activation of type I interferon (Deng et al. 2017; Kindler et al. 2017).

In addition to the replicase complex and structural proteins, coronavirus encode a series of accessory proteins. These proteins display significant divergence between, and within, coronavirus lineages, resulting in diverse nomenclature and functions, with the majority of their functions remaining unknown (Michel et al. 2020). Many of the characterized proteins function in evading and antagonizing the innate immune response and in turn play a key role in viral pathogenesis (Narayanan, Huang, and Makino 2008; Yoshimoto 2020; Comar et al. 2019; Michel et al. 2020; Lee, Bae, and Myoung 2019).

1.1.4 Coronavirus Replication and Transcription

Upon exposure to coronaviruses, the coronavirus lifecycle begins and proceeds as depicted in Figure 2. The newly introduced virus attaches to the specific host cell receptor by the S protein, which triggers entry via direct fusion of the viral membrane with the plasma

membrane or endocytosis followed by fusion with the endocytic membrane (Chen, Liu, and Guo 2020; V'Kovski et al. 2021; Wang, Grunewald, and Perlman 2020). Fusion allows for the release of the viral genome into the cytoplasm which marks the onset of viral replication. The positive-sense genome acts as the template for primary translation of the replicase genes encoded by polyproteins 1a and 1ab. A translational frame shift that occurs between ORF1a and ORF1b is responsible for directing whether pp1a or pp1ab is produced, with pp1a being generated about twice as often as pp1ab depending on the virus (Chen, Liu, and Guo 2020; Rohaim et al. 2021; V'Kovski et al. 2021; Wang, Grunewald, and Perlman 2020; Finkel et al. 2021). The polyproteins are processed by the proteolytic domains of NSP3 and NSP5 resulting in the 16 individual non-structural proteins which come together to antagonize the innate immune response, induce membrane rearrangements for replication centers, and form the RTC for viral RNA synthesis to occur (Anand et al. 2003; Harcourt et al. 2004; Rohaim et al. 2021; V'Kovski et al. 2021; Wang, Grunewald, and Perlman 2020; Hagemeijer, Rottier, and de Haan 2012; Neuman 2016; Angelini et al. 2013). The RTC synthesizes negative-sense anti-genomes that act as the template for replication of more positive-sense genomes to be made leading to a constant cycle of NSP translation and genome production. Additionally, the positive-sense genome provides a platform for discontinuous transcription, the process by which the sub-genomic mRNAs encoding the structural and accessory proteins are made. Discontinuous transcription starts with the RTC being recruited to the 3’ end of the genome and beginning to transcribe a negative sense strand until the transcription-regulating sequence (TRS) at the 5’ end of the first ORF is reached. This sequence signals the RTC to fall off and jump to the complementary sequence at the 5’ most end of the genome and complete the transcription process by adding this sequence at the 5’ 3’ end of the newly synthesized negative strand. Each ORF on the 3’ end of

the genome contains a TRS at its 5' end allowing this process to continue with the RTC making its way further and further down the genome each time until a series of nested negative-strand sub-genomic (sg) RNAs all containing the same anti-leader at their 3' end have been produced. The sg mRNAs will be produced from the negative-strand sgRNA pieces, and the first ORF of each mRNA will be translated to produce the individual structural and accessory proteins (Sola et al. 2015; V'Kovski et al. 2021; Sawicki and Sawicki 1995; Wang, Grunewald, and Perlman 2020; Di, McIntyre, and Brinton 2018; Sawicki and Sawicki 1998).

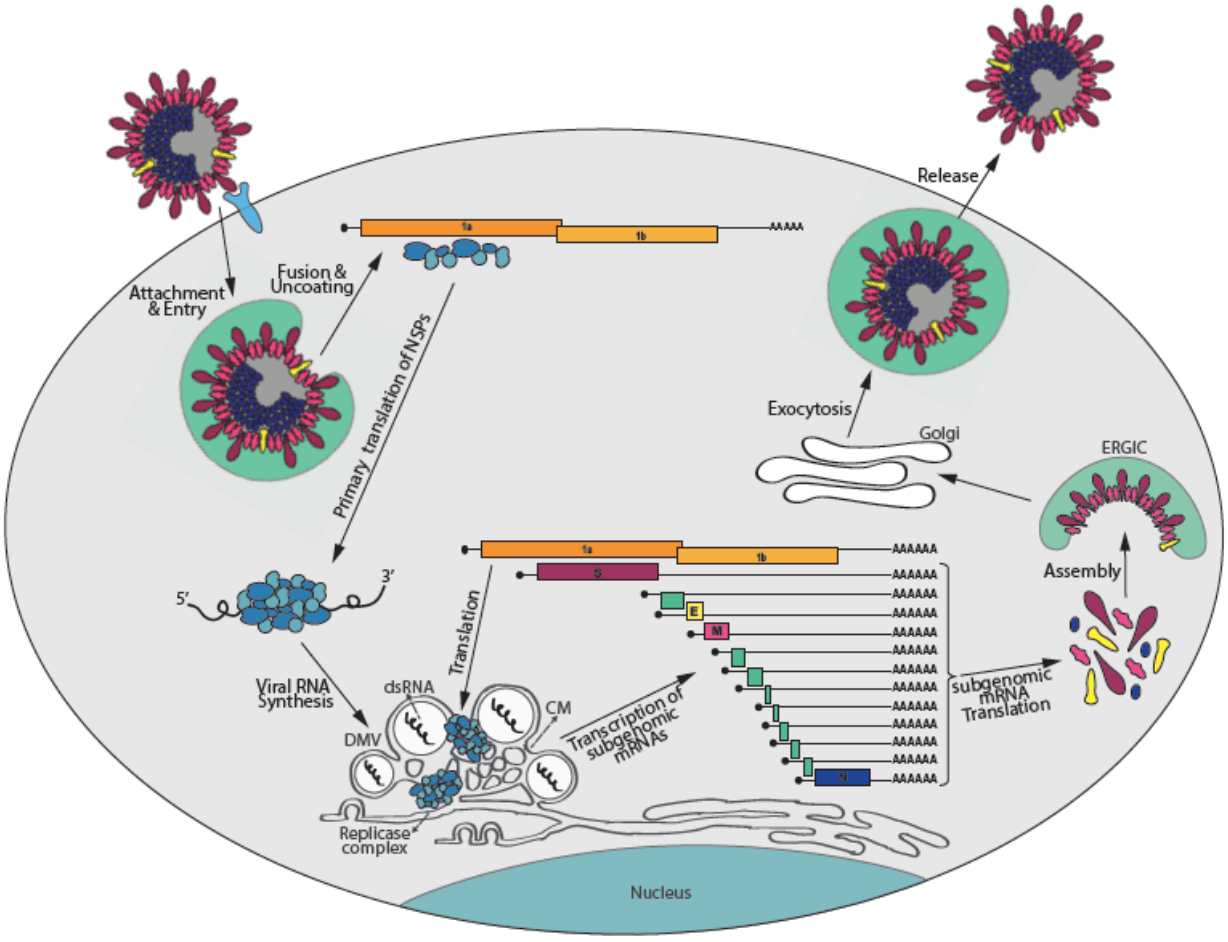

Figure 2 Schematic of the coronavirus life cycle

Schematic representation of the Coronavirus life cycle including entry and attachment, transcription, translation, viral genome replication, assembly, and release. Clusters of teal-colored proteins corresponds to the viral RTC.

As the cycle proceeds and structural and non-structural proteins are produced, virion assembly begins to occur. The main structural proteins are embedded in the ER membrane and hijack the secretory pathway to make their way to the ER-Golgi intermediate compartment (ERGIC) where virion assembly is thought to initiate (Krijnse-Locker et al. 1994; Tooze, Tooze, and Warren 1984; Siu et al. 2008; Ye and Hogue 2007; Stertz et al. 2007). An additional component of trafficking for the purpose of assembly, is the trafficking of N encapsidated viral genomes from sites of replication to join the structural proteins at the ERGIC membranes where N interacts with M to anchor the newly synthesized genomes into the newly forming virions (Siu et al. 2008; Hurst et al. 2005; de Haan and Rottier 2005). Upon completion of formation and assembly, the virions are trafficked in intracellular vesicles to the Golgi and then to the plasma membrane to be released by exocytosis (V'Kovski et al. 2021; Wang, Grunewald, and Perlman 2020; Artika, Dewantari, and Wiyatno 2020; Orenstein, Banach, and Baker 2008).

1.1.5 Coronavirus Induced Membrane Rearrangements

A common facet of cytoplasmic viral replication is the formation of structures to provide a more ideal microenvironment for viral processes. CoVs are known to form a complex network of membranous structures through reorganization and recruitment host cell membranes and lipid metabolism that concentrate viral components and promote efficient viral replication and virion formation (Hagemeijer et al. 2014; Prentice et al. 2004; Reggiori, de Haan, and Molinari 2011; Reggiori et al. 2010; Snijder et al. 2020; V'Kovski et al. 2021; Yan et al. 2019; Heaton and Randall 2011). These rearrangements lead to formation of double-membrane vesicles (DMVs), double-membrane spherules (DMSs), convoluted membranes (CMs), and vesicle packets (VPs) (Figure 3) (Knoops et al. 2008; Snijder et al. 2020). In addition to providing a localized environment for replication and RNA synthesis to occur, these structures supply a secluded

environment for newly synthesized RNAs to hide from host sensors preventing activation of the host immune response (Artika, Dewantari, and Wiyatno 2020; Oudshoorn et al. 2016; V'Kovski et al. 2021; Snijder et al. 2020).

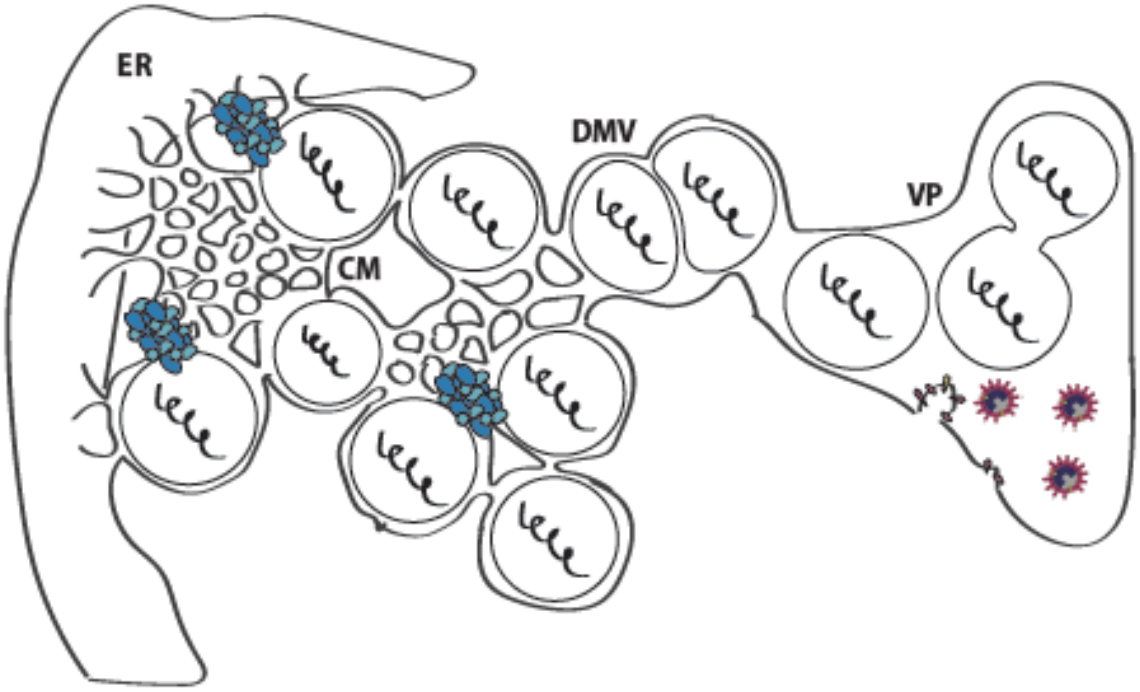

Figure 3 Schematic of coronavirus induced membrane rearrangements for viral replication
Schematic of proposed network of coronavirus induced membrane rearrangements for viral replication and virion production including the endoplasmic reticulum (ER), convoluted membranes (CM), double membrane vesicles (DMV), and vesicle packets (VP). Clusters of teal-colored proteins on the CM and DMVs corresponds to the viral RTC. Multicolored particles within the VPs correspond to newly assembled virions.

While the importance and basic functionality of these structures is relatively known, the overall formation mechanism is still largely unknown. Previous studies have observed DMVs colocalizing with LC3, a protein with well-known functions in autophagy (Reggiori, de Haan, and Molinari 2011; Reggiori et al. 2010). However, studies on mouse hepatitis virus (MHV), a model *betacoronavirus*, have produced conflicting data on whether or not autophagy is necessary for replication (Prentice et al. 2004; Zhao et al. 2007). Alternate models for membrane remodeling implicate EDEMosomes, vesicles originating from the ER that associate with non-

lipidated LC3 (Reggiori, de Haan, and Molinari 2011; Reggiori et al. 2010). Additionally, other RNA viruses that induce comparable membrane rearrangements and DMV formation usurp host cell lipid droplets, cellular organelles that store neutral lipids, and lipid metabolism as an underlying platform and energy source for replication (Cloherty et al. 2020; Heaton and Randall 2011). The likelihood that any single one of these mechanisms acts as the basis for replication center formation is low; it is more likely that a combination of these processes come together to form structures with a unique composition ideal for providing the exact microenvironment needed for effective progression of the viral life cycle.

What is known, however, is that onset of CoV induced membrane rearrangement coincides with interaction between early viral NSPs, namely NSP3, NSP4, and NSP6, and host proteins (Angelini et al. 2013; Hagemeijer et al. 2014; Knoops et al. 2008; Oudshoorn et al. 2017; Prentice et al. 2004; Reggiori, de Haan, and Molinari 2011; Reggiori et al. 2010; Gosert et al. 2002; Sims, Ostermann, and Denison 2000). Ultrastructural analysis and electron microscopy tracking of membrane rearrangement progression revealed a reticulovesicular network with substantial entanglement between the various membrane structures and the ER providing a likely origin and predetermined path for viral RNA synthesis (Knoops et al. 2008; Snijder et al. 2020). Within this network there are convoluted membranes (CM) that may act as sites of polyprotein processing and allow replicase subunits to make their way from the ER to double membrane vesicles (DMVs) (Hagemeijer et al. 2014; Knoops et al. 2008; Oudshoorn et al. 2017; Snijder et al. 2020). DMV are spherical structures with a double membrane that are interconnected with the CMs that are thought to act as the primary replication centers for coronaviruses. Tracking of dsRNA implicates DMVs as the primary site of RNA synthesis with almost all identifiable newly synthesized RNA being located withing these structures (Gosert et al. 2002; Hagemeijer et al.

2014; Knoops et al. 2008; Snijder et al. 2020). Additionally, there are structures called double membrane spherules (DMSs) that seem to be an intermediate structure between CMs and DMVs. DMSs appear as uniform spherical structures interconnected with CMs like DMVs, but unlike DMVs are not fully formed structures isolated from the external environment and are dsRNA negative. While their exact function is unknown, DMSs are hypothesized to be the result of non-productive replication events, an intermediary structure that eventually matures in to a fully functional DMV, or a secondary structure that potentially houses host factors and resources necessary for efficient replication (Oudshoorn et al. 2017; Knoops et al. 2008; Snijder et al. 2020). The last identified component of the membrane network are the vesicle packets (VPs), which appear as a large single membrane packet surrounding single membrane vesicles that strongly resemble the internal components of DMVs, suggesting a progression in the formation of these rearrangements where DMVs come together and merge via their outer membranes creating a single larger compartment (Knoops et al. 2008; Goldsmith et al. 2004). VPs have been observed to contain both single membrane vesicles and newly forming virions, suggesting that these structures may also act as sites for concentrating newly synthesized genomes and structural proteins for assembly (Knoops et al. 2008). How this hypothesis ties into the previously described models of assembly and ERGIC utilization is still unclear (Krijnse-Locker et al. 1994; Snijder et al. 2020; Goldsmith et al. 2004; Stertz et al. 2007; Tooze, Tooze, and Warren 1984; Klumperman et al. 1994).

1.1.6 Coronavirus Utilization of Fatty Acid Metabolism

Host-cell fatty acid metabolism involves a series of interconnected pathways that take glucose and metabolize it into various fatty acid and lipid products (Figure 4). Fatty-acid metabolism begins with catalysis of acetyl-CoA carboxylation by acetyl-CoA carboxylase

(ACC) to produce malonyl-CoA. Acetyl-CoA and malonyl-CoA are then further metabolized into fatty acids, namely palmitic acid, by fatty acid synthase (FASN), which marks the beginning of the branching points of the pathway. The resulting fatty acids can be processed by three major pathways. First, palmitic acid, the direct product of FASN, can be used for protein palmitoylation by palmitoyl acyltransferases (PAT). Additionally, the fatty acids produced by FASN can be processed into acyl-CoA by long chain acyl-CoA synthetase (ACS) at which point it can either be translocated to the mitochondria by carnitine palmitoyltransferase 1A (CPT1A) for fatty acid β-oxidation and energy production, or further processed into the neutral lipid triacylglycerol (DAG) by a series of acyltransferase enzymes and trigger lipid droplet formation.

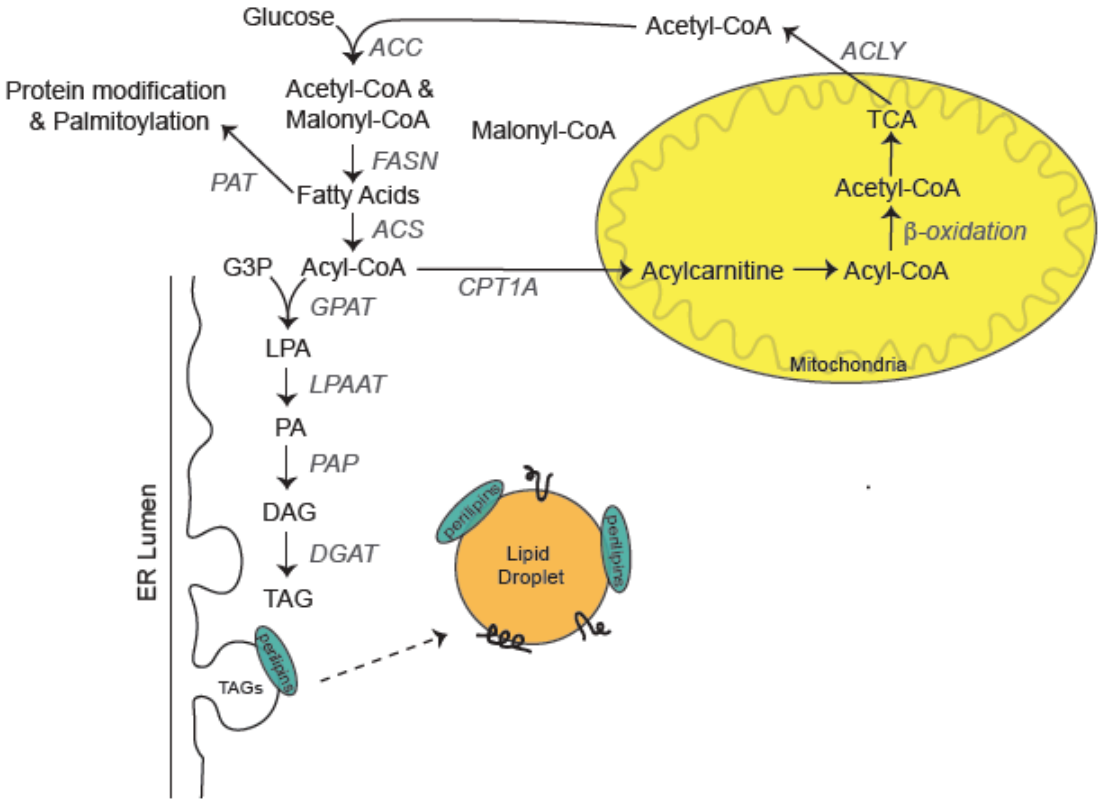

Figure 4 Schematic of host cell fatty acid metabolism

Simplified schematic of host-cell fatty acid metabolism showing the major steps required to process glucose and acetyl-CoA into downstream fatty acid and lipid products.

Usurpation of fatty acid metabolism for replication is a common theme amongst viruses. The resulting changes in fatty acid and lipid products can be used for production of receptors or cofactors at the cell surface, production of signaling molecules, structural and function components of virally induced replication centers, protein modification and proper protein trafficking, or as an energy source for replication (Chandrasekharan, Marginean, and Sharma-Walia 2016; Chazal and Gerlier 2003; Heaton and Randall 2011; Hsu et al. 2010; Xu and Nagy 2015; Yan et al. 2019). Inhibition of upstream metabolism enzymes like ACC or FASN decreases replication of several positive sense RNA viruses including Coxsackievirus B, Chickungunya virus (CHIKV), and several flaviviruses (Ammer et al. 2015; Gaunt et al. 2013; Hitakarun et al. 2020; Merino-Ramos et al. 2016; Tongluan et al. 2017). Fatty acid protein palmitoylation is also required for HCV infection, NS4B and the core protein both require protein palmitoylation for their function in replication and virus particle formation, respectively (Majeau et al. 2009; Yu et al. 2006). Fatty acid β-oxidation in the mitochondria is upregulated by Dengue virus (DENV) infection to process fatty acids produced from lipid droplet catabolism into energy for replication (Heaton and Randall 2011). Conversely, the production of neutral lipids and lipid droplets by enzymes like ACS or diglyceride acyltransferases (DGATs), has been shown to be important for rotavirus (RV) and hepatitis C virus (HCV) replication, reflecting a dependence of these viruses on lipid droplets for replication center formation (Cheung et al. 2010; Kim et al. 2012; Liefhebber et al. 2014).

Coronaviruses are no exception to this pattern of fatty acid utilization. During infection, coronaviruses modify host-cell lipid metabolism to upregulate and downregulate specific lipid populations based on viral necessity (Yan et al. 2019). Among the upregulated populations were fatty acids. While the use of fatty acids by coronavirus during infection is still largely

uncharacterized, there is evidence of fatty acid and neutral lipid involvement in proper protein function, replication, and pathogenesis. Protein palmitoylation of the spike proteins of MHV and SARS-CoV have also been shown to be critical to virion assembly, cell-cell fusion, and infectivity (McBride and Machamer 2010; Petit et al. 2007; Thorp et al. 2006). Palmitoylation of coronavirus envelope (E) proteins has also been described and thought to be responsible for the ability of E to alter the morphology of vesicle membranes for assembly and release (Boscarino et al. 2008; Tseng et al. 2014). In addition to protein palmitoylation, neutral lipids and lipid droplets have recently been implicated as a critical components for SARS-CoV-2 replication. Lipid droplets and neutral lipids were found to closely co-localize with viral particles and newly synthesized RNA in infected cells, and inhibition of DGAT1, a terminal enzyme in lipid TAG production and lipid droplet formation, resulted in a significant reduction in viral replication, suggesting a potential role for lipid droplets in replication and/or replication center formation (Dias et al. 2020).

The extensive involvement of fatty acid metabolism in viral replication, combined with the little that is known about the necessity of fatty acids for coronavirus replication, provides a rationale for complete investigation into additional enzymes and products of fatty acid metabolism pathways and how they contribute to coronavirus replication. Chapter one of this dissertation will begin to address this.

1.1.7 Coronavirus Recruitment of Autophagy Machinery

VPS34, a class III phosphoinositol-3 kinase (PI3K) that phosphorylates phosphatydlinositol-3 (PI3) into phosphatydlinositol-3-phosphate (PI3P), and plays roles in autophagy, endosomal trafficking, and other aspects of membrane biology (Figure 5). VPS34 integrates into two separate complexes, complex I and complex II, that vary by a single protein

that determines the localization and activities of VPS34 (Ohashi et al. 2020). When associated with complex I, which contains VPS15, Beclin1, and ATG14L, VPS34 functions in cellular macroautophagy and the turnover and degradation of cellular components. VPS34 initiates autophagy by phosphorylating PI3 at the ER and recruiting additional proteins that work together with VPS34 to activate autophagosomal initiation and lipidation of LC3 for the progression of cellular autophagy flux and lysosomal degradation of the autophagosome (Jaber and Zong 2013; Backer 2016; Ohashi et al. 2020). Separate from autophagy, VPS34 associates with complex II, which contains VPS15, Beclin1, and UVRAG, and localizes to endocytic vesicles for vesicular trafficking and sorting. VPS34 is recruited to endosomes by VPS15 binding to Rab5 in early endosomes and uses its kinase activity to produce PI3P to recruit additional factors, like Rab7, involved in maturation to a late endosome. Additional phosphorylation of phosphoinositol-3 allows for recruitment of the endosomal sorting complex required for transport (ESCRT) proteins for the formation of multivesicular bodies or proper functioning of the Retromer complex for endosome-to-Golgi transport (Backer 2016; Ohashi et al. 2020).

Regardless of which complex it is associated with, VPS34 activity has been implicated in the coronavirus lifecycle for recruitment of factors for replication or DMV formation (Feng et al. 2019; Su et al. 2011; Wang et al. 2021). For members of the positive-sense RNA tombusviruses (TBSV), VPS34 has been shown to be recruited to replication compartments providing increased levels of phosphoinositol-3-phosphate, which allows for the recruitment of Rab5-positive early endosomes to provide phosphatidylethanolamine-enriched membranes at sites of viral replication and for replication center formation (Feng et al. 2019). Additionally, HCV protein NS4b uses VPS34 to induce autophagy, possibly for initiation of DMV formation, but the exact mechanism is not yet fully characterized (Su et al. 2011; Romero-Brey et al. 2012).

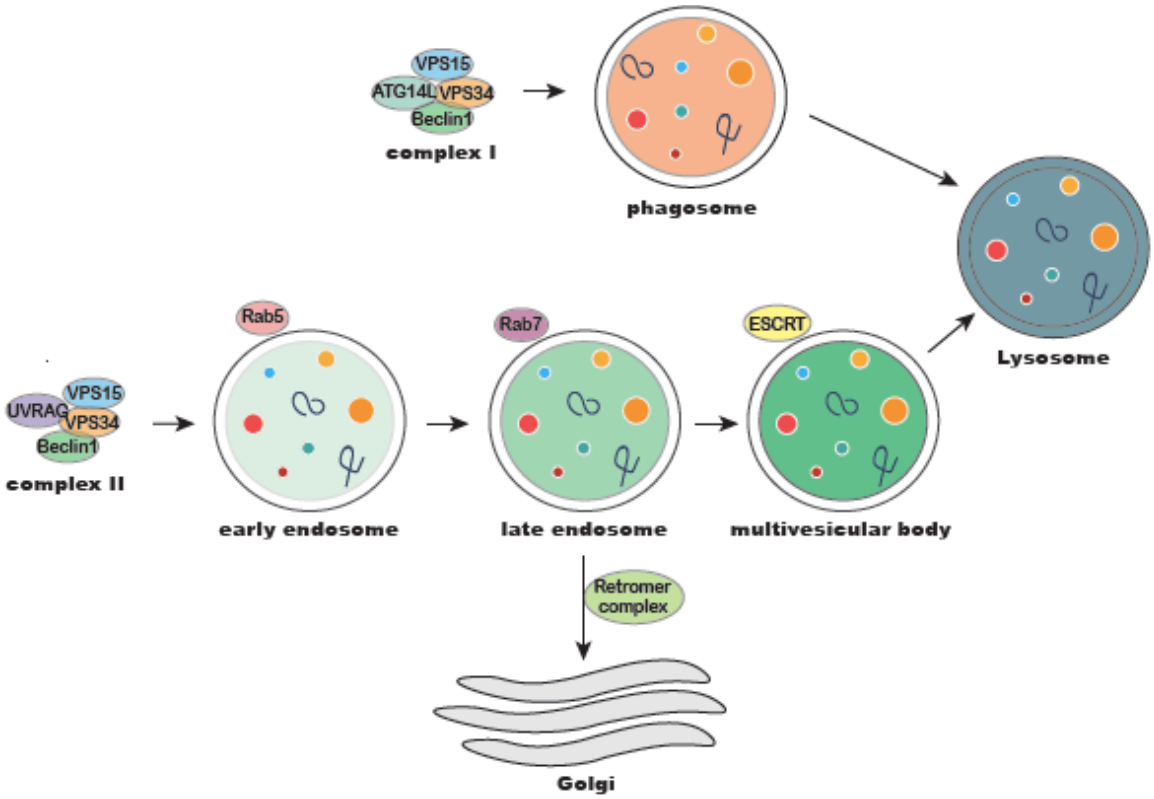

Figure 5 Schematic of VPS34 function

Simplified schematic of normal VPS34 function including the complex I autophagy pathway and complex II endocytic trafficking pathway.

For coronaviruses, multiple studies have observed DMVs colocalizing with LC3, a protein implicated in autophagy and autophagosome membranes, but the exact mechanism of recruitment has yet to be fully linked to autophagy and could be the result of alternate VPS34 pathways or alternate mechanisms all together (Reggiori, de Haan, and Molinari 2011; Reggiori et al. 2010; de Haan, Molinari, and Reggiori 2010). However, studies on mouse hepatitis virus (MHV), a common model *betacoronavirus*, have found conflicting data on whether or not autophagy is necessary for replication depending on the cell line used. Embryonic stem cells lacking ATG5, an essential autophagy protein involved in autophagosome precursor formation, appeared to lack proper DMV formation; however, in bone marrow derived macrophages and

mouse embryonic fibroblasts ATG5 was found to have no effect on replication (Prentice et al. 2004; Zhao et al. 2007).

More recent studies suggest that coronaviruses interfere with autophagy, and that activation of autophagy can inhibit replication of various coronaviruses (Gassen et al. 2019; Guo et al. 2016; Schneider et al. 2021). In transmissible gastroenteritis virus (TGEV) infected cells it was found that viral replication induced autophagy flux and increased the levels of lipidated LC3 and vesicles consistent with autophagy, and compound inhibition of autophagy resulted in an enhancement in replication (Guo et al. 2016). Consistent with these data, it was found that MERS-CoV reduces Beclin1 levels and in turn blocks autophagosome-lysosome fusion. Inhibition of S-phase kinase-associated protein 2 (SKP2), a negative regulator of Beclin1 and autophagy, counteracts this process and enhances autophagic flux resulting in reduced replication of MERS-CoV (Gassen et al. 2019). Conversely, host protein TMEM41B, which is also implicated in autophagy, has been demonstrated to facilitate SARS-CoV-2 growth, suggesting that some coronaviruses may also usurp some autophagy functions for pro-viral function (Schneider et al. 2021).

1.1.8 Current strategies in antiviral development

The current SARS-CoV-2 pandemic has been continuing on for close to two years now and is still causing major concern in many areas of the world. The geographic reach and duration of this pandemic has made the need for anti-coronavirus antivirals very apparent. When major public health events like this occur and new viruses emerge, it is common to implement high throughput drug repurposing screens to identify potential FDA approved antivirals that can be quickly applied to the ongoing situation (Pizzorno et al. 2019; Garcia-Serradilla, Risco, and Pacheco 2019; Lundstrom 2020). To date, this has been the major strategy for coronavirus

outbreaks with treatment for SARS, MERS, and SARS-CoV-2 consisting of repurposed broad spectrum antiviral treatments including exogenous IFN-α/β, protease inhibitors like Lopinavir and Ritonavir, and nucleoside analogs like Remdesivir and Ribavirin (Chong et al. 2015; Sheahan et al. 2020; Wu, Wu, and Lai 2020; Pizzorno et al. 2019; Gordon, Tchesnokov, et al. 2020). The aforementioned treatments have been found to be useful and effective in many cases, they are not the only viable option.

A potential strategy to identify additional drugs for repurposing, or even novel therapeutic options, is determining the host proteins and pathways involved in the virus life cycle and using small molecule inhibitors against these components to prevent propagation of the virus. There have been several screens employing this strategy that have led to proposed potential therapeutic options, such as drugs targeting entry by inhibiting angiotensin converting enzyme 2 (ACE2), the specific receptor for SARS-CoV-2, disrupting cap dependent translation by targeting eukaryotic initiation factor 4a (eIF4a), and sigma nonopioid receptor 1 (SIGMAR1) that is thought to act through various mechanisms that have yet to be confirmed (Gordon, Hiatt, et al. 2020; Schneider et al. 2021; Gordon, Jang, et al. 2020; Santos et al. 2020). Another screen looked at the presentation of COVID-19 in patients and identified overlap between the inflammatory response generated by severe virus-induced disease and neoplasia and sought to determine whether or not there were cancer treatments targeting chronic inflammation that could be used to inhibit replication. Currently there are 14 classes of drugs used in cancer treatment that are being tested, or have been tested, in patients with COVID-19 (Saini et al. 2020). There is also work being done to determine if lipid metabolism pathways are viable candidates for targeting coronavirus infection with an emphasis on disrupting the structural involvement of lipid

metabolism for viral entry, assembly, and egress (Dias et al. 2020; Abu-Farha et al. 2020; Schneider et al. 2021; Chen et al. 2018).

While there is a good amount of research being done to work towards new antivirals effective against coronaviruses, there are still many possibilities that have yet to be pursued. A continued effort to better understand the viral lifecycle and viral usurpation of host-cell machinery will help to uncover additional viable targets for treatment. In chapter one of this dissertation, we will discuss the involvement of fatty acid metabolism and VPS34 in coronavirus replication in the context of SARS-CoV-2 infection, and attempt to pinpoint specific steps of these pathways that are critical for virus propagation. The results may suggest host pathways with therapeutic potential for SARS-CoV-2 and other coronaviruses.

1.2 Filoviruses

1.2.1 Filovirus Taxonomy

Filoviridae is a family of zoonotic viruses within the order *Mononegavirales (Maes et al. 2019; Kuhn et al. 2019)*. The family is divided into six different genera based on genome sequence similarity (Table 2). The *Ebolavirus*, *Marburgvirus*, *Cuevavirus*, *Dianlovirus*, *Striavirus*, and *Thamnovirus* genera differ between 55-58% at the nucleotide level, with species divergence within the genera being less than 30% (Bào et al. 2017). The genus most prevalent in causing human disease, *Ebolavirus*, contains six species: Bombali *ebolavirus* (BOMV), Bundibugyo *ebolavirus* (BDBV), Reston *ebolavirus* (RESTV), Sudan *ebolavirus* (SUDV), Tai Forest *ebolavirus* (TAFV), Zaire *ebolavirus* (EBOV) (Kuhn et al. 2019). *Marburgvirus*, the second genus known to contain human disease-causing viruses, contains one species, Marburg *marburgvirus*, that is divided into two distinct lineages Marburg *marburgvirus* (MARV) and Ravn *marburgvirus* (RAVV) (Towner et al. 2006; Kuhn et al. 2019; Brauburger, Hume,

Mühlberger, et al. 2012). The additional four genera were identified through RNA sequencing of samples from bats and fish from which viral RNA, but not infectious virus, was isolated and identified (Yang et al. 2019; Shi et al. 2018; Negredo et al. 2011; Kemenesi et al. 2018; Hume and Mühlberger 2019). Genus *cuevavirus* contains a single species, Lloviu *cuevavirus* (LLOV), the RNA of which was isolated from a colony of Schreiber's bats in Spain that became of interest after a large portion of the colony had died (Negredo et al. 2011; Kemenesi et al. 2018). Similarly, Měnglà *dianlovirus* (MLAV), the only species of the genus *Dianlovirus*, was discovered when its RNA was isolated from a single Rousettus bat in China in 2018 (Yang et al. 2019). The genera *striavirus* and *thamnovirus*, containing Xīlǎng *striavirus* (XILV) and Huángjiāo *thamnovirus* (HUJV), respectively, were identified in China after being isolated from fish (Shi et al. 2018; Negredo et al. 2011).

Table 2. Filovirus phylogeny including order, family, genus, and species.

Order	Family	Genus	Species
Mononegavirales	Filoviridae	Ebolavirus	Bombali virus (BOMV) Bundibugyo virus (BDBV) Reston virus (RESTV) Sundan virus (SUDV) Tai Forest virus (TAFV) Zaire virus (EBOV)
		Marburgvirus	Marburg virus (MARV) Ravn virus (RAVV)
		Cuevavirus	Lloviu virus (LLOV)
		Dianlovirus	Měnglà virus (MLAV)
		Striavirus	Xīlǎng virus (XILV)
		Thamnovirus	Huángjiāo virus (HUJV)

1.2.2 Filovirus Outbreaks

The first reported filovirus outbreak occurred in 1967 when laboratory workers in Germany and Yugoslavia were isolating kidney cells for culturing poliomyelitis vaccine strains contracted an unknown infectious agent. The kidney cells were from infected African green monkeys imported from Uganda (Smith et al. 1967; Brauburger, Hume, Mühlberger, et al. 2012).

The outbreak resulted in a total of 32 cases and seven fatalities (Smith et al. 1967; Brauburger, Hume, Mühlberger, et al. 2012). In the months following the outbreak, the virus become the first filovirus to be isolated and characterized, and it would subsequently be named Marburg *marburgvirus* after the city in Germany with the highest prevalence of disease. Following the initial identification of MARV, several small outbreaks occurred sporadically in Africa, each affecting only a small number of people (Table 3). This pattern of small outbreaks was interrupted in 1998, and again in 2004, when MARV emerged in the Democratic Republic of Congo (DRC) and Angola, respectively. These two outbreaks caused a total of 406 cases with respective fatality rates of 83% and 90%, revealing the public health threat of Marburg virus (WHO 2018; Languon and Quaye 2019; CDC 2014; Brauburger, Hume, Mühlberger, et al. 2012). In the last fifteen years there have been a handful of outbreaks, but they have all been small and minimally consequential from a global public health perspective (WHO 2018; Languon and Quaye 2019; CDC 2014).

Table 3. Documented Marburgvirus outbreaks since the first occurrence

Year	Lineage	Country	Number of cases	Number of fatalities	Case fatality (%)
1967	MARV	Germany	30	7	23.3%
		Yugoslavia	2	0	0%
1975	MARV	South Africa	1	3	33%
1980	MARV	Kenya	1	2	50%
1987	RAVV	Kenya	1	1	100%
1988	MARV	Russia	1	1	100%
1998-2000	MARV/RAVV	DRC	154	128	83%
2004-2005	MARV	Angola	252	227	90%
2007	MARV/RAVV	Uganda	4	1	25%
2008	MARV	USA	1	0	0%
2008	MARV	Netherlands	1	1	100%
2012	MARV	Uganda	15	4	27%
2014	MARV	Uganda	1	1	100%
2017	MARV	Uganda	3	3	100%

Table adapted from (Brauburger, Hume, Muhlberger, et al. 2012; CDC 2014; Languon and Quaye 2019; WHO 2018)

In addition to outbreaks caused by members of the *Marburgvirus* genus, members of the *Ebolavirus* genus have been of great significance with regard to public health. 1976 marked the first emergence of both Zaire *ebolavirus* and Sudan *ebolavirus*, when simultaneous outbreaks occurred in the DRC and Sudan, respectively (Pattyn et al. 1977; Languon and Quaye 2019; Bowen et al. 1977). Both outbreaks were suspected to have animal origin, coming from bushmeat purchased on an excursion and bats hanging in a cotton factory for EBOV and SUDV, respectively (Languon and Quaye 2019). Since the first occurrence of Ebola virus disease (EVD), new cases have been identified every year or two, with less than one percent of cases occurring outside of African countries (Table 4). Outbreaks resulted in anywhere from a few to a few hundred cases with death rates between 30-90% (WHO 2021a; Languon and Quaye 2019; CDC 2021b). This pattern continued until 2013 when an outbreak started in Guinea and quickly spread to other parts of West Africa and beyond. The epidemic became the largest Ebola outbreak in history causing 28,646 confirmed cases and 11,323 deaths with only a fraction of a percentage of cases and deaths occurring outside of West Africa (Languon and Quaye 2019; Jacob et al. 2020). This outbreak marked a critical turning point in the history of Ebola, not only because of the scale of the outbreak, but also because it provided new insights into the ability of Ebola to establish latent infection. Since the conclusion of the West Africa outbreak in 2016 there have been six more outbreaks, with two being of particular importance. First, the tenth outbreak in the Democratic Republic of Congo (DRC) which was the largest occurrence in that region and the second largest Ebola outbreak overall. It began in August 2018, and despite global best efforts to contain the virus lasted until June 2020 resulting in an outbreak affecting thousands of people and a case fatality rate of 66% (Languon and Quaye 2019; CDC 2021b). Second, the recent outbreaks in DRC and Guinea, which have been identified by sequencing to

be tied to the 2013-2016 outbreak and the result of recurrence due to latent infection (Kupferschmidt 2021; CDC 2021b, 2021a).

Table 4. Documented Ebolavirus outbreaks since the first occurrence

Year	Species	Country	Number of cases	Number of fatalities	Case fatality (%)
1976	SUDV	Sudan	284	151	53%
	EBOV	DRC	318	280	88%
	SUDV	England	1	0	0%
1977	EBOV	DRC	1	1	100%
1979	SUDV	Sudan	34	22	65%
1989-1990	RESTV	Philippines/USA	7	0	0%
1992	RESTV	Italy	0	0	0%
1994	EBOV	Gabon	52	31	60%
	TAFV	Côte d Ivoire	1	0	0%
1995	EBOV	DRC	315	254	81%
1996	EBOV	Gabon	31	21	68%
	EBOV	Gabon	60	45	75%
	EBOV	South Africa	1	1	100%
	RESTV	USA	0	0	0%
	RESTV	Philippines	0	0	0%
	EBOV	Russia	1	1	100%
2000-2001	SUDV	Uganda	425	224	53%
2001-2002	EBOV	Gabon	65	53	82%
	EBOV	Republic of Congo	59	44	75%
2002-2003	EBOV	Republic of Congo	143	128	90%
2003	EBOV	Republic of Congo	35	29	83%
2004	SUDV	Sudan	17	7	41%
	EBOV	Russia	1	1	100%
2005	EBOV	Republic of Congo	12	10	83%
2007	EBOV	DRC	264	187	71%
2007-2008	BDBV	Uganda	131	42	32%
2008	RESTV	Philippines	6	0	0%
2008-2009	EBOV	DRC	32	15	47%
2011	SUDV	Uganda	1	1	100%
2012	SUDV	Uganda	11	4	36%
	BDBV	DRC	38	13	34%
	SUDV	Uganda	6	3	50%
2013-2016	EBOV	Multiple Countries	28,646	11,323	40%
2014	EBOV	DRC	69	49	71%
2017	EBOV	DRC	8	4	50%
2018	EBOV	DRC	54	33	61%
	EBOV	DRC, Uganda	3,470	2,287	66%
2020	EBOV	DRC	130	55	42%
2021	EBOV	DRC	12	6	50%
2021	EBOV	Guinea	23	12	52%

Table is adapted from (CDC 2021b; Languon and Quaye 2019; WHO 2021a)

1.2.3 Filovirus Structure and Proteins

Filoviruses are enveloped, non-segmented, negative-sense viruses with encapsidated genomes around 19 kilobases that get packaged into filamentous virions of pleomorphic nature (Beniac et al. 2012; Bharat et al. 2011; Noda et al. 2006; Noda et al. 2010; Sugita et al. 2018; Wan et al. 2017; Welsch et al. 2010). The particle envelope is derived from host cell membranes and contains the encapsidated genome that is associated with the nucleocapsid complex (NC) containing the nucleoprotein (NP) directly coating the ssRNA genome and the four viral proteins (VP) required for initiation of the viral lifecycle in newly infected cells: VP24, VP35, VP30, and the RdRp large protein (L). The virion membrane itself is decorated with the viral matrix protein (VP40) on the inside and the viral glycoprotein (GP) on the surface (Figure 6B) (Becker et al. 1998; Bharat et al. 2012; Bharat et al. 2011; Booth, Rabb, and Beniac 2013; Noda et al. 2006; Hofmann-Winkler, Kaup, and Pohlmann 2012; Kuhn et al. 2006; Manicassamy et al. 2007; Olejnik et al. 2011).

The genome contains seven open reading frames that can produce up to ten proteins depending on the virus (Figure 6A) (Elliott, Kiley, and McCormick 1985; Emanuel, Marzi, and Feldmann 2018; Feldmann et al. 1992; Hume and Mühlberger 2019; Kirchdoerfer et al. 2017; Sanchez et al. 1993; Sanchez et al. 1989). The filovirus proteins are multifunctional and partake in interactions between themselves and other viral proteins and host proteins to carry out their various functions.

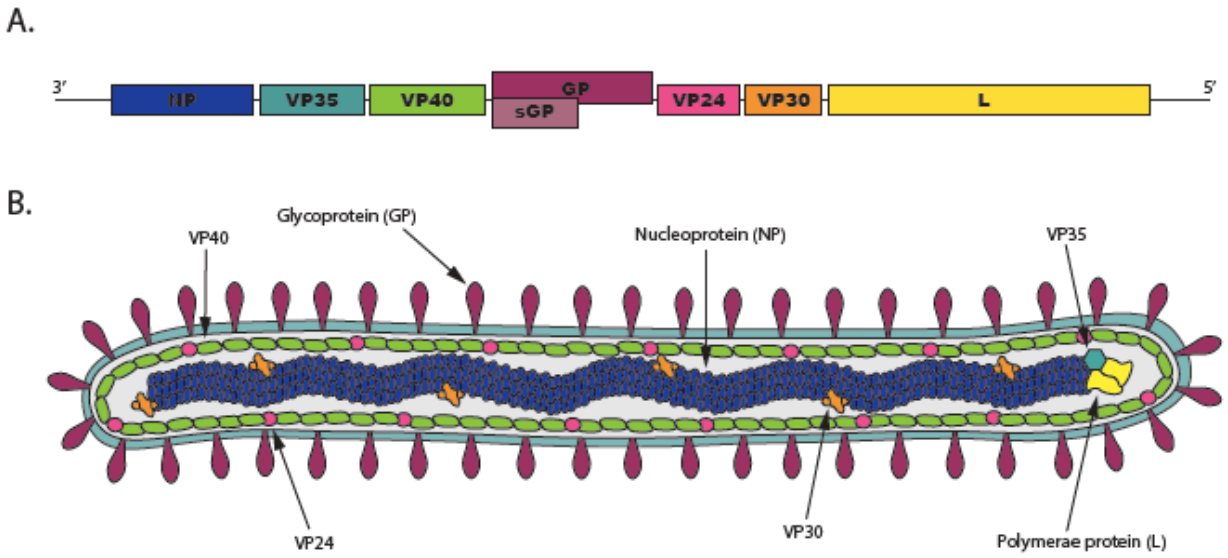

Figure 6 Genome organization and morphology of filoviruses

Schematic representation of Filovirus genome organization (A). Schematic representation of the Filovirus virion and structural protein organization (B).

There are two major complexes formed by viral protein interactions for the purposes of replication and assembly. NP, VP35, VP30, and the RdRp L protein make up the replication transcription complex (RTC) and directly function in genome replication and transcription of mRNAs (Mühlberger et al. 1999; Mühlberger et al. 1998; Enterlein et al. 2006). The nucleocapsid complex (NC) contains NP, VP35, VP24, and L with the first three being required for virion formation and transport to the plasma membrane for budding (Bharat et al. 2012; Bharat et al. 2011; Noda et al. 2010; Takamatsu, Kolesnikova, and Becker 2018; Wan et al. 2017).

In addition to forming complexes for replication and assembly the aforementioned proteins have further functions in creating an ideal environment for the progression of infection. NP has been shown to be necessary and sufficient for the formation of perinuclearly localized punctate structures that act as the sites of viral replication that encompass RTC components, host proteins, and newly synthesized RNA (Baskerville et al. 1985; Hoenen et al. 2012; Miyake et al.

2020; Nanbo et al. 2013). The VP35 protein is a critical factor in innate immune antagonism and engages in a multitude of interactions with host factors to surpass host responses to viral infection (Messaoudi, Amarasinghe, and Basler 2015; Olejnik, Hume, Leung, Amarasinghe, Basler, and Mühlberger 2017; Basler and Amarasinghe 2009). Complementing its role in the RTC, VP30 has been shown to participate in interactions regulating replication and the phosphorylation status of VP30 is important to these functions (Batra et al. 2018; Dong et al. 2020; Nanbo et al. 2013; Xu et al. 2017). VP40 and VP24 function as the two matrix proteins, and VP40 itself is the major constituent required for virion formation and budding (Martin et al. 2016; Kolesnikova et al. 2002; Stahelin 2014; Timmins et al. 2001). In addition to their role as matrix proteins, the VP40 and VP24 proteins of various filovirus family members function in blocking components of the IFN signaling pathway (Feagins and Basler 2015b; Reid et al. 2006; Valmas and Basler 2011b; Messaoudi, Amarasinghe, and Basler 2015; Olejnik, Hume, Leung, Amarasinghe, Basler, and Mühlberger 2017). Uniquely, the VP24 of MARV can also activate the host cytoprotective antioxidant response as a means of prolonging the lifespan of host-cells (Edwards et al. 2014; Page et al. 2014).

Lastly, the viral glycoprotein (GP), is a type I transmembrane protein present on the surface of viral particles that acts as the major determinant of cell tropism and is the major antigenic determinant of the virus (Carette et al. 2011; Chandran et al. 2005; Hofmann-Winkler, Kaup, and Pohlmann 2012; Martin et al. 2016; Takada et al. 1997; Wool-Lewis and Bates 1998; Becquart et al. 2014; Dahlke et al. 2017). Depending on the species, filoviruses either produce a single membrane bound version of GP or utilize editing of the GP open reading frame to produce membrane bound GP, as well as soluble GP (sGP), that acts as a decoy substrate for GP specific

antibodies, and small soluble GP (ssGP) with unknown function (He, Melnik, et al. 2017; Mohan et al. 2012; Sanchez et al. 1996).

1.2.4 Filovirus Replication and Transcription

The viral life cycle proceeds as depicted in Figure 7. After exposure to virus, membrane bound GP on the outside of the virion will contact and bind the host cell receptor triggering entry through micropinocytosis and fusion of the viral membrane and host endosomal membrane to allow for release of the genome into the cytoplasm (Aleksandrowicz et al. 2011; Carette et al. 2011; Chandran et al. 2005; Hofmann-Winkler, Kaup, and Pohlmann 2012; Martin, Canard, and Decroly 2017; Wool-Lewis and Bates 1998). Upon release, the negative-sense genome acts as the template for the accompanying RTC proteins to carry out primary transcription, producing capped polyadenylated mRNAs that will be translated into proteins using the host translation machinery (Dolnik et al. 2010; Mühlberger 2007; Whelan, Barr, and Wertz 2004). The increasing pool of viral proteins within the cell allows production of positive-sense antigenomes to be copied into more negative-sense genomes that will be packaged into new virions. The mechanism involved in the switch between these two processes is not completely understood but is thought to be tightly regulated and dependent on the concentration of NP within the cell (Dolnik et al. 2010; Mühlberger 2007; Whelan, Barr, and Wertz 2004). The process of viral replication occurs within cytoplasmic inclusion bodies that are postulated to act to concentrate replication machinery and sequester it from the external cellular environment (Baskerville et al. 1985; Hoenen et al. 2012; Miyake et al. 2020; Nanbo et al. 2013). As the cycle continues, producing new proteins and genomes, interactions with VP40 will trigger formation of new nucleocapsids that will assemble and bud into virions and be released from the host cell membrane (Bharat et al. 2012; Dolnik et al. 2010; Harty et al. 2000; Jasenosky et al. 2001a;

Kolesnikova et al. 2004; Kolesnikova et al. 2002; Noda et al. 2002; Noda et al. 2007b; Timmins et al. 2001; Wu, Jin, et al. 2020; Licata et al. 2003; Yasuda et al. 2003).

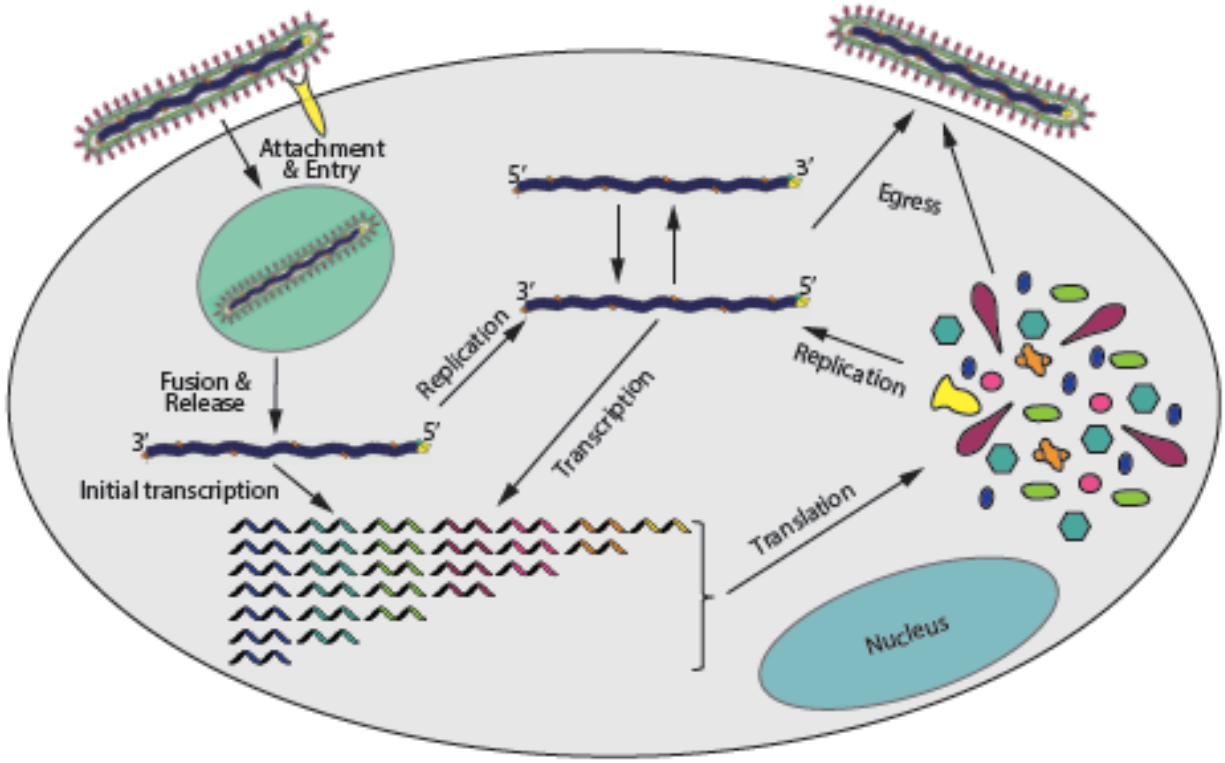

Figure 7 Schematic of the filovirus life cycle

Schematic representation of the Filovirus life cycle including entry and attachment, transcription, translation, viral genome replication, assembly, and release.

1.2.5 Disruption of Signaling Pathways to Enhance Filoviral Infection

1.2.5.1 Type I interferon production and signaling pathway

Type I interferons like IFN-α and IFN-β are produced as a cellular defense mechanism in response to pathogens. The pathway functions as a cycle; the production side of the pathway involves pathogen detection and production of IFN, which then stimulates the signaling side of the pathway leading to the upregulation if IFN-stimulated genes (ISGs), in turn producing more IFNs, and this continues until the threat is neutralized (Figure 8) (Majzoub, Wrensch, and Baumert 2019; McNab et al. 2015; Pestka, Krause, and Walter 2004; Secombes and Zou 2017).

The production of type I IFNs is triggered by the recognition of pathogens by host-cell pattern recognition receptors (PRRs) that include C-type lectin receptors (CLRs), nucleotide-binding oligomerization domain-like receptors (NLRs), retinoic acid-inducible gene I (RIG-I)-like receptors (RLRs), toll-like receptors (TLRs), and DNA sensors. Each type of receptor is capable of distinguishing between host and non-host material through the recognition of motifs commonly associated with non-host invaders called pathogen-associated molecular patterns (PAMPs). Pathogen recognition by a PRR leads to complex signaling cascades involving an array of signaling proteins and kinases that ultimately result in the translocation of transcription factors to the nucleus for the activation of the IFN-α/β promotor (Amarante-Mendes et al. 2018; Chow, Gale, and Loo 2018; Honda et al. 2005; Hopfner and Hornung 2020; Kato, Takahasi, and Fujita 2011; Okamoto et al. 2017; Panne, Maniatis, and Harrison 2007; Takeuchi and Akira 2010).

Activation of the IFNα/β promotor results in production and secretion of IFNα/β that can be recognized by the interferon receptor (IFNAR) on the producing cell and surrounding cells to initiate IFN signaling and the antimicrobial response to eliminate infection within the producing cell and prevent progression of infection in neighboring cells. The IFNAR receptors are coupled to two well characterized signaling molecules: janus kinase (Jak1) and tyrosine kinase 2 (Tyk2) (Piehler et al. 2012). The binding of type I IFNs to the receptor causes phosphorylation of Jak1 and Tyk2, initiating a phosphorylation signaling cascade that recruits signal transducer and activator of transcription (STAT) proteins. STAT1 and STAT2 are phosphorylated and come together with interferon regulatory factor 9 (IRF9) to form the interferon-stimulated gene factor 3 (ISGF3) complex that is translocated to the nucleus by the karyopherin alpha (KPNA) nuclear transport proteins. Once inside the nucleus the complex will bind to the interferon response

elements (ISREs) and promote production of large numbers of ISGs that work together to combat the initial infection that triggered the IFN response (Au et al. 1995; Darnell, Kerr, and Stark 1994; McBride and Reich 2003; Mogensen 2019; Schneider, Chevillotte, and Rice 2014; Schoggins 2014; Sekimoto et al. 1997).

Activation of the IFN response by non-segmented negative-sense RNA (NNS RNA) viruses, including filoviruses, is well characterized and involves triggering two main PRRs (Chow, Gale, and Loo 2018; Messaoudi, Amarasinghe, and Basler 2015; Okamoto et al. 2017). Retinoic-acid inducible gene I (RIG-I) preferentially recognizes 5'-triphosphates (5'ppp) of short segments of double and single stranded RNAs and melanoma differentiation association gene 5 (MDA5) senses longer segments of double stranded RNA. When a cell is infected by a NNS RNA virus, RIG-I will recognize the viral PAMP and become activated. Once active, RIG-I travels to the mitochondria and interacts with mitochondrial antiviral-signaling protein (MAVS) to recruit the additional signaling factors TANK binding kinase 1 (TBK1) and inhibitor of nuclear factor kappa-B kinase subunit epsilon (IKKε). The result of these interaction is the phosphorylation, dimerization, and nuclear translocation of interferon regulatory factor (IRF)-3 or IRF-7 to stimulate the IFNα/β promotor (Figure 8) (Chow, Gale, and Loo 2018; Messaoudi, Amarasinghe, and Basler 2015; Okamoto et al. 2017; Ren et al. 2020).

1.2.5.1 Filovirus antagonism of type I interferon

Filoviruses are known to counteract the host IFN response through unique interactions made by VP35, VP40, and VP24 (Basler and Amarasinghe 2009; Basler et al. 2000; Edwards et al. 2016b; Olejnik, Hume, Leung, Amarasinghe, Basler, and Muhlberger 2017). VP35 is the main multifunction IFN antagonist that takes part in numerous interactions to prevent activation of IFN production. First, VP35 acts as a dsRNA binding protein and is thought to sequester viral

RNA away from recognition by RIG-I through its dsRNA binding capabilities (Albariño et al. 2015; Bale et al. 2013b; Bale et al. 2012; Cardenas et al. 2006; Edwards et al. 2016b; Hartman, Towner, and Nichol 2004; Leung et al. 2009b; Leung, Prins, et al. 2010; Leung, Shabman, et al. 2010; Ramanan et al. 2012). Additionally, VP35 interacts with protein activator of interferon induced protein (PACT), a dsRNA binding protein that interacts with, and facilitates activation of, RIG-I; VP35 prevents RIG-I activation through disruption of this interaction (Cardenas et al. 2006; Luthra et al. 2013). VP35 also functions as a decoy substrate for IRF3 phosphorylation by TBK1 and IKKe (Basler et al. 2003; Prins, Cardenas, and Basler 2009). All of these points of inhibition by VP35 result in a loss of IRF3 phosphorylation and nuclear translocation, preventing the activation of the IFN promotor.

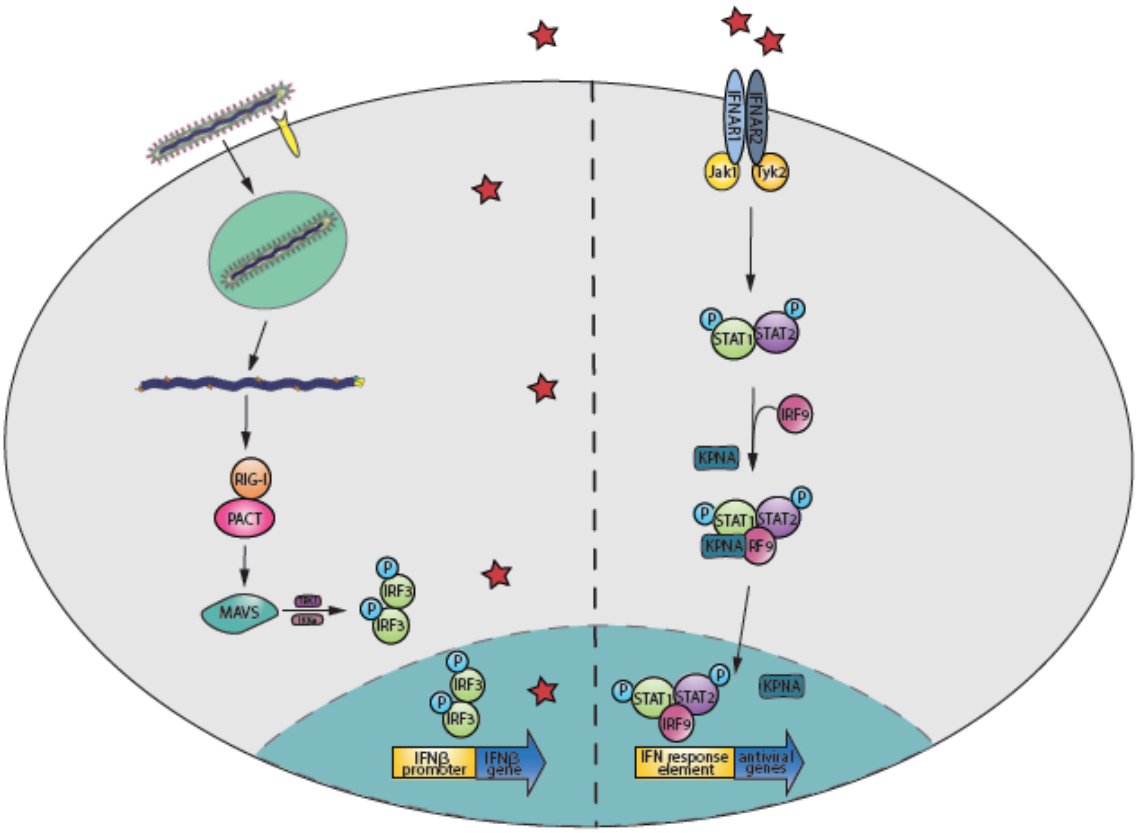

Figure 8 Schematic of the host-cell IFN signaling pathway in response to viral stimulus
Schematic representation of the virally induced type I IFN response including both production and signaling.

In addition to the direct antagonism of the RIG-I pathway, VP35 has the ability to prevent phosphorylation and activation of protein kinase R (PKR) on the signaling side of the pathway; however, the exact mechanism of antagonism is not known. There is some speculation that this inhibition could be tied to VP35s ability to disrupt stress granule formation and downstream translational arrest by preventing the PKR dependent activation of eukaryotic initiation factor 2 alpha (eIF2α) (Nelson et al. 2016; Le Sage et al. 2017; Feng et al. 2007b; Hume and Muhlberger 2018; Williams et al. 2020).

For MARV and MLAV, the VP40 protein has been found to be a potent inhibitor of exogenous IFN and Jak1 overexpression induced STAT1 phosphorylation on the signaling side of the IFN pathway. The blocking of phosphorylation prevents formation and nuclear translocation of the ISGF3 complex, preventing ISG production. The mechanism by which the phosphorylation is blocked has yet to be fully elucidated but is suspected to occur upstream of Jak1 phosphorylation (Guito et al. 2017; Valmas and Basler 2011b; Valmas et al. 2010; Williams et al. 2020).

Lastly, EBOV VP24 has been shown to interact with KPNA1, KPNA5, and KPNA6. The nuclear translocation of phosphorylated STAT1 requires interaction with KPNA, and the binding of VP24 to KPNA family members disrupts this interaction and prevents translocation. Without the translocation of STAT1 to the nucleus, ISG production cannot be activated, and IFN signaling cannot occur (Darnell, Kerr, and Stark 1994; Reid et al. 2006; Reid et al. 2007; Sekimoto et al. 1997; Xu et al. 2014). LLOV VP24 also inhibits IFN signaling, and while the mechanism has not been fully confirmed, it is thought to act in a similar manner (Feagins and Basler 2015b).

The details of filovirus innate immune antagonism as it applies to the newly identified MLAV will be discussed in chapter two.

1.2.5.2 Nrf2 dependent antioxidant response

As a means of counteracting oxidative stress, host-cells use a cytoprotective antioxidant response that is turned on upon activation of the antioxidant response element (ARE) by the transcription factor nuclear factor erythroid-2 related factor 2 (Nrf2). During normal cellular homeostasis, Kelch-like ECH-associated protein 1 (Keap1) interacts with and ubiquitinates Nrf2 to tag it for degradation and prevent it from making its way to the nucleus to activate an ARE response. If the cell is exposed to oxidative stress, this interaction is disrupted and Nrf2 accumulates and moves into the nucleus to activate the ARE and stimulate production of antioxidant genes for cellular protection (Figure 9) (Baird and Dinkova-Kostova 2011; Jain, Bloom, and Jaiswal 2005; Stenvinkel et al. 2020).

While MARV VP24 does not have an identified role in IFN antagonism, it has been shown to interact with Keap1 through a short sequence specific domain called the K-loop. VP24 induced disruption of the Keap1-Nrf2 interaction triggers the activation of the cytoprotective antioxidant response. This interaction is thought to be a pro-viral function of MARV VP24 to increase cell health and during replication (Edwards et al. 2014; Page et al. 2014; Williams et al. 2020).

In chapter two we will revisit the VP24-Keap1 interaction in the context on MLAV and further confirm the necessity of the K-loop sequence for this pro-viral function.

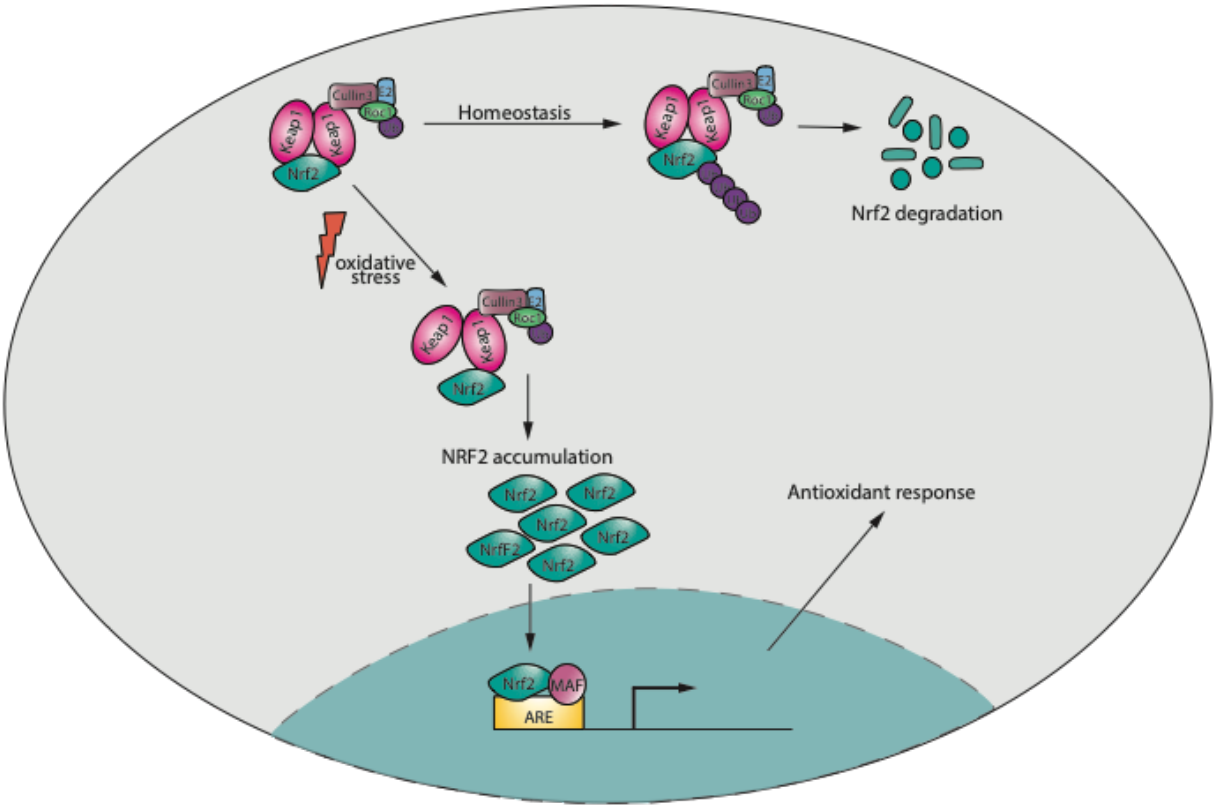

Figure 9 Schematic of the ARE antioxidant response pathway

Schematic representation of the Nrf2 dependent antioxidant response and its progression from normal homeostatic state to its active state.

2 INHIBITORS OF VPS34 AND FATTY-ACID METABOLISM SUPPRESS SARS-COV-2 REPLICATION

2.1 Author figure contributions

Caroline G. Williams – Figure 13 and Figures 15-19

Alexander S. Jureka – Figures 10-13 and Figures 15-19

Jesus A. Silvas – Figures 13-14

2.2 Abstract

Coronaviruses rely on host membranes for entry, establishment of replication centers, and egress. Compounds targeting cellular membrane biology and lipid biosynthetic pathways have previously shown promise as antivirals and are actively being pursued as treatments for other conditions. Here, we tested small molecule inhibitors that target the PI3 kinase VPS34 or fatty acid metabolism for anti-SARS-CoV-2 activity. Our studies determined compounds targeting VPS34 are potent SARS-CoV-2 inhibitors. Mechanistic studies with compounds targeting multiple steps up- and downstream of fatty acid synthase (FASN) identified the importance of triacylglycerol production and protein palmitoylation as requirements for efficient viral RNA synthesis and infectious virus production. Further, FASN knockout results in significantly impaired SARS-CoV-2 replication that can be rescued with fatty acid supplementation. Together, these studies clarify roles for VPS34 and fatty acid metabolism in SARS-CoV-2 replication and identify promising avenues for the development of novel countermeasures against SARS-CoV-2.

2.3 Introduction

SARS-CoV-2, the causative agent of COVID-19, is an enveloped positive-sense RNA virus of the *Betacoronavirus* genus (Holshue et al. 2020; Lundstrom 2020; Zhu et al. 2020). Since its emergence, SARS-CoV-2 is responsible for the most significant pandemic in the last century and has resulted in worldwide social and economic disruption. The severity of the pandemic has prompted urgent efforts to understand the requirements of the viral life cycle and identify potential therapeutic strategies (Bouhaddou et al. 2020; Gordon, Jang, et al. 2020; Hoffmann et al. 2020; Wang, Wang, et al. 2020). Repurposing drugs developed for other diseases and conditions may provide a shortcut to antiviral development (Garcia-Serradilla, Risco, and Pacheco 2019; Li and De Clercq 2020; Pizzorno et al. 2019; Saini et al. 2020). The use of compounds known to target specific host factors may also elucidate key pathways and processes utilized in SARS-CoV-2 replication.

Coronaviruses (CoV) interact with host cell membranes and membrane machinery at many different stages of their life cycle including entry, genome replication, and virion maturation and release (Hagemeijer et al. 2014; Prentice et al. 2004; Reggiori, de Haan, and Molinari 2011; Reggiori et al. 2010; Snijder et al. 2020; V'Kovski et al. 2021). One of the most striking features of CoV infection is the reorganization and recruitment of host cell membranes to form replication organelles. These rearrangements lead to formation of double-membrane vesicles (DMVs), double-membrane spherules (DMSs), convoluted membranes (CMs), and vesicle packets (VPs) (Knoops et al. 2008; Snijder et al. 2020). While there are several existing models that suggest these various membranous structures originate from modified ER membranes and that DMVs are the primary sites of replication, the mechanistic basis of their formation and CoV utilization remains incompletely understood (Angelini et al. 2013; Knoops et

al. 2008; Oudshoorn et al. 2017; Reggiori et al. 2010; Snijder et al. 2020). Previous studies have observed DMVs colocalizing with LC3, a protein with well-known functions in autophagy (Reggiori, de Haan, and Molinari 2011; Reggiori et al. 2010). However, studies on mouse hepatitis virus (MHV), a model *betacoronavirus*, have found conflicting data on whether or not autophagy is necessary for replication (Prentice et al. 2004; Zhao et al. 2007). Alternate models for membrane remodeling implicate EDEMosomes, vesicles originating from the ER that associate with non-lipidated LC3 (Reggiori, de Haan, and Molinari 2011; Reggiori et al. 2010). Additionally, other positive-sense RNA viruses that induce comparable membrane rearrangements and DMV formation utilize host cell lipid droplets, cellular organelles that store neutral lipids, and lipid metabolism as an underlying platform and energy source for replication (Cloherty et al. 2020; Heaton and Randall 2011).

Inhibitors of metabolic and biosynthesis pathways related to membranes and their precursors inhibit the replication of a number of viruses. One example of this is the inhibition of VPS34, a class III phosphoinositol-3 kinase (PI3K) that plays roles in autophagy, endosomal trafficking, and other aspects of membrane biology, which has been shown to impair hepatitis C virus (HCV), tombusvirus (TBSV) and coronavirus infection (Feng et al. 2019; Su et al. 2011; Wang et al. 2021).

Targeting enzymes involved in late steps of the neutral lipid synthesis pathway, such as long chain acyl-CoA synthetase (ACS) or diglyceride acyltransferases (DGATs) has been shown to inhibit rotavirus (RV) and HCV, possibly reflecting a dependence of these viruses on lipid droplets (Cheung et al. 2010; Kim et al. 2012; Liefhebber et al. 2014). Targeting upstream enzymes in fatty acid metabolism such as acetyl-CoA carboxylase (ACC) or fatty acid synthase (FASN) also decreases replication of several different viruses including Coxsackievirus B,

Chickungunya virus (CHIKV), and several flaviviruses (Ammer et al. 2015; Gaunt et al. 2013; Hitakarun et al. 2020; Merino-Ramos et al. 2016; Tongluan et al. 2017).

In this study, we sought out to determine the susceptibility of SARS-CoV-2 to modulators of VPS34, fatty acid and lipid metabolism. Compounds targeting VPS34 strongly impaired SARS-CoV-2 replication *in vitro*. Additionally, Orlistat and Triacsin C, inhibitors of FASN and ACS respectively (Carvalho et al. 2008; Igal, Wang, and Coleman 1997; Kridel et al. 2004), effectively inhibited SARS-CoV-2. Time of addition studies revealed that each of these inhibitors exert antiviral effects post-entry, with the VPS34 inhibitors also inhibiting an early step in the replication cycle. Experiments using additional inhibitors of enzymes upstream and downstream of FASN and ACS point to palmitoylation and neutral lipid production as necessary for virus replication. Immunofluorescence studies of compound-treated cells demonstrate disruption of dsRNA positive viral replication centers, and the same inhibitors also impact viral RNA synthesis. Studies in FASN knock-out Caco2 cells confirmed the critical role of fatty acid biosynthesis in SARS-CoV-2 replication. Taken together, the data presented here demonstrate that specific fatty acid and lipid metabolism pathways are critical for SARS-CoV-2 replication and provide novel mechanistic insights that may serve as a basis for the potential repurposing and development of therapeutics targeting these pathways for the treatment of COVID-19.

2.4 Materials and Methods

2.4.1 Viruses and cell lines

Vero E6 (ATCC# CRL-1586), Calu-3 (ATCC# HTB-55), and Caco-2 (ATCC# HTB-37) were maintained in DMEM (Corning) supplemented with 10% heat inactivated fetal bovine serum (FBS; GIBCO). Cells were kept in a 37°C, 5% CO2 incubator without antibiotics or antimycotics. Non-targeting wild type (NT-WT) Caco-2 and FASN KO Caco-2 cells were

produced by CRISPR editing (Synthego, Redwood City, CA) and maintained the same as their Caco2 parental cell line. SARS-CoV-2, strain USA_WA1/2020, was obtained from the World Reference Collection for Emerging Viruses and Arboviruses at the University of Texas Medical Branch-Galveston.

2.4.2 sgRNA selection

sgRNAs were designed according to Synthego's multi-guide gene knockout. Briefly, two or three sgRNAs are bioinformatically designed to work in a cooperative manner to generate small, knockout-causing, fragment deletions in early exons. These fragment deletions are larger than standard indels generated from single guides. The genomic repair patterns from a multi-guide approach are highly predictable based on the guide-spacing and design constraints to limit off-targets, resulting in a higher probability protein knockout phenotype.

2.4.3 sgRNA synthesis

RNA oligonucleotides were chemically synthesized on the Synthego solid-phase synthesis platform, using CPG solid support containing a universal linker. 5-Benzylthio-1H-tetrazole (BTT, 0.25 M solution in acetonitrile) was used for coupling, (3-((Dimethylamino-methylidene)amino)-3H-1,2,4-dithiazole-3-thione (DDTT, 0.1 M solution in pyridine) was used for thiolation, dichloroacetic acid (DCA, 3% solution in toluene) for used for detritylation. Modified sgRNA were chemically synthesized to contain 2'-O-methyl analogs and 3' phosphorothioate nucleotide interlinkages in the terminal three nucleotides at both 5' and 3' ends of the RNA molecule. After synthesis, oligonucleotides were subject to series of deprotection steps, followed by purification by solid phase extraction (SPE). Purified oligonucleotides were analyzed by ESI-MS.

2.4.4 RNP formation and transfection

To deliver CRISPR-Cas9 ribonucleoprotein (RNP) complexes, 10 pmol Streptococcus pyogenes NLS-Sp.Cas9-NLS (SpCas9) nuclease (Aldevron Cat. #9212) was combined with 30 pmol total synthetic sgRNA (Synthego,10 pmol each sgRNA) to form RNPs in 20 uL total volume with SF Buffer (Lonza Cat #V5SC-2002) and allowed to complex at room temperature for 10 minutes. Cells were dissociated into single cells using TrypLE Express (Gibco), as described above, resuspended in culture media and then counted. 100,000 cells per nucleofection reaction were pelleted by centrifugation at 100 xg for 3 minutes. Following centrifugation, cells were resuspended in transfection buffer according and diluted to $2x10^4$ cells/µL. 5 µL of cell solution was added to preformed RNP solution and gently mixed. Nucleofections were performed on a Lonza 96-well nucleofector shuttle system using program CM-150. Immediately following nucleofection each reaction was transferred to a tissue-culture treated 96-well plate containing 100µL normal culture media and seeded at a density of 50,000 cells per well. Transfected cells were incubated following standard protocols.

2.4.5 Genomic analysis

Two days post-nucleofection, DNA was extracted from using DNA QuickExtract (Lucigen Cat. #QE09050). Briefly, cells were lysed by removal of the spent media followed by addition of 50 µL of QuickExtract solution to each well. Once the QuickExtract DNA Extraction Solution was added, the cells were scraped off the plate into the buffer. Following transfer to compatible plates, DNA extract was then incubated at 68°C for 15 minutes followed by 95°C for 10 minutes in a thermocycler before being stored for downstream analysis.

Amplicons for indel analysis were generated by PCR amplification AmpliTaq Gold 360 polymerase (Thermo Fisher Scientific Cat. #4398881) according to the manufacturer's protocol.

Primers were designed to create amplicons between 400 – 800 bp, with both primers at least 100 bp distance from any of the sgRNA target sites. PCR products were cleaned-up and analyzed by Sanger sequencing (Genewiz). Sanger data files and sgRNA target sequences were input into Inference of CRISPR Edits (ICE) analysis (ice.synthego.com) to determine editing efficiency and to quantify generated indels (Hsiau et al. 2019). Percentage of alleles edited is expressed an ice-d score. This score is a measure of how discordant the Sanger trace is before versus after the edit. It is a simple and robust estimate of editing efficiency in a pool, especially suited to highly disruptive editing techniques like multi-guide.

2.4.6 Compounds

VPS34 IN-1 (#17392), PIK-III (#17002), Triacsin C (#10007448), Orlistat (#10005426), TOFA (#10005263), C75 (#10005270), Etomoxir (#11969), Trimetazidine (#18165), and A-922500 (#10012708) were purchased from Cayman Chemical (Ann Arbor, Michigan, USA). Remdesivir was purchased from Target Molecule Corp. (T7766, Boston, Massachusetts, USA). 2-bromopalmitate was purchased from Sigma-Aldrich (#21604, St. Louis, MO, USA). All compounds were resuspended in dimethylsulfoxide (DMSO).

2.4.7 Virus propagation and virus tittering

A lyophilized ampule of SARS-CoV-2 was initially resuspended in DMEM supplemented with 2% FBS. Vero E6 cells were inoculated in duplicate with a dilution of 1:100 with an adsorption period of 1 hour at 37°C and shaking every 15 minutes. Cells were observed for cytopathic effect (CPE) every 24 hours. Stock SARS-CoV-2 virus was harvested at 72 hours post infection (hpi) and supernatants were collected, clarified, aliquoted, and stored at -80°C.

Plaque assays were performed as previously described (Jureka, Silvas, and Basler 2020). Briefly, Vero E6 cells were seeded onto 24-well plates 24 hours before infection. 100 ul of

SARS-CoV-2 serial dilutions were added and adsorbed for 1 hour at 37°C with shaking at 15-minute intervals. After the absorption period, 1 mL of 0.6% microcrystalline cellulose overlay (MCC; Sigma-Aldrich 435244, St. Louis, MO, USA) was added and plates were returned to the incubator for the indicated amount of time. To stain plaque assays, MCC was removed by aspiration and 10% neutral buffered formalin (NBF) added for one hour at room temperature. Formalin was removed and monolayers were washed with water and stained with 0.4% crystal violet. Plaques were quantified and recorded as plaque forming units (PFU)/mL.

Focus forming assays were performed as previously described (Gordon, Hiatt, et al. 2020; Jureka, Silvas, and Basler 2020). Briefly, Vero E6 cells were pre-seeded in 96-well plates and grown to confluency. 50 μL of SARS-CoV-2 serial dilutions were added and adsorbed for 1 hour at 37°C. Post-adsorption, 50 μL of 2.4% microcrystalline cellulose overlay (MCC; Sigma-Aldrich 435244, St. Louis, MO, USA) was added and plates were returned to the incubator for 24 hours. Cell monolayers were inactivated with 10% NBF for one hour at room temperature, washed with deionized water and fixed/permeabilized with ice cold methanol containing 0.3% hydrogen peroxide for 10 minutes at -20°C followed by 20 minutes at room temperature. Prior to primary antibody addition, plates were washed with PBS and blocked for one hour at room temperature with 5% milk. Primary antibody detection with SARS N diluted in milk occurred overnight at 4°C. The next day, plates were washed with PBS and anti-rabbit-HRP diluted in milk was added for 1 hour at room temperature. After final washing, plates were developed using TrueBlue HRP substrate (ThermoFisher, Waltham, MA, USA). Focuses were quantified and graphed as focus forming units (FFU)/mL.

2.4.8 Maestro Z impedance experiments

Prior to cell plating, CytoView-Z 96-well electrode plates (Axion BioSystems, Atlanta, GA, USA) were coated with 5 μg/mL human fibronectin (Corning, Tewksbury, MA, USA) for 1 hr at 37°C. After coating, fibronectin was removed and 100 μL of DMEM containing 10% FBS was added to each well. The plate was then docked into the Maestro Z instrument to measure impedance electrode baseline. Vero E6 cells were then plated to confluency (~75,000 cells/well) in the coated CytoView-Z plates and left at room temperature for 1 hour to ensure even coverage of the well. Plates containing Vero E6 cells were docked into the Maestro Z for 24 hours at 37°C with 5% CO2 to allow the cells to attach and the monolayer to stabilize, as measured by resistance, a component of impedance. The Maestro Z was used to monitor the resistance of the monolayer as it formed, very similar to transepithelial electrical resistance (TEER) (Benson, Cramer, and Galla 2013). In this study, resistance was measured at 10 kHz, which reflects both cell coverage over the electrode and strength of the barrier formed by the cell monolayer. For compound treatments, media was removed from wells of the CytoView-Z plates and 195 μL of pre-warmed DMEM containing 2% FBS was added with the indicated concentration of compound. Infections with SARS-CoV-2 at an MOI of 0.01 were carried out by directly adding 5 μL of virus to each well. Plates were then docked within the Maestro Z and resistance measurements were continuously recorded for 48-72 hours post infection. All plates contained media only, full lysis, uninfected, and SARS-CoV-2 infected controls. For calculation of percent inhibition, raw resistance values for each well were normalized to the value at 1 hour post infection within the Axis Z software, and percent inhibition was calculated with the following formula: Percent Inhibition = 100*(1-(1- average of treated cells)/(1-average of infected control)). Median time to death calculations were performed by fitting the Boltzmann sigmoid

equation to raw kinetic resistance data in GraphPad Prism. Fifty percent maximum velocity (V50) values obtained from the Boltzmann sigmoid fits were used to determine median time to death for each MOI.

2.4.9 Cell viability assay

Vero E6 or Calu-3 cells were seeded in 96-well black walled microplates and incubated overnight. Media was replaced with fresh DMEM containing 2% FBS and CellTox Green Dye (Promega, Madison, WI, USA) as described in the manufacturer's protocol. Cells were then treated with compound in parallel with the corresponding experiment and put back in the incubator for the indicated duration. Fluorescence (Excitation: 485nm, Emission: 520nm) was measured at the designated end point. Percent viability was determined using the minimum fluorescence obtained from media only cells and the maximum value obtained by wells lysed with the included lysis solution.

2.4.10 Quantification of vRNA and mRNA

Calu-3 cells were seeded in 24-well plates and allowed to grow to confluency. Infection with SARS-CoV-2 was carried out at an MOI of 0.01 and 1.0. Media containing the indicated compound was added 2 hours post infection. Supernatants were collected at 24 hours post infection for titering, and RNA was extracted from cell monolayers using TRIzol reagent (ThermoFisher). Post extraction, RNA was DNase treated using ezDNase (ThermoFisher, Waltham, MA, USA) and subjected to first strand synthesis using SuperScript IV (ThermoFisher, Waltham, MA, USA) using the included random hexamer primers. qPCR was performed using PerfeCTa CYBR Green FastMix (VWR, Radnor, PA, USA) and primers for SARS-CoV-2 N (genomic and subgenomic), SARS-CoV-2 NSP14, and RPS11 as an internal control (Schneider et al. 2021). Each assay was performed in triplicate with three technical

replicates, and each assay contained no-template controls. Data were analyzed by the ΔΔCt method with RPS11 serving as the housekeeping gene and uninfected DMSO treated Calu3 cells as a mock control.

2.4.11 Confocal microscopy

For confocal microscopy analysis, cells were pre-seeded in 24-well plates on fibronectin coated glass coverslips and allowed to grow to confluency. Cells were infected with SARS-CoV-2 at an MOI of 1 and media containing compound treatments was added 2 hours post infection. At 24 hours post infection, the supernatant was removed and samples were fixed with 10% NBF for 1 hour at room temperature. Post-fixation, the cells were washed with PBS and permeabilized with sterile filtered 0.1% Saponin and 0.15% glycine in PBS. Cells were blocked with 0.1% Saponin in 1x Fluorescent Blocker (ThermoFisher, Waltham, MA, USA) for 1 hour at room temperature. Primary antibodies were diluted in blocking buffer, added to the wells and incubated overnight at 4°C. The following day, coverslips were washed with PBS and incubated with secondary antibodies diluted in 0.1% saponin in PBS for 1 hour. AlexaFluor 488 and 647 conjugated secondary antibodies (ThermoFisher, Waltham, MA, USA) were used. Cover slips were mounted using ProLong Glass Antifade mountant with NucBlue stain (ThermoFisher, Waltham, MA, USA). Samples were imaged on a Zeiss LSM800 Confocal and images were rendered in ZenBlue (Zeiss, White Plains, NY, USA).

2.4.12 Supplementation

Supplementation with fatty acids and lipids was achieved by pre-complexing the supplements to fatty acid free bovine serum albumin (FAF-BSA). Briefly, FAF-BSA was dissolved in tissue culture grade water to achieve a final concentration of 10%. Stock solutions of palmitic acid (150 mM in ethanol, Sigma-Aldrich St. Louis, MO, USA) and oleic acid (3 M,

Sigma-Aldrich St. Louis, MO, USA) were diluted to 2.5 mM in 10% FAF-BSA and incubated at 37°C with frequent mixing for 30 minutes. The pre-complexed solutions were then added to DMEM at a final concentration of 2% FAF-BSA and 0.25 mM supplement. For the infection, NT-WT and FASN KO Caco2 cells were pre-seeded in 96 well plates and allowed to grow to confluency. Infection with SARS-CoV-2 was performed at an MOI of 0.01 in the serum-free media. One hour post adsorption, virus inoculum was removed and medium containing the designated serum/lipid treatment was added. Cells were incubated at 37°C with 5% CO2 until the designated end point. Supernatants were collected and quantified by plaque assay.

2.4.13 GFP-2xFYVE assay

Huh7 cells were seeded in 96-well black walled plates and transfected with a pEGFP-2xFYVE plasmid obtained from Addgene (#140047) using Lipofectamine 2000 (Invitrogen St. Louis, MO, USA). 24 hours post transfection (hpt) media was removed and replaced with media containing either DMSO, VPS34-IN1 (2 μM), PIK-III (5 μM), SAR405 (5 μM), Compound 19 (5 μM), or Orlistat (200 μM). 24 hours post treatment cells were imaged using a BioTek Cytation 5 to determine the localization pattern of eGFP-2xFYVE.

2.5 Results

2.5.1 Development of a 96-well format impedance-based assay to measure SARS-CoV-2 cytopathic affect

SARS-CoV-2 induces significant cytopathic effects in infected Vero E6 cells. Based on this property, we standardized a 96-well format assay that provides continuous real-time, label free monitoring of the integrity of cell monolayers as a direct correlation of virus growth and infection. This assay was standardized using the Maestro Z platform (Axion BioSystems, Atlanta, GA), an instrument that uses plates containing electrodes in each well (CytoView-Z

plates) to measure electrical impedance across the cell monolayer every minute throughout the course of the experiment. As SARS-CoV-2 induced cytopathic effects damage the cell monolayer, impedance measurements decrease over time providing a detailed assessment of infection kinetics. To determine the capacity of the system to differentiate levels of virus replication, confluent Vero E6 monolayers in CytoView-Z plates were infected with SARS-CoV-2 at multiple MOIs (0.0001 to 10) and resistance measurements were acquired for 72 hours post infection (Figure 10A). The progression of infection at each MOI was clearly distinct. A decrease in resistance could be observed as early as 18-20 hours post-infection (hpi) at an MOI of 1 and 10, and as late as 56 hpi at an MOI of 0.0001. All sample signals reached their lowest point between 32 to 72 hpi in an MOI dependent manner. The raw kinetic data was used to determine the median time to cell death for each MOI which shows a direct correlation with a decrease in resistance (Figure 10B). MOI of 0.01 was chosen for antiviral assays based on its desirable infection kinetics.

To establish the Maestro Z as a potential instrument for screening of anti-SARS-CoV-2 therapeutics, we first tested Remdesivir, a well-described inhibitor of SARS-CoV-2 that has been granted emergency use authorization (EUA) for the treatment of COVID-19 (Gordon, Tchesnokov, et al. 2020; Wu, Wu, and Lai 2020). Vero E6 cells were seeded on a CytoView-Z plate, incubated overnight to allow cells to stabilize, pretreated with 6-fold dilutions of Remdesivir for 1 hour and infected with SARS-CoV-2. Resistance measurements were recorded for 48 hpi (Figure 10C). In agreement with previous studies, we determined a 50% inhibitory concentration (IC50) for Remdesivir of 1.54 μM (Figure 10D) (Gordon, Tchesnokov, et al. 2020). Taken together, these data validate the impedance-based assay described as a tool for screening of potential SARS-CoV-2 therapeutics.

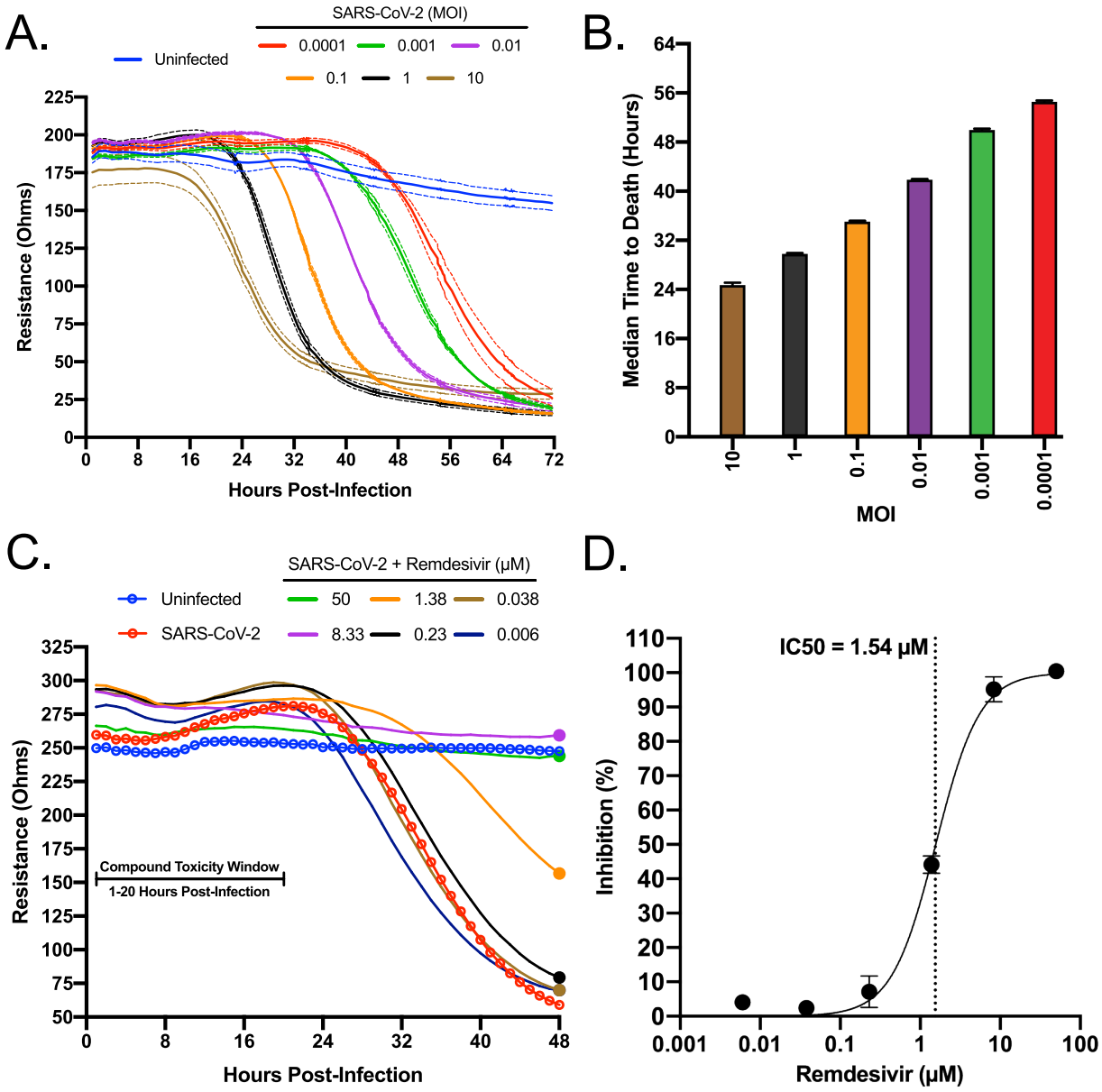

Figure 10 Standardization of an electrical resistance-based assay as a measure of SARS CoV-2 induced CPE and anti-SARS-CoV-2 activity

Vero E6 cells were seeded into a CytoView-Z 96-well plate and allowed to stabilize overnight, as measured by electrical resistance. A) Resistance was measured every minute over the course of 72 hours in wells that were mock infected or infected with SARS-CoV-2 in 10-fold dilutions ranging from an MOI of 10-0.0001. Solid lines indicate the mean, dotted lines indicate the standard error of three replicates. B) Median time-to-death calculations based on raw resistance data for each MOI. C) Remdesivir was titrated in 6-fold dilutions ranging from 50-0.006 μM. After infection at an MOI of 0.01, resistance was monitored for 48 hpi and D) percent inhibition for Remdesivir based on the data from the 48-hour time point is presented (solid circles).

2.5.2 Inhibitors of VPS34 activity impair SARS-CoV-2 growth

VPS34 is a multifunctional protein involved in autophagy and membrane trafficking (Jaber and Zong 2013; Ohashi et al. 2020). On account of the significant role of membrane rearrangements in coronavirus replication, we wanted to determine if VPS34 activity was essential for SARS-CoV-2 growth. We tested two well characterized VPS34 inhibitors, VPS34-IN1 and PIK-III (Bago et al. 2014; Dowdle et al. 2014). This was done over a 10-point dose response using the resistance assay described above. Briefly, pre-plated Vero E6 cells were treated with compound 1 hour prior to infection with SARS-CoV-2. Both VPS34-IN1 and PIK-III induced rapid cytotoxicity at 50 μM and 16.67 μM as indicated by a rapid decrease in resistance measurements between 1 and 20 hpi. (Figure 11A, C). At the remaining concentrations, no toxicity was observed. For several concentrations, the integrity of the monolayer was preserved relative to the mock-treated infected control indicating an antiviral effect of both VPS34-IN1 and PIK-III. Based on normalized resistance measurements at 48 hpi for non-toxic doses, we estimated IC50 values of <600 nM for VPS34-IN1 and PIK-III (Figure 11B, D, respectively). These data suggest that the VPS34 kinase plays a significant role in SARS-CoV-2 replication.

2.5.3 Inhibition of fatty acid metabolism impairs SARS-CoV-2 growth

Fatty acid metabolism contributes to various host processes including production of lipid-based molecules such as triglycerides, phospholipids, and cholesterol, as well as protein modifications, such as palmitoylation and myristoylation (Baenke et al. 2013; Chen et al. 2018; Wakil and Abu-Elheiga 2009). Modulation of fatty acid metabolism has been shown to impact replication and virion maturation for numerous flaviviruses,

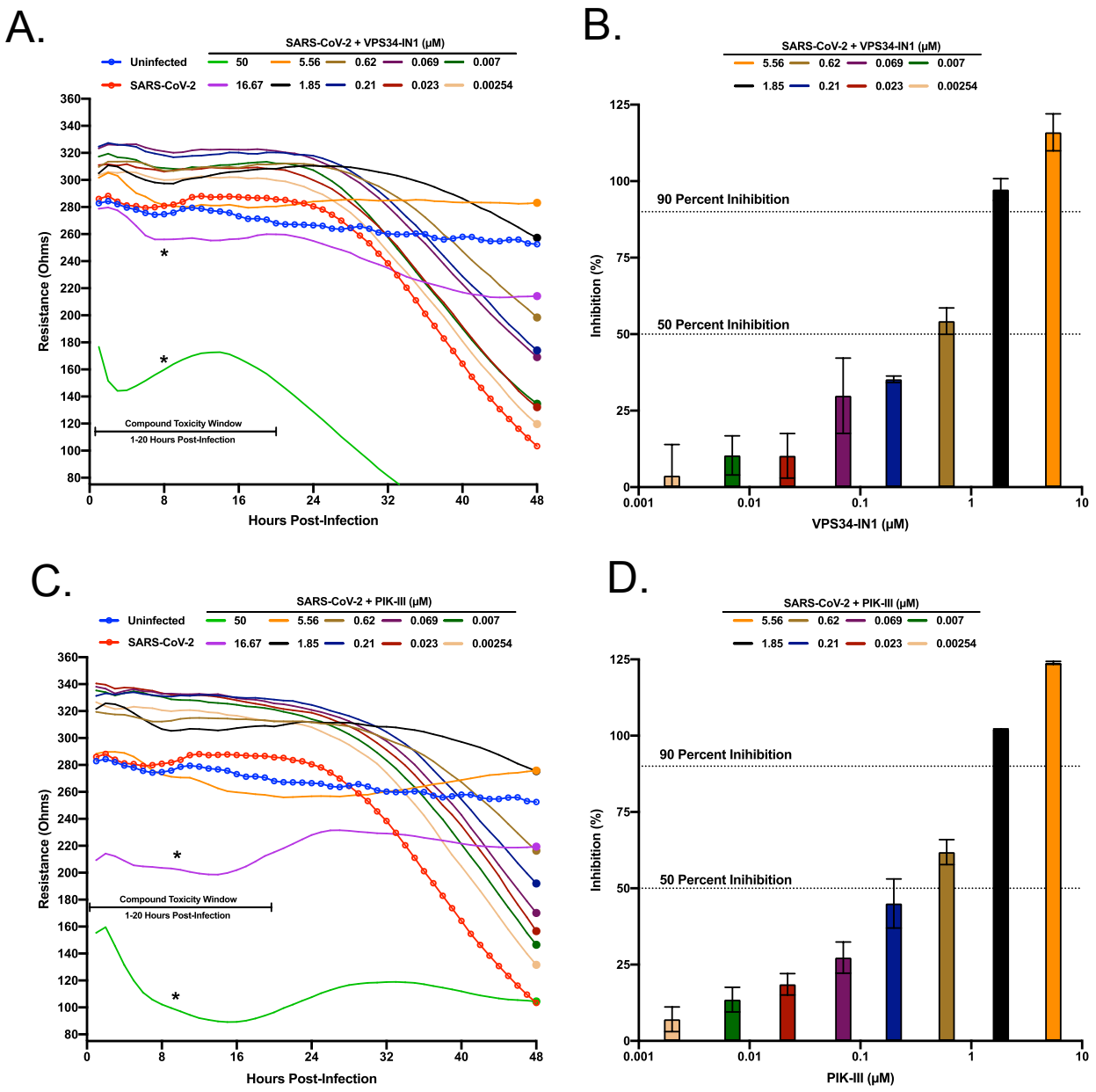

Figure 11 VPS34 inhibitors exhibit anti-SARS-CoV-2 activity

Vero E6 cells were seeded into a CytoView-Z 96-well plate and allowed to stabilize overnight. Cells were pre-treated with serial half-log dilutions of VPS34-IN1 (A-B) or PIK-III (C-D) and infected with SARS-CoV-2 at an MOI of 0.01. Resistance (A and C) was measured every minute over the course of 48 hours and percent inhibition (B and D) was determined at the 48-hour timepoint (solid circles) as compared to the infected DMSO treated control (red). Uninfected cells are indicated in blue.

enteroviruses, and alphaviruses (Ammer et al. 2015; Bakhache et al. 2019; Cheung et al. 2010; Gaunt et al. 2013; Hitakarun et al. 2020; Liefhebber et al. 2014; Merino-Ramos et al. 2016;

Nasheri et al. 2013; Tongluan et al. 2017). Two well-described compounds that inhibit fatty acid metabolism are Orlistat, an FDA-approved drug that inhibits gastric lipases and fatty acid synthase (FASN), and Triacsin C, an inhibitor of long chain Acyl-CoA synthetase (ACS), both of which have been shown to have antiviral activity (Ammer et al. 2015; Hitakarun et al. 2020; Kim et al. 2012; Nasheri et al. 2013).To test the efficacy of these compounds against SARS-CoV-2 infection, Vero E6 cells were pre-seeded onto a CytoView-Z plate, allowed to stabilize, and then pre-treated with Orlistat or Triacsin C for 1 hour prior to infection. Based on the toxicity window of 1-20 hours post-treatment (hpt) determined with the VPS34 inhibitors, neither Orlistat nor Triacsin C induced early cytotoxic effects, even at the highest concentrations of 50 μM and 500 μM, respectively (Figure 12A, C). Both compounds exhibited inhibition of viral cytopathic effects at higher concentrations, although complete inhibition was not achieved even with 500 μM of Orlistat. Based on normalized resistance measurements at 48 hpi, we estimated IC50s of ~500 μM for Orlistat and ~20 μM for Triacsin C (Figure 12B, D). This data suggests that fatty acid metabolism and neutral lipid synthesis likely play an important role in SARS-CoV-2 infection.

2.5.4 VPS34 and fatty acid metabolism inhibitors exhibit activity on post-entry steps of the viral life cycle

Next, we performed time of addition studies with VPS34-IN1, PIK-III, Orlistat, or Triacsin C. This allowed us to identify if the anti-viral activity of each compound impacted the viral life cycle at steps pre- or post- entry. As indicated in Figure 13A, three conditions were tested: 1) single treatment 1 hour prior to viral infection, with compound removed prior to infection; 2) dosing at 2 hpi; and 3) dosing at 4 hpi. We observed that a single 5 μM treatment of VPS34-IN1 or PIK-III prior to infection inhibited SARS-CoV-2 replication, and inhibition could

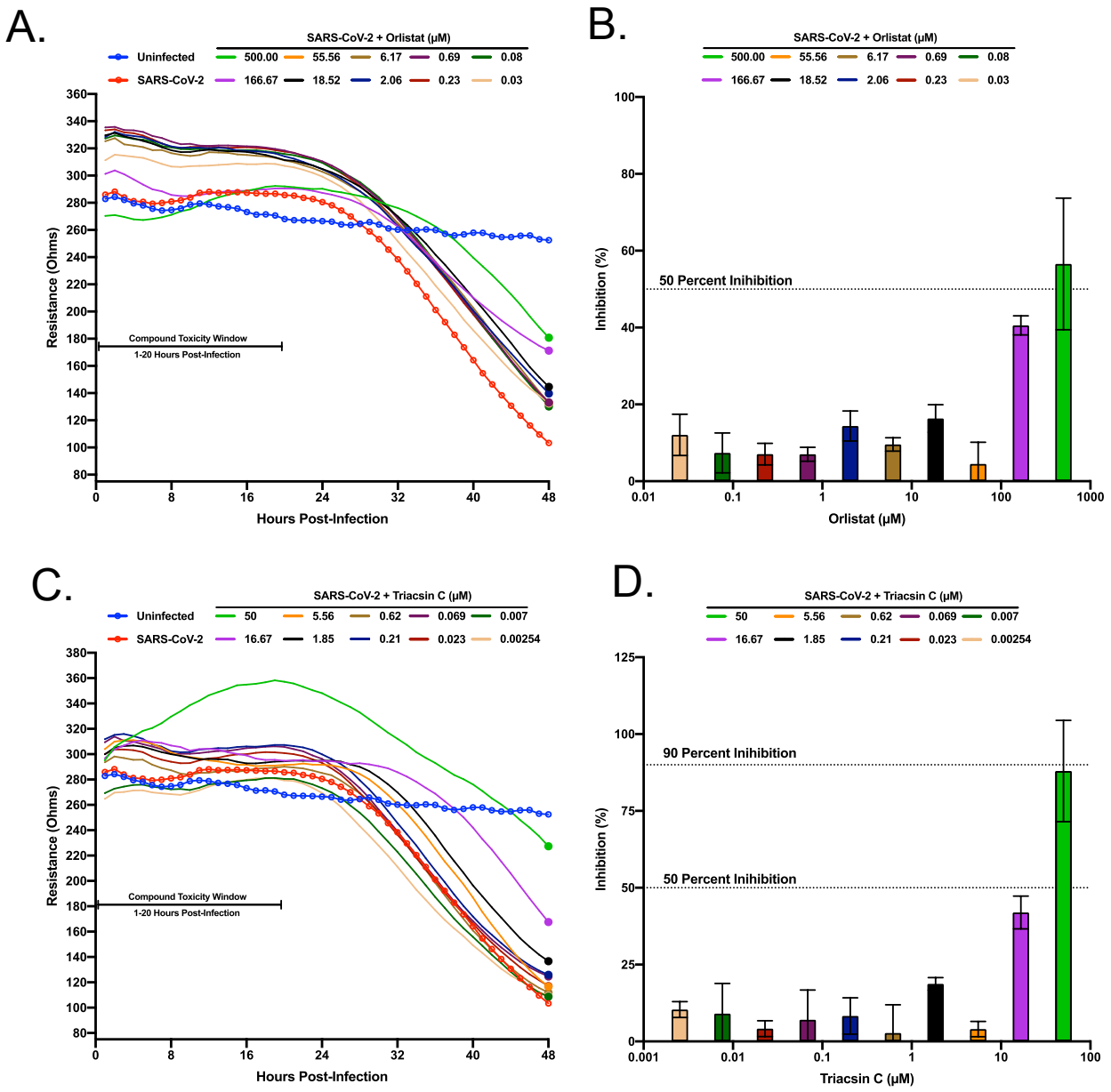

Figure 12 Screening of fatty acid inhibitors for potential anti-SARS-CoV-2 activity

Vero E6 cells were seeded into a CytoView-Z 96-well plate and allowed to stabilize overnight. Cells were pre-treated with serial half-log dilutions of Orlistat (A-B) or Triacsin C (C-D) and infected with SARS CoV-2 at an MOI of 0.01. Resistance (A and C) was measured every minute over the course of 48 hours and percent inhibition (B and D) was determined at the 48-hour timepoint (solid circles) as compared to the infected DMSO treated control (red). Uninfected cells are indicated in blue.

be observed even when added up to 4 hpi (Figure 13B). In contrast, Orlistat or Triacsin C showed minimal efficacy when removed prior to infection but remained inhibitory when added up to 4 hpi. Altogether, these data demonstrate that the VPS34 inhibitors likely act on viral entry and at later steps in the replication cycle; and inhibition by Orlistat and Triacsin C occurs post-entry.

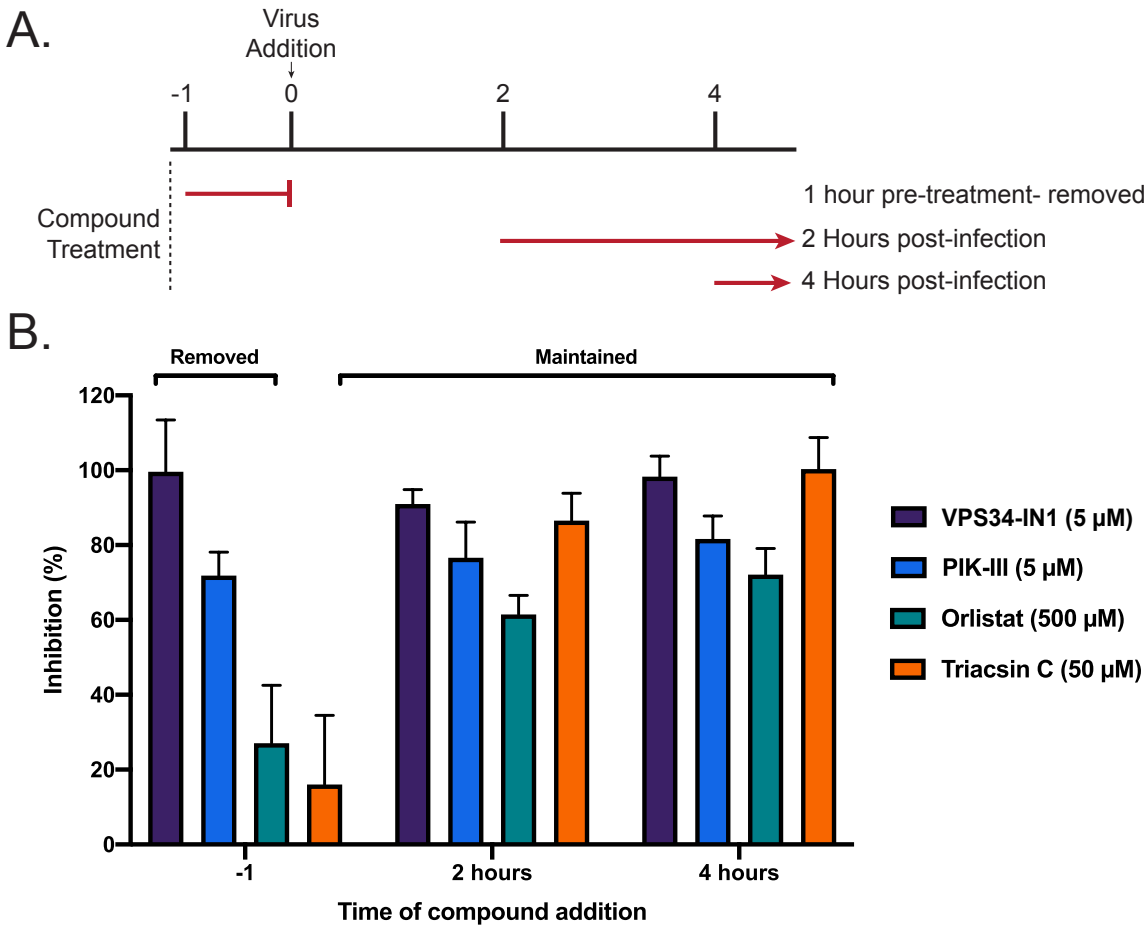

Figure 13 Time of addition studies

VeroE6 cells were seeded into a CytoView-Z 96-well plate and allowed to stabilize overnight. A) Timeline for the time-of-addition experiment. B) VeroE6 cells were either pre-treated for one hour with compound removed prior to infection (-1) or treated at 2 (+2) or 4 (+4) hours post-infection. All conditions were infected with an MOI of 0.01. Resistance was measured every minute over the course of 48 hours and percent inhibition was determined at the 48-hour timepoint. Data is representative of the mean and standard error of three replicates.

2.5.5 Attenuation of VPS34 kinase activity and fatty acid metabolism inhibit SARS-CoV-2 in a human airway epithelial cell line

To determine whether or not the previously observed inhibition could be maintained in a cell line more functionally relevant to human infection by SARS-CoV-2, we directly measured the impact of compounds on production of infectious virus and cell viability in Calu-3 cells. These cells are derived from human airway epithelium and are highly susceptible to infection, establishing them as a standard for infection studies with SARS-CoV-1, MERS-CoV and SARS-CoV-2 (Sims et al. 2005; Sims et al. 2008). For these studies, Calu-3 cells were plated onto 96-well plates and allowed to reach confluency. Cells were either pre-treated with a range of concentrations of VPS34-IN1, PIK-III, Triacsin C and Orlistat, DMSO, or mock treated with media alone for 1 hour, then infected with SARS-CoV-2 at an MOI of 0.01. Supernatants were collected at 48 hpi and viral titer determined by plaque assay. Cytotoxicity of the compounds was determined in parallel. Consistent with results from infected Vero E6 cells, each of the compounds tested above inhibited production of infectious virus (Figure 14) and cytotoxicity was only observed in Calu-3 cells at the highest concentrations of some compounds. We observed IC50s of 0.55 μM (VPS34-IN1; A), 0.12 μM (PIK-III; B), 21.25 μM (Orlistat; C), and 0.04 μM (Triacsin C; D). Notably, the IC50s measured for VPS34-IN1 and PIK-III by plaque assay are in close agreement with estimated IC50s determined in Vero E6 cells using the resistance-based assay. The IC50s for Orlistat and Triacsin C were substantially lower than those estimated in VeroE6 cells.

To determine the specificity of inhibition to the class III PI3 kinase VPS34, we extended our Calu-3 compound study to include two additional VPS34 inhibitors: SAR405 and compound 19 (Honda et al. 2016; Pasquier 2015; Ronan et al. 2014). SAR405 and compound 19 each

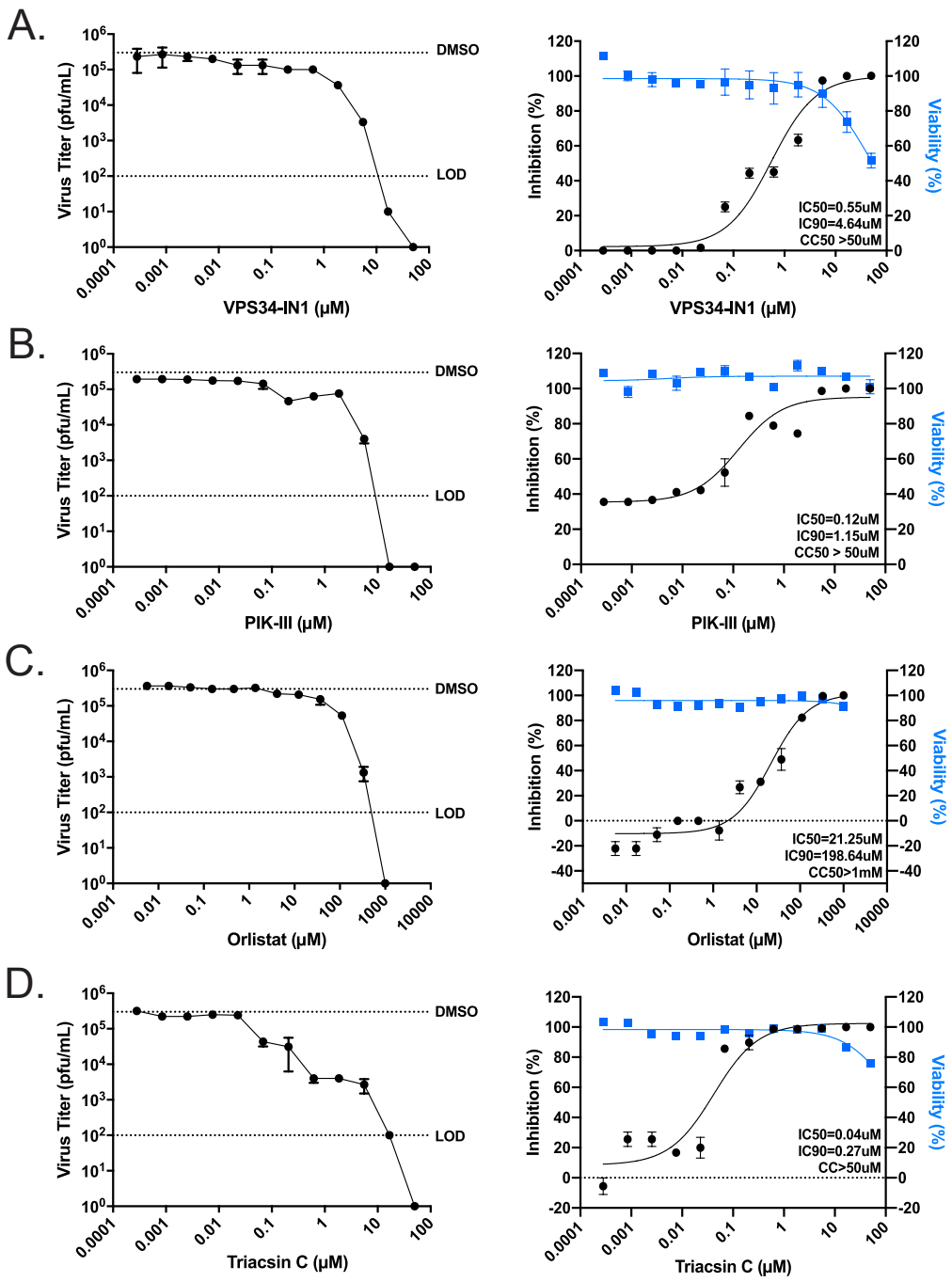

Figure 14 Attenuation of VPS34 kinase activity and fatty acid metabolism inhibit SARS-CoV-2 replication in human airway epithelial cell line

Calu-3 cells were plated onto a 96-well plate and allowed to reach confluency. Cells were then pre-treated with a series of 3-fold dilutions of VPS34-IN1 (A), PIK-III (B), Orlistat (C), Triacsin C (D), DMSO, or mock-treated with media alone for 1 hour, then infected with SARS-CoV-2 at an MOI of 0.01. Supernatants were collected at 48 hpi and virus was quantified by plaque assay on VeroE6 cells. The data is reported as plaque forming units per milliliter (pfu/ml) (left panels) and percent inhibition (right panels). Cell viability over 48 hours was determined in parallel and plotted with the percent inhibition data. IC50 and IC90 were calculated from the plaque assay data and are indicated on the curves. For the plaque assay data, the dotted lines labeled DMSO and LOD indicate the level of virus growth in the DMSO control and the limit of detection, respectively.

inhibited with IC50s of 0.376 μM and 5.843 μM, respectively (Figure 15A-B). This data further supports the importance of the class III PI3 kinase during SARS-CoV-2 replication. To confirm that the compounds were able to inhibit VPS34 activity, we assessed in Huh7 cells the effect of the inhibitors on GFP-2xFYVE localization to endosomes, indicating a loss of phosphoinositol-3 phosphorylation by VPS34 (Gillooly et al. 2000; Gillooly, Simonsen, and Stenmark 2001; Kutateladze 2007; Ronan et al. 2014). Huh7 cells were chosen for their favorable characteristics, such as transfectability and large cytoplasm that facilitates imaging. While DMSO or Orlistat did not affect GFP-2xFYVE localization, the four VPS34 inhibitors disrupted GFP-2xFYVE puncta, consistent with loss of PI-3 phosphorylation (Figure 15C).

2.5.6 Protein palmitoylation and triacylglycerol production are implicated in SARS-CoV-2 infection

Several recent reports have identified that pathways related to lipid metabolism and cholesterol homeostasis are required for SARS-CoV-2 replication; however, the precise mechanism by which these pathways contribute to the SARS-CoV-2 replication cycle remains unclear (Abu-Farha et al. 2020; Daniloski et al. 2021; Schneider et al. 2021; Zang et al. 2020). Given that our data suggests a role for fatty acid metabolism, we set out to further clarify the enzymatic steps required for SARS-CoV-2 replication.

To further evaluate the importance of de novo fatty acid synthesis, TOFA, a competitive inhibitor of acetyl-CoA carboxylase (ACC), the enzyme directly upstream of FASN, and C75, an additional inhibitor of FASN, were used (Halvorson and McCune 1984; Kuhajda et al. 2000). Both compounds exhibited activity against SARS-CoV-2 infection with IC50s of 1.339 μM and 22.81 μM respectively (Figure 16A, B-C).

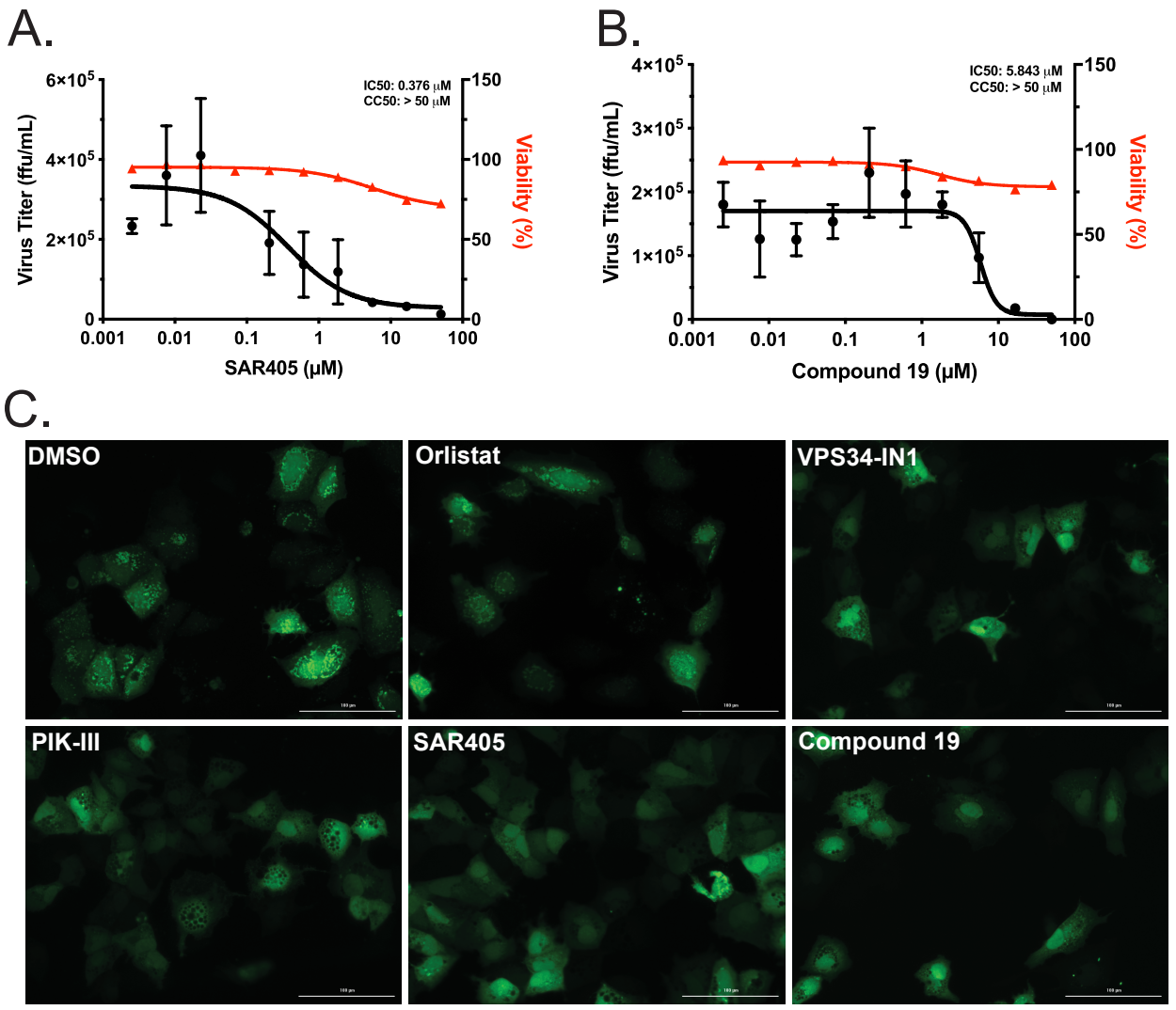

Figure 15 VPS34 inhibitors actively block VPS34 activity

The inhibitory abilities of two additional compounds against VPS34 was tested. Calu-3 cells were seeded in 96-well format and grown to confluency. Cells were pre-treated with a series of 3-fold dilutions of the indicated compounds or DMSO for 1 hour, then infected with SARS-CoV-2 at an MOI of 0.01. Supernatants were collected at 48 hpi and infectious virus was quantified by focus forming assay on VeroE6 cells and presented as focus forming units (ffu)/mL. Cytotoxicity assays were performed in parallel and used to calculate percent viability as show in red (A). To determine whether VPS34 inhibitors actively block VPS34 kinase activity, Huh7 cells were seeded in black walled 96-well plates and transfected with a 2X-FYVE-GFP plasmid. 24 hpt cells were treated with DMSO, VPS34-IN1 (2 μM), PIK-III (5 μM), SAR405 (5 μM), Compound 19 (5 μM), or Orlistat (200 μM). Cells were imaged to determine 2X-FYVE-GFP localization (B) using a BioTek Cytation 5.

Inhibition of fatty acid synthesis at early enzymatic steps like FASN can lead to dysregulation of three main downstream pathways: fatty acid based protein modification, fatty acid β-oxidation in the mitochondria, and neutral lipid synthesis (Baenke et al. 2013). To further determine which branches and enzymatic steps of fatty acid metabolism contribute to anti-SARS-CoV-2 activity, a series of additional compounds were tested for inhibitory activity and cytotoxicity (Figure 16).

To assess the contribution of decreased protein palmitoylation, 2-bromoplamitate, an inhibitor of palmitoyl acyltransferases (PAT), was used (Davda et al. 2013). 2-bromopalmitate inhibited infectious virus production at concentrations greater than 10 μM with an IC50 of 23.02 μM (Figure 16A, D). To determine if fatty acid β-oxidation in the mitochondria contributes to inhibition of SARS-CoV-2, two compounds were tested: Etomoxir, a compound that targets carnitine palmitoyltransferase 1A (CPT1A), blocking translocation of fatty acids into the mitochondria, and Trimetazidine, an inhibitor of long-chain 3-ketoacyl-CoA thiolase (Ma et al. 2020). Neither compound showed any inhibition, indicating that fatty acid β-oxidation is not required for SARS-CoV-2 replication (Figure 16A, F-G). Lastly, the importance of the terminal steps of the fatty acid metabolism pathways was assessed by inhibiting neutral lipid production and lipid droplet formation using A922500, a potent inhibitor of diacylglycerol acyltransferase 1 (DGAT1) (Zhao et al. 2008). Treatment with A922500 potently inhibited SARS-CoV-2 with an IC50 value of 4.017 μM (Figure 16A, E). All together, these data suggest that protein palmitoylation and neutral lipid synthesis are needed for efficient SARS-CoV-2 replication.

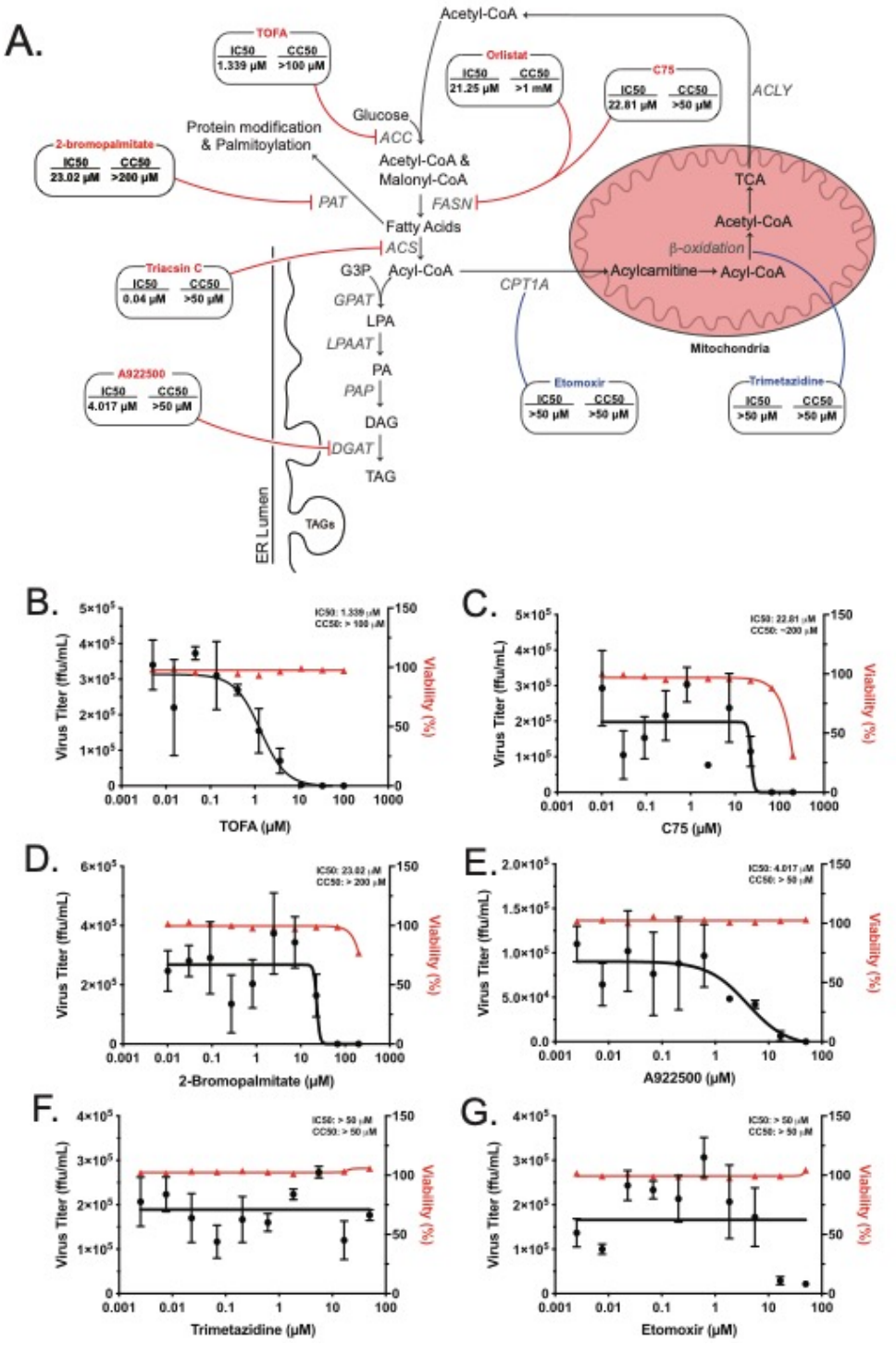

Figure 16 Fatty acid metabolism involvement in SARS-CoV-2 replication

To determine which steps involved in fatty acid metabolism contribute to the observed anti-SARS-CoV-2 activity, Calu-3 cells were pre-treated with DMSO or a series of 3-fold dilutions of the indicated compounds, or mock-treated with media alone for 1 hour, then infected with SARS-CoV-2 at an MOI of 0.01. Supernatants were collected at 48 hpi and infectious virus was quantified by focus forming assay on VeroE6 cells and presented as focus forming units ffu/mL (black). Cytotoxicity assays were performed in parallel and used to calculate percent viability (red) (B-G). IC50 and CC50 values were calculated for each (A).

2.5.7 Inhibition of VPS34 kinase activity and fatty acid metabolism alters SARS-CoV-2 replication centers

As time-of-addition studies implicated post-entry steps as targets of the compounds, we sought to assess the status of sites of viral RNA synthesis, which can be detected with anti-dsRNA antibodies (Knoops et al. 2008; Reggiori et al. 2010; Weber et al. 2006). Foci of dsRNA staining in coronavirus infected cells reflect the formation of membrane-associated viral replication compartments (Knoops et al. 2008; Oudshoorn et al. 2017; Prentice et al. 2004; Reggiori et al. 2010). Calu-3 cells were seeded onto fibronectin coated glass cover slips and allowed to reach partial confluency. Cells were infected with SARS-CoV-2 at a MOI of 1, treated at 2 hpi with concentrations of VPS34-IN1, PIK-III, Orlistat, Triacsin C, TOFA, 2-bromopalmitate, A922500, or Remdesivir determined to

result in significant inhibition without cytoxicity, or with DMSO. At 24 hpi cells were fixed, permeabilized, and stained for indirect immunofluorescence using primary antibodies against SARS-CoV-2 N and dsRNA.

DMSO-treated control cells displayed distinct puncta positive for dsRNA consistent with CoV replication centers (Knoops et al. 2008; Reggiori et al. 2010). These structures were also positive for the SARS-CoV-2 nucleocapsid protein (N). Treatments with VPS34-IN1, Orlistat, TOFA, or A922500 resulted in a loss of these distinct puncta and dispersion of dsRNA and SARS-CoV-2 N. When treated with Triacsin C and 2-bromopalmitate, cells exhibited fewer but larger foci positive for both markers. Treatment with a non-sterilizing concentration of Remdesivir (1 μM) served as a control and yielded a distribution of N and dsRNA similar to the DMSO control (Figure 17). Taken together, these data suggest inhibition VPS34 activity and fatty acid metabolism may affect SARS-CoV-2 replication by affecting viral replication centers.

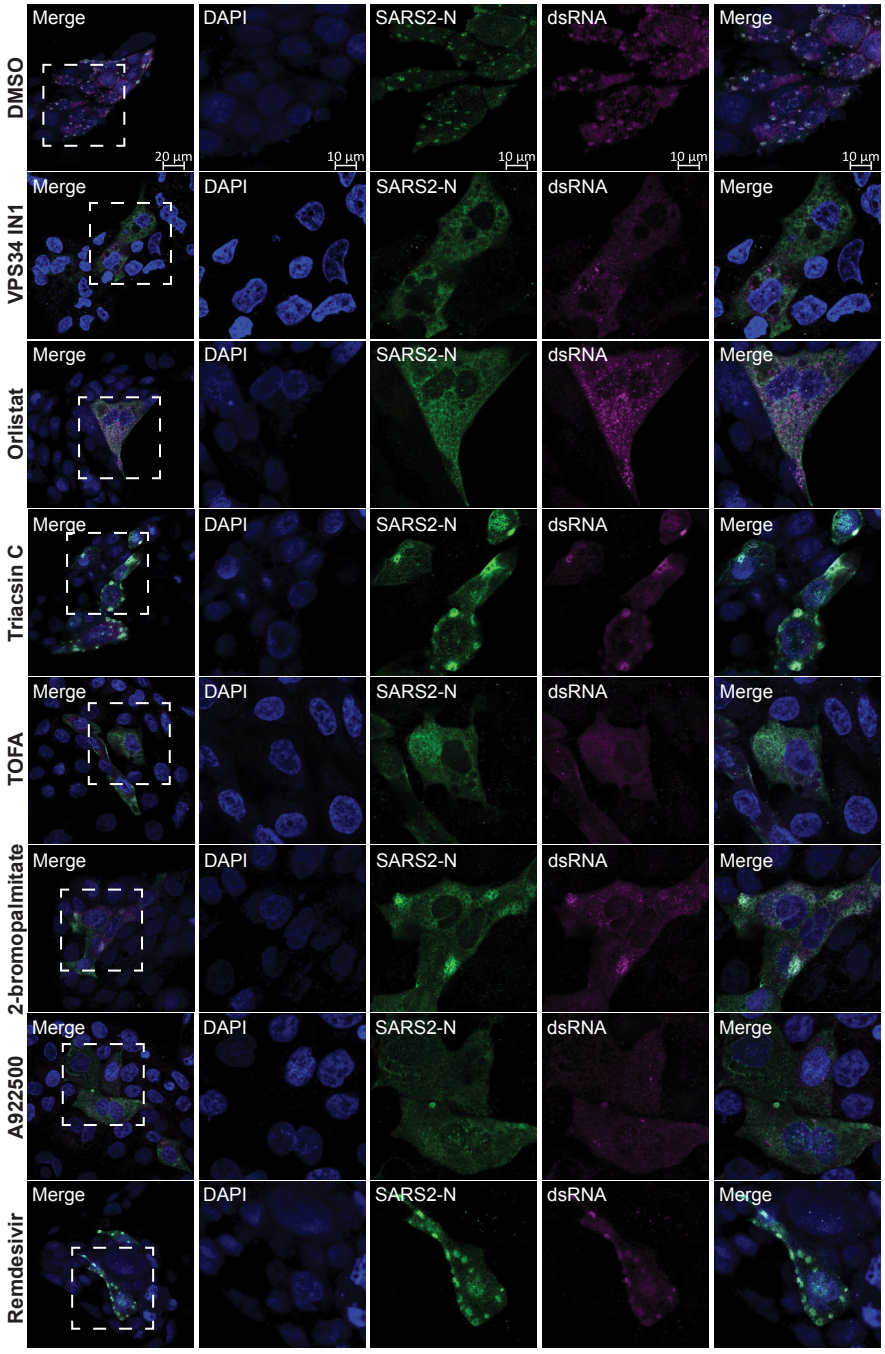

Figure 17 Inhibition of VPS34 kinase activity and fatty acid metabolism affect formation of SARS-CoV-2 replication centers

Calu-3 cells were pre-seeded in 24-well format on fibronectin coated glass coverslips, allowed to grow to partial confluency, and infected at an MOI of 1. Inoculum was removed 2 hpi and replaced with media containing VPS34-IN1 (5 µM), Orlistat (500 µM), Triacsin C (5 µM), TOFA (50 µM), 2-bromopalmitate (50 µM), A922500 (30 µM), Remdesivir (1 µM), or DMSO. 24 hours post infection, cells were fixed and indirect immunofluorescence was performed using primary antibodies against SARS-CoV-2 N and dsRNA, and AlexaFluor488 and AlexaFluor647 conjugated secondaries, respectively. Cover slips were mounted using ProLong Glass Antifade mountant with NucBlue stain (ThermoFisher). Samples were imaged on Zeiss LSM800 Confocal and images were rendered in ZenBlue. Representative images are shown.

2.5.8 Inhibition of VPS34 and fatty acid metabolism impacts genomic and subgenomic RNA levels

The effects on dsRNA and N distribution suggested possible effects on viral RNA synthesis. To determine if the production of viral RNA was affected, Calu-3 cells were infected at an MOI of either 0.01 or 1. Two hours post-infection, cells were treated with DMSO or concentrations of each inhibitor determined to result in significant inhibition at an MOI of 0.01 without toxicity. At 4, 10, and 24 hpi, levels of genomic and subgenomic N and NSP14 RNA were quantified by RT-PCR. Supernatants corresponding to 24 hpi were used to quantify viral titers to ensure inhibition was achieved. Remdesivir was used as a positive control compound that inhibits SARS-CoV-2 RNA synthesis.

Compound treatments resulted in a 1- to 4-log10 reduction of viral titers at both MOIs at 24 hpi (Figure 18A, E). Consistent with the decrease in viral titers, all compounds reduced the amounts of genomic RNA at the 24 h time point. Remdesivir inhibited RNA synthesis at earlier time points as well. At 4 and 10 hpi at MOI of 1, the inhibition was more apparent with the N genomic RNA and NSP14 primers as compared with the N sub-genomic RNA primers. The degree of inhibition was magnified at an MOI of 0.01 (Figure 18B-D, F-H). Similarly, treatment with VPS34-IN1, Orlistat, Triacsin C, and 2-bromopalmitate reduced RNA levels at both MOI 0.01 and 1. In general, there were minimal differences in fold-inhibition at 4 versus 10 hpi. (Figure 18B-D, F-H). The inhibition of RNA synthesis resulting from treatment with TOFA and A922500 followed a similar pattern to the other compounds at each MOI and time point. However, the reduction in RNA synthesis at 24 hpi was significantly less substantial than the reduction in viral titers. (Figure 18B-D, F-H). This discordance suggests that these compounds have additional effects beyond viral RNA synthesis that explain their inhibition of virus growth.

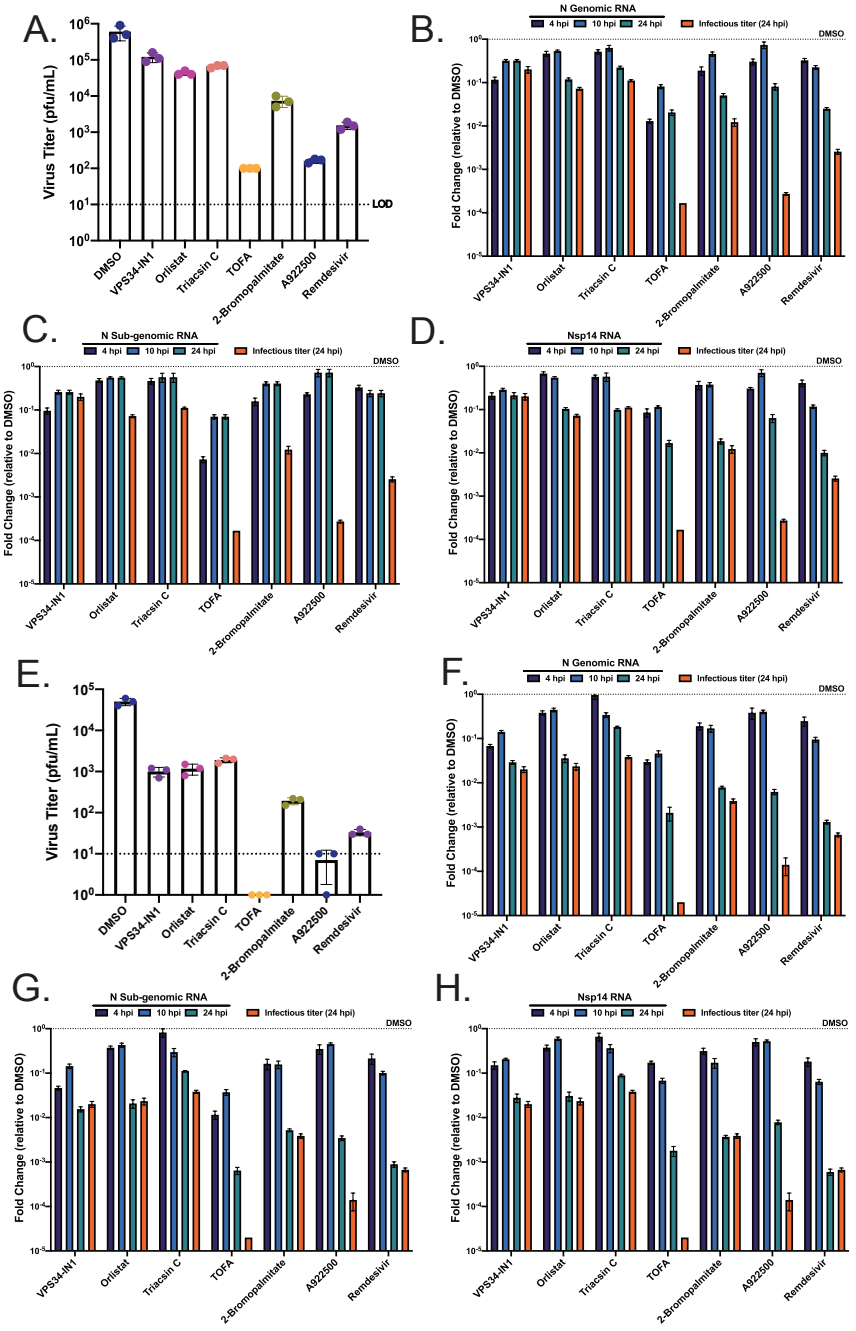

Figure 18 Mechanistic characterization of anti-SARS-CoV-2 activity on RNA synthesis

To discern whether or not genomic and subgenomic RNA levels are affected by compound treatment, Calu-3 cells were pre-seeded in 24-well format, allowed to grow to confluency, and infected at an MOI of 1 (A-D) or 0.01 (E-H). 2 hours post-infection cells were treated with VPS34-IN1 (5 μM), Orlistat (500 μM), Triacsin C (5 μM), TOFA (50 μM), 2-bromopalmitate (50 μM), A922500 (30 μM), Remdesivir (1 μM), or DMSO. At 4, 10, and 24 hpi total RNA was extracted from the cell monolayers, and 24 hpi supernatants were harvested for viral titers. Virus titers were determined by plaque assay (A, E). Levels of genomic RNA, subgenomic N RNA, and NSP14 RNA were quantified via qPCR (see materials and methods). Data are represented as fold change of RNA levels in infected compound treated samples versus infected DMSO treated samples (B-D, F-H). The virus titer at 24 hpi for compound treated cells (orange bars) are plotted alongside the qPCR data and represented as fold-change compared to titers from DMSO treated cells.

2.5.9 Genetic knockout confirms a critical role of de novo fatty acid synthesis for SARS-CoV-2 replication

As a genetic correlate to the studies described above, we compared the growth of SARS-CoV-2 in non-targeting control (NT) and FASN knockout Caco2 (FASN KO) cells in the presence of 2% FBS or 1% fatty acid free (FAF)-BSA. The latter condition addressed the possible contribution of exogenous fatty acids supplied by the FBS. Consistent with the previous compound data, SARS-CoV-2 replicated to substantially lower titers in the FASN KO cells as compared to WT cells when the cells were maintained in medium with 2% fetal bovine serum (FBS) (Figure 19A). The inhibition was enhanced when cells were maintained in 1% FAF-BSA media, reaching an almost 2-log10 reduction in titer as early as 48 hpi (Figure 19B). For each experiment, FASN knockout was confirmed by western blot. In addition, SARS-CoV-2 N protein levels were decreased in FASN KO cells as compared to NT cells. At later timepoints, N protein levels in FASN KO cells decline consistent with the changes in virus titer. The diminished replication and protein production in cells lacking FASN confirms our earlier findings and suggests that fatty acid metabolism is necessary for efficient, sustained replication during SARS-CoV-2 infection.

Based on our observations that the reduction in protein palmitoylation and neutral lipid synthesis are likely responsible for the inhibition seen when blocking fatty acid metabolism, we asked whether viral replication in FASN knockout cells would be restored by supplementing with substrates that feed into these two sub-pathways. Supplementation was achieved by infecting FASN KO Caco2 cells in minimal media and adding back media containing 2% FAF-BSA pre-complexed to a combination of 250 μM palmitic acid and 250 μM oleic acid. Cell supernatants were collected at 1, 24, 48, and 72 hpi and viral titers were determined by plaque

assay. Consistent with our previous data, growth in FASN KO cells was significantly reduced as compared to NT control cells. Supplementation with palmitate and oleic acid partially rescued virus growth further confirming the importance of fatty acid metabolism in SARS-CoV-2 replication (Figure 19C).

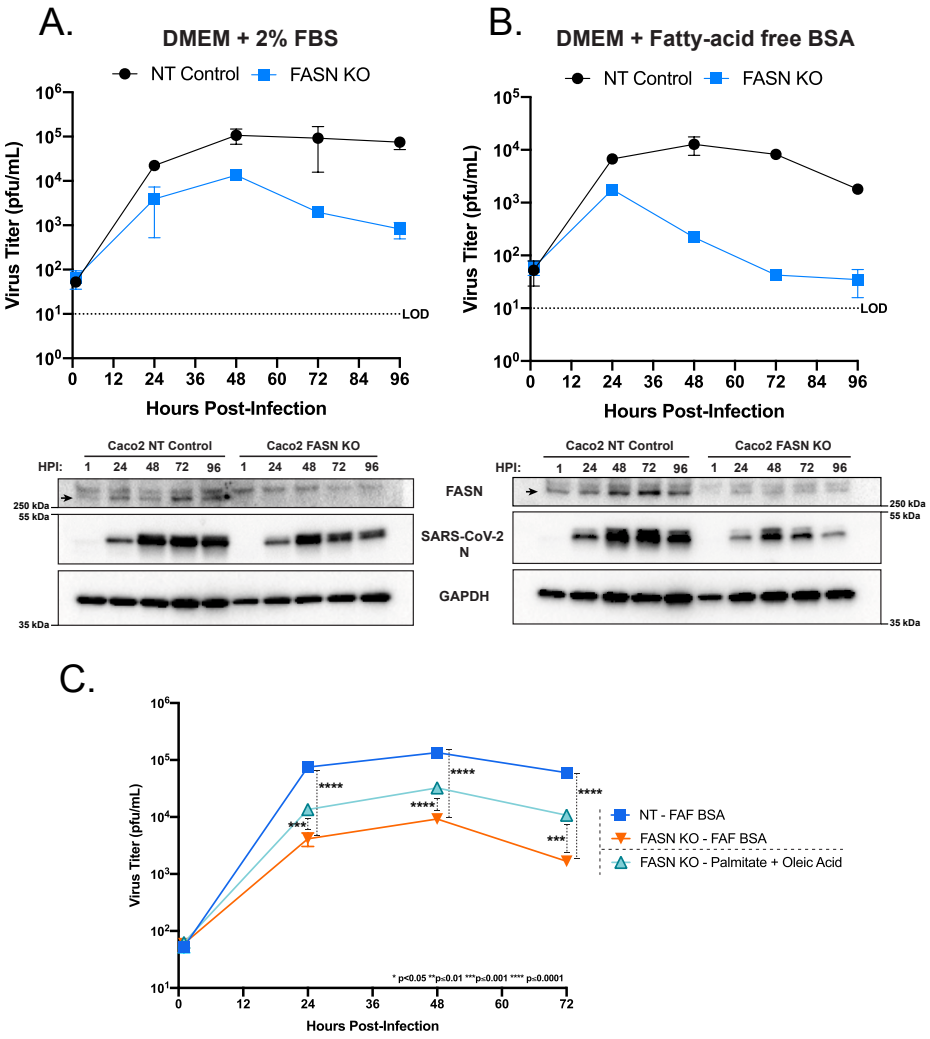

Figure 19 Fatty acid metabolism is essential for efficient SARS-CoV-2 replication

FASN CRISPR KO Caco2 cells and corresponding NT Caco2 cells were pre-seeded in 96-well plates, grown to confluency, and then infected at an MOI 0.01 in minimal media. Post adsorption, cells were maintained in either 2% FBS DMEM (A) or 1% fatty-acid free (FAF)-BSA DMEM (B). Supernatants were collected at 1, 24, 48, 72, and 96 hpi and viral titers were determined by plaque assay. Protein samples were obtained from cell monolayers and analyzed by western blot to confirm FASN knockout and look for changes in SARS-CoV-2 N levels. FASN KO and WT cells were pre-seeded and infected as previously described. Post adsorption, inoculum was removed and replaced with 2% FAF-BSA DMEM or 2% FAF-BSA DMEM containing 250 µM palmitic acid + 250 µM oleic acid (C). Supernatants were collected at 1, 24, 48, and 72 hpi and viral titers were determined via plaque assay.

2.6 Discussion

Engagement with and usurpation of host membranes is central to coronavirus biology. We therefore sought to identify potential host factors and pathways relevant to lipid metabolism that are critical for SARS-CoV-2 replication. In addition to providing insights into virus-host interactions, such approaches might also suggest new therapeutic strategies. Our results demonstrate the importance of both the class III PI3 kinase VPS34, and enzymes involved in fatty acid metabolism for SARS-CoV-2 replication. Treatment of infected cells with inhibitors against VPS34 and various steps of fatty acid metabolism impairs virus growth, reduces viral RNA synthesis, and perturbs the formation of dsRNA positive replication centers. Compounds targeting ACC and DGAT1 likely also inhibit additional steps in the virus replication cycle.

VPS34 is a class III phosphoinositide 3-kinase that plays important roles in autophagy and endosomal trafficking, as well as other cellular functions (Backer 2016; Ohashi et al. 2020). In our inquiry into host factors relevant for SARS-CoV-2 replication we tested two well characterized specific and structurally similar inhibitors of VPS34: VPS34-IN1 and PIK-III (Bago et al. 2014; Dowdle et al. 2014). Both inhibitors showed potent inhibition of viral titers at sub-micromolar concentrations in both Vero E6 and Calu-3 cells as measured by resistance assay and plaque assay, respectively. To further confirm the specificity to VPS34 activity we tested the anti-SARS-CoV-2 activity of two additional inhibitors, Compound 19 and SAR405, the latter of which is structurally distinct from the others (Honda et al. 2016; Pasquier 2015; Ronan et al. 2014). Each compound inhibited virus growth, further validating the importance of VPS34 for virus replication, consistent with recent reports (Wang et al. 2021; Yuen et al. 2021). Mechanistically, our data point to early steps, potentially viral entry, and later steps, including viral RNA synthesis as sensitive to VPS34 inhibition.

While our inhibitor studies do not differentiate between the various functions of VPS34 that might be involved in SARS-CoV-2 replication, studies in different cell types suggest autophagy is not essential for MHV growth and more recent studies suggest that coronaviruses interfere with autophagy, and that activation of autophagy can inhibit replication of SARS-CoV, MERS CoV, and SARS-CoV-2 (Gassen et al. 2019; Guo et al. 2016; Prentice et al. 2004; Zhao et al. 2007). Given that inhibition of VPS34 results in the inhibition of autophagy, it would be expected that inhibition of VPS34 would eliminate these anti-CoV effects of autophagy and promote SARS-CoV-2 replication. At the same time, host protein TMEM41B which is also implicated in autophagy has been demonstrated to facilitate SARS-CoV-2 growth, suggesting that the virus may usurp some autophagy functions (Schneider et al. 2021). It will therefore be of interest to determine whether the disruptions in SARS-CoV-2 replication due to VPS34 targeting reflect inhibition of autophagy or non-autophagy related functions.

Separate from autophagy, VPS34 has several other roles, most notably in vesicular trafficking and sorting. VPS34 phosphorylation of phosphoinositol-3 allows for recruitment of various proteins for endosomal fusion and tethering, recruitment of the endosomal sorting complex required for transport (ESCRT) proteins for the formation of multivesicular bodies, and proper functioning of the Retromer complex for endosome-to-Golgi transport (Backer 2016; Ohashi et al. 2020). For members of the positive-sense RNA tombusviruses, VPS34 has been shown to be recruited to replication compartments providing increased levels of phosphoinositol-3-phosphate, which allows for recruitment of Rab5-positive early endosomes to provide phosphatidylethanolamine-enriched membranes for replication centers formation (Feng et al. 2019). Based on our observation that the VPS34 inhibitor VPS34-IN1 interferes with the formation of dsRNA positive SARS-CoV-2 replication centers, it is possible that VPS34

functions to facilitate membrane availability for SARS-CoV-2 replication organelle formation. Disruption of endocytic trafficking might also explain our observation that pre-treatment followed by removal of VPS34 inhibitors alone had significant effects on early phases of SARS-CoV-2 replication. Alternatively, the significant effects on SARS-CoV-2 replication observed by pre-treatment alone could also be due to an extended in vitro half-life of these compounds or irreversible binding to VPS34 leading to inhibition of later steps in the virus lifecycle without continuous treatment. Further studies will be required to fully deconvolute these possibilities.

Fatty acid metabolism is co-opted by viruses for a variety of purposes including as a means to provide energy for replication, the establishment of membrane-associated replication centers and the proper assembly and budding of newly synthesized viral particles (Heaton and Randall, 2011). Orlistat, an FDA approved inhibitor of fatty acid synthase (FASN), and Triacsin C, an inhibitor of long chain acyl-CoA synthetase (ACS) have previously been examined for their antiviral activities against viruses the utilize fatty acids and neutral lipids for replication (Ammer et al. 2015; Cheung et al. 2010; Gaunt et al. 2013; Hitakarun et al. 2020; Kim et al. 2012; Liefhebber et al. 2014; Tongluan et al. 2017; Wakil and Abu-Elheiga 2009). In our study on SARS-CoV-2, we found that Orlistat and Triacsin C both exhibited antiviral activity but only when maintained throughout infection, consistent with the post-entry inhibition previously described for other viruses.

Inhibition of upstream steps in the metabolic pathway, like FASN and ACS, can lead to dysregulation of multiple downstream pathways. In this case, the viral inhibition we observe from Orlistat and Triacsin C could be the result of downregulating fatty acid protein modification, β-oxidation of fatty acids in the mitochondria, or neutral lipid synthesis and lipid droplet formation (Baenke et al. 2013). In HCV infection, NS4B and the core protein both

require protein palmitoylation for their function in replication and virus particle formation, respectively (Majeau et al. 2009; Yu et al. 2006). Protein palmitoylation of the spike proteins of MHV and SARS-CoV have also been shown to be critical to virion assembly, cell-cell fusion, and infectivity (McBride and Machamer 2010; Petit et al. 2007; Thorp et al. 2006). Palmitoylation of coronavirus envelope proteins has also been described (Boscarino et al. 2008; Tseng et al. 2014). DENV activates pathways that trigger breakdown of lipid droplets and neutral lipids to redirect fatty acids to the mitochondria for β-oxidation and energy production (Heaton and Randall 2011). Conversely to this, rotavirus directly utilizes lipid droplets as a platform for replication center formation and a protected environment for virion maturation (Cheung et al. 2010; Lever and Desselberger 2016). To gain further mechanistic insight into the role of fatty acid metabolism in the SARS-CoV-2 lifecycle we tested a series of compounds that targeted enzymatic steps involved in each one of the aforementioned pathways downstream of FASN. Our results showed that the palmitoyl acetyltransferase (PAT) inhibitor 2-bromopalmitate, which should block protein palmitoylation, led to a substantial reduction in SARS-CoV-2 replication. This may reflect a requirement for spike modification and/or palmitoylation of envelope and host proteins. Additionally, A922500, a specific inhibitor of DGAT1, resulted in significant reduction of SARS-CoV-2. This inhibition is indicative of a need for neutral lipid synthesis and suggests a role for lipid droplets, which have been implicated in SARS-CoV-2 growth and a role for lipid droplets in SARS-CoV-2 assembly (Dias et al. 2020). Our data with A922500 are consistent with such a model, given that its effects on production of infectious virus were substantially greater than on viral RNA synthesis.

Previous studies tracking newly synthesized RNA during CoV infection show that RNA synthesis occurs at foci referred to as replication centers that correspond to double membrane

vesicles produced during coronavirus infection (Snijder et al. 2020). It was striking that treatment of infected cells with VPS34-IN1 and inhibitors of different aspects of fatty acid metabolism all resulted in aberrant dsRNA and N localization while treatment with Remdesivir did not. The distribution of dsRNA and N varied, depending on the compound used. These data suggest VPS34 and various aspects of fatty acid metabolism play a role in proper formation SARS-CoV-2 replication centers and possibly in virally induced membrane rearrangements.

VPS34-IN1, Triacsin C, Orlistat, and 2-bromopalmitate all reduced genomic N and NSP14 RNA levels to a degree that roughly correlated with the reduction in viral titer, while subgenomic N was only moderately affected in comparison. Determining whether these compounds selectively impact viral genome replication versus subgenomic mRNA production will be of interest. Treatment with TOFA and A922500 reduced genomic N and NSP14 RNA to a substantially lesser degree than the reductions in viral titers. The discrepancy between the reduction in RNA synthesis and infectious virus is consistent with models like rotavirus, where RNA synthesis and virion formation utilize the production of specialized replication organelles. Disruption of these structures moderately reduces RNA synthesis but has a much larger impact on virus assembly and release (Cheung et al. 2010; Gaunt et al. 2013; Kim et al. 2012; Lever and Desselberger 2016).

The demonstration that SARS-CoV-2 replication is impaired in FASN KO cells as compared to cells that received a non-targeting guide RNA further confirms the requirement for fatty acids. In cells lacking FASN there was a significant reduction in viral titers that was sustained throughout infection. That this attenuation is due to loss of fatty acid production is supported by the increased attenuation when the cells were maintained in the presence of fatty acid free medium as compared to medium containing FBS that might provide exogenous fatty

acids. To further address this issue, supplementation was performed with two primary substrates downstream of FASN, palmitic acid and oleic acid (Ackerman et al. 2018; Alsabeeh et al. 2018; Baenke et al. 2013). This resulted in a significant rescue of SARS-CoV-2 replication in FASN KO cells when compared to cells without supplementation. The ability to rescue infection using fatty acid metabolism products provides a potentially useful approach to further mechanistic characterization of fatty acid metabolism is in the SARS-CoV-2 life cycle.

Cumulatively, these data support lipid metabolism as a potential therapeutic target for SARS-CoV-2 infection. The specific mechanisms by which VPS34 promotes SARS-CoV-2 replication and the precise manner in which the VSP34 inhibitors impair replication warrant further investigation. Additionally, the identification of fatty acid metabolism, and more specifically protein palmitoylation and lipid droplet production, as key components for replication provides important insights into SARS-CoV-2-host interaction.

2.7 Acknowledgments

This work was supported by NIH grants R01AI125453 and P01AI120943 (Amarasinghe), by a Fast Grant for COVID-19 from the Emergent Ventures program at the Mercatus Center of George Mason University and by The Augusta University–Georgia State University Seed Grant program to C.F.B. We would like to thank the Georgia State University High Containment team Natasha Griffith, Martin Wildes, and Robert “Mike” Walsh for their continuous support. We would also like to thank Authors Anthony M. Nicolini and Stacie A. Chvatal from Axion BioSystems who provided the Axion Maestro Z instrument used in these studies and Jared Carlson-Stevermer, Jennifer Oki, and Kevin Holden from Synthego, Inc. who generated and provided the FASN knockout cells.

3 IMPACT OF MĚNGLÀ VIRUS PROTEINS ON HUMAN AND BAT INNATE IMMUNE PATHWAYS

DOI: 10.1128/JVI.00191-20]

3.1 Author figure contribution

Caroline G. Williams – Figure 20 E, Figure 21, Figure 23 A-C, Figure 24 A-C, Figure 29 C, and Figure 30 B

Joyce Sweeney Gibbons – Figure 20 A-D, Figure 22 A-C, Figure 25 A-C, Figure 26, Figure 27 A-C, Figure 28 A-D, Figure 29 A-B, and Figure 30 A

Timothy Keiffer – Figure 25 A-B

3.2 Abstract

Měnglà virus (MLAV), identified in Rousettus bats, is a phylogenetically distinct member of the family Filoviridae. Because the filoviruses Ebola virus (EBOV) and Marburg virus (MARV) modulate host innate immunity, MLAV VP35, VP40 and VP24 proteins were compared with their EBOV and MARV homologs for innate immune pathway modulation. In human and Rousettus cells, MLAV VP35 behaved like EBOV and MARV VP35s, inhibiting virus-induced activation of the interferon (IFN)-β promoter and IRF3 phosphorylation. MLAV VP35 also interacted with PACT, a host protein engaged by EBOV VP35 to inhibit RIG-I signaling. MLAV VP35 also inhibits PKR activation. MLAV VP40 was demonstrated to inhibit type I IFN induced gene expression in human and bat cells. It blocked STAT1 tyrosine phosphorylation induced either by type I IFN or over-expressed Jak1, paralleling MARV VP40. MLAV VP40 also inhibited virus-induced IFNβ promoter activation, a property shared by MARV VP40 and EBOV VP24. A Jak kinase inhibitor did not recapitulate this inhibition in the

absence of viral proteins. Therefore, inhibition of Jak-STAT signaling is insufficient to explain inhibition of IFNβ promoter activation. MLAV VP24 did not inhibit IFN-induced gene expression or bind karyopherin α proteins, properties of EBOV VP24. MLAV VP24 differed from MARV VP24 in that it failed to interact with Keap1 or activate an antioxidant response element reporter gene, due to the absence of a Keap1-binding motif. These functional observations support a closer relationship of MLAV to MARV than to EBOV but also are consistent with MLAV belonging to a distinct genus.

3.3 Importance

EBOV and MARV, members of the family Filoviridae, are highly pathogenic zoonotic viruses that cause severe disease in humans. Both viruses use several mechanisms to modulate the host innate immune response, and these likely contribute to severity of disease. Here, we demonstrate that MLAV, a filovirus newly discovered in a bat, suppresses antiviral type I interferon responses in both human and bat cells. Inhibitory activities are possessed by MLAV VP35 and VP40, which parallels how MARV blocks IFN responses. However, whereas MARV activates cellular antioxidant responses through an interaction between its VP24 protein and host protein Keap1, MLAV VP24 lacks a Keap1 binding motif and fails to activate this cytoprotective response. These data indicate that MLAV possesses immune suppressing functions that could facilitate human infection. They also support the placement of MLAV in a different genus than either EBOV or MARV.

3.4 Introduction

Měnglà virus (MLAV) was discovered when its genomic RNA was identified in the liver of a bat of the *Rousettus* genus that had been collected in Měnglà County, Yunnan Province, China (Yang et al. 2019). To date, only RNA sequence is available and viable MLAV has not

yet been isolated. MLAV has been proposed to represent a new genus, *Dianlovirus,* within the family *Filoviridae*. The filovirus family includes three additional genera, *Ebolavirus*, *Marburgvirus* and *Cuevavirus,* that contain viral species isolated from or identified in mammals (Maes et al. 2019). Placement of MLAV in a distinct genus was based on its comparatively low sequence identity to other filoviruses, phylogenetic and pairwise sequence comparison (PASC) analyses (Yang et al. 2019). It was also noted to have, compared to other filoviruses, unique gene overlaps and a unique transcription start signal (Yang et al. 2019). MLAV displays some features more reminiscent of *Marburgvirus* members than *Ebolavirus* members. Specifically, MLAV RNA was identified in tissue from a *Rousettus* bat, the same genus of bat which serves as a MARV reservoir in Africa (Schuh, Amman, and Towner 2017). In addition, the MLAV Large (L) protein exhibits closer phylogenetic relatedness to *Marburgvirus* L than to the L of other filoviruses, and in contrast to *Ebolavirus* and *Cuevavirus* members, MLAV can express its glycoprotein (GP) without the need for editing of the GP mRNA (Messaoudi, Amarasinghe, and Basler 2015).

Filoviruses are noteworthy because of their capacity to cause severe human disease (Messaoudi, Amarasinghe, and Basler 2015). Some members of the *Ebolavirus* and *Marburgvirus* genera are zoonotic pathogens that have caused repeated outbreaks with substantial lethality in humans (Rougeron et al. 2015). The largest such outbreak on record was caused by *Zaire ebolavirus* (EBOV) and occurred in West Africa between 2013 and 2016. This resulted in upwards of 28,000 infections, more than 11,000 deaths, and the export of infected cases to the United States and Europe (Team et al. 2016). EBOV is also the cause of the second largest filovirus outbreak, which was first recognized in August 2018 and has continued well into

2019 (Organization 2019).The largest outbreak of MARV occurred in Angola between 2004-2005 and had a reported case fatality rate of 88 percent (Rougeron et al. 2015).

Likely contributing to the virulence of filoviruses are viral encoded proteins that target host cell innate immune signaling pathways (Messaoudi, Amarasinghe, and Basler 2015). Filovirus VP35 proteins suppress interferon (IFN)-α/β responses that play critical roles in innate antiviral immunity (Basler et al. 2000). VP35 impairment of IFN-α/β production occurs by inhibition of RIG-I-like receptor (RLR) signaling through several mechanisms, including VP35 binding to RLR activating dsRNAs and the interaction of VP35 with PACT, a host protein that facilitates RIG-I activation (Cardenas et al. 2006; Edwards et al. 2016a; Leung et al. 2009a; Leung, Prins, et al. 2010; Luthra et al. 2013; Prins et al. 2010; Yen et al. 2014; Hartman, Towner, and Nichol 2004; Kimberlin et al. 2010; Bale et al. 2013a; Bale et al. 2012; Dilley et al. 2017). VP35s also inhibit the phosphorylation and activation of the IFN-induced kinase PKR (Feng et al. 2007a; Schumann, Gantke, and Muhlberger 2009; Hume and Muhlberger 2018; Edwards et al. 2018). EBOV VP24, but not MARV VP24, interacts with the NPI-1 subfamily of karyopherin alpha (KPNA) (also known as importin alpha) nuclear transport proteins, which includes KPNA1, KPNA5 and KPNA6 (Reid et al. 2006; Reid et al. 2007). The NPI-1 subfamily also mediates nuclear import of STAT1 following its activation by IFN (McBride et al. 2002; Reid et al. 2007; Sekimoto et al. 1997). The interaction of EBOV VP24 with KPNA competes with tyrosine phosphorylated STAT1 (pY-STAT1), blocking pY-STAT1 nuclear import and suppressing expression of IFN stimulated genes (ISGs), a response that mediates the antiviral effects of IFN (Mateo et al. 2010; Reid et al. 2006; Reid et al. 2007; Xu et al. 2014). MARV VP40 protein has been demonstrated to suppress IFN-induced signaling and ISG expression, while EBOV VP40 has no known role in IFN antagonism (Valmas et al. 2010). Activation of

the Jak family of kinases associated with IFN receptors is inhibited by MARV VP40, blocking phosphorylation and activation of the downstream STAT proteins, including STAT1 (Valmas et al. 2010; Valmas and Basler 2011a; Feagins and Basler 2015a). EBOV VP24 and MARV VP40 have also been described to modestly inhibit IFN-α/β production, although the mechanism(s) are not defined (He, Melen, et al. 2017; Guito et al. 2017). While MARV VP24 does not appear to block IFN responses, it has been demonstrated to interact with Kelch-like ECH-associated protein 1 (Keap1). Under homeostatic conditions, Keap1, a cellular substrate adaptor protein of the Cullin3/Rbx1 ubiquitin E3 ligase complex, targets the transcription factor Nuclear factor erythroid 2-related factor 2 (Nrf2) for polyubiquitination and proteasomal degradation (Edwards et al. 2014; Page et al. 2014; Johnson et al. 2016). MARV VP24 disrupts the Keap1-Nrf2 interaction, leading to Nrf2-induced expression of genes possessing antioxidant response elements (ARE) (Edwards et al. 2014; Page et al. 2014; Johnson et al. 2016). This activity induces a cytoprotective state that may prolong the life of MARV infected cells. MARV VP24 also relieves Keap1 repression of the NF-κB pathway (Edwards and Basler 2015).

Given the link between EBOV and MARV innate immune suppressors and virulence, and the unknown potential of MLAV to cause human disease, this study sought to determine whether MLAV possesses effective suppressors of innate immunity. Given the differences in innate immune evasion mechanisms between EBOV and MARV, it was also of interest to determine whether MLAV innate immune evasion mechanisms more closely resemble EBOV or MARV. The data demonstrate that MLAV VP35 functions as an IFN antagonist by mechanisms that mirror those of EBOV and MARV VP35. MLAV VP40 is demonstrated to act as a suppressor of IFN-induced signaling, whereas MLAV VP24 does not, mirroring the inhibitory functions of MARV. Both MLAV VP35 and VP40 effectively suppressed IFN responses in human and

Rousettus cells. Interestingly, MLAV VP24 does not detectably interact with Keap1 or activate ARE gene expression due to the absence of Keap1-binding sequences found in MARV VP24. Cumulatively, the data demonstrate the presence of IFN evasion functions in MLAV that are effective in human cells, suggesting the virus may have the capacity to cause human disease. The similarities in VP40 immune evasion functions are consistent with a closer genetic relationship of MLAV to MARV than EBOV, but the differences in VP24 function are consistent with MLAV occupying a distinct genus within the filovirus family.

3.5 Materials and methods

3.5.1 Viruses and cell lines

HEK293T cells were maintained in Dulbecco's Modified Eagle Medium (DMEM), supplemented with 10% fetal bovine serum (FBS) and cultured at 37°C and 5% CO2. RO6E cells, immortalized fetal cells from Rousettus aegyptiacus, were obtained from BEI Resources and maintained in DMEM F12 and supplemented with 5% FBS. Sendai Virus Cantell (SeV) was grown in 10-day-old embryonating chicken eggs for forty-eight hours at 37°C.

3.5.2 Plasmids

MLAV NP, VP35, VP40, VP30 and VP24 coding sequences (based on accession number KX371887) were synthesized by Genscript. The synthesized open ¬reading frames were cloned into a pCAGGS expression vector with a FLAG-tag at the N-terminus of each coding sequence. EBOV and MARV viral proteins, GFP-STAT1, HA-Jak1, HA-PACT, HA-KPNA5, HA-Keap1 and IRF3 expression plasmids were previously described (Cardenas et al., 2006; Edwards et al., 2014; Luthra et al., 2013; Reid et al., 2006; Valmas & Basler, 2011). VP24 K-loop chimeras were made using overlapping PCR. MARV VP24 residues 202-RRIDIEPCCGETVLSESV-219 were inserted into MLAV VP24 between residues 202 and 219 (MLAV VP24MARV 202-219)

and the corresponding MLAV residues 202- RAINASGRENESVVQNPI- 219 were inserted into MARV VP24 at the same position (MARV VP24MLAV 202-219).

3.5.3 Cytokines

Universal type I IFN (UIFN) (PBL) was used at 1000 U/mL in DMEM supplemented with 0.3% FBS for 30 minutes at 37°C, unless otherwise stated.

3.5.4 Phosphorylation assays

HEK293T cells ($1x10^6$) were transfected using Lipofectamine 2000® (Life Technologies)**.** The amount of transfected IRF3 was 100 ng per well. Twenty-four hours post transfection, cells were mock-treated, UIFN-treated or SeV-infected, depending on the assay. Subsequently, cells were lysed in NP40 buffer (50mM Tris-HCl {pH 8.0}, 280mM NaCl, 0.5% NP-40) supplemented with cOmplete™ protease inhibitor cocktail (Roche) and PhosSTOP (Roche). Lysates were incubated for ten minutes on ice and clarified for ten minutes at 21,100 x g at 4°C. Phosphorylation status of the proteins was determined by western blot.

3.5.5 IFNβ- and ISG54-promotor reporter gene assay

HEK293T cells ($5x10^4$) and RO6E cells ($2x10^5$) were co-transfected using Lipofectamine 2000® with 25 ng of an IFNβ promoter-firefly luciferase reporter plasmid or an interferon stimulated gene 54 (ISG54) promoter-firefly luciferase reporter plasmid, 25 ng of a constitutively expressing *Renilla* luciferase plasmid (pRL-TK, Promega) and the indicated viral protein expression plasmids – HEK293T cells: 62.5, 6.25, and 0.625 ng for VP35 and VP40 and 25, 2.5, and 0.25 ng for VP24; RO6E cells: 250, 25, and 2.5 ng for EBOV and MARV proteins and 125, 12.5, and 1.25 ng for MLAV proteins. Twenty-four hours post transfection cells were mock-treated, SeV-infected (150 hemagglutinin activity units (HAU)) or UIFN-treated (1000 U/mL). Eighteen hours post-infection or treatment, cells were lysed and analyzed for luciferase

activity using a Dual Luciferase® Reporter Assay System (Promega) per the manufacturer's protocol. Firefly luciferase activity was normalized to *Renilla* luciferase activity. Assays were performed in triplicate; error bars indicate the standard error of the mean (SEM) for the triplicate. Viral protein expression was confirmed by western blot.

3.5.6 IFNβ promotor reporter gene assay in the presence of Jak1/Jak2 inhibitor

HEK293T cells ($5x10^4$) were co-transfected using Lipofectamine 2000® with 25 ng of an IFNβ promoter firefly luciferase reporter plasmid, 25 ng of pRL-TK *Renilla* luciferase reporter plasmid and 62.5, 6.25, and 0.625 ng of the indicated viral protein expression plasmids. Twenty-four hours post-transfection, cells were pre-treated for one hour with 5 μM of Ruxolitinib (SelleckChem), a Jak1/Jak2 inhibitor, and then mock- or SeV- infected in the presence of the inhibitor (Quintas-Cardama et al. 2010). Eighteen hours post-infection or treatment, cells were lysed and assayed using a dual luciferase assay and analyzed as above. To verify inhibition of Jak1/Jak2 by Ruxolitnib, cells were transfected with 25 ng of an ISG54 promoter-firefly luciferase reporter plasmid and 25 ng of pRL-TK reporter plasmid. Twenty-four hours post-transfection, cells were pre-treated for one hour with 5 μM of Ruxolitinib and then mock- or UIFN-treated for eighteen hours in the presence of the inhibitor and assayed for luciferase activity as above.

3.5.7 Measurements of endogenous gene expression

HEK293T cells ($5x10^4$) were transfected with 125 ng of empty vector or viral expression plasmids using Lipofectamine 2000®**.** Twenty-four hours post-transfection, cells were either mock-treated, SeV-infected, or UIFN treated (1000U/mL). At fourteen-hours post-treatment or infection, total cellular RNA was extracted using RNeasy® Mini Kit (Qiagen), as per the manufacturer's protocol. SuperScript™ IV (Thermo Fisher Scientific) was used to generate oligo

dT cDNA which served as the template for quantitative PCR (qPCR). qPCR was performed using PerfeCTa® SYBR Green FastMix® (VWR Scientific) along with gene specific primers for human β-actin, IFNβ and ISG54.

3.5.8 ARE reporter assay

HEK293T cells ($5x10^4$) were co-transfected using Lipofectamine 2000® with an antioxidant response element (ARE) reporter gene, pGL4.37 {luc2P/ARE/Hygro} (Promega) (30 ng) and a pRL-TK reporter plasmid (25 ng) along with either empty vector or 62.5, 6.25, and 0.625 ng of EBOV, MARV, MLAV VP24 or chimeric MARV and MLAV expression plasmids. Eighteen hours post-transfection, luciferase activity was assessed and analyzed as above.

3.5.9 Co-immunoprecipitation assays

HEK293T cells were co-transfected using Lipofectamine 2000® with plasmids for FLAG-tagged MLAV proteins, HA-tagged host proteins, and pCAGGS empty vector. Twenty-four hours post-transfection cells were rinsed with PBS and lysed in NP40 buffer supplemented with cOmplete™ protease inhibitor cocktail (Roche). Lysates were clarified by centrifugation and incubated with anti-FLAG M2 (Sigma-Aldrich) or anti-HA (Thermo Fisher) magnetic beads for two hours at 4°C. Beads were washed five times in NP40 buffer and precipitated proteins were eluted by boiling with SDS sample loading buffer or elution with 3X FLAG peptide (Sigma-Aldrich). Whole cell lysates and immunoprecipitated samples were analyzed by western blot.

3.5.10 Western blot analysis

Blots were probed with anti-FLAG (Sigma-Aldrich), anti-β-tubulin (Sigma-Aldrich), anti-HA (Sigma-Aldrich), anti-phospho-IRF3 (S396) (Cell Signaling), anti-IRF3 (Santa Cruz), anti-phospho-STAT1 (Y701) (BD Transduction Laboratories), anti-STAT1 (BD Transduction

Laboratories), anti-phospho-PKR (T446) (Abcam), or anti-PKR (Cell Signaling) antibodies, as indicated. Antibodies were diluted in Tris-buffered saline with 0.1% Tween-20 (TBS-T) with 5% milk or, when detecting phospho-proteins, 5% bovine serum albumin.

3.5.11 VP40 budding assays

10 µg of EBOV, MARV and MLAV VP40 expression plasmids were transfected into either HEK293T ($3x10^6$) or RO6E ($2x10^6$) cells using Lipofectamine 2000® (Life Technologies). Media was harvested 48 hours post-transfection, briefly clarified by centrifugation, and layered over a 20% sucrose cushion in NTE buffer (10 mM NaCl, 10 mM Tris {pH 7.5}, 1 mM EDTA {pH 8.0}). The samples were then subjected to ultracentrifugation in a Beckman SW41 rotor at 222,200 x g for 2 hours at 10°C; media was aspirated after ultracentrifugation and virus-like particles (VLPs) were solubilized in NTE buffer at 4°C overnight. Cellular lysates were generated by washing transfected cells with PBS and lysing cells in NP40 buffer containing cOmplete™ protease inhibitor cocktail (Roche). To detect the presence of VP40, 5% of cell lysates and 10% of VLPs were analyzed by western blotting. To confirm that VP40s from isolated VLPs had a membrane that can protect internal components from protease digestion, 10% of VLPs were incubated in NTE buffer with 500 ng/µl of trypsin solution (Corning), either in the absence or presence of 0.5% Triton X-100 (Sigma), at 37°C for 1 hour prior to western blot analysis.

3.5.12 Statistics

Statistical significance was determined by one-way ANOVA followed with Tukey multiple comparison as compared to the indicated control; $**p < 0.0001$, $* p < 0.001$ (GraphPad PRISM8).

3.6 Results

3.6.1 MLAV VP35 blocks virus induced IFNβ promotor activation in both human and bat cells

As a measure of the capacity of MLAV VP35, VP40 and VP24 to modulate type I IFN production, the human cell line HEK293T or the *Rousettus* bat cell line RO6E were assessed by reporter gene assay for their effect on Sendai virus (SeV) induced IFNβ promoter activation. Either empty vector or FLAG-tagged expression plasmids for the VP35, VP40 and VP24 proteins of EBOV, MARV and MLAV were co-transfected with an IFNβ promoter firefly luciferase reporter and a constitutively expressing *Renilla* luciferase plasmid. Twenty-four hours post-transfection, cells were either mock-infected or infected for an additional 18 hours with SeV, a potent activator of the IFNβ promoter(Baum, Sachidanandam, and Garcia-Sastre 2010). As expected, SeV infection activated the IFNβ promoter in the absence of viral protein expression. EBOV and MARV VP35 impaired IFNβ reporter activation in a dose-dependent manner in both cell lines, with EBOV exhibiting greater potency as previously shown (Figure 20A-B) (Edwards et al. 2016a; Dilley et al. 2017). Similarly, MLAV VP35 dramatically diminished IFNβ promoter activity in a dose dependent manner (Figure 20A-B).

Expression of EBOV VP24, Lloviu virus (LLOV) VP24 or MARV VP40 has also been reported to impair IFNβ and, in the case of EBOV VP24, IFNλ production (Guito et al. 2017; He, Melen, et al. 2017; Feagins and Basler 2015b). In the present study, in HEK293T cells, modest inhibition of IFNβ promoter activation was evident for EBOV VP24, EBOV VP40, and MARV VP40. MLAV VP40 exhibited potent dose-dependent inhibition of IFNβ promoter activation (Figure 20A). Weak, but statistically significant inhibition of IFNβ reporter gene expression was detected for MARV VP24 and MLAV VP24, however, the biological

significance of this minimal inhibition is uncertain. In RO6E cells, MLAV VP40 inhibition of IFNβ promoter activation was also detected but only at the highest concentration of transfected plasmid (Figure 20B).

To evaluate whether or not the inhibition of the IFNβ reporter also correlates with inhibition of endogenous IFNβ gene expression, qRT-PCR assays were performed. MLAV VP35 and VP40 showed significant inhibition of IFNβ transcripts consistent with the results of the reporter assays. Expression of MLAV VP24 had no effect on IFNβ copy numbers, which may suggest that the minor inhibition observed in the luminescence assay is not biologically relevant (Figure 20C).

EBOV and MARV VP35 inhibition of RLR signaling pathways results in inhibition of the phosphorylation and activation of transcription factor interferon regulatory factor 3 (IRF3) (Cardenas et al. 2006; Hartman et al. 2006; Ramanan et al. 2012). In order to determine whether MLAV VP35 can inhibit activation of IRF3, HEK293T cells were co-transfected with either empty vector or an IRF3 expression plasmid and plasmids that express FLAG-tagged EBOV, MARV, and MLAV VP35 (Figure 20D). Twenty-four hours post-transfection, cells were either mock- or SeV-infected to induce IRF3 phosphorylation. Over-expression of IRF3 substantially increased detection of the phosphorylated form. As previously reported, EBOV VP35 potently inhibited IRF3 phosphorylation. MARV VP35 also inhibited IRF3 phosphorylation, although less efficiently, consistent with less robust inhibition of RIG-I signaling as compared to EBOV VP35 (Dilley et al. 2017; Edwards et al. 2016a). MLAV VP35 inhibited IRF3 phosphorylation comparable to EBOV VP35 (Figure 20D).

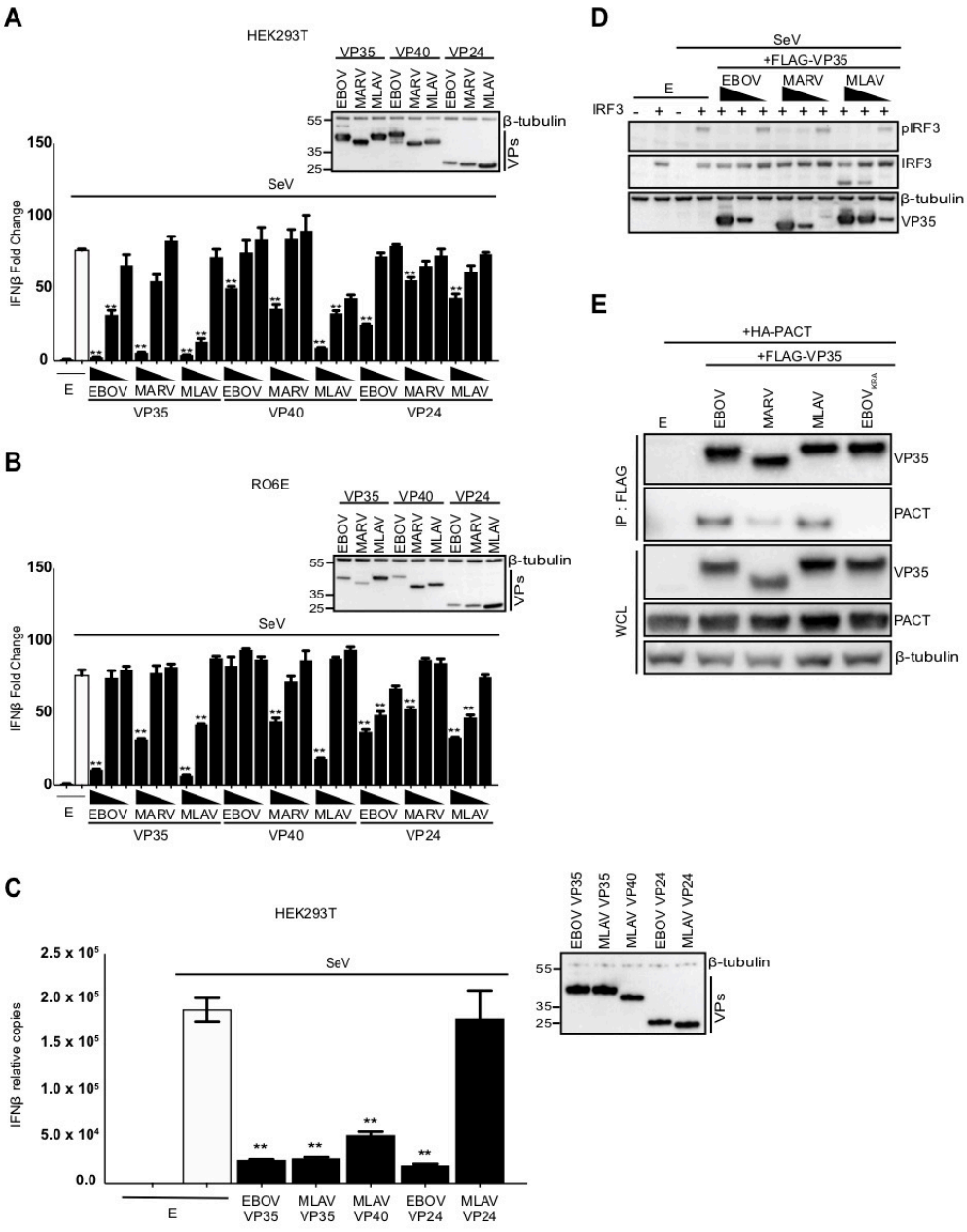

Figure 20 MLAV VP35 blocks Sendai virus-induced IFNβ promoter activation in both human and bat cells

HEK293T cells were transfected with an IFNβ promoter firefly luciferase reporter plasmid, a constitutively-expressed Renilla luciferase reporter plasmid and either empty vector (E) or the specified FLAG-tagged viral proteins. The amounts of VP35 and VP40 plasmids were 62.5 ng, 6.25 ng and 0.625 ng; the amounts of VP24 plasmids were 25 ng, 2.5 ng and 0.25 ng. Twenty-four hours post-transfection, cells were either mock or Sendai virus (SeV)-infected. Firefly and Renilla luciferase activities were determined eighteen hours post-infection using a dual luciferase assay. Fold induction was determined relative to the vector only, mock-infected samples (A). RO6E cells were assayed as described above, except the amounts of EBOV and MARV VP35, VP40 and VP24 plasmids were 250 ng, 25 ng and 2.5 ng and the amounts of MLAV VP35, VP40 and VP24 plasmids were 125 ng, 12.5 ng and 1.25 ng (B). HEK293T cells were transfected with 125 ng of empty vector or the indicated protein expression plasmids, mock- or SeV-infected for eighteen hours and endogenous human IFNβ mRNA

levels were measured and normalized to human β-actin mRNA levels. For all experiments in A-C, cell lysates were analyzed by western blot with anti-FLAG and anti-β-tubulin antibodies (insets) (C). Experiments were performed in triplicate, error bars represent the SEM for the triplicate, and statistical significance was determined by performing a one-way ANOVA followed with Tukey multiple comparison as compared to SeV-infected control (white bar); **$p < 0.0001$, * $p < 0.001$. VPs – viral proteins. HEK293T cells were transfected with empty vector (E) or IRF3 expression plasmid (100 ng), as indicated, and FLAG-tagged EBOV, MARV, MLAV VP35. The amounts of VP35 plasmids were 2,000 ng, 400 ng and 80 ng. Cells were mock or SeV-infected for four hours. Whole cell lysates were analyzed by western blot with anti-pIRF3 (S396), anti-total IRF3, anti-FLAG (VP35), and anti-β-tubulin antibodies (D). HEK293T cells were transfected with empty vector (E), or plasmids that express FLAG-tagged EBOV VP35, MARV VP35, MLAV VP35, or dsRNA binding mutant EBOV $VP35_{KRA}$ and HA-tagged PACT, as indicated (E). Immunoprecipitations (IP) were performed with anti-FLAG antibody. Western blots were performed for detection of VP35 (anti-FLAG antibody), PACT (anti-HA antibody), and β-tubulin. WCL, whole cell lysate. ***Experiments in A-D performed by Joyce Sweeney Gibbons.**

EBOV and MARV VP35 interact with host protein PACT, and this interaction contributes to VP35 inhibition of RIG-I signaling (Hume and Muhlberger 2018; Luthra et al. 2013). To determine if MLAV VP35 might suppress IFN production through a similar mechanism, the PACT-VP35 interactions were evaluated by co-immunoprecipitation assay (Figure 10E). FLAG-tagged EBOV, MARV, and MLAV VP35 or empty vector expression plasmids were co-transfected with HA-tagged PACT in HEK293T cells. A VP35 dsRNA binding mutant ($VP35_{KRA}$) that has previously been shown to lack the ability to interact with PACT was included as a negative control (Luthra et al. 2013). All three wildtype VP35 proteins were demonstrated to interact with PACT, with MLAV VP35 interacting comparably to EBOV VP35 (Figure 10E). Together, these data suggest that MLAV VP35 employs mechanisms similar to EBOV and MARV VP35 for inhibition of RIG-I dependent activation of type I IFN responses and that the potency of inhibition is similar to EBOV VP35.

3.6.2 MLAV VP35 protein inhibits phosphorylation of PKR in human cells

To assess whether MLAV VP35 can inhibit activation of PKR, HEK293T cells were transfected with FLAG-tagged EBOV, MARV, and MLAV VP35, or empty vector expression plasmids. Consistent with previous literature, EBOV VP35 and MARV VP35 inhibited SeV-

induced PKR phosphorylation (Figure 21). MLAV VP35 also inhibited activation of PKR in a concentration dependent manner (Figure 21).

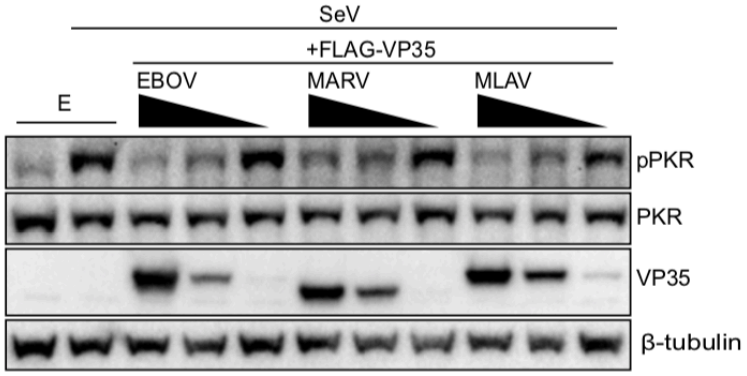

Figure 21 MLAV VP35 inhibits Sendai virus-induced PKR activation

HEK293T cells were transfected with empty vector (E) or expression plasmids for FLAG-tagged EBOV, MARV and MLAV VP35, as indicated (2000 ng, 400 ng and 80 ng). Twenty-four hours post-transfection, cells were mock- or SeV-infected. Eighteen hours post infection, whole cell lysates were assessed by western blot for levels of total and phosphorylated PKR using anti-FLAG (VP35), anti-total PKR, anti-phospho-PKR (T446) (pPKR) and anti-β-tubulin antibodies.

3.6.3 MLAV VP40 protein responses to type I IFN in both human and bat cells

To test the effects of MLAV VP35, VP40 and VP24 on the response of cells to exogenous type I IFN, empty vector or expression plasmids for FLAG-tagged VP35, VP40 and VP24 proteins of EBOV, MARV and MLAV were co-transfected with an IFN-responsive ISG54 promoter firefly luciferase reporter plasmid and a plasmid that constitutively expresses *Renilla* luciferase. Twenty-four hours post-transfection, cells were either mock- or type I IFN-treated. The ISG54 reporter was activated by IFN-treatment in the absence of viral protein expression (Figure 22B). As expected, both MARV VP40 and EBOV VP24 strongly inhibited ISG54 reporter activity in both human and bat cell lines (Figure 22A-B). Similar to MARV VP40, MLAV VP40 potently inhibited the ISG54 reporter in both cell types. Each of the VP35s and MARV and MLAV VP24 modestly inhibited the ISG54 reporter when higher amounts of expression plasmid were tested.

To further address this function, endogenous ISG54 transcripts were measured by qRT-PCR. Inhibition of IFN-induced gene expression was demonstrated for MARV VP40, EBOV VP24 and MLAV VP40 (Figure 22C), consistent with the reporter gene results. Notably, no inhibition was detected with either MLAV VP35 or MLAV VP24 in this assay.

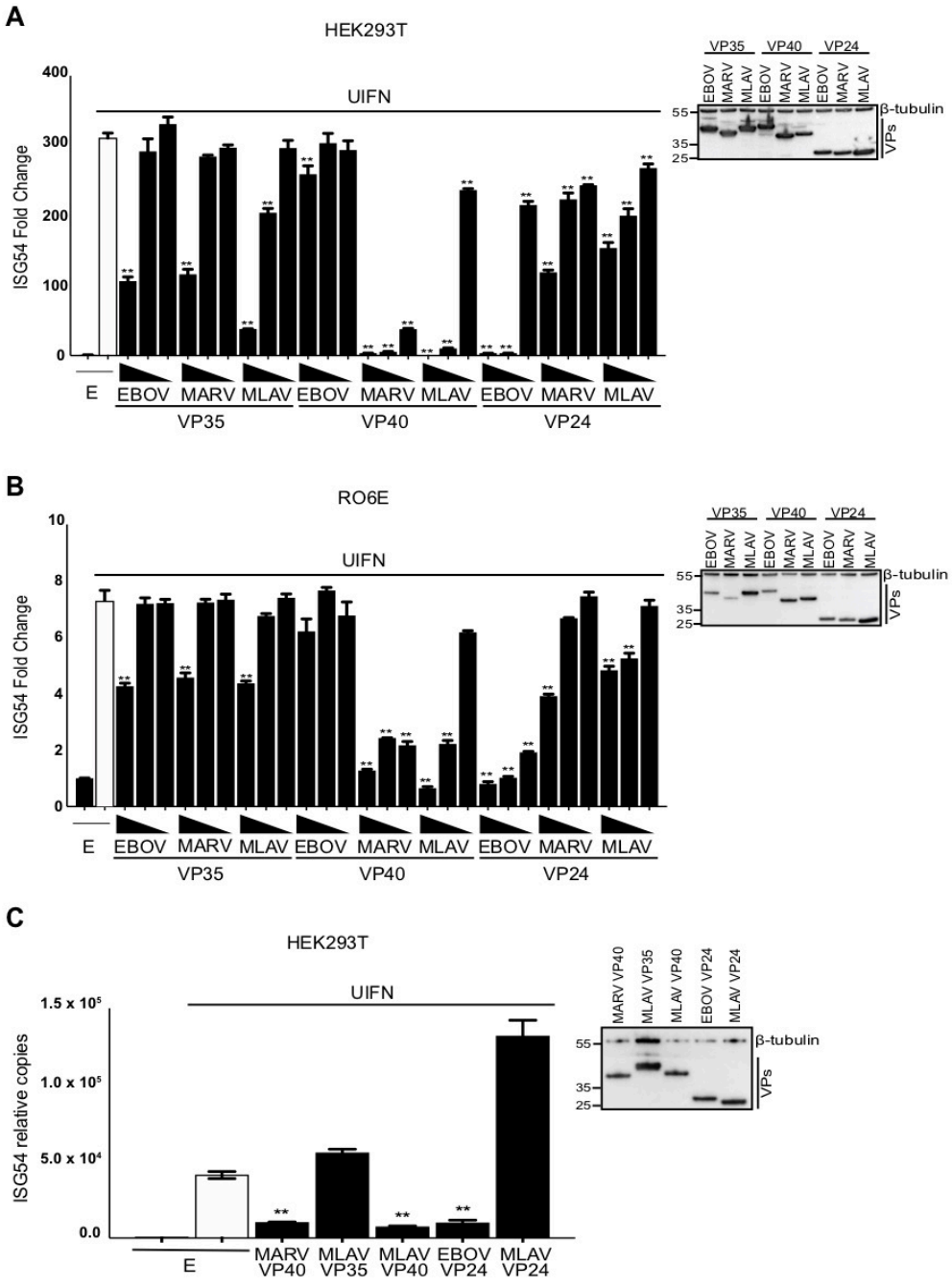

Figure 22 MLAV VP40 protein inhibits responses to type I IFN in both human and bat cells

*HEK293T cells were transfected with an ISG54 promoter firefly luciferase reporter plasmid, a constitutively-expressed Renilla luciferase reporter plasmid and either empty vector (E) or the specified FLAG-tagged viral proteins. The amounts of VP35 and VP40 plasmids were 62.5 ng, 6.25 ng and 0.625 ng; the amounts of VP24 plasmids were 25 ng, 2.5 ng and 0.25 ng. Twenty-four hours post-transfection, cells were either mock- or UIFN-treated. Eighteen hours post-treatment, firefly and Renilla luciferase activities were determined. Firefly luciferase values were normalized to Renilla luciferase values and fold induction was calculated relative to the vector only, mock-treated samples (A). RO6E cells were transfected as described above, except the amounts of EBOV and MARV VP35, VP40 and VP24 plasmids were 250 ng, 25 ng and 2.5 ng and the amounts of MLAV VP35, VP40 and VP24 plasmids were 125 ng, 12.5 ng and 1.25 ng (B). HEK293T cells were assessed for endogenous human ISG54 mRNA levels in the presence of empty vector or expression plasmids for the indicated viral proteins, 125 ng. Results were normalized to human β–actin mRNA levels. All experiments were performed in triplicate, error bars represent the SEM for the triplicate. Whole cell lysates were analyzed by western blot with anti-FLAG and anti-β-tubulin antibodies (inset) (C). Statistical significance was determined by performing a one-way ANOVA followed with Tukey's multiple comparison test as compared to UIFN-treated control (white bar); **p < 0.0001, *p < 0.001.* ***Experiments performed by Joyce Sweeney Gibbons.***

MARV VP40 has been shown to be a potent inhibitor of IFN-α/β induced phosphorylation of STAT1; whereas EBOV VP24 inhibits this pathway by blocking nuclear transport of pY-STAT1(Reid et al. 2006; Reid et al. 2007; Xu et al. 2014). To determine whether inhibition of IFN responses is due to inhibition of STAT1 phosphorylation, HEK293T cells were co-transfected with empty vector or expression plasmids for FLAG-tagged EBOV, MARV, and MLAV VP24 or VP40. GFP-STAT1 was (Figure 23A) or was not (Figure 23B) included in the transfection. Addition of IFN triggered the phosphorylation of GFP-STAT1 and endogenous STAT1 in the vector only samples. Among the EBOV and MARV constructs, only MARV VP40 was inhibitory. MLAV VP40 inhibited STAT1 tyrosine phosphorylation to a similar degree as MARV VP40. MLAV VP24 did not detectably affect STAT1 phosphorylation.

MARV VP40 inhibits STAT1 phosphorylation following over-expression of Jak1(Valmas et al. 2010). To determine whether MLAV VP40 can prevent Jak1 induced STAT1 phosphorylation, HA-tagged Jak1 was co-transfected with empty vector or FLAG-tagged EBOV, MARV or MLAV VP40. As expected, expression of exogenous Jak1 induced STAT1 tyrosine phosphorylation, and this was suppressed in the presence of MARV VP40 (Figure 23C).

Similarly, MLAV VP40 prevented Jak1-dependent STAT1 phosphorylation, suggesting that MLAV VP40 inhibits IFN signaling through mechanisms similar to those used by MARV VP40.

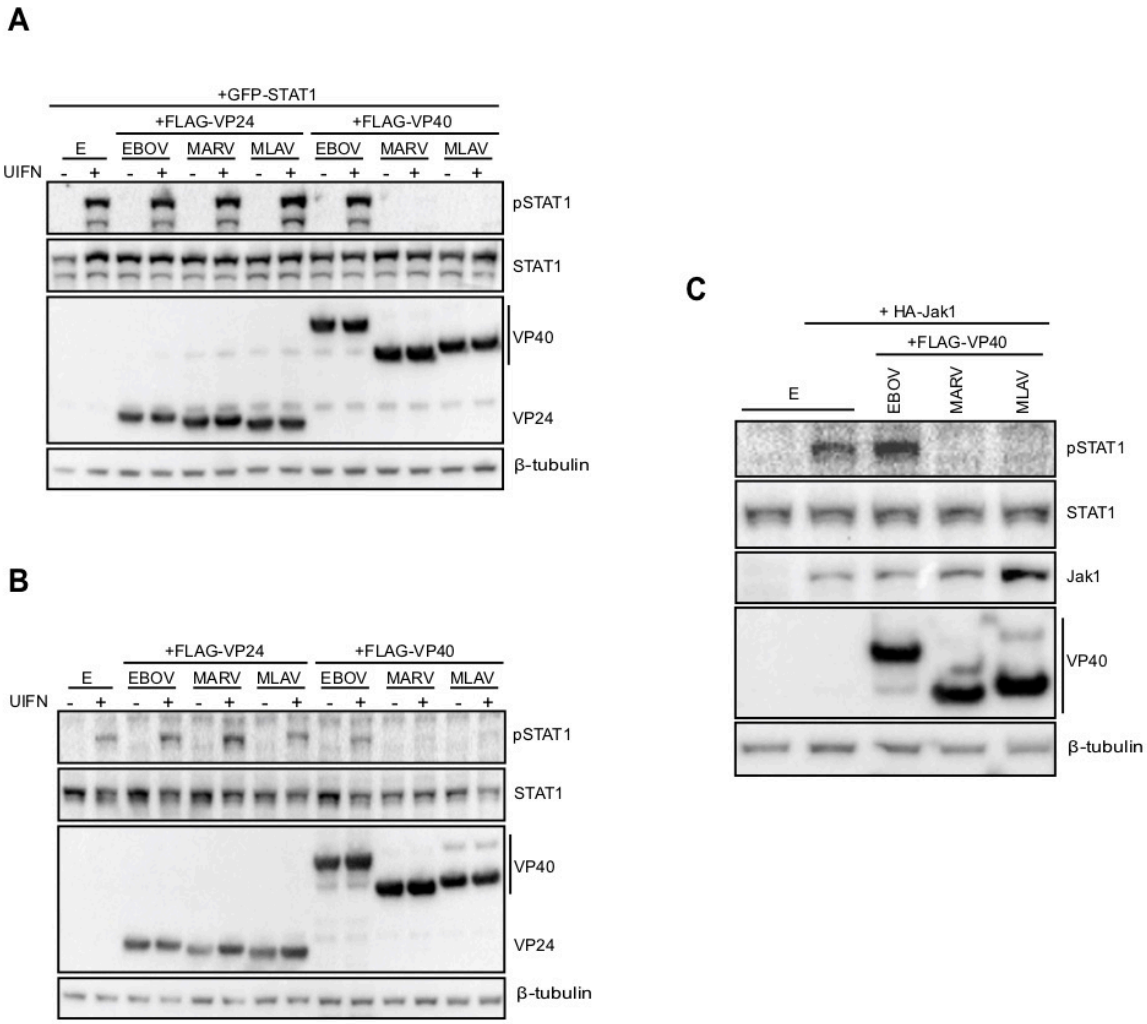

Figure 23 MLAV VP40 protein inhibits type I IFN induced gene expression and Jak-STAT signaling

HEK293T cells were transfected with empty vector (E), FLAG-tagged VP24s or VP40s from EBOV, MARV and MLAV, as indicated. Twenty-four hours post-transfection, cells were treated with UIFN for 30 minutes and the phosphorylation status of exogenous GFP-STAT1 (A) or endogenous STAT1 (B) was assessed by western blotting. HEK293T cells were co-transfected with empty vector (E) or FLAG-tagged VP40s from EBOV, MARV and MLAV and HA-tagged Jak1 expression plasmids. Twenty-four hours post-transfection cells were lysed and the phosphorylation status of endogenous STAT1 was analyzed (C). Western blotting was performed with anti-FLAG, anti-STAT1, anti-pSTAT1 (Y701), and anti-β-tubulin antibodies.

EBOV VP24 interacts with NPI-1 subfamily members of the KPNA nuclear transporters, including KPNA5, to block nuclear import of pY-STAT1(Reid et al. 2006; Reid et al. 2007; Xu

et al. 2014). To assess whether MLAV VP24 interacts with KPNA5, co-immunoprecipitation assays were performed in HEK293T cells (Figure 24A). KPNA5 did not precipitate in the absence of a co-expressed protein. Among FLAG-tagged EBOV, MARV, and MLAV VP24, only EBOV VP24 detectably interacted with KPNA5. To determine if MLAV VP24 might interact with other KPNA family members, additional co-immunoprecipitation assays were performed between MLAV VP24 and KPNA1-6. EBOV VP24 was used in parallel as a control. As expected, EBOV VP24 co-precipitated with KPNA1, KPNA5, and KPNA6. MLAV VP24 failed to detectably co-precipitate with any of the KPNA family members (Figure 24B and 24C). The absence of MLAV VP24-KPNA interactions is consistent with the inability of MLAV VP24 to inhibit IFN-induced gene expression and identifies a functional difference from EBOV VP24.

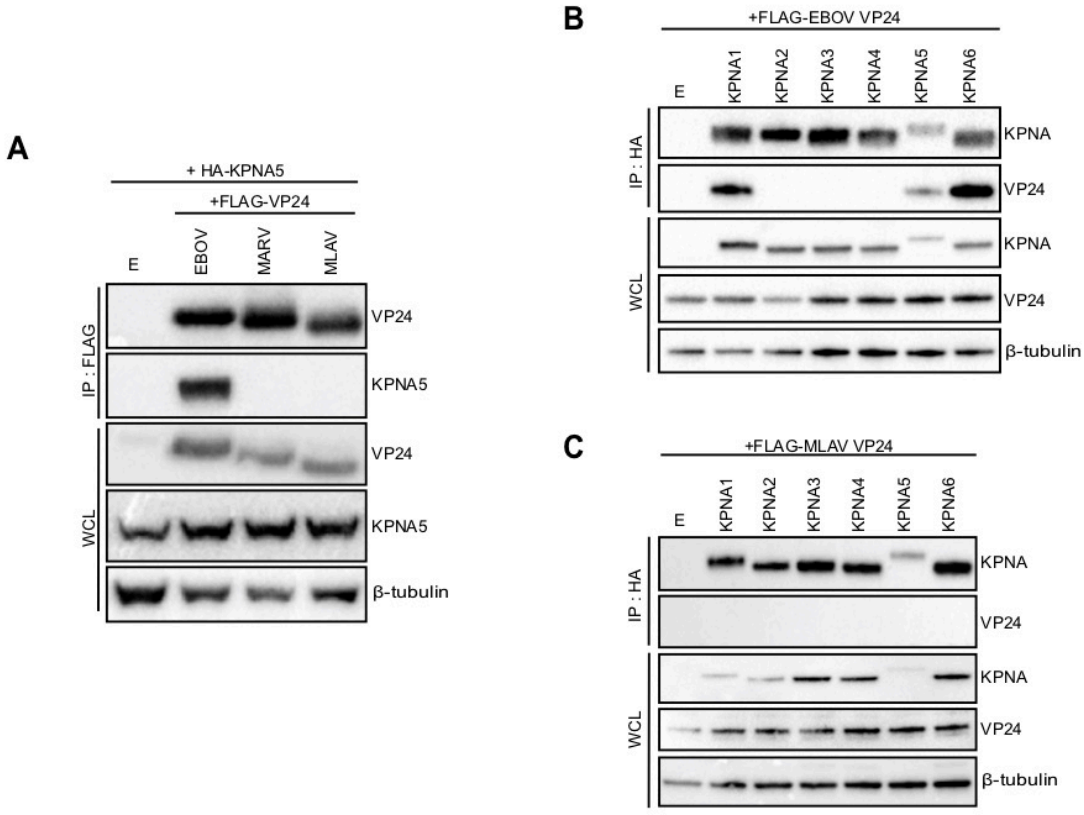

Figure 24 MLAV VP24 does not interact with KPNAs

HEK293T cells were co-transfected with FLAG-tagged EBOV, MARV, MLAV VP24, and HA-tagged KPNA5. Immunoprecipitation (IP) was performed with anti-FLAG antibody and precipitates and whole cell lysates (WCL) were assessed by western blotting with anti-FLAG (VP24), anti-HA (KPNA5) and anti-β-tubulin

antibodies (D). HEK293T cells were co-transfected with either FLAG-tagged EBOV or MLAV VP24, and HA-tagged KPNA1-6 (E-F). Immunoprecipitation (IP) was performed with anti-HA antibody and precipitates and whole cell lysates (WCL) were assessed by western blotting with anti-FLAG (VP24), anti-HA (KPNA) and anti-β-tubulin antibodies.

3.6.4 MLAV and MARV VP40 bud with similar efficiencies from human and bat cells

Filovirus VP40 proteins play a critical role in budding of new virus particles, and expression of VP40 is sufficient for formation and budding of VLPs (Timmins et al. 2001; Harty et al. 2000; Jasenosky et al. 2001b; Kolesnikova et al. 2002; Kolesnikova et al. 2004). MLAV VP40 displays more potent activity than MARV VP40 in several assays. To determine whether this might reflect altered cellular accumulation due to different levels of budding from cells, the capacity of EBOV, MARV and MLAV VP40s to bud as VLPs was assessed. Upon expression in human and bat cells, each VP40 budded from both cell types. Furthermore, significant portions of the EBOV, MARV, and MLAV VP40 in cell supernatants were only trypsin-sensitive upon addition of Triton X-100 detergent, consistent with the VP40s from both HEK293T and RO6E cells being protected by a membrane, as is characteristic of filovirus particles (Figure 25A-B).

3.6.5 MLAV VP40 and EBOV VP24 inhibition of IFNβ promotor activation occurs independently of Jak-STAT signaling

The type I IFN response includes a positive feedback loop whereby secreted IFN upregulates pattern recognition receptors, such as RIG-I and transcription factors such as IRF7, to amplify the response (Michalska et al. 2018). It was therefore of interest to test the hypothesis that MLAV VP40, MARV VP40 and EBOV VP24 inhibit virus-induced induction of the IFN response as a result of their inhibition of IFN-induced positive

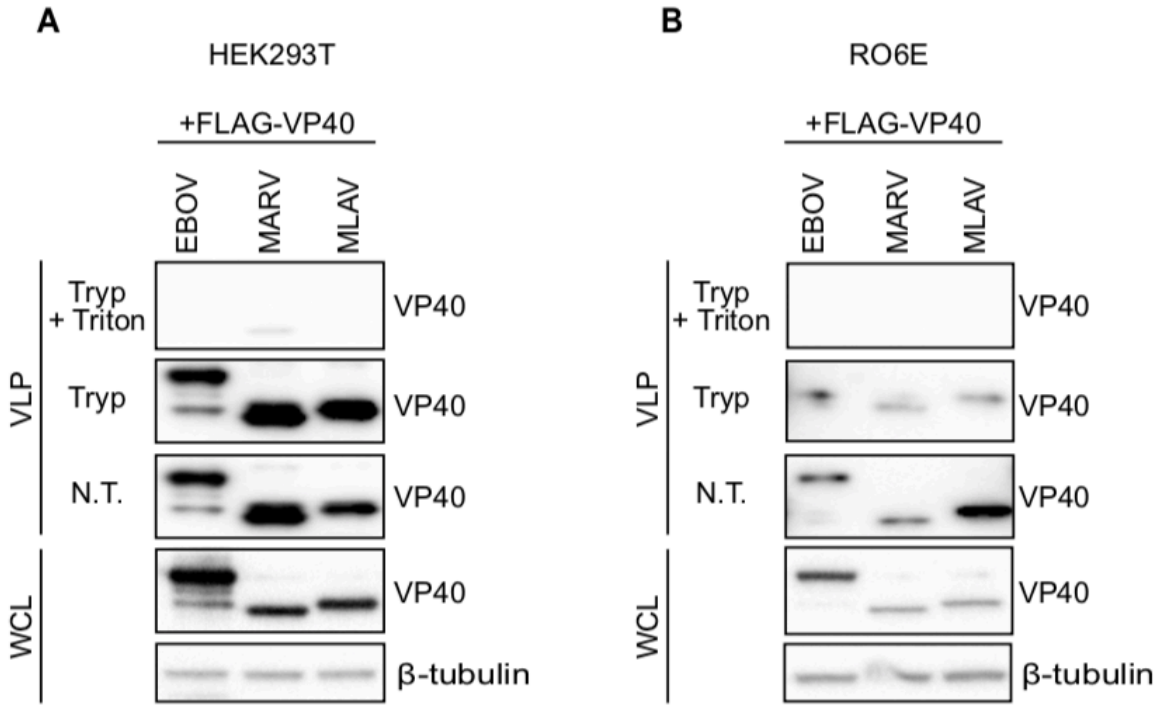

Figure 25 MLAV VP40 is capable of forming virus-like particles from both human and bat cells

To compare the budding of EBOV, MARV, and MLAV VP40 proteins from different cell lines, VLP assays were performed in a HEK293T cells **(A)** and RO6E cells **(B)**. Ten percent of each VLP preparation was subjected to treatment with trypsin (Tryp) or trypsin and Triton X-100 (Tryp+Triton) to determine whether VP40 was contained within a membrane. The presence of VP40 in non-treated (N.T.) and treated VLPs and whole cell lysates (WCL) was assessed by western blot with anti-FLAG antibody. Anti-β-tubulin served as a loading control for the WCL. ***Experiments in A-D performed by Timothy Keiffer.**

feedback loop. Activation of the IFNβ promoter by SeV was therefore assessed by reporter gene assay in the absence or presence of the Jak1/Jak2 inhibitor Ruxolitinib. In this experiment, cells were transfected with empty vector or FLAG-tagged expression plasmids for the EBOV VP35, EBOV, MARV and MLAV VP40 and EBOV VP24, pre-treated with DMSO or Ruxolitinib and then mock- or SeV- infected, in the absence or presence of the inhibitor (Figure 26A). EBOV VP35 acted as a potent suppressor of IFNβ promoter activation under these conditions. MARV VP40, MLAV VP40, and EBOV VP24 all suppressed IFNβ promoter activation to similar extents in the absence or presence of the Jak kinase inhibitor. To confirm that inhibition of IFN

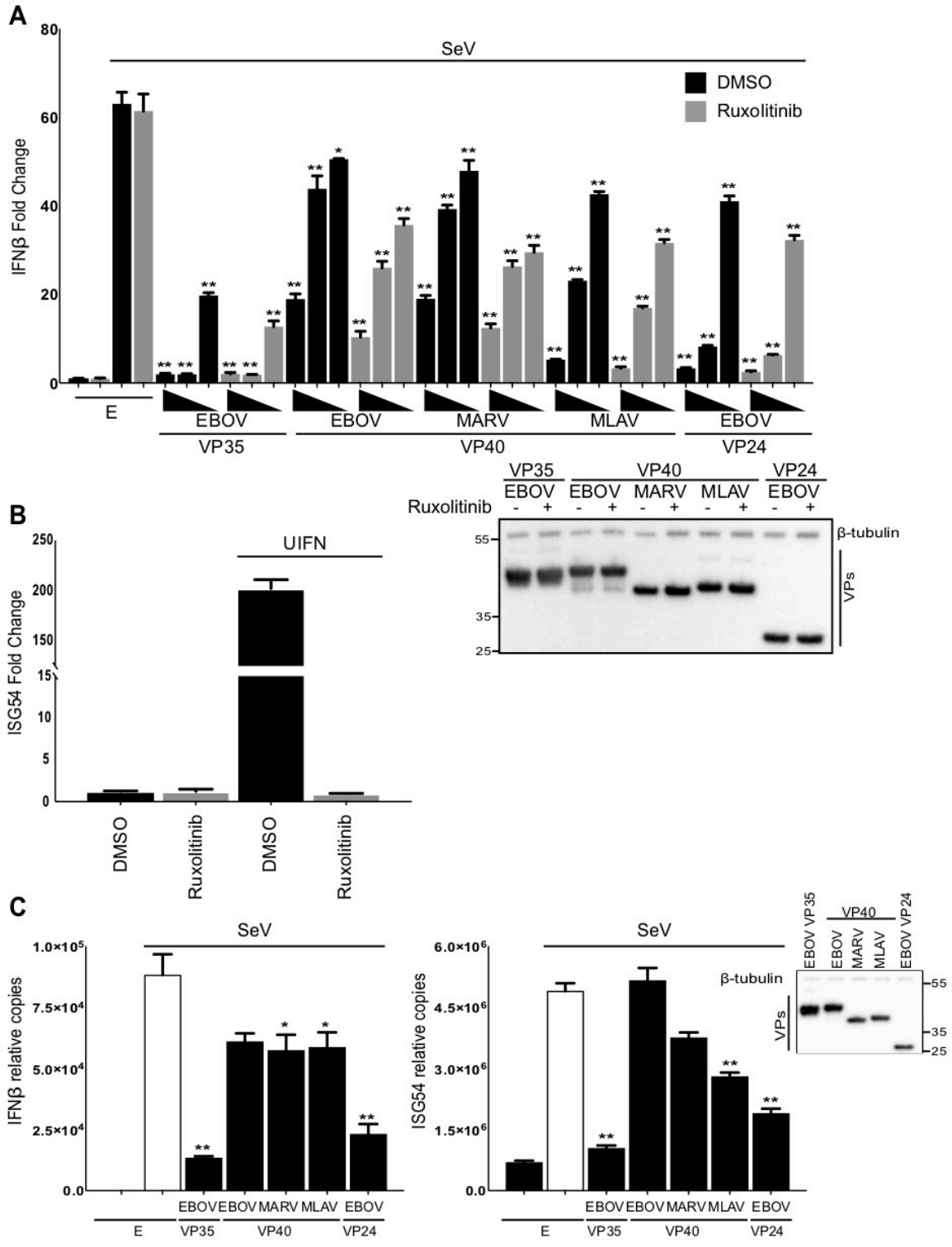

Figure 26 MLAV VP40 blocks Sendai virus-induced IFNβ promoter activation independently of Jak-STAT signaling

HEK293T cells were transfected with an IFNβ promoter firefly luciferase reporter plasmid, a constitutively-expressed *Renilla* luciferase reporter plasmid and either empty vector (E) or the specified FLAG-tagged viral proteins. The amounts of VP35, VP40, and VP24 plasmids were 62.5 ng, 6.25 ng, and 0.625 ng. Twenty-four hours post-transfection, cells were pre-treated with either DMSO or the Jak1/Jak2 inhibitor Ruxolitinib for one hour. Post treatment, cells were mock- or SeV-infected in the presence of DMSO or Ruxolitinib. Firefly and *Renilla* luciferase activities were determined eighteen hours later using a dual luciferase assay (Promega). Fold induction was determined relative to the DMSO vector only, mock-infected samples. Viral protein expression was confirmed by western blotting with anti-FLAG antibody (inset). Anti-β-tubulin served as a loading control (A). HEK293T cells were transfected with an ISG54 promotor firefly luciferase reporter plasmid, a constitutively-expressing *Renilla* luciferase reporter plasmid and empty vector. Twenty-four hours post-transfection, cells were pre-treated with DMSO or Ruxolitinib for one hour. Post-treatment, cells were mock- or UIFN-treated in the presence of DMSO or Ruxolitinib. Firefly and *Renilla* luciferase activities were determined eighteen hours later using a dual luciferase assay (Promega). Fold induction was determined relative to the DMSO, mock-treated samples (B). HEK293T cells were assessed for endogenous human IFNβ and ISG54 mRNA levels in the presence of viral expression plasmids, 125 ng. Results were normalized to human β-actin mRNA levels. Assays were performed in triplicate. Cell lysates were analyzed by western blot with anti-FLAG and anti-β-tubulin antibodies (inset) (C). For A and C, error bars represent the SEM for the triplicate. Statistical significance was determined by performing a one-way ANOVA followed with Tukey multiple comparison as compared to SeV-infected control; **$p < 0.0001$, * $p < 0.001$. ***Experiments performed by Joyce Sweeney Gibbons.**

induced signaling was complete, cells transfected with an ISG54 promoter reporter gene were DMSO or Ruxolitinib treated and then mock or IFN-treated. As expected, IFN activated the ISG54 promoter in the presence of DMSO but not Ruxolitinib (Figure 26B). To validate the inhibitory activities detected in the reporter gene assays, quantitative RT-PCR was performed to detect expression of the endogenous IFNβ and ISG54 mRNA. Consistent with the reporter assays, IFNβ and ISG54 copy numbers were significantly inhibited in the presence of EBOV VP35, EBOV VP24 and both MARV and MLAV VP40 (Figure 26C). It is notable that inhibition of SeV-induced IFN responses by EBOV VP35 was more robust than for the other proteins. That degrees of inhibition were unaffected by the presence of the Ruxolitinib, these data suggest that MARV VP40, MLAV VP40 and EBOV VP24 all utilize mechanisms independent of inhibition of STAT1 phosphorylation to impair induction of type I IFN responses.

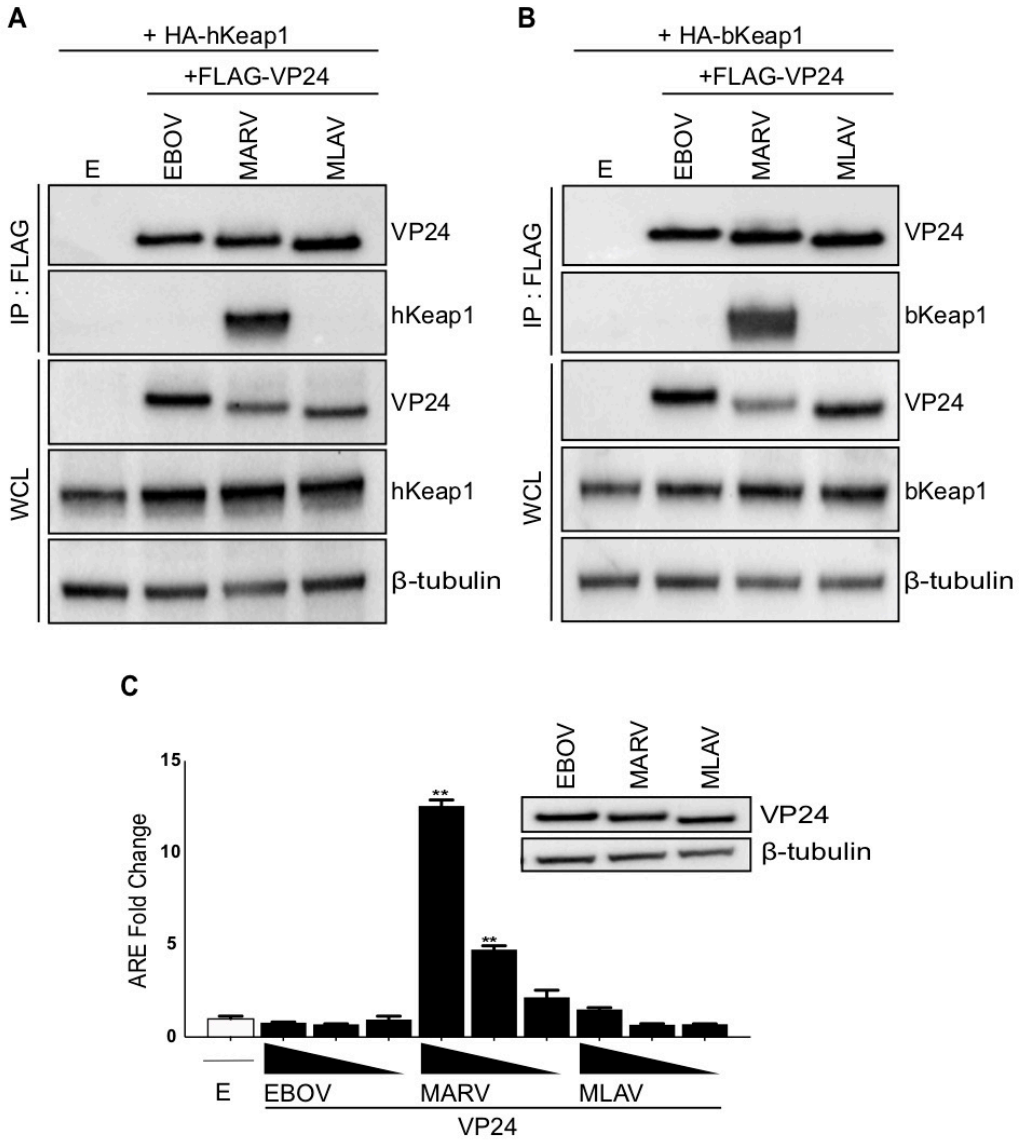

Figure 27 MLAV VP24 does not interact with KEAP1 or activate the ARE response

HEK293T cells were co-transfected with FLAG-tagged EBOV, MARV, MLAV VP24, as indicated, and HA-tagged human Keap1 (hKeap1) (A) or HA-tagged bat Keap1 (bKeap1) (B). Co-immunoprecipitation (IP) was performed with anti-FLAG antibody and precipitates and whole cell lysates (WCL) were assessed by using anti-FLAG (VP24), anti-HA (Keap1) and anti-β-tubulin antibodies. HEK293T cells were transfected with a reporter plasmid with the firefly luciferase gene under the control of an ARE promoter, a reporter plasmid that constitutively expresses *Renilla* luciferase and either empty vector (E) or the indicated FLAG-VP24 proteins. The amounts of VP24 plasmids were 62.5 ng, 6.25 ng and 0.625 ng. Firefly and *Renilla* luciferase activities were determined eighteen hours post-transfection. Firefly luciferase activity was normalized to *Renilla* luciferase activities and fold activity is reported, relative to the empty vector only sample. Protein expression was analyzed by western blot using anti-FLAG (VP24) and anti-β-tubulin antibodies (inset) (C). The reporter gene assays were performed in triplicate; error bars represent the SEM for the triplicate. Statistical significance was determined by performing a one-way ANOVA followed with Tukey multiple comparison as compared to vector only control (white bar); **$p < 0.0001$, * $p < 0.001$. ***Experiments performed by Joyce Sweeney Gibbons.**

3.6.6 MLAV VP24 fails to interact with Keap1 or activate ARE gene expression due to the absence of a Keap1-interacting K-loop

MARV VP24 interacts with Keap1 to activate ARE promoters (Edwards et al. 2014; Page et al. 2014). To determine whether MLAV VP24 possesses similar properties, co-immunoprecipitation experiments were performed with HA-tagged human Keap1 (hKeap1) or HA-tagged Keap1 derived from the bat *Myotis lucifugus* (bKeap1), which is 96.8% identical, at the amino acid level, to the predicted *Rousettus aegypticus* Keap1 (data not shown). As previously described, MARV VP24 interacted with both human and bat Keap1, whereas EBOV and MLAV VP24 did not interact (Figure 27A and 27B). Consistent with these data, when tested in an ARE promoter reporter gene assay, MARV VP24 activated the ARE reporter, relative to an empty vector control, while neither EBOV nor MLAV VP24 activated the ARE response (Figure 27C).

MARV VP24 interaction with Keap1 occurs via a specific motif, the K-loop, and transfer of this sequence to EBOV VP24 confers binding to Keap1 (Edwards et al. 2014). To determine whether this sequence could confer interaction with Keap1 and activation of ARE responses upon MLAV VP24, the MARV VP24 K-loop sequence (amino acid residues 202-219) was transferred to MLAV VP24, replacing the corresponding amino acid residues (MLAV VP24$_{\text{MARV 202-219}}$). The reverse chimera was also generated, with MLAV sequences replacing the K-loop in MARV VP24 (MARV VP24$_{\text{MLAV 202-219}}$) (Figure 8A). Transferring the MARV K-loop sequence to MLAV VP24 conferred the capacity to activate an ARE response while transfer of the MLAV sequence to MARV VP24 abolished the activation (Figure 28B). Interaction with human Keap1 (Figure 28C) and bat Keap1 (Figure 28D) yielded corresponding data, where interaction was

dependent on the MARV VP24 K-loop. Collectively, these data demonstrate that the lack of ARE gene expression by MLAV VP24 is due to the lack of a Keap1 binding motif.

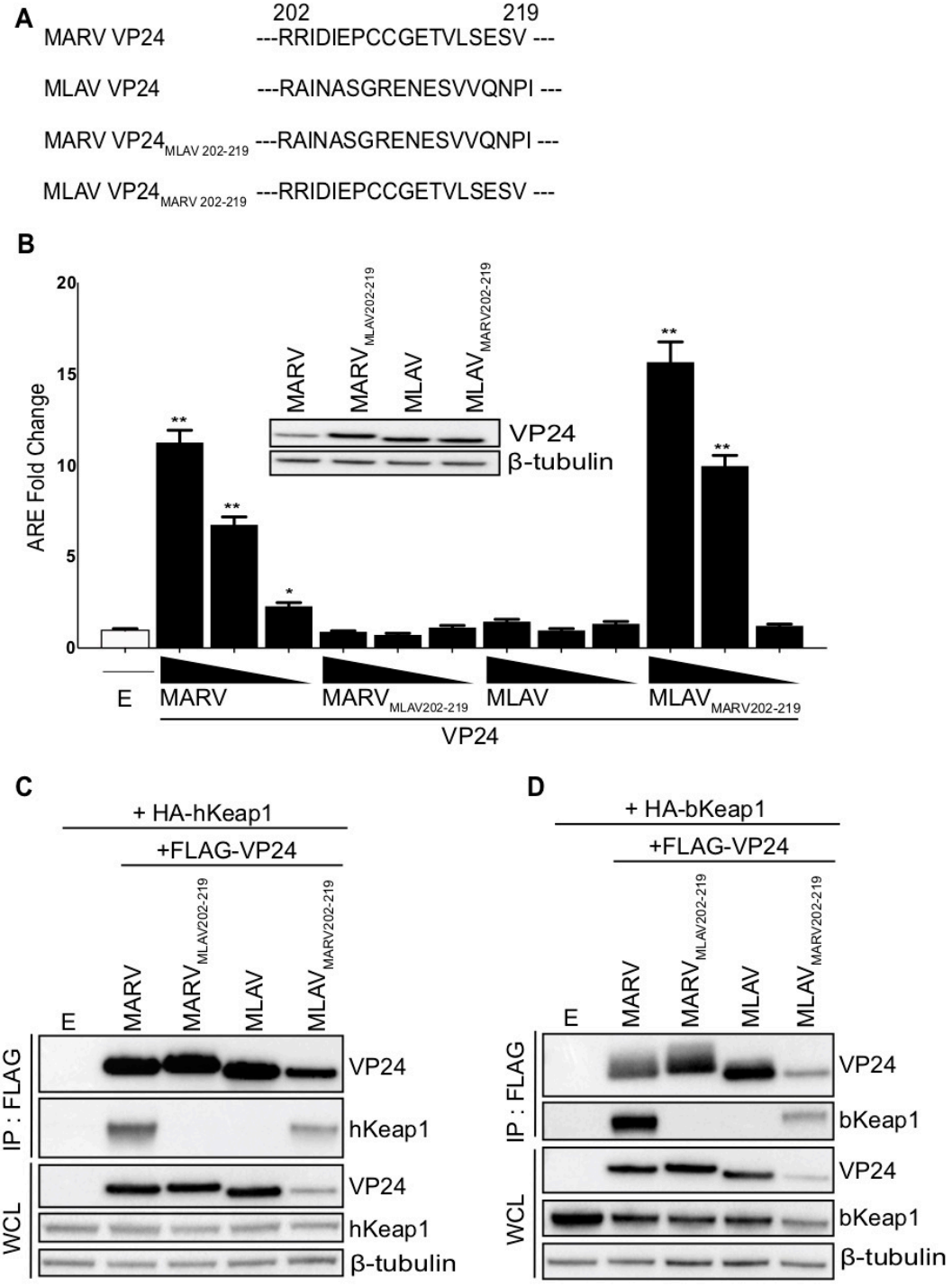

Figure 28 Transfer of the MARV K-Loop sequence confers on MLAV VP24 interaction with Keap1 and activation of ARE signaling

Sequences for amino acid residues 202-219, which correspond to the MARV VP24 K-loop, for MARV VP24, MLAV VP24 and the VP24 chimera constructs MLAV VP24 $_{\text{MARV 202-219}}$ and MARV VP24$_{\text{MLAV 202-219}}$ (A). HEK293T cells were transfected with reporter plasmid with the firefly luciferase gene under the control of an ARE promoter, a reporter plasmid that constitutively expresses *Renilla* luciferase and either empty vector (E) or the indicated FLAG-VP24 proteins. The amounts of VP24 plasmids were 62.5 ng, 6.25 ng and 0.625 ng. Firefly and *Renilla* luciferase activities were determined eighteen hours post transfection. Firefly luciferase activity was normalized to *Renilla* luciferase activities and fold activity is reported, relative to the empty vector only sample. The experiment was performed in triplicate, error bars represent the SEM for the triplicate. Statistical significance was determined by performing a one-way ANOVA followed with Tukey multiple comparison as compared to vector only control (white bar); **$p < 0.0001$, * $p < 0.001$. Cell lysates were analyzed by western blot with anti-FLAG (VP24) and anti-β-tubulin antibodies (Inset) (B). HEK293T cells were transfected with FLAG-tagged constructs, as indicated and either (C) HA-tagged human Keap1 (hKeap1) or (D) HA-tagged bat Keap1 (bKeap1). Co-immunoprecipitation (IP) was performed with anti-FLAG antibody. IPs were analyzed by western blotting with anti-FLAG (VP24), anti-HA (Keap1) and anti-β-tubulin antibodies. WCL, whole cell lysate.

3.6.7 MLAV VP35 and VP40 proteins maintain their ability to inhibit the IFN response in the presence of other viral proteins

In addition to inhibiting IFN responses, VP35 and VP40 are known to form complexes with other viral proteins at various stages of the viral life cycle (Bharat et al. 2012; Huang et al. 2002; Noda et al. 2007a; Watanabe, Noda, and Kawaoka 2006). Both VP35 and VP40 are known to independently interact with the nucleoprotein (NP) and together with the VP24 protein NP and VP35 can form mature nucleocapsids. To determine if the formation of the nucleocapsid complex impacted the ability of VP35 to inhibit IFNβ production, varying amounts of EBOV and MLAV VP35 were transfected in the presence of EBOV or MLAV NP and VP24, respectively. Both EBOV and MLAV VP35 were still able to inhibit SeV-induced activation of the IFNβ promoter in the presence of NP and VP24. (Figure 29A). Similarly, to assess if NP could interfere with the ability of VP40 to inhibit IFN production and signaling we co-transfected varying amounts of MARV VP40 or MLAV VP40 in the presence of NP. MLAV VP40 was still a potent repressor of both SeV-induced activation of the IFNβ promoter and the UIFN-induced activation of the ISG54 promoter in the presence of NP (Figure 29B-C).

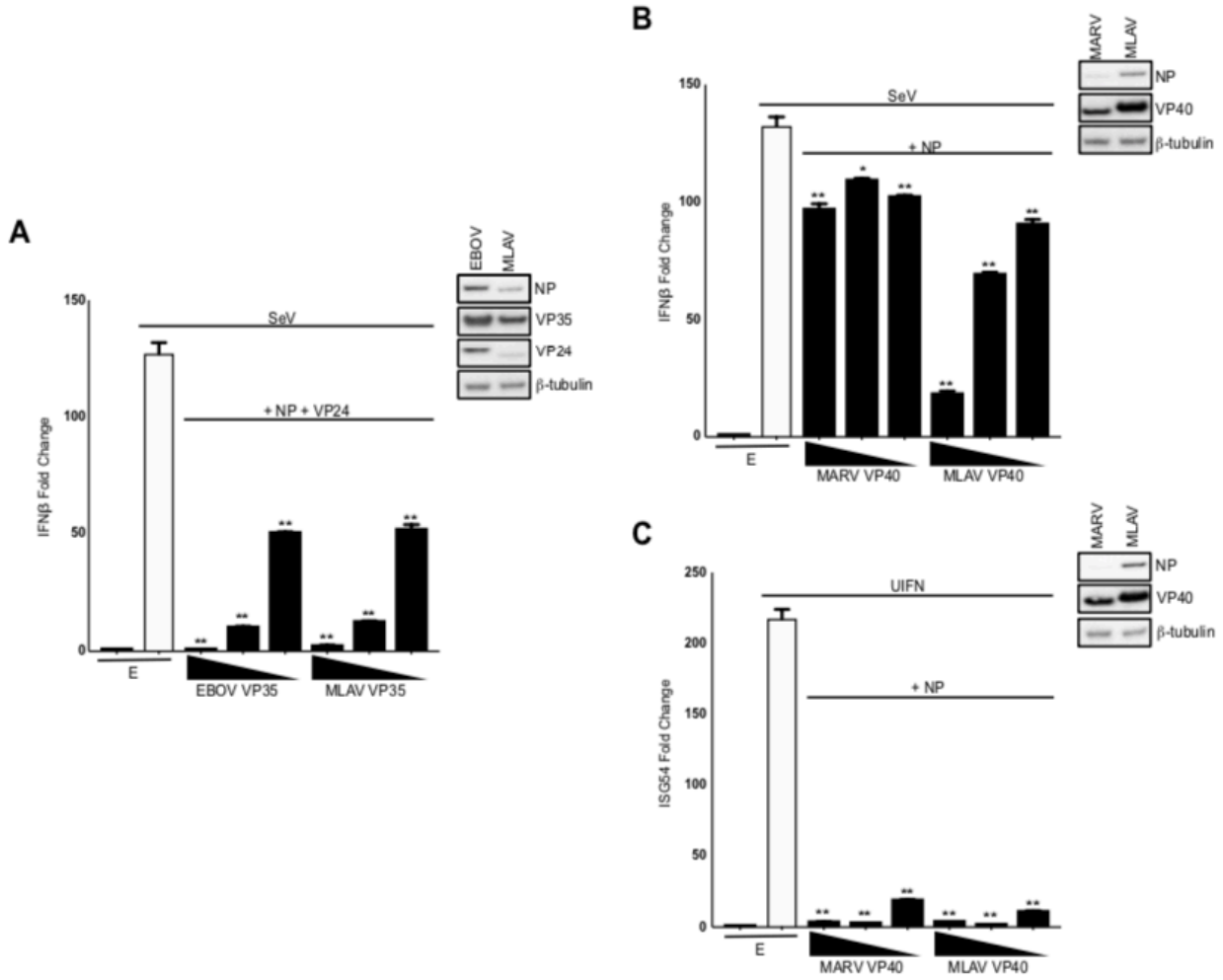

Figure 29 MLAV VP35 and VP40 maintain their ability to inhibit the IFN response in the presence of other viral proteins (Part I)

HEK293T cells were transfected with either an IFNβ (A-B) or an ISG54 (C) promoter firefly luciferase reporter plasmid, a constitutively-expressed Renilla luciferase reporter plasmid and either empty vector (E) or the specified FLAG-tagged viral proteins. **(A)** 62.5 ng, 6.25 ng and 0.625 ng of VP35 plasmid and 6.25 ng of NP and VP24 plasmids. **(B-C)** 62.5 ng, 6.25 ng and 0.625 ng of VP40 plasmid and 6.25 ng of NP plasmid. Twenty-four hours post-transfection, cells were either mock, SeV-infected (A-B), or UIFN-treated (C). Eighteen hours post-treatment, firefly and Renilla luciferase activities were determined. Firefly luciferase values were normalized to Renilla luciferase values and fold induction was calculated relative to the vector only, mock-treated samples Whole cell lysates were analyzed by western blot with anti-FLAG and anti-β-tubulin antibodies (insets). Statistical significance was determined by performing a one-way ANOVA followed with Tukey's multiple comparison test as compared to SeV-infected (A-B) or UIFN-treated (C) control (white bar); **p < 0.0001, *p < 0.001. ***Experiments in A-B performed by Joyce Sweeney Gibbons.**

Lastly, we evaluated the effect of co-transfecting multiple viral proteins together on the inhibitory capabilities of EBOV, MARV, and MLAV. The respective NP, VP35, VP40, VP30 and VP24 plasmids were transfected together in either the IFNβ or ISG54 promotor assay. Upon

activation with either SeV or UIFN, respectively, it was observed that the combination of proteins inhibited the SeV-induced activation of the IFNβ promoter and the UIFN-induced activation of the ISG54 promoter (Figure 30A-B).

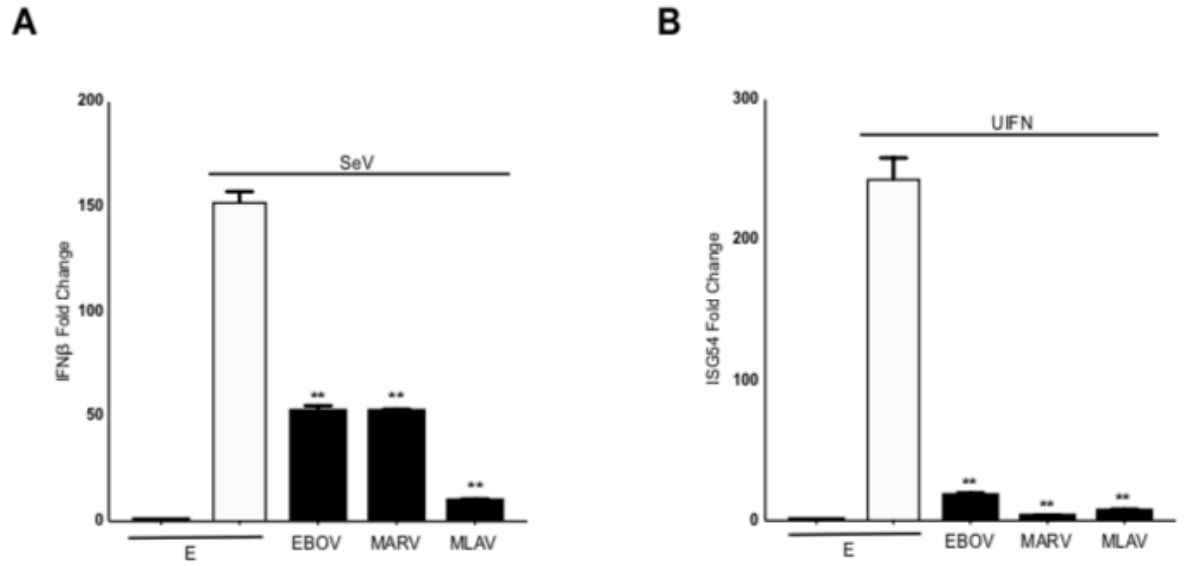

Figure 30 MLAV VP35 and VP40 maintain their ability to inhibit the IFN response in the presence of other viral proteins (Part II)

HEK293T cells were transfected with either an IFNβ (D) or an ISG54 (E) promoter firefly luciferase reporter plasmid, a constitutively-expressed *Renilla* luciferase reporter plasmid and either empty vector (E) or the specified FLAG-tagged viral proteins. 6.25 ng of NP, VP35, VP40, VP30, and VP24 plasmids. Twenty-four hours post-transfection, cells were either mock, SeV-infected (D) or UIFN-treated (E). Eighteen hours post-treatment, firefly and *Renilla* luciferase activities were determined. Firefly luciferase values were normalized to *Renilla* luciferase values and fold induction was calculated relative to the vector only, mock-treated samples. Whole cell lysates were analyzed by western blot with anti-FLAG and anti-β-tubulin antibodies (insets). Statistical significance was determined by performing a one-way ANOVA followed with Tukey's multiple comparison test as compared to SeV-infected (A) or UIFN-treated (B) control (white bar); **$p < 0.0001$, *$p < 0.001$. ***Experiments in A performed by Joyce Sweeney Gibbons.**

3.7 Discussion

The data in this study provide functional evidence that MLAV is biologically distinct from other filoviruses and support its classification in its own genus. The placement of MLAV in a distinct genus was based on its relatively low sequence identity to other filoviruses (Yang et al. 2019). It was also noted to have, compared to other filoviruses, unique gene overlaps and a unique

transcription start signal. Despite these distinctions, MLAV mechanisms of entry and RNA synthesis, based on pseudotype and minigenome assays, mirror those of both EBOV and MARV. MLAV also possesses some features that suggest a closer genetic relationship to members of the *Marburgvirus* genus as opposed to the *Ebolavirus* and *Cuevavirus* genera. This includes similarities in Large (L) protein sequence and the absence of RNA editing sites in GP (Yang et al. 2019). In addition, MLAV was identified in *Rousettus* bats, and *Rousettus* bats in Africa serve as a reservoir for MARV and RAVV (Schuh, Amman, and Towner 2017). The present study demonstrates commonalities and distinctions between MLAV and either EBOV or MARV in terms of how viral proteins antagonize the innate immune response in both bat and human cells. Inhibition of RIG-I induced IFN responses is thus far a common feature of filoviruses (Olejnik, Hume, Leung, Amarasinghe, Basler, and Muhlberger 2017). The suppression of IFN-induced signaling and gene expression by VP40, rather than via VP24, parallels MARV and draws a functional distinction between MLAV and EBOV. The absence of MLAV VP24 interaction with human or bat Keap1, and its lack of ARE transcriptional activation is consistent with MLAV having evolved unique virus-host interactions that are distinct from MARV. These findings further support placement of MLAV in a distinct genus, but also suggest a closer relationship to MARV than EBOV.

The data also demonstrate that MLAV encodes mechanisms to counteract both type I IFN production and cellular responses to exogenous IFN, and that this virus has the potential to antagonize these innate antiviral responses in both bat and human cells. MLAV VP35 was demonstrated to effectively block activation of the IFNβ promoter in response to SeV infection, a known inducer of the RIG-I signaling pathway. In addition, inhibition of SeV-induced phosphorylation of IRF3 was demonstrated. Together, these data indicate that MLAV can block

RIG-I signaling, consistent with the function of other filovirus VP35s (Rehwinkel et al. 2010; Baum, Sachidanandam, and Garcia-Sastre 2010). Mechanistically, inhibition of IFN-α/β production by EBOV or MARV VP35 correlates with dsRNA binding activity (Cardenas et al. 2006; Hartman, Towner, and Nichol 2004; Leung, Prins, et al. 2010; Prins et al. 2010; Bale et al. 2012; Dilley et al. 2017; Luthra et al. 2013; Ramanan et al. 2012; Edwards et al. 2016a). This may reflect binding and sequestration of RIG-I activating dsRNAs (Luthra et al. 2013; Dilley et al. 2017). The VP35 dsRNA binding domain, also known as the interferon inhibitory domain (IID), directly contacts the phosphodiester backbone of dsRNA, via residues that comprise a central basic patch, to mediate this interaction (Edwards et al. 2016a; Kimberlin et al. 2010; Leung et al. 2009a; Leung, Prins, et al. 2010; Ramanan et al. 2012; Bale et al. 2013a). EBOV VP35 also caps the ends of dsRNA in a manner that likely masks 5'-triphosphates, which contribute to recognition of RNAs by RIG-I (Kimberlin et al. 2010; Leung, Prins, et al. 2010). VP35 interaction with host protein PACT, which interacts with and facilitates activation of RIG-I, also contributes to inhibition (Luthra et al. 2013; Kok et al. 2011). Because the residues that make up the central basic patch are conserved between MLAV and other filoviral VP35s, MLAV is likely to bind to dsRNA. Given that it also interacts with PACT, its mechanisms of inhibition are likely similar to other filoviral VP35s.

EBOV, MARV and LLOV VP35 have also been demonstrated to inhibit activation of PKR, an IFN-induced, dsRNA-activated protein kinase that exerts antiviral effects by suppressing translation (Hume and Muhlberger 2018; Edwards et al. 2018; Feagins and Basler 2015b; Schumann, Gantke, and Muhlberger 2009; Feng et al. 2007a). The mechanism by which VP35s inhibit PKR remains ambiguous, however, mutation of multiple central basic patch residues in EBOV or MARV VP35 disrupts the inhibitory activity (Schumann, Gantke, and Muhlberger 2009;

Hume and Muhlberger 2018). In contrast, single point mutations that disrupt EBOV VP35 dsRNA binding activity leave PKR inhibition intact, suggesting that inhibition of PKR is not dependent upon VP35-dsRNA interaction or sequestration (Feng et al. 2007a; Schumann, Gantke, and Muhlberger 2009). Consistent with PKR inhibition being an important function for filoviruses, this activity is conserved in MLAV as well. That the inhibition can occur in human cells further supports the likelihood that MLAV could counter human innate antiviral defenses.

The IFN-inhibitory activities of both EBOV and MARV VP35 have been demonstrated to be important for efficient virus replication in IFN-competent systems (Hartman et al. 2006; Prins et al. 2010). In addition to blocking the production of antiviral IFNs, VP35 inhibition of RIG-I also suppresses maturation of dendritic cells when expressed alone or in the context of EBOV infection (Yen and Basler 2016; Yen et al. 2014; Lubaki et al. 2013). This activity impairs adaptive immunity to EBOV (Lubaki et al. 2016; Ilinykh et al. 2015). Therefore, VP35 likely inhibits adaptive, as well as innate, antiviral defenses. Disruption of VP35 anti-IFN function in the context of recombinant EBOVs has been demonstrated to render the virus avirulent in mice, guinea pigs and non-human primates (Hartman et al. 2008; Prins et al. 2010; Woolsey et al. 2019). Based on these data, VP35 suppression of RIG-I signaling appears to be critical for virulence. The effective function in human cells of MLAV VP35 satisfies one apparent criterion for virulence in humans. It should be noted however, that suppression of RIG-I signaling by VP35 is not sufficient on its own to confer virulence. Even though MARV VP35 functions in *Rousettus* cells and likely has evolved in this species, MARV does not appear to cause significant disease in these animals (Paweska et al. 2012; Jones et al. 2015; Amman et al. 2015). It does seem likely that in the reservoir host, VP35 IFN-antagonist function will be important for efficient replication and transmission, although this remains to be tested experimentally.

For MARV, either infection or VP40 expression alone blocks IFN induced phosphorylation of Jak kinases, inhibiting activation and downstream signaling. The absence of these phosphorylation events in response to IFN-α/β or IFNγ is consistent with the phenotype of Jak1-deficient cells, suggesting that Jak1 function may be targeted by MARV VP40, although there is no evidence to date of VP40-Jak1 interaction (Valmas et al. 2010). Consistent with MARV VP40 impairing Jak1 function, MARV VP40 expression is sufficient to prevent phosphorylation of STAT proteins following Jak1 over-expression or treatment by IFN-α/β or IFNγ (type II IFN) (Valmas et al. 2010). MLAV VP40 likewise blocks ISG expression and inhibits STAT1 phosphorylation following IFN treatment or over-expression of Jak1. Therefore, inhibition of IFN signaling by MLAV VP40 seems likely to proceed by a mechanism similar to that employed by MARV VP40.

MARV VP24 binds directly to Keap1, a cellular substrate adaptor protein of the Cullin-3/Rbx1 E3 ubiquitin ligase complex (Edwards et al. 2014; Johnson et al. 2016; Zhang et al. 2014; Page et al. 2014). Keap1 regulates the cellular antioxidant response (Copple 2012). Under homeostatic conditions, Keap1 promotes Nrf2 polyubiquitination and degradation. Cell stresses, including oxidative stress, disrupt the Keap1-mediated ubiquitination of Nrf2, stabilizing it and promoting Nrf2 dependent expression of antioxidant response genes. Biophysical studies demonstrated that MARV VP24 interacts with the Keap1 Kelch domain at a site that overlaps the region that binds Nrf2 (Johnson et al. 2016). This interaction disrupts Nrf2-Keap1 interaction and activates ARE gene expression (Johnson et al. 2016; Edwards et al. 2014; Page et al. 2014). Keap1 similarly interacts with host kinase IKKβ to repress NF-κB responses and MARV VP24 can also disrupt this interaction, thereby relieving Keap1 repression on the NF-κB transcriptional response (Edwards and Basler 2015). In contrast, EBOV and LLOV VP24 targets KPNA proteins in a

manner that prevents pY-STAT1 nuclear transport, inhibiting ISG expression (Mateo et al. 2010; Reid et al. 2006; Reid et al. 2007; Xu et al. 2014; Feagins and Basler 2015b).

Given that MLAV VP40 mirrored MARV VP40 in its inhibition of the IFN response, it was of interest to determine whether MLAV VP24 would similarly mimic MARV VP24 in terms of interaction with the Keap1-Nrf2 pathway. However, MLAV VP24 lacks a sequence that resembles the MARV VP24 K-loop and, correspondingly, did not interact with human or a bat-derived Keap1 and did not activate an ARE promoter. Chimeric MARV-MLAV VP24 proteins confirmed that the absence of the K-loop sequence can explain the lack of MLAV VP24 effects on antioxidant responses. Furthermore, consistent with the absence of MLAV VP24 inhibitory activity in IFN-signaling assays, it also fails to interact with KPNA1, 5 and 6, which can mediate nuclear import of pY-STAT1. The interface between EBOV VP24 and KPNA covers a large surface area and involves multiple points of contact (Xu et al. 2014). This precluded the mapping of specific amino acid residues that explain the lack of MLAV VP24-KPNA interactions. Nonetheless, these data presented here indicate that MLAV VP24 does not reflect the functions of either MARV or EBOV VP24. It will be of interest to determine whether MLAV VP24 engages different host signaling pathway(s).

The inhibition of IFNβ promoter activity by MLAV VP40 parallels the inhibition by EBOV VP24 and MARV VP40, although inhibition by MLAV VP40 appeared to be more potent. Interestingly, MLAV VP40 inhibits SeV-induced IFNβ gene expression with an efficiency comparable to EBOV VP35, although MLAV VP35 appears to be more potent than MLAV VP40 in this assay. It will be of interest to determine to what extent VP35 and VP40 contribute to suppression of IFN induction in MLAV infected cells. MARV VP40 and EBOV VP24 inhibition of IFN-α/β production and, in the case of EBOV VP24, production of IFN-λ as well, have been

previously reported (Guito et al. 2017; He, Melen, et al. 2017). However, the mechanism(s) for these inhibitory activities are incompletely defined, although EBOV VP24 was implicated as having an effect post-IRF3 phosphorylation (He, Melen, et al. 2017). Inhibition of STAT1 activation and IFN-induced gene expression would be expected to impair the positive feedback loop in which IFN-α/β induces expression of IFN stimulated genes, including RIG-I and IRF7, to amplify IFN responses (Michalska et al. 2018). This prompted additional experiments to determine whether the detected inhibition was a product of blocking a positive feedback loop involving Jak-STAT signaling. Treatment of empty vector-transfected cells with a Jak1/Jak2 inhibitor did not inhibit SeV-induced IFNβ promoter activation, suggesting that in the system used, Jak-STAT signaling does not contribute to the IFNβ response. Further, the dose response of EBOV VP24, MARV VP40 and MLAV VP40 in the IFNβ promoter assay were unaffected. These data suggest MLAV VP40 has an additional mechanism(s) of IFN antagonism that requires further exploration.

Infectious MLAV is not available to allow us to confirm that suppression of IFN responses occurs in infected cells. As an alternative, we asked whether other viral proteins might modulate these activities. We co-transfected MLAV VP35 and MLAV VP40 with other viral proteins that, based on data from EBOV and MARV, would be expected to form functional complexes. VP35, when co-expressed with NP and VP24, forms nucleocapsid structures (Huang et al. 2002; Watanabe, Noda, and Kawaoka 2006). Despite this, NP and VP24 co-expression did not prevent inhibition of the IFNβ promoter by either EBOV or MLAV. Similarly, VP40 interacts with NP (Noda et al. 2007a). However, NP affected neither VP40 suppression of the IFNβ nor the ISG54 promoter. Additionally, co-expression of the internal viral proteins except the Large (L) protein which is expressed at low levels in filovirus-infected cells, also did not prevent suppression of IFN

responses. These findings suggest that these innate immune evasion functions will be active during MLAV infection.

Cumulatively, the present study has identified several functions of MLAV proteins that, in conjunction with previously published data, indicate a compatibility with infection of humans. These include the capacity of MLAV GP to mediate entry into human cells via interaction with NPC1 and suppression of IFN responses through several mechanisms (Yang et al. 2019). Notably, given that MLAV VP24 does not detectably interact with the KPNAs or Keap1, it is likely that it may make unique interactions with host cells. Therefore, the existing data also suggests that the outcome of MLAV infection in humans could differ from that of the typical outcome of EBOV or MARV infection.

3.8 Acknowledgements

The following reagent was obtained through BEI Resources, NIAID, NIH: RO6E, *Rousettus aegyptiacus* (Egyptian fruit bat), Immortalized Fetal Cell Line, NR-49168. This work was supported by NIH grants P01AI120943 and U19AI109945 and Department of the Defense, Defense Threat Reduction Agency grant HDTRA1-16-1-0033. The content of the information does not necessarily reflect the position or the policy of the federal government, and no official endorsement should be inferred. C.F.B. is a Georgia Research Alliance Eminent Scholar in Microbial Pathogenesis.

4 DISCUSSION AND FUTURE DIRECTIONS

4.1 Utilization of VPS34 and fatty acid metabolism by coronaviruses

In late 2019, a novel coronavirus appeared in China and quickly initiated not only the largest coronavirus outbreak on record, but also the most significant pandemic in the last century, resulting in almost a billion cases and worldwide social and economic disruption. The severity of the pandemic prompted urgent efforts to stop the spread and treat those infected, which manifested as a concerted effort to utilize existing antivirals and better understand the requirements of the viral life cycle (Bouhaddou et al. 2020; Gordon, Jang, et al. 2020; Hoffmann et al. 2020; Wang, Wang, et al. 2020). Repurposing of drugs developed for other diseases and conditions that target host factors has been a large part of the process to better understand how SARS-CoV-2 interacts with host-cells to promote infection, not only because it provides a higher-throughput way to identify required enzymes and pathways, but also due to the likelihood of it providing a shortcut to antiviral development (Garcia-Serradilla, Risco, and Pacheco 2019; Li and De Clercq 2020; Pizzorno et al. 2019; Saini et al. 2020).

A known facet of CoV infection is the ability of viral proteins to interact with host cell membranes and membrane machinery to induce rearrangements that promote effective entry, RNA replication, and virion production (Hagemeijer et al. 2014; Prentice et al. 2004; Reggiori, de Haan, and Molinari 2011; Reggiori et al. 2010; Snijder et al. 2020; V'Kovski et al. 2021). A major result of these rearrangements is the formation of a complex reticulovesicular network of interconnected convoluted membranes (CMs), double membrane vesicles (DMVs), and vesicle packets (VPs) thought to function in concentrating and protecting viral replication processes (Knoops et al. 2008; Snijder et al. 2020). Previous studies have observed DMVs colocalizing with LC3, a protein with well-known functions in autophagy; however, studies on mouse

hepatitis virus (MHV) disagree on whether or not autophagy itself is necessary for replication (Reggiori, de Haan, and Molinari 2011; Reggiori et al. 2010; Prentice et al. 2004; Zhao et al. 2007). Alternate models for membrane remodeling implicate EDEMosomes, vesicles originating from the ER that associate with non-lipidated LC3 (Reggiori, de Haan, and Molinari 2011; Reggiori et al. 2010). A common entity in the underlying pathways in these models is VPS34, a class III phosphoinositide 3-kinase that plays important roles in autophagy and endosomal trafficking, as well as other cellular functions (Backer 2016; Ohashi et al. 2020). Inhibition of VPS34 kinase activity has been shown to impair hepatitis C virus (HCV), tombusvirus (TBSV) and coronavirus infections (Feng et al. 2019; Su et al. 2011; Wang et al. 2021).

Additionally, other RNA viruses that induce comparable membrane rearrangements and DMV formation usurp host cell fatty acid metabolism and lipid droplets, cellular organelles that store neutral lipids, as a scaffold and energy source for replication (Cloherty et al. 2020; Heaton and Randall 2011). Pharmacological inhibition of long chain acyl-CoA synthetase (ACS) or diglyceride acyltransferases (DGATs), enzymes involved in the neutral lipid synthesis pathway, inhibits rotavirus (RV) and HCV, possibly reflecting a dependence of these viruses on lipid droplets (Cheung et al. 2010; Kim et al. 2012; Liefhebber et al. 2014). It has also been shown that, targeting upstream fatty acid metabolism enzymes, acetyl-CoA carboxylase (ACC) and fatty acid synthase (FASN), impairs replication of several different viruses including Coxsackievirus B, Chickungunya virus (CHIKV), and several flaviviruses (Ammer et al. 2015; Gaunt et al. 2013; Hitakarun et al. 2020; Merino-Ramos et al. 2016; Tongluan et al. 2017).

Together, this information provided two major pathways for consideration in SARS-CoV-2 membrane rearrangement formation and replication. Chapter one of this dissertation

discusses how VPS34 and fatty acid metabolism are involved in the viral life cycle of SARS-CoV-2 and their attractiveness for potential therapeutic development.

In our investigation into the involvement of VPS34, we tested two well characterized specific and structurally similar inhibitors of VPS34: VPS34-IN1 and PIK-III (Bago et al. 2014; Dowdle et al. 2014). Both inhibitors showed potent inhibition of viral titers at sub-micromolar concentrations in both Vero E6 and Calu-3 cells as measured by resistance assay and plaque assay, respectively (Figure 11 and Figure 14). To further contribute the observed anti-SARS-CoV-2 activity to VPS34 activity, the panel of inhibitors was extended to include Compound 19 and SAR405, the latter of which is structurally distinct from the others (Honda et al. 2016; Pasquier 2015; Ronan et al. 2014). The importance of VPS34 for virus replication was validated by the inhibition of virus growth, consistent with recent reports (Figure 15) (Wang et al. 2021; Yuen et al. 2021). Time of addition studies with VPS34-IN1 and PIK-III suggest inhibition occurs at both early steps, potentially at viral entry, and later steps, including viral RNA synthesis as being sensitive to VPS34 inhibition (Figure 13).

While our inhibitor studies implicate VPS34 as a critical host factor for SARS-CoV-2 replication, they do not differentiate between the various functions of VPS34 that might be involved. Studies in different cell types suggest autophagy is not essential for MHV growth and more recent studies suggest that coronaviruses interfere with autophagy, and that activation of autophagy can inhibit replication of SARS-CoV, MERS CoV, and SARS-CoV-2 (Gassen et al. 2019; Guo et al. 2016; Prentice et al. 2004; Zhao et al. 2007). Using this logic and the fact that inhibitors of VPS34 result in the inhibition of autophagy, it would be expected that inhibition of VPS34 would eliminate these anti-CoV effects of autophagy and promote SARS-CoV-2 replication, contradicting what we are seeing. At the same time, host protein TMEM41B, which

is also implicated in autophagy, has been demonstrated to facilitate SARS-CoV-2 growth, suggesting that the virus may usurp some autophagy functions (Schneider et al. 2021). Separate from autophagy, VPS34 has several other roles, most notably in vesicular trafficking and sorting. VPS34 phosphorylation of phosphoinositol-3 allows for recruitment of various proteins for endosomal fusion and tethering, recruitment of the endosomal sorting complex required for transport (ESCRT) proteins for the formation of multivesicular bodies, and proper functioning of the Retromer complex for endosome-to-Golgi transport (Backer 2016; Ohashi et al. 2020). It will be of interest to further determine whether the diminished replication of SARS due to targeting VPS34 reflects inhibition of autophagy or non-autophagy related functions. VPS34 associates with two main complexes: complex I, which functions in autophagy, and complex II, which functions in endosomal maturation (Backer 2016; Ohashi et al. 2020). One potential option for determining how VPS34 regulates replication, would be to retain VPS34 activity but prevent autophagy flux or endosomal maturation by eliminating factors closely tied to VPS34 in each of the two major pathways. If we can independently disrupt either pathway and obtain comparable inhibition to what we see with VPS34-IN1, we can begin to focus in on one pathway for further characterization of the key host factors utilized by SARS-COV-2.

Interestingly, VPS34 has been shown to be recruited to tombusvirus replication compartments providing increased levels of phosphoinositol-3-phosphate, which allows for recruitment of Rab5-positive early endosomes to provide phosphatidylethanolamine-enriched membranes for replication center formation (Feng et al. 2019). Based on our observation that VPS34-IN1 interferes with the formation of dsRNA positive SARS-CoV-2 replication centers (Figure 17), it is possible that VPS34 functions to facilitate membrane availability for SARS-CoV-2 replication organelle formation. Disruption of endocytic trafficking might also explain

our observation that pre-treatment followed by removal of VPS34 inhibitors had significant effects on early phases of SARS-CoV-2 replication. This provides us with an additional ultrastructural characterization dependent pipeline to pursue in determining the mechanism by which SARS-CoV-2 utilizes VPS34.

Orlistat, an FDA approved inhibitor of fatty acid synthase (FASN), and Triacsin C, an inhibitor of long chain acyl-CoA synthetase (ACS) have previously been examined for their antiviral activities against viruses the utilize fatty acids and neutral lipids for replication (Ammer et al. 2015; Cheung et al. 2010; Gaunt et al. 2013; Hitakarun et al. 2020; Kim et al. 2012; Liefhebber et al. 2014; Tongluan et al. 2017; Wakil and Abu-Elheiga 2009). To begin our study on fatty acid metabolism involvement in SARS-CoV-2 replication, we tested both Orlistat and Triacsin C and found that both exhibited antiviral activity in Vero E6 and Calu-3 cells, with more than ten times higher inhibition being observed in Calu-3 cells (Figure 12 and Figure 14). Inhibition was only observed when treatment was maintained throughout infection, consistent with the post-entry inhibition previously described for other viruses (Figure 13).

Due to the upstream nature of steps in the metabolic pathway inhibited by Orlistat and Triacsin C, we are likely dysregulating downstream pathways, such that the inhibition we see could be the result of downregulation of fatty acid protein modification, β-oxidation of fatty acids in the mitochondria, or neutral lipid synthesis and lipid droplet formation (Baenke et al. 2013). To further determine the mechanistic role of fatty acid metabolism involvement for SARS-CoV-2, we tested a series of compounds that targeted enzymatic steps involved in each one of the aforementioned pathways downstream of FASN. Our results showed that the palmitoyl acetyltransferase (PAT) inhibitor 2-bromopalmitate, which should block protein palmitoylation, led to a substantial reduction in SARS-CoV-2 replication. This may reflect a

requirement for spike modification and/or palmitoylation of envelope and host proteins that has been previously described for other coronaviruses (Figure 16) (McBride and Machamer 2010; Petit et al. 2007; Thorp et al. 2006; Boscarino et al. 2008; Tseng et al. 2014). Additionally, treatment with A922500, a specific inhibitor of DGAT1, resulted in significant reduction of SARS-CoV-2. This inhibition is indicative of a need for neutral lipid synthesis and suggests a critical role for lipid droplets, which have previously been implicated in SARS-CoV-2 replication and assembly (Figure 16) (Dias et al. 2020). Our data with A922500 are consistent with such a model, given that its effects on production of infectious virus were substantially greater than on viral RNA synthesis (Figure 17 and Figure 18). Inhibition of multiple steps of fatty acid β-oxidation by Etomoxir and Trimetazidine (TMZ) has no effect on SARS-CoV-2 replication, ruling out a direct role for fatty-acid catabolism in virus replication (Figure 16).

As previously mentioned, VPS34 and fatty acid metabolism are closely tied to membranes and virally induced membrane rearrangements. Studies tracking newly synthesized RNA during CoV infection show that RNA synthesis occurs at foci referred to as replication centers that correspond to double membrane vesicles produced during coronavirus infection (Snijder et al. 2020). We looked at whether SARS-CoV-2 replication centers might be affected and found that treatment of infected cells with VPS34-IN1 and the inhibitors of different steps of fatty acid metabolism all resulted in aberrant dsRNA and N localization, and the distribution varied depending on the compound used. These data suggest VPS34 and various aspects of fatty acid metabolism play a critical role in proper formation SARS-CoV-2 replication centers and virally induced membrane rearrangements. The conclusion that the observed change in localization is specific to the mechanism by which each inhibitor effects SARS-CoV-2 is further

supported by the lack of localization disruption in samples treated Remdesivir, a compound that specifically inhibits RNA replication (Figure 17).

When investigating whether the change in localization is coupled to changes in RNA synthesis, we found that VPS34-IN1, Triacsin C, Orlistat, and 2-bromopalmitate all reduced genomic N and NSP14 RNA levels to a degree that roughly correlated with the reduction in viral titer, while subgenomic N was only moderately affected in comparison (Figure 18). Determining whether these compounds selectively impact viral genome replication versus subgenomic mRNA production is of interest and warrants future studies. Treatment with TOFA and A922500 reduced genomic N and NSP14 RNA to a substantially lesser degree than the reductions in viral titers. The discrepancy between the reduction in RNA synthesis and infectious virus is consistent with models like rotavirus, where specialized replication organelles function not only as sites of RNA synthesis, but also as sites of virion assembly and maturation. Disruption of these structures moderately reduces RNA synthesis but has a much larger impact on virus assembly and release (Cheung et al. 2010; Gaunt et al. 2013; Kim et al. 2012; Lever and Desselberger 2016). It has been speculated that vesicle packets are the result of merging DMVs to provide a site to bring together newly synthesized RNA and viral proteins for virion assembly (Knoops et al. 2008; Goldsmith et al. 2004). One way we can assess whether this is a contributing factor to the discrepancies we see in RNA levels and titer, would be to do ultrastructural analysis to determine how treatment alters membrane rearrangements and how that effects the localization and quantity of newly forming virions.

The demonstration that SARS-CoV-2 replication is impaired in CRISPR knockout cells lacking FASN expression cells but not in cells that received a non-targeting guide RNA further confirms the requirement for fatty acids. In cells lacking FASN there was a significant reduction

in viral titers that was sustained throughout infection. Further support that the attenuation of replication is due to loss of fatty acid production, is the increased attenuation when the cells were maintained in the presence of fatty acid free medium that lacks potential sources of exogenous fatty acids like FBS. As a means of trying to rescue the phenotype, supplementation was performed with two primary substrates downstream of FASN, palmitic acid and oleic acid (Ackerman et al. 2018; Alsabeeh et al. 2018; Baenke et al. 2013). The result was a significant increase in SARS-CoV-2 replication in FASN KO cells with supplementation when compared to cells without (Figure 19). The ability to rescue infection using fatty acid metabolism products provides a potentially useful approach for further mechanistic characterization of fatty acid metabolism in the SARS-CoV-2 life cycle.

The identification of fatty acid metabolism, and more specifically protein palmitoylation and lipid droplet production, as key components for replication provides important insights into SARS-CoV-2-host interactions. The significant reduction in viral titers observed by inhibiting FASN and DGAT1 offers potential targets for therapeutic design and drug repurposing efforts. For FASN specifically, there are several classes of molecules that are either currently undergoing late phase clinical trials or already FDA approved for various diseases and conditions with differing properties and mechanisms of action (Kridel et al. 2004; Lupu and Menendez 2006; Syed-Abdul et al. 2020; Zaytseva et al. 2018). Investigation of these compounds, alone or in the presence of Remdesivir, could lead to viable treatment options worth further consideration and pre-clinical studies.

4.2 Characterization of filovirus protein immune antagonism

Filoviruses are highly pathogenic zoonotic pathogens that have case fatality rates ranging from 30-90% (Languon and Quaye 2019). As a zoonotic pathogen, filoviruses follow a two-part

transmission cycle with an enzootic phase in which the virus transmits among its natural animal hosts and an epizootic or epidemic phase in which the virus spills over into the human population from its animal host and begins human-to-human transmission (CDC 2016; Plowright et al. 2017). With the looming possibility of spillover from animals to humans, surveillance and sampling of possible host species has been of great importance. Testing of samples isolated from various bats found RNA and virus for *Marburgviruses* and RNA and antibodies for *Ebolaviruses*, making bats the prime suspect for being the natural asymptomatic reservoir for the enzootic transmission phase (Towner et al. 2009; He et al. 2013; Olival et al. 2013; Yuan et al. 2012; Olival and Hayman 2014). As global viral surveillance measures continue, more and more novel filoviruses have been identified including LLOV, BOMV, and the most recently discovered MLAV (Yang et al. 2019; Towner et al. 2009; Goldstein et al. 2018).

As a newly discovered virus in a family of zoonotic pathogens, it is necessary to determine whether there is a possibility of successful human infection by MLAV. An important factor in the pathogenesis of viral infection is the ability of the virus to evade or disrupt the host innate immune response (Plowright et al. 2017; Messaoudi, Amarasinghe, and Basler 2015). For filoviruses, the importance of viral-host interactions that dysregulate the host immune response is well demonstrated (Basler and Amarasinghe 2009; Messaoudi, Amarasinghe, and Basler 2015). Disruption of the anti-IFN function of EBOV VP35 by abrogating its ability to bind to dsRNA has been shown to render the virus avirulent in mice, guinea pigs and non-human primates (Hartman et al. 2008; Prins et al. 2010; Woolsey et al. 2019). While VP35 suppression of RIG-I signaling appears to be critical for virulence, the suppression of RIG-I signaling by VP35 is not sufficient on its own to confer virulence, as is apparent with MARV in *Rousettus* cells where VP35 is functional, but MARV does not appear to cause significant disease in these animals

(Paweska et al. 2012; Jones et al. 2015; Amman et al. 2015). This finding supports the idea that productive infection likely requires the antagonistic functions of multiple proteins, including VP40 and/or VP24. The importance of these proteins in the pathogenicity of filoviruses in new host species was demonstrated during mouse adaption of MARV, EBOV, and RAVV, where serial passaging of the viruses in mice caused mutations in VP40 for MARV and RAVV and VP24 for EBOV that resulted in successful inhibition of IFN signaling (Feagins and Basler 2015a; Valmas and Basler 2011a; Lofts et al. 2011; Warfield et al. 2009; Volchkov et al. 2000; Lofts et al. 2007; Ebihara et al. 2006).

Chapter two of this dissertation investigates MLAV as a novel species in a newly proposed genus and characterizes the capabilities of VP35, VP40, and VP24 as compared to their EBOV and MARV counterparts.

The residues that make up the central basic patch of other filovirus VP35s are conserved in MLAV, suggesting MLAV VP35 is able to bind to dsRNA. Given this information, it was not surprising to see that MLAV VP35 was able to potently inhibit SeV-induced IFNβ promotor activation and phosphorylation of PKR and IRF in a dose dependent manner (Figure 20 and Figure 21). Additionally, MLAV VP35 was found to interacts with PACT (Figure 20). These data together suggest a mechanism of inhibition similar that to other filoviral VP35s, likely blocking RIG-I signaling through shielding dsRNA and acting as a decoy substrate during IRF3 phosphorylation (Rehwinkel et al. 2010; Baum, Sachidanandam, and Garcia-Sastre 2010; Messaoudi, Amarasinghe, and Basler 2015). Determining the RNA binding capabilities of MLAV and whether it sequesters dsRNA by binding the backbone or the backbone and the ends like MARV and EBOV, respectively, is of interest for better understanding the IFN-antagonism

and which of its counterparts it more closely resembles (Bale et al. 2013b; Bale et al. 2012; Basler et al. 2000; Edwards et al. 2016b).

MARV VP40 expression is sufficient to prevent phosphorylation of STAT proteins following Jak1 over-expression or treatment with type I IFN, blocking downstream ISG production (Valmas et al. 2010). Consistent with this, we observed potent inhibition of UIFN-induced ISG54 promotor activation by MLAV VP40 (Figure 22) and inhibition of UIFN- and Jak1 overexpression-induced STAT1 phosphorylation (Figure 23). Our data suggest disruption of IFN signaling by MLAV VP40 seems likely to proceed by a mechanism similar to that employed by MARV VP40. Interestingly, MLAV also showed potent inhibition of SeV-induced IFNβ promoter activity comparable to the inhibition seen by EBOV and MARV VP35. This finding led us to determine whether the observed inhibition was a possible biproduct of blocking a positive feedback loop involving the inhibition Jak-STAT signaling. Treatment with a Jak1/Jak2 inhibitor in the absence of VP40 did not inhibit SeV-induced IFNβ promoter activation, suggesting that Jak-STAT signaling does not contribute to the IFNβ response (Figure 26). Similar, albeit less potent, inhibition was observed for MARV VP40, consistent with previously reports, however no mechanism has been determined (Guito et al. 2017). A potential starting point for future investigation into the mechanism of inhibition is the ability of MARV VP40 to localize to the nucleus (Han et al. 2020). If MARV and MLAV can shuttle in and out of the nucleus, it will be of interest to identify the means by which this trafficking occurs. Neither VP40 contains a classical nuclear localization signal (NLS); however, patches of basic residues, like the one found in MARV and MLAV VP40, can be involved in nuclear transport, providing a starting point for analyzing sequence specific nuclear localization (Oka and Yoneda 2018). Matrix proteins of other NNS RNA viruses are implicated in nuclear mechanisms ranging from

regulating cellular transcription, to IFN antagonism, and regulating viral assembly and budding (Wang et al. 2010; Ciancanelli and Basler 2006; Ghildyal et al. 2003; von Kobbe et al. 2000; Bharaj et al. 2016). The ability to block nuclear localization can help determine the purpose for trafficking and help us better understand the inhibition of IFN production. Additionally, this inhibition can be assessed independently of the nuclear localization using the samepreviously described IFNβ promotor assay coupled to stimulation with components of the signaling pathway that activate RIG-I signaling downstream of SeV activation.

EBOV VP24 disrupts IFN signaling though interaction with KPNA family members to prevent the localization of phosphorylated STATs to the nucleus while MARV VP24 interacts with Keap1 to activate cytoprotective ARE gene expression (Edwards et al. 2014; Johnson et al. 2016; Zhang et al. 2014; Page et al. 2014; Mateo et al. 2010; Reid et al. 2006; Reid et al. 2007). MLAV VP24 appears to lack both of these functions. We observed no significant inhibition of either SeV-induced IFNβ promotor activity or UIFN-induced ISG54 promotor activity (Figure 20 and Figure 22). Consistent with the lack of inhibition of IFN signaling, MLAV VP24 failed to interact with any of the KPNA family members (Figure 24). Additionally, MLAV VP24 lacks a sequence that resembles the MARV VP24 Keap1 binding K-loop and therefore lacked the corresponding interaction with Keap1 and the resulting ARE promoter activation (Figure 27). Chimeric MARV-MLAV VP24 proteins confirmed the absence of the K-loop sequence as the cause for the lack of antioxidant response activation by MLAV VP24 (Figure 28). Since EBOV and MARV function by separate mechanisms, it cannot be ruled out that MLAV VP24 utilizes its own unique strategy to contribute to pathogenicity and virulence. Protein interactome mass spectrometry screens using the EBOV and MARV viral proteins as bait were responsible for identifying the host factors involved in the respective VP24 functions (Pichlmair et al. 2012;

Garcia-Dorival et al. 2014). As this has been successful previously, it is of interest to repeat a similar process for MLAV VP24 to pinpoint any potential novel host interactions and elucidate the functionality, if any, of MLAV VP24.

Lastly, we were interested in seeing whether or not the aforementioned inhibition of host defenses was likely to be relevant in the context of virus infection. The inhibitory activities of MLAV VP35, VP40, and VP24 were assessed in the presence of the NC or RTC proteins depending on the relevant interaction that occurs in a natural infection. The presence of the additional viral proteins had no effect on the previously observed inhibition, further supporting the potential for these proteins to shut down host immune responses and allow for productive human infection (Figure 29 and Figure 30). Unfortunately, the isolated genomic sequence for MLAV is lacking the terminal most non-coding regions that are important for making an artificial replication system, and no live virus was isolated from the bat (Yang et al. 2019). The production of a chimeric minigenome system to study replication and a transcription- and replication- competent virus like particle (trVLP) system to study replication, transcription, and assembly, would be useful in pursuing further studies into more holistic mechanisms of the viral MLAV proteins. If those studies are successful, it would be of interest to try and get an additional step closer to true infection studies by creating a chimeric virus through reverse genetics by incorporating the terminal ends from another filovirus to compensate for what is currently missing from the MLAV sequences.

4.3 Concluding Remarks

Cumulatively, this dissertation has provided evidence for VPS34 and fatty acid metabolism, and more specifically protein palmitoylation and lipid droplet production, as key components for the newly identified SARS-CoV-2 replication. Not only does this provide

important insights into novel host interactions of SARS-CoV-2, but also supports the potential for lipid metabolism as a viable candidate for therapeutic targeting and development. Furthermore, we have characterized the ability of viral proteins from the newest member of the filovirus family, MLAV, to interact with, and antagonize, host innate immune responses in human and bat cells, as compared to their EBOV and MARV counterparts. The results support placement of MLAV in a unique genus, *Dianlovirus*, exhibiting similarities to both the *Ebolavirus* and *Marburgvirus* genera, and the potential for MLAV to cause productive human disease should a spillover event occur. Insight into the mechanism by which these proteins interact with the host should prove valuable in identifying novel pro-viral host factors for the development of filovirus specific antivirals.

References:

Abu-Farha, M., T. A. Thanaraj, M. G. Qaddoumi, A. Hashem, J. Abubaker, and F. Al-Mulla. 2020. 'The Role of Lipid Metabolism in COVID-19 Virus Infection and as a Drug Target', *Int J Mol Sci*, 21.

Ackerman, D., S. Tumanov, B. Qiu, E. Michalopoulou, M. Spata, A. Azzam, H. Xie, M. C. Simon, and J. J. Kamphorst. 2018. 'Triglycerides Promote Lipid Homeostasis during Hypoxic Stress by Balancing Fatty Acid Saturation', *Cell Rep*, 24: 2596-605 e5.

Adedeji, A. O., and H. Lazarus. 2016. 'Biochemical Characterization of Middle East Respiratory Syndrome Coronavirus Helicase', *mSphere*, 1.

Adedeji, A. O., B. Marchand, A. J. Te Velthuis, E. J. Snijder, S. Weiss, R. L. Eoff, K. Singh, and S. G. Sarafianos. 2012. 'Mechanism of nucleic acid unwinding by SARS-CoV helicase', *PLoS One*, 7: e36521.

Al-Omari, A., A. A. Rabaan, S. Salih, J. A. Al-Tawfiq, and Z. A. Memish. 2019. 'MERS coronavirus outbreak: Implications for emerging viral infections', *Diagn Microbiol Infect Dis*, 93: 265-85.

Al-Osail, A. M., and M. J. Al-Wazzah. 2017. 'The history and epidemiology of Middle East respiratory syndrome corona virus', *Multidiscip Respir Med*, 12: 20.

Albariño, César G., Lisa Wiggleton Guerrero, Jessica R. Spengler, Luke S. Uebelhoer, Ayan K. Chakrabarti, Stuart T. Nichol, and Jonathan S. Towner. 2015. 'Recombinant Marburg viruses containing mutations in the IID region of VP35 prevent inhibition of Host immune responses', *Virology*, 476: 85-91.

Aleksandrowicz, Paulina, Andrea Marzi, Nadine Biedenkopf, Nadine Beimforde, Stephan Becker, Thomas Hoenen, Heinz Feldmann, and Hans-Joachim Schnittler. 2011. 'Ebola virus enters host cells by macropinocytosis and clathrin-mediated endocytosis', *The Journal of Infectious Diseases*, 204 Suppl 3: S957-S67.

Alsabeeh, N., B. Chausse, P. A. Kakimoto, A. J. Kowaltowski, and O. Shirihai. 2018. 'Cell culture models of fatty acid overload: Problems and solutions', *Biochim Biophys Acta Mol Cell Biol Lipids*, 1863: 143-51.

Amarante-Mendes, Gustavo P., Sandy Adjemian, Laura Migliari Branco, Larissa C. Zanetti, Ricardo Weinlich, and Karina R. Bortoluci. 2018. 'Pattern Recognition Receptors and the Host Cell Death Molecular Machinery', *Frontiers in Immunology*, 9.

Amman, B. R., M. E. Jones, T. K. Sealy, L. S. Uebelhoer, A. J. Schuh, B. H. Bird, J. D. Coleman-McCray, B. E. Martin, S. T. Nichol, and J. S. Towner. 2015. 'Oral shedding of Marburg virus in experimentally infected Egyptian fruit bats (Rousettus aegyptiacus)', *J Wildl Dis*, 51: 113-24.

Ammer, E., S. Nietzsche, C. Rien, A. Kuhnl, T. Mader, R. Heller, A. Sauerbrei, and A. Henke. 2015. 'The anti-obesity drug orlistat reveals anti-viral activity', *Med Microbiol Immunol*, 204: 635-45.

Anand, K., J. Ziebuhr, P. Wadhwani, J. R. Mesters, and R. Hilgenfeld. 2003. 'Coronavirus main proteinase (3CLpro) structure: basis for design of anti-SARS drugs', *Science*, 300: 1763-7.

Angelini, M. M., M. Akhlaghpour, B. W. Neuman, and M. J. Buchmeier. 2013. 'Severe acute respiratory syndrome coronavirus nonstructural proteins 3, 4, and 6 induce double-membrane vesicles', *mBio*, 4.

Annan, A., F. Ebach, V. M. Corman, R. Krumkamp, Y. Adu-Sarkodie, A. M. Eis-Hubinger, T. Kruppa, A. Simon, J. May, J. Evans, M. Panning, C. Drosten, and J. F. Drexler. 2016. 'Similar virus spectra and seasonality in paediatric patients with acute respiratory disease, Ghana and Germany', *Clin Microbiol Infect*, 22: 340-46.

Anthony, S. J., K. Gilardi, V. D. Menachery, T. Goldstein, B. Ssebide, R. Mbabazi, I. Navarrete-Macias, E. Liang, H. Wells, A. Hicks, A. Petrosov, D. K. Byarugaba, K. Debbink, K. H. Dinnon, T. Scobey, S. H. Randell, B. L. Yount, M. Cranfield, C. K. Johnson, R. S. Baric, W. I. Lipkin, and J. A. Mazet. 2017. 'Further Evidence for Bats as the Evolutionary Source of Middle East Respiratory Syndrome Coronavirus', *mBio*, 8.

Arora, P., M. Jafferany, T. Lotti, R. Sadoughifar, and M. Goldust. 2020. 'Learning from history: Coronavirus outbreaks in the past', *Dermatol Ther*, 33: e13343.

Artika, I. M., A. K. Dewantari, and A. Wiyatno. 2020. 'Molecular biology of coronaviruses: current knowledge', *Heliyon*, 6: e04743.

Au, W. C., P. A. Moore, W. Lowther, Y. T. Juang, and P. M. Pitha. 1995. 'Identification of a member of the interferon regulatory factor family that binds to the interferon-stimulated response element and activates expression of interferon-induced genes', *Proc Natl Acad Sci U S A*, 92: 11657-61.

Backer, J. M. 2016. 'The intricate regulation and complex functions of the Class III phosphoinositide 3-kinase Vps34', *Biochem J*, 473: 2251-71.

Baenke, F., B. Peck, H. Miess, and A. Schulze. 2013. 'Hooked on fat: the role of lipid synthesis in cancer metabolism and tumour development', *Dis Model Mech*, 6: 1353-63.

Bago, R., N. Malik, M. J. Munson, A. R. Prescott, P. Davies, E. Sommer, N. Shpiro, R. Ward, D. Cross, I. G. Ganley, and D. R. Alessi. 2014. 'Characterization of VPS34-IN1, a selective inhibitor of Vps34, reveals that the phosphatidylinositol 3-phosphate-binding SGK3 protein kinase is a downstream target of class III phosphoinositide 3-kinase', *Biochem J*, 463: 413-27.

Baird, L., and A. T. Dinkova-Kostova. 2011. 'The cytoprotective role of the Keap1-Nrf2 pathway', *Arch Toxicol*, 85: 241-72.

Bakhache, W., A. Neyret, J. McKellar, C. Clop, E. Bernard, J. Weger-Lucarelli, and L. Briant. 2019. 'Fatty acid synthase and stearoyl-CoA desaturase-1 are conserved druggable cofactors of Old World Alphavirus genome replication', *Antiviral Res*, 172: 104642.

Bale, S., J. P. Julien, Z. A. Bornholdt, C. R. Kimberlin, P. Halfmann, M. A. Zandonatti, J. Kunert, G. J. Kroon, Y. Kawaoka, I. J. MacRae, I. A. Wilson, and E. O. Saphire. 2012. 'Marburg virus VP35 can both fully coat the backbone and cap the ends of dsRNA for interferon antagonism', *PLoS Pathog*, 8: e1002916.

Bale, S., J. P. Julien, Z. A. Bornholdt, A. S. Krois, I. A. Wilson, and E. O. Saphire. 2013a. 'Ebolavirus VP35 coats the backbone of double-stranded RNA for interferon antagonism', *J Virol*, 87: 10385-8.

Bale, Shridhar, Jean-Philippe Julien, Zachary A. Bornholdt, Alexander S. Krois, Ian A. Wilson, and Erica Ollmann Saphire. 2013b. 'Ebolavirus VP35 Coats the Backbone of Double-Stranded RNA for Interferon Antagonism', *Journal of Virology*, 87: 10385.

Banerjee, A., K. Kulcsar, V. Misra, M. Frieman, and K. Mossman. 2019. 'Bats and Coronaviruses', *Viruses*, 11.

Bào, Yīmíng, Gaya K. Amarasinghe, Christopher F. Basler, Sina Bavari, Alexander Bukreyev, Kartik Chandran, Olga Dolnik, John M. Dye, Hideki Ebihara, Pierre Formenty, Roger Hewson, Gary P. Kobinger, Eric M. Leroy, Elke Mühlberger, Sergey V. Netesov, Jean L. Patterson, Janusz T. Paweska, Sophie J. Smither, Ayato Takada, Jonathan S. Towner, Viktor E. Volchkov, Victoria Wahl-Jensen, and Jens H. Kuhn. 2017. 'Implementation of Objective PASC-Derived Taxon Demarcation Criteria for Official Classification of Filoviruses', *Viruses*, 9.

Baskerville, A., S. P. Fisher-Hoch, G. H. Neild, and A. B. Dowsett. 1985. 'Ultrastructural pathology of experimental Ebola haemorrhagic fever virus infection', *J Pathol*, 147: 199-209.

Basler, C. F., and G. K. Amarasinghe. 2009. 'Evasion of interferon responses by Ebola and Marburg viruses', *J Interferon Cytokine Res*, 29: 511-20.

Basler, C. F., A. Mikulasova, L. Martinez-Sobrido, J. Paragas, E. Mühlberger, M. Bray, H. D. Klenk, P. Palese, and A. García-Sastre. 2003. 'The Ebola virus VP35 protein inhibits activation of interferon regulatory factor 3', *J Virol*, 77: 7945-56.

Basler, C. F., X. Wang, E. Muhlberger, V. Volchkov, J. Paragas, H. D. Klenk, A. Garcia-Sastre, and P. Palese. 2000. 'The Ebola virus VP35 protein functions as a type I IFN antagonist', *Proc Natl Acad Sci U S A*, 97: 12289-94.

Batra, J., J. F. Hultquist, D. Liu, O. Shtanko, J. Von Dollen, L. Satkamp, G. M. Jang, P. Luthra, T. M. Schwarz, G. I. Small, E. Arnett, M. Anantpadma, A. Reyes, D. W. Leung, R. Kaake, P. Haas, C. B. Schmidt, L. S. Schlesinger, D. J. LaCount, R. A. Davey, G. K. Amarasinghe, C. F. Basler, and N. J. Krogan. 2018. 'Protein Interaction Mapping Identifies RBBP6 as a Negative Regulator of Ebola Virus Replication', *Cell*, 175: 1917-30.e13.

Baum, A., R. Sachidanandam, and A. Garcia-Sastre. 2010. 'Preference of RIG-I for short viral RNA molecules in infected cells revealed by next-generation sequencing', *Proc Natl Acad Sci U S A*, 107: 16303-8.

Becker, S., C. Rinne, U. Hofsäss, H. D. Klenk, and E. Mühlberger. 1998. 'Interactions of Marburg virus nucleocapsid proteins', *Virology*, 249: 406-17.

Becquart, Pierre, Tanel Mahlakõiv, Dieudonné Nkoghe, and Eric M. Leroy. 2014. 'Identification of Continuous Human B-Cell Epitopes in the VP35, VP40, Nucleoprotein and Glycoprotein of Ebola Virus', *PLoS One*, 9: e96360.

Beniac, D. R., P. L. Melito, S. L. Devarennes, S. L. Hiebert, M. J. Rabb, L. L. Lamboo, S. M. Jones, and T. F. Booth. 2012. 'The organisation of Ebola virus reveals a capacity for extensive, modular polyploidy', *PLoS One*, 7: e29608.

Benson, K., S. Cramer, and H. J. Galla. 2013. 'Impedance-based cell monitoring: barrier properties and beyond', *Fluids Barriers CNS*, 10: 5.

Bharaj, P., Y. E. Wang, B. E. Dawes, T. E. Yun, A. Park, B. Yen, C. F. Basler, A. N. Freiberg, B. Lee, and R. Rajsbaum. 2016. 'The Matrix Protein of Nipah Virus Targets the E3-Ubiquitin Ligase TRIM6 to Inhibit the IKKepsilon Kinase-Mediated Type-I IFN Antiviral Response', *PLoS Pathog*, 12: e1005880.

Bharat, T. A., T. Noda, J. D. Riches, V. Kraehling, L. Kolesnikova, S. Becker, Y. Kawaoka, and J. A. Briggs. 2012. 'Structural dissection of Ebola virus and its assembly determinants using cryo-electron tomography', *Proc Natl Acad Sci U S A*, 109: 4275-80.

Bharat, T. A., J. D. Riches, L. Kolesnikova, S. Welsch, V. Krahling, N. Davey, M. L. Parsy, S. Becker, and J. A. Briggs. 2011. 'Cryo-electron tomography of Marburg virus particles and their morphogenesis within infected cells', *PLoS Biol*, 9: e1001196.

Booth, T. F., M. J. Rabb, and D. R. Beniac. 2013. 'How do filovirus filaments bend without breaking?', *Trends Microbiol*, 21: 583-93.

Boscarino, J. A., H. L. Logan, J. J. Lacny, and T. M. Gallagher. 2008. 'Envelope protein palmitoylations are crucial for murine coronavirus assembly', *J Virol*, 82: 2989-99.

Bouhaddou, M., D. Memon, B. Meyer, K. M. White, V. V. Rezelj, M. Correa Marrero, B. J. Polacco, J. E. Melnyk, S. Ulferts, R. M. Kaake, J. Batra, A. L. Richards, E. Stevenson, D. E. Gordon, A. Rojc, K. Obernier, J. M. Fabius, M. Soucheray, L. Miorin, E. Moreno, C. Koh, Q. D. Tran, A. Hardy, R. Robinot, T. Vallet, B. E. Nilsson-Payant, C. Hernandez-Armenta, A. Dunham, S. Weigang, J. Knerr, M. Modak, D. Quintero, Y. Zhou, A. Dugourd, A. Valdeolivas, T. Patil, Q. Li, R. Huttenhain, M. Cakir, M. Muralidharan, M. Kim, G. Jang, B. Tutuncuoglu, J. Hiatt, J. Z. Guo, J. Xu, S. Bouhaddou, C. J. P. Mathy, A. Gaulton, E. J. Manners, E. Felix, Y. Shi, M. Goff, J. K. Lim, T. McBride, M. C. O'Neal, Y. Cai, J. C. J. Chang, D. J. Broadhurst, S. Klippsten, E. De Wit, A. R. Leach, T. Kortemme, B. Shoichet, M. Ott, J. Saez-Rodriguez, B. R. tenOever, R. D. Mullins, E. R. Fischer, G. Kochs, R. Grosse, A. Garcia-Sastre, M. Vignuzzi, J. R. Johnson, K. M. Shokat, D. L. Swaney, P. Beltrao, and N. J. Krogan. 2020. 'The Global Phosphorylation Landscape of SARS-CoV-2 Infection', *Cell*, 182: 685-712 e19.

Bouvet, M., I. Imbert, L. Subissi, L. Gluais, B. Canard, and E. Decroly. 2012. 'RNA 3'-end mismatch excision by the severe acute respiratory syndrome coronavirus nonstructural protein nsp10/nsp14 exoribonuclease complex', *Proc Natl Acad Sci U S A*, 109: 9372-7.

Bouvet, M., A. Lugari, C. C. Posthuma, J. C. Zevenhoven, S. Bernard, S. Betzi, I. Imbert, B. Canard, J. C. Guillemot, P. Lecine, S. Pfefferle, C. Drosten, E. J. Snijder, E. Decroly, and X. Morelli. 2014. 'Coronavirus Nsp10, a critical co-factor for activation of multiple replicative enzymes', *J Biol Chem*, 289: 25783-96.

Bowen, E. T., G. Lloyd, W. J. Harris, G. S. Platt, A. Baskerville, and E. E. Vella. 1977. 'Viral haemorrhagic fever in southern Sudan and northern Zaire. Preliminary studies on the aetiological agent', *Lancet*, 1: 571-3.

Brauburger, K., A. J. Hume, E. Muhlberger, and J. Olejnik. 2012. 'Forty-five years of Marburg virus research', *Viruses*, 4: 1878-927.

Brauburger, Kristina, Adam J. Hume, Elke Mühlberger, and Judith Olejnik. 2012. 'Forty-Five Years of Marburg Virus Research', *Viruses*, 4.

Cardenas, W. B., Y. M. Loo, M. Gale, Jr., A. L. Hartman, C. R. Kimberlin, L. Martinez-Sobrido, E. O. Saphire, and C. F. Basler. 2006. 'Ebola virus VP35 protein binds double-stranded RNA and inhibits alpha/beta interferon production induced by RIG-I signaling', *J Virol*, 80: 5168-78.

Carette, Jan E., Matthijs Raaben, Anthony C. Wong, Andrew S. Herbert, Gregor Obernosterer, Nirupama Mulherkar, Ana I. Kuehne, Philip J. Kranzusch, April M. Griffin, Gordon Ruthel, Paola Dal Cin, John M. Dye, Sean P. Whelan, Kartik Chandran, and Thijn R. Brummelkamp. 2011. 'Ebola virus entry requires the cholesterol transporter Niemann–Pick C1', *Nature*, 477: 340-43.

Carvalho, M. A., K. G. Zecchin, F. Seguin, D. C. Bastos, M. Agostini, A. L. Rangel, S. S. Veiga, H. F. Raposo, H. C. Oliveira, M. Loda, R. D. Coletta, and E. Graner. 2008. 'Fatty acid

synthase inhibition with Orlistat promotes apoptosis and reduces cell growth and lymph node metastasis in a mouse melanoma model', *Int J Cancer*, 123: 2557-65.

CDC. 2013. 'CDC SARS Response Timeline'. https://www.cdc.gov/about/history/sars/timeline.htm.

———. 2014. 'Outbreaks Chronology: Marburg Hemorrhagic Fever'. https://www.cdc.gov/vhf/marburg/outbreaks/chronology.html.

———. 2016. 'Virus Ecology- Ebola'. https://www.cdc.gov/vhf/ebola/resources/virus-ecology.html.

———. 2019. 'Middle East Respiratory Syndrome (MERS)'. https://www.cdc.gov/coronavirus/mers/about/index.html.

———. 2021a. '2021 Democratic Republic of the Congo, North Kivu Province'. https://www.cdc.gov/vhf/ebola/outbreaks/drc/2021-february.html.

———. 2021b. 'History of Ebola Virus Disease (EVD) Outbreaks'. https://www.cdc.gov/vhf/ebola/history/chronology.html#anchor_1526565058132.

Chandran, K., N. J. Sullivan, U. Felbor, S. P. Whelan, and J. M. Cunningham. 2005. 'Endosomal proteolysis of the Ebola virus glycoprotein is necessary for infection', *Science*, 308: 1643-5.

Chandrasekharan, J. A., A. Marginean, and N. Sharma-Walia. 2016. 'An insight into the role of arachidonic acid derived lipid mediators in virus associated pathogenesis and malignancies', *Prostaglandins Other Lipid Mediat*, 126: 46-54.

Chazal, N., and D. Gerlier. 2003. 'Virus entry, assembly, budding, and membrane rafts', *Microbiol Mol Biol Rev*, 67: 226-37, table of contents.

Chen, B., S. Fang, J. P. Tam, and D. X. Liu. 2009. 'Formation of stable homodimer via the C-terminal alpha-helical domain of coronavirus nonstructural protein 9 is critical for its function in viral replication', *Virology*, 383: 328-37.

Chen, B., Y. Sun, J. Niu, G. K. Jarugumilli, and X. Wu. 2018. 'Protein Lipidation in Cell Signaling and Diseases: Function, Regulation, and Therapeutic Opportunities', *Cell Chem Biol*, 25: 817-31.

Chen, Y., H. Cai, J. Pan, N. Xiang, P. Tien, T. Ahola, and D. Guo. 2009. 'Functional screen reveals SARS coronavirus nonstructural protein nsp14 as a novel cap N7 methyltransferase', *Proc Natl Acad Sci U S A*, 106: 3484-9.

Chen, Y., Q. Liu, and D. Guo. 2020. 'Emerging coronaviruses: Genome structure, replication, and pathogenesis', *J Med Virol*, 92: 418-23.

Chen, Y., J. Tao, Y. Sun, A. Wu, C. Su, G. Gao, H. Cai, S. Qiu, Y. Wu, T. Ahola, and D. Guo. 2013. 'Structure-function analysis of severe acute respiratory syndrome coronavirus RNA cap guanine-N7-methyltransferase', *J Virol*, 87: 6296-305.

Cheung, W., M. Gill, A. Esposito, C. F. Kaminski, N. Courousse, S. Chwetzoff, G. Trugnan, N. Keshavan, A. Lever, and U. Desselberger. 2010. 'Rotaviruses associate with cellular lipid droplet components to replicate in viroplasms, and compounds disrupting or blocking lipid droplets inhibit viroplasm formation and viral replication', *J Virol*, 84: 6782-98.

Chong, Y. P., J. Y. Song, Y. B. Seo, J. P. Choi, H. S. Shin, and Team Rapid Response. 2015. 'Antiviral Treatment Guidelines for Middle East Respiratory Syndrome', *Infect Chemother*, 47: 212-22.

Chow, K. T., M. Gale, Jr., and Y. M. Loo. 2018. 'RIG-I and Other RNA Sensors in Antiviral Immunity', *Annu Rev Immunol*, 36: 667-94.

Ciancanelli, M. J., and C. F. Basler. 2006. 'Mutation of YMYL in the Nipah virus matrix protein abrogates budding and alters subcellular localization', *J Virol*, 80: 12070-8.

Cloherty, A. P. M., A. D. Olmstead, C. M. S. Ribeiro, and F. Jean. 2020. 'Hijacking of Lipid Droplets by Hepatitis C, Dengue and Zika Viruses-From Viral Protein Moonlighting to Extracellular Release', *Int J Mol Sci*, 21.

Comar, C. E., S. A. Goldstein, Y. Li, B. Yount, R. S. Baric, and S. R. Weiss. 2019. 'Antagonism of dsRNA-Induced Innate Immune Pathways by NS4a and NS4b Accessory Proteins during MERS Coronavirus Infection', *mBio*, 10.

Copple, I. M. 2012. 'The Keap1-Nrf2 cell defense pathway--a promising therapeutic target?', *Adv Pharmacol*, 63: 43-79.

Corman, V. M., D. Muth, D. Niemeyer, and C. Drosten. 2018. 'Hosts and Sources of Endemic Human Coronaviruses', *Adv Virus Res*, 100: 163-88.

Cui, J., F. Li, and Z. L. Shi. 2019. 'Origin and evolution of pathogenic coronaviruses', *Nat Rev Microbiol*, 17: 181-92.

Dabravolski, S. A., and Y. K. Kavalionak. 2020. 'SARS-CoV-2: Structural diversity, phylogeny, and potential animal host identification of spike glycoprotein', *J Med Virol*, 92: 1690-94.

Dahlke, Christine, Sebastian Lunemann, Rahel Kasonta, Benno Kreuels, Stefan Schmiedel, My L. Ly, Sarah K. Fehling, Thomas Strecker, Stephan Becker, Marcus Altfeld, Abdourahmane Sow, Ansgar W. Lohse, César Muñoz-Fontela, and Marylyn M. Addo. 2017. 'Comprehensive Characterization of Cellular Immune Responses Following Ebola Virus Infection', *The Journal of Infectious Diseases*, 215: 287-92.

Daniloski, Z., T. X. Jordan, H. H. Wessels, D. A. Hoagland, S. Kasela, M. Legut, S. Maniatis, E. P. Mimitou, L. Lu, E. Geller, O. Danziger, B. R. Rosenberg, H. Phatnani, P. Smibert, T. Lappalainen, B. R. tenOever, and N. E. Sanjana. 2021. 'Identification of Required Host Factors for SARS-CoV-2 Infection in Human Cells', *Cell*, 184: 92-105 e16.

Darnell, J. E., I. M. Kerr, and G. R. Stark. 1994. 'Jak-STAT pathways and transcriptional activation in response to IFNs and other extracellular signaling proteins', *Science*, 264: 1415.

Davda, D., M. A. El Azzouny, C. T. Tom, J. L. Hernandez, J. D. Majmudar, R. T. Kennedy, and B. R. Martin. 2013. 'Profiling targets of the irreversible palmitoylation inhibitor 2-bromopalmitate', *ACS Chem Biol*, 8: 1912-7.

de Haan, C. A., M. Molinari, and F. Reggiori. 2010. 'Autophagy-independent LC3 function in vesicular traffic', *Autophagy*, 6: 994-6.

de Haan, C. A., and P. J. Rottier. 2005. 'Molecular interactions in the assembly of coronaviruses', *Adv Virus Res*, 64: 165-230.

Decroly, E., C. Debarnot, F. Ferron, M. Bouvet, B. Coutard, I. Imbert, L. Gluais, N. Papageorgiou, A. Sharff, G. Bricogne, M. Ortiz-Lombardia, J. Lescar, and B. Canard. 2011. 'Crystal structure and functional analysis of the SARS-coronavirus RNA cap 2'-O-methyltransferase nsp10/nsp16 complex', *PLoS Pathog*, 7: e1002059.

Decroly, E., I. Imbert, B. Coutard, M. Bouvet, B. Selisko, K. Alvarez, A. E. Gorbalenya, E. J. Snijder, and B. Canard. 2008. 'Coronavirus nonstructural protein 16 is a cap-0 binding enzyme possessing (nucleoside-2'O)-methyltransferase activity', *J Virol*, 82: 8071-84.

DeDiego, M. L., E. Alvarez, F. Almazan, M. T. Rejas, E. Lamirande, A. Roberts, W. J. Shieh, S. R. Zaki, K. Subbarao, and L. Enjuanes. 2007. 'A severe acute respiratory syndrome coronavirus that lacks the E gene is attenuated in vitro and in vivo', *J Virol*, 81: 1701-13.

Deng, X., M. Hackbart, R. C. Mettelman, A. O'Brien, A. M. Mielech, G. Yi, C. C. Kao, and S. C. Baker. 2017. 'Coronavirus nonstructural protein 15 mediates evasion of dsRNA sensors and limits apoptosis in macrophages', *Proc Natl Acad Sci U S A*, 114: E4251-E60.

Denison, M. R., B. Yount, S. M. Brockway, R. L. Graham, A. C. Sims, X. Lu, and R. S. Baric. 2004. 'Cleavage between replicase proteins p28 and p65 of mouse hepatitis virus is not required for virus replication', *J Virol*, 78: 5957-65.

Di, H., A. A. McIntyre, and M. A. Brinton. 2018. 'New insights about the regulation of Nidovirus subgenomic mRNA synthesis', *Virology*, 517: 38-43.

Dias, S. S. G., V. C. Soares, A. C. Ferreira, C. Q. Sacramento, N. Fintelman-Rodrigues, J. R. Temerozo, L. Teixeira, M. A. Nunes da Silva, E. Barreto, M. Mattos, C. S. de Freitas, I. G. Azevedo-Quintanilha, P. P. A. Manso, M. D. Miranda, M. M. Siqueira, E. D. Hottz, C. R. R. Pao, D. C. Bou-Habib, D. F. Barreto-Vieira, F. A. Bozza, T. M. L. Souza, and P. T. Bozza. 2020. 'Lipid droplets fuel SARS-CoV-2 replication and production of inflammatory mediators', *PLoS Pathog*, 16: e1009127.

Dilley, K. A., A. A. Voorhies, P. Luthra, V. Puri, T. B. Stockwell, H. Lorenzi, C. F. Basler, and R. S. Shabman. 2017. 'The Ebola virus VP35 protein binds viral immunostimulatory and host RNAs identified through deep sequencing', *PLoS One*, 12: e0178717.

Dolnik, O., L. Kolesnikova, L. Stevermann, and S. Becker. 2010. 'Tsg101 is recruited by a late domain of the nucleocapsid protein to support budding of Marburg virus-like particles', *J Virol*, 84: 7847-56.

Donaldson, E. F., R. L. Graham, A. C. Sims, M. R. Denison, and R. S. Baric. 2007. 'Analysis of murine hepatitis virus strain A59 temperature-sensitive mutant TS-LA6 suggests that nsp10 plays a critical role in polyprotein processing', *J Virol*, 81: 7086-98.

Dong, Shishang, Kangning Wen, Hongguan Chu, Hui Li, Qianqian Yu, Changhui Wang, and Xiaochun Qin. 2020. 'Crystal structure of the Měnglà virus VP30 C-terminal domain', *Biochemical and Biophysical Research Communications*, 525: 392-97.

Dowdle, W. E., B. Nyfeler, J. Nagel, R. A. Elling, S. Liu, E. Triantafellow, S. Menon, Z. Wang, A. Honda, G. Pardee, J. Cantwell, C. Luu, I. Cornella-Taracido, E. Harrington, P. Fekkes, H. Lei, Q. Fang, M. E. Digan, D. Burdick, A. F. Powers, S. B. Helliwell, S. D'Aquin, J. Bastien, H. Wang, D. Wiederschain, J. Kuerth, P. Bergman, D. Schwalb, J. Thomas, S. Ugwonali, F. Harbinski, J. Tallarico, C. J. Wilson, V. E. Myer, J. A. Porter, D. E. Bussiere, P. M. Finan, M. A. Labow, X. Mao, L. G. Hamann, B. D. Manning, R. A. Valdez, T. Nicholson, M. Schirle, M. S. Knapp, E. P. Keaney, and L. O. Murphy. 2014. 'Selective VPS34 inhibitor blocks autophagy and uncovers a role for NCOA4 in ferritin degradation and iron homeostasis in vivo', *Nat Cell Biol*, 16: 1069-79.

Ebihara, H., A. Takada, D. Kobasa, S. Jones, G. Neumann, S. Theriault, M. Bray, H. Feldmann, and Y. Kawaoka. 2006. 'Molecular determinants of Ebola virus virulence in mice', *PLoS Pathog*, 2: e73.

Eckerle, L. D., X. Lu, S. M. Sperry, L. Choi, and M. R. Denison. 2007. 'High fidelity of murine hepatitis virus replication is decreased in nsp14 exoribonuclease mutants', *J Virol*, 81: 12135-44.

Edwards, M. R., and C. F. Basler. 2015. 'Marburg Virus VP24 Protein Relieves Suppression of the NF-kappaB Pathway Through Interaction With Kelch-like ECH-Associated Protein 1', *J Infect Dis*, 212 Suppl 2: S154-9.

Edwards, M. R., B. Johnson, C. E. Mire, W. Xu, R. S. Shabman, L. N. Speller, D. W. Leung, T. W. Geisbert, G. K. Amarasinghe, and C. F. Basler. 2014. 'The Marburg virus VP24

protein interacts with Keap1 to activate the cytoprotective antioxidant response pathway', *Cell Rep*, 6: 1017-25.

Edwards, M. R., G. Liu, C. E. Mire, S. Sureshchandra, P. Luthra, B. Yen, R. S. Shabman, D. W. Leung, I. Messaoudi, T. W. Geisbert, G. K. Amarasinghe, and C. F. Basler. 2016a. 'Differential Regulation of Interferon Responses by Ebola and Marburg Virus VP35 Proteins', *Cell Rep*, 14: 1632-40.

Edwards, M. R., H. Liu, R. S. Shabman, G. M. Ginell, P. Luthra, P. Ramanan, L. J. Keefe, B. Kollner, G. K. Amarasinghe, D. J. Taylor, D. W. Leung, and C. F. Basler. 2018. 'Conservation of Structure and Immune Antagonist Functions of Filoviral VP35 Homologs Present in Microbat Genomes', *Cell Rep*, 24: 861-72 e6.

Edwards, Megan R., Gai Liu, Chad E. Mire, Suhas Sureshchandra, Priya Luthra, Benjamin Yen, Reed S. Shabman, Daisy W. Leung, Ilhem Messaoudi, Thomas W. Geisbert, Gaya K. Amarasinghe, and Christopher F. Basler. 2016b. 'Differential Regulation of Interferon Responses by Ebola and Marburg Virus VP35 Proteins', *Cell reports*, 14: 1632-40.

Egloff, M. P., F. Ferron, V. Campanacci, S. Longhi, C. Rancurel, H. Dutartre, E. J. Snijder, A. E. Gorbalenya, C. Cambillau, and B. Canard. 2004. 'The severe acute respiratory syndrome-coronavirus replicative protein nsp9 is a single-stranded RNA-binding subunit unique in the RNA virus world', *Proc Natl Acad Sci U S A*, 101: 3792-6.

Elliott, L. H., M. P. Kiley, and J. B. McCormick. 1985. 'Descriptive analysis of Ebola virus proteins', *Virology*, 147: 169-76.

Emanuel, J., A. Marzi, and H. Feldmann. 2018. 'Filoviruses: Ecology, Molecular Biology, and Evolution', *Adv Virus Res*, 100: 189-221.

Enterlein, S., V. Volchkov, M. Weik, L. Kolesnikova, V. Volchkova, H. D. Klenk, and E. Muhlberger. 2006. 'Rescue of recombinant Marburg virus from cDNA is dependent on nucleocapsid protein VP30', *J Virol*, 80: 1038-43.

Feagins, A. R., and C. F. Basler. 2015a. 'Amino Acid Residue at Position 79 of Marburg Virus VP40 Confers Interferon Antagonism in Mouse Cells', *J Infect Dis*, 212 Suppl 2: S219-25.

———. 2015b. 'Lloviu virus VP24 and VP35 proteins function as innate immune antagonists in human and bat cells', *Virology*, 485: 145-52.

Feldmann, H., E. Muhlberger, A. Randolf, C. Will, M. P. Kiley, A. Sanchez, and H. D. Klenk. 1992. 'Marburg virus, a filovirus: messenger RNAs, gene order, and regulatory elements of the replication cycle', *Virus Res*, 24: 1-19.

Feng, Z., M. Cerveny, Z. Yan, and B. He. 2007a. 'The VP35 protein of Ebola virus inhibits the antiviral effect mediated by double-stranded RNA-dependent protein kinase PKR', *J Virol*, 81: 182-92.

Feng, Z., K. Xu, N. Kovalev, and P. D. Nagy. 2019. 'Recruitment of Vps34 PI3K and enrichment of PI3P phosphoinositide in the viral replication compartment is crucial for replication of a positive-strand RNA virus', *PLoS Pathog*, 15: e1007530.

Feng, Zongdi, Melissa Cerveny, Zhipeng Yan, and Bin He. 2007b. 'The VP35 Protein of Ebola Virus Inhibits the Antiviral Effect Mediated by Double-Stranded RNA-Dependent Protein Kinase PKR', *Journal of Virology*, 81: 182.

Finkel, Y., O. Mizrahi, A. Nachshon, S. Weingarten-Gabbay, D. Morgenstern, Y. Yahalom-Ronen, H. Tamir, H. Achdout, D. Stein, O. Israeli, A. Beth-Din, S. Melamed, S. Weiss, T. Israely, N. Paran, M. Schwartz, and N. Stern-Ginossar. 2021. 'The coding capacity of SARS-CoV-2', *Nature*, 589: 125-30.

Forster, P., L. Forster, C. Renfrew, and M. Forster. 2020. 'Phylogenetic network analysis of SARS-CoV-2 genomes', *Proc Natl Acad Sci U S A*, 117: 9241-43.

Garcia-Dorival, I., W. Wu, S. Dowall, S. Armstrong, O. Touzelet, J. Wastling, J. N. Barr, D. Matthews, M. Carroll, R. Hewson, and J. A. Hiscox. 2014. 'Elucidation of the Ebola virus VP24 cellular interactome and disruption of virus biology through targeted inhibition of host-cell protein function', *J Proteome Res*, 13: 5120-35.

Garcia-Serradilla, M., C. Risco, and B. Pacheco. 2019. 'Drug repurposing for new, efficient, broad spectrum antivirals', *Virus Res*, 264: 22-31.

Gassen, N. C., D. Niemeyer, D. Muth, V. M. Corman, S. Martinelli, A. Gassen, K. Hafner, J. Papies, K. Mosbauer, A. Zellner, A. S. Zannas, A. Herrmann, F. Holsboer, R. Brack-Werner, M. Boshart, B. Muller-Myhsok, C. Drosten, M. A. Muller, and T. Rein. 2019. 'SKP2 attenuates autophagy through Beclin1-ubiquitination and its inhibition reduces MERS-Coronavirus infection', *Nat Commun*, 10: 5770.

Gaunt, E. R., W. Cheung, J. E. Richards, A. Lever, and U. Desselberger. 2013. 'Inhibition of rotavirus replication by downregulation of fatty acid synthesis', *J Gen Virol*, 94: 1310-17.

Gaunt, E. R., A. Hardie, E. C. Claas, P. Simmonds, and K. E. Templeton. 2010. 'Epidemiology and clinical presentations of the four human coronaviruses 229E, HKU1, NL63, and OC43 detected over 3 years using a novel multiplex real-time PCR method', *J Clin Microbiol*, 48: 2940-7.

Ghildyal, R., C. Baulch-Brown, J. Mills, and J. Meanger. 2003. 'The matrix protein of Human respiratory syncytial virus localises to the nucleus of infected cells and inhibits transcription', *Arch Virol*, 148: 1419-29.

Gillooly, D. J., I. C. Morrow, M. Lindsay, R. Gould, N. J. Bryant, J. M. Gaullier, R. G. Parton, and H. Stenmark. 2000. 'Localization of phosphatidylinositol 3-phosphate in yeast and mammalian cells', *EMBO J*, 19: 4577-88.

Gillooly, D. J., A. Simonsen, and H. Stenmark. 2001. 'Cellular functions of phosphatidylinositol 3-phosphate and FYVE domain proteins', *Biochem J*, 355: 249-58.

Goldsmith, C. S., K. M. Tatti, T. G. Ksiazek, P. E. Rollin, J. A. Comer, W. W. Lee, P. A. Rota, B. Bankamp, W. J. Bellini, and S. R. Zaki. 2004. 'Ultrastructural characterization of SARS coronavirus', *Emerg Infect Dis*, 10: 320-6.

Goldstein, T., S. J. Anthony, A. Gbakima, B. H. Bird, J. Bangura, A. Tremeau-Bravard, M. N. Belaganahalli, H. L. Wells, J. K. Dhanota, E. Liang, M. Grodus, R. K. Jangra, V. A. DeJesus, G. Lasso, B. R. Smith, A. Jambai, B. O. Kamara, S. Kamara, W. Bangura, C. Monagin, S. Shapira, C. K. Johnson, K. Saylors, E. M. Rubin, K. Chandran, W. I. Lipkin, and J. A. K. Mazet. 2018. 'The discovery of Bombali virus adds further support for bats as hosts of ebolaviruses', *Nat Microbiol*, 3: 1084-89.

Gorbalenya, A. E., E. V. Koonin, A. P. Donchenko, and V. M. Blinov. 1989. 'Coronavirus genome: prediction of putative functional domains in the non-structural polyprotein by comparative amino acid sequence analysis', *Nucleic Acids Res*, 17: 4847-61.

Gordon, C. J., E. P. Tchesnokov, E. Woolner, J. K. Perry, J. Y. Feng, D. P. Porter, and M. Gotte. 2020. 'Remdesivir is a direct-acting antiviral that inhibits RNA-dependent RNA polymerase from severe acute respiratory syndrome coronavirus 2 with high potency', *J Biol Chem*, 295: 6785-97.

Gordon, D. E., J. Hiatt, M. Bouhaddou, V. V. Rezelj, S. Ulferts, H. Braberg, A. S. Jureka, K. Obernier, J. Z. Guo, J. Batra, R. M. Kaake, A. R. Weckstein, T. W. Owens, M. Gupta, S. Pourmal, E. W. Titus, M. Cakir, M. Soucheray, M. McGregor, Z. Cakir, G. Jang, M. J.

O'Meara, T. A. Tummino, Z. Zhang, H. Foussard, A. Rojc, Y. Zhou, D. Kuchenov, R. Huttenhain, J. Xu, M. Eckhardt, D. L. Swaney, J. M. Fabius, M. Ummadi, B. Tutuncuoglu, U. Rathore, M. Modak, P. Haas, K. M. Haas, Z. Z. C. Naing, E. H. Pulido, Y. Shi, I. Barrio-Hernandez, D. Memon, E. Petsalaki, A. Dunham, M. C. Marrero, D. Burke, C. Koh, T. Vallet, J. A. Silvas, C. M. Azumaya, C. Billesbolle, A. F. Brilot, M. G. Campbell, A. Diallo, M. S. Dickinson, D. Diwanji, N. Herrera, N. Hoppe, H. T. Kratochvil, Y. Liu, G. E. Merz, M. Moritz, H. C. Nguyen, C. Nowotny, C. Puchades, A. N. Rizo, U. Schulze-Gahmen, A. M. Smith, M. Sun, I. D. Young, J. Zhao, D. Asarnow, J. Biel, A. Bowen, J. R. Braxton, J. Chen, C. M. Chio, U. S. Chio, I. Deshpande, L. Doan, B. Faust, S. Flores, M. Jin, K. Kim, V. L. Lam, F. Li, J. Li, Y. L. Li, Y. Li, X. Liu, M. Lo, K. E. Lopez, A. A. Melo, F. R. Moss, 3rd, P. Nguyen, J. Paulino, K. I. Pawar, J. K. Peters, T. H. Pospiech, Jr., M. Safari, S. Sangwan, K. Schaefer, P. V. Thomas, A. C. Thwin, R. Trenker, E. Tse, T. K. M. Tsui, F. Wang, N. Whitis, Z. Yu, K. Zhang, Y. Zhang, F. Zhou, D. Saltzberg, Qcrg Structural Biology Consortium, A. J. Hodder, A. S. Shun-Shion, D. M. Williams, K. M. White, R. Rosales, T. Kehrer, L. Miorin, E. Moreno, A. H. Patel, S. Rihn, M. M. Khalid, A. Vallejo-Gracia, P. Fozouni, C. R. Simoneau, T. L. Roth, D. Wu, M. A. Karim, M. Ghoussaini, I. Dunham, F. Berardi, S. Weigang, M. Chazal, J. Park, J. Logue, M. McGrath, S. Weston, R. Haupt, C. J. Hastie, M. Elliott, F. Brown, K. A. Burness, E. Reid, M. Dorward, C. Johnson, S. G. Wilkinson, A. Geyer, D. M. Giesel, C. Baillie, S. Raggett, H. Leech, R. Toth, N. Goodman, K. C. Keough, A. L. Lind, Consortium Zoonomia, R. J. Klesh, K. R. Hemphill, J. Carlson-Stevermer, J. Oki, K. Holden, T. Maures, K. S. Pollard, A. Sali, D. A. Agard, Y. Cheng, J. S. Fraser, A. Frost, N. Jura, T. Kortemme, A. Manglik, D. R. Southworth, R. M. Stroud, D. R. Alessi, P. Davies, M. B. Frieman, T. Ideker, C. Abate, N. Jouvenet, G. Kochs, B. Shoichet, M. Ott, M. Palmarini, K. M. Shokat, A. Garcia-Sastre, J. A. Rassen, R. Grosse, O. S. Rosenberg, K. A. Verba, C. F. Basler, M. Vignuzzi, A. A. Peden, P. Beltrao, and N. J. Krogan. 2020. 'Comparative host-coronavirus protein interaction networks reveal pan-viral disease mechanisms', *Science*, 370.

Gordon, D. E., G. M. Jang, M. Bouhaddou, J. Xu, K. Obernier, K. M. White, M. J. O'Meara, V. V. Rezelj, J. Z. Guo, D. L. Swaney, T. A. Tummino, R. Huttenhain, R. M. Kaake, A. L. Richards, B. Tutuncuoglu, H. Foussard, J. Batra, K. Haas, M. Modak, M. Kim, P. Haas, B. J. Polacco, H. Braberg, J. M. Fabius, M. Eckhardt, M. Soucheray, M. J. Bennett, M. Cakir, M. J. McGregor, Q. Li, B. Meyer, F. Roesch, T. Vallet, A. Mac Kain, L. Miorin, E. Moreno, Z. Z. C. Naing, Y. Zhou, S. Peng, Y. Shi, Z. Zhang, W. Shen, I. T. Kirby, J. E. Melnyk, J. S. Chorba, K. Lou, S. A. Dai, I. Barrio-Hernandez, D. Memon, C. Hernandez-Armenta, J. Lyu, C. J. P. Mathy, T. Perica, K. B. Pilla, S. J. Ganesan, D. J. Saltzberg, R. Rakesh, X. Liu, S. B. Rosenthal, L. Calviello, S. Venkataramanan, J. Liboy-Lugo, Y. Lin, X. P. Huang, Y. Liu, S. A. Wankowicz, M. Bohn, M. Safari, F. S. Ugur, C. Koh, N. S. Savar, Q. D. Tran, D. Shengjuler, S. J. Fletcher, M. C. O'Neal, Y. Cai, J. C. J. Chang, D. J. Broadhurst, S. Klippsten, P. P. Sharp, N. A. Wenzell, D. Kuzuoglu-Ozturk, H. Y. Wang, R. Trenker, J. M. Young, D. A. Cavero, J. Hiatt, T. L. Roth, U. Rathore, A. Subramanian, J. Noack, M. Hubert, R. M. Stroud, A. D. Frankel, O. S. Rosenberg, K. A. Verba, D. A. Agard, M. Ott, M. Emerman, N. Jura, M. von Zastrow, E. Verdin, A. Ashworth, O. Schwartz, C. d'Enfert, S. Mukherjee, M. Jacobson, H. S. Malik, D. G. Fujimori, T. Ideker, C. S. Craik, S. N. Floor, J. S. Fraser, J. D. Gross, A. Sali, B. L. Roth, D. Ruggero, J. Taunton, T. Kortemme, P. Beltrao, M. Vignuzzi, A. Garcia-Sastre, K. M.

Shokat, B. K. Shoichet, and N. J. Krogan. 2020. 'A SARS-CoV-2 protein interaction map reveals targets for drug repurposing', *Nature*, 583: 459-68.

Gosert, R., A. Kanjanahaluethai, D. Egger, K. Bienz, and S. C. Baker. 2002. 'RNA replication of mouse hepatitis virus takes place at double-membrane vesicles', *J Virol*, 76: 3697-708.

Guan, Y., B. J. Zheng, Y. Q. He, X. L. Liu, Z. X. Zhuang, C. L. Cheung, S. W. Luo, P. H. Li, L. J. Zhang, Y. J. Guan, K. M. Butt, K. L. Wong, K. W. Chan, W. Lim, K. F. Shortridge, K. Y. Yuen, J. S. Peiris, and L. L. Poon. 2003. 'Isolation and characterization of viruses related to the SARS coronavirus from animals in southern China', *Science*, 302: 276-8.

Guito, J. C., C. G. Albarino, A. K. Chakrabarti, and J. S. Towner. 2017. 'Novel activities by ebolavirus and marburgvirus interferon antagonists revealed using a standardized in vitro reporter system', *Virology*, 501: 147-65.

Gumel, A. B., S. Ruan, T. Day, J. Watmough, F. Brauer, P. van den Driessche, D. Gabrielson, C. Bowman, M. E. Alexander, S. Ardal, J. Wu, and B. M. Sahai. 2004. 'Modelling strategies for controlling SARS outbreaks', *Proc Biol Sci*, 271: 2223-32.

Guo, L., H. Yu, W. Gu, X. Luo, R. Li, J. Zhang, Y. Xu, L. Yang, N. Shen, L. Feng, and Y. Wang. 2016. 'Autophagy Negatively Regulates Transmissible Gastroenteritis Virus Replication', *Sci Rep*, 6: 23864.

Hagemeijer, M. C., I. Monastyrska, J. Griffith, P. van der Sluijs, J. Voortman, P. M. van Bergen en Henegouwen, A. M. Vonk, P. J. Rottier, F. Reggiori, and C. A. de Haan. 2014. 'Membrane rearrangements mediated by coronavirus nonstructural proteins 3 and 4', *Virology*, 458-459: 125-35.

Hagemeijer, M. C., P. J. Rottier, and C. A. de Haan. 2012. 'Biogenesis and dynamics of the coronavirus replicative structures', *Viruses*, 4: 3245-69.

Halvorson, D. L., and S. A. McCune. 1984. 'Inhibition of fatty acid synthesis in isolated adipocytes by 5-(tetradecyloxy)-2-furoic acid', *Lipids*, 19: 851-6.

Hamre, D., and J. J. Procknow. 1966. 'A new virus isolated from the human respiratory tract', *Proc Soc Exp Biol Med*, 121: 190-3.

Han, Z., S. Dash, C. A. Sagum, G. Ruthel, C. K. Jaladanki, C. T. Berry, M. P. Schwoerer, N. M. Harty, B. D. Freedman, M. T. Bedford, H. Fan, S. S. Sidhu, M. Sudol, O. Shtanko, and R. N. Harty. 2020. 'Modular mimicry and engagement of the Hippo pathway by Marburg virus VP40: Implications for filovirus biology and budding', *PLoS Pathog*, 16: e1008231.

Harcourt, B. H., D. Jukneliene, A. Kanjanahaluethai, J. Bechill, K. M. Severson, C. M. Smith, P. A. Rota, and S. C. Baker. 2004. 'Identification of severe acute respiratory syndrome coronavirus replicase products and characterization of papain-like protease activity', *J Virol*, 78: 13600-12.

Hartman, A. L., B. H. Bird, J. S. Towner, Z. A. Antoniadou, S. R. Zaki, and S. T. Nichol. 2008. 'Inhibition of IRF-3 activation by VP35 is critical for the high level of virulence of ebola virus', *J Virol*, 82: 2699-704.

Hartman, A. L., J. E. Dover, J. S. Towner, and S. T. Nichol. 2006. 'Reverse genetic generation of recombinant Zaire Ebola viruses containing disrupted IRF-3 inhibitory domains results in attenuated virus growth in vitro and higher levels of IRF-3 activation without inhibiting viral transcription or replication', *J Virol*, 80: 6430-40.

Hartman, A. L., J. S. Towner, and S. T. Nichol. 2004. 'A C-terminal basic amino acid motif of Zaire ebolavirus VP35 is essential for type I interferon antagonism and displays high identity with the RNA-binding domain of another interferon antagonist, the NS1 protein of influenza A virus', *Virology*, 328: 177-84.

Harty, R. N., M. E. Brown, G. Wang, J. Huibregtse, and F. P. Hayes. 2000. 'A PPxY motif within the VP40 protein of Ebola virus interacts physically and functionally with a ubiquitin ligase: implications for filovirus budding', *Proc Natl Acad Sci U S A*, 97: 13871-6.

He, B., Z. Li, F. Yang, J. Zheng, Y. Feng, H. Guo, Y. Li, Y. Wang, N. Su, F. Zhang, Q. Fan, and C. Tu. 2013. 'Virome profiling of bats from Myanmar by metagenomic analysis of tissue samples reveals more novel Mammalian viruses', *PLoS One*, 8: e61950.

He, F., K. Melen, S. Maljanen, R. Lundberg, M. Jiang, P. Osterlund, L. Kakkola, and I. Julkunen. 2017. 'Ebolavirus protein VP24 interferes with innate immune responses by inhibiting interferon-lambda1 gene expression', *Virology*, 509: 23-34.

He, J., L. I. Melnik, A. Komin, G. Wiedman, T. Fuselier, C. F. Morris, C. G. Starr, P. C. Searson, W. R. Gallaher, K. Hristova, R. F. Garry, and W. C. Wimley. 2017. 'Ebola Virus Delta Peptide Is a Viroporin', *J Virol*, 91.

Heaton, N. S., and G. Randall. 2011. 'Multifaceted roles for lipids in viral infection', *Trends Microbiol*, 19: 368-75.

Hitakarun, A., S. Khongwichit, N. Wikan, S. Roytrakul, S. Yoksan, S. Rajakam, A. D. Davidson, and D. R. Smith. 2020. 'Evaluation of the antiviral activity of orlistat (tetrahydrolipstatin) against dengue virus, Japanese encephalitis virus, Zika virus and chikungunya virus', *Sci Rep*, 10: 1499.

Hoenen, Thomas, Reed S. Shabman, Allison Groseth, Astrid Herwig, Michaela Weber, Gordian Schudt, Olga Dolnik, Christopher F. Basler, Stephan Becker, and Heinz Feldmann. 2012. 'Inclusion Bodies Are a Site of Ebolavirus Replication', *Journal of Virology*, 86: 11779.

Hoffmann, H. H., W. M. Schneider, F. J. Sanchez-Rivera, J. M. Luna, A. W. Ashbrook, Y. M. Soto-Feliciano, A. A. Leal, J. Le Pen, I. Ricardo-Lax, E. Michailidis, Y. Hao, A. F. Stenzel, A. Peace, C. D. Allis, S. W. Lowe, M. R. MacDonald, J. T. Poirier, and C. M. Rice. 2020. 'Functional interrogation of a SARS-CoV-2 host protein interactome identifies unique and shared coronavirus host factors', *bioRxiv*.

Hofmann-Winkler, H., F. Kaup, and S. Pohlmann. 2012. 'Host cell factors in filovirus entry: novel players, new insights', *Viruses*, 4: 3336-62.

Holshue, M. L., C. DeBolt, S. Lindquist, K. H. Lofy, J. Wiesman, H. Bruce, C. Spitters, K. Ericson, S. Wilkerson, A. Tural, G. Diaz, A. Cohn, L. Fox, A. Patel, S. I. Gerber, L. Kim, S. Tong, X. Lu, S. Lindstrom, M. A. Pallansch, W. C. Weldon, H. M. Biggs, T. M. Uyeki, S. K. Pillai, and V. Case Investigation Team Washington State -nCo. 2020. 'First Case of 2019 Novel Coronavirus in the United States', *N Engl J Med*, 382: 929-36.

Honda, A., E. Harrington, I. Cornella-Taracido, P. Furet, M. S. Knapp, M. Glick, E. Triantafellow, W. E. Dowdle, D. Wiedershain, W. Maniara, C. Moore, P. M. Finan, L. G. Hamann, B. Firestone, L. O. Murphy, and E. P. Keaney. 2016. 'Potent, Selective, and Orally Bioavailable Inhibitors of VPS34 Provide Chemical Tools to Modulate Autophagy in Vivo', *ACS Med Chem Lett*, 7: 72-6.

Honda, Kenya, Hideyuki Yanai, Akinori Takaoka, and Tadatsugu Taniguchi. 2005. 'Regulation of the type I IFN induction: a current view', *International Immunology*, 17: 1367-78.

Hopfner, Karl-Peter, and Veit Hornung. 2020. 'Molecular mechanisms and cellular functions of cGAS–STING signalling', *Nature Reviews Molecular Cell Biology*, 21: 501-21.

Hsiau, Tim, David Conant, Nicholas Rossi, Travis Maures, Kelsey Waite, Joyce Yang, Sahil Joshi, Reed Kelso, Kevin Holden, Brittany L. Enzmann, and Rich Stoner. 2019. 'Inference of CRISPR Edits from Sanger Trace Data', *bioRxiv*: 251082.

Hsu, N. Y., O. Ilnytska, G. Belov, M. Santiana, Y. H. Chen, P. M. Takvorian, C. Pau, H. van der Schaar, N. Kaushik-Basu, T. Balla, C. E. Cameron, E. Ehrenfeld, F. J. van Kuppeveld, and N. Altan-Bonnet. 2010. 'Viral reorganization of the secretory pathway generates distinct organelles for RNA replication', *Cell*, 141: 799-811.

Huang, Y., L. Xu, Y. Sun, and G. J. Nabel. 2002. 'The assembly of Ebola virus nucleocapsid requires virion-associated proteins 35 and 24 and posttranslational modification of nucleoprotein', *Mol Cell*, 10: 307-16.

Huang, Y., C. Yang, X. F. Xu, W. Xu, and S. W. Liu. 2020. 'Structural and functional properties of SARS-CoV-2 spike protein: potential antivirus drug development for COVID-19', *Acta Pharmacol Sin*, 41: 1141-49.

Hume, A., and E. Muhlberger. 2018. 'Marburg Virus Viral Protein 35 Inhibits Protein Kinase R Activation in a Cell Type-Specific Manner', *J Infect Dis*, 218: S403-S08.

Hume, Adam J., and Elke Mühlberger. 2019. 'Distinct Genome Replication and Transcription Strategies within the Growing Filovirus Family', *Journal of Molecular Biology*, 431: 4290-320.

Hurst, K. R., L. Kuo, C. A. Koetzner, R. Ye, B. Hsue, and P. S. Masters. 2005. 'A major determinant for membrane protein interaction localizes to the carboxy-terminal domain of the mouse coronavirus nucleocapsid protein', *J Virol*, 79: 13285-97.

Igal, R. A., P. Wang, and R. A. Coleman. 1997. 'Triacsin C blocks de novo synthesis of glycerolipids and cholesterol esters but not recycling of fatty acid into phospholipid: evidence for functionally separate pools of acyl-CoA', *Biochem J*, 324 (Pt 2): 529-34.

Ilinykh, P. A., N. M. Lubaki, S. G. Widen, L. A. Renn, T. C. Theisen, R. L. Rabin, T. G. Wood, and A. Bukreyev. 2015. 'Different Temporal Effects of Ebola Virus VP35 and VP24 Proteins on Global Gene Expression in Human Dendritic Cells', *J Virol*, 89: 7567-83.

Imbert, I., J. C. Guillemot, J. M. Bourhis, C. Bussetta, B. Coutard, M. P. Egloff, F. Ferron, A. E. Gorbalenya, and B. Canard. 2006. 'A second, non-canonical RNA-dependent RNA polymerase in SARS coronavirus', *EMBO J*, 25: 4933-42.

Imbert, I., E. J. Snijder, M. Dimitrova, J. C. Guillemot, P. Lecine, and B. Canard. 2008. 'The SARS-Coronavirus PLnc domain of nsp3 as a replication/transcription scaffolding protein', *Virus Res*, 133: 136-48.

Ivanov, K. A., V. Thiel, J. C. Dobbe, Y. van der Meer, E. J. Snijder, and J. Ziebuhr. 2004. 'Multiple enzymatic activities associated with severe acute respiratory syndrome coronavirus helicase', *J Virol*, 78: 5619-32.

Ivanov, K. A., and J. Ziebuhr. 2004. 'Human coronavirus 229E nonstructural protein 13: characterization of duplex-unwinding, nucleoside triphosphatase, and RNA 5'-triphosphatase activities', *J Virol*, 78: 7833-8.

Jaber, N., and W. X. Zong. 2013. 'Class III PI3K Vps34: essential roles in autophagy, endocytosis, and heart and liver function', *Ann N Y Acad Sci*, 1280: 48-51.

Jacob, Shevin T., Ian Crozier, William A. Fischer, Angela Hewlett, Colleen S. Kraft, Marc-Antoine de La Vega, Moses J. Soka, Victoria Wahl, Anthony Griffiths, Laura Bollinger, and Jens H. Kuhn. 2020. 'Ebola virus disease', *Nature Reviews Disease Primers*, 6: 13.

Jain, Abhinav K., David A. Bloom, and Anil K. Jaiswal. 2005. 'Nuclear Import and Export Signals in Control of Nrf2 *', *Journal of Biological Chemistry*, 280: 29158-68.

Jasenosky, L. D., G. Neumann, I. Lukashevich, and Y. Kawaoka. 2001a. 'Ebola virus VP40-induced particle formation and association with the lipid bilayer', *Journal of Virology*, 75: 5205-14.

———. 2001b. 'Ebola virus VP40-induced particle formation and association with the lipid bilayer', *J Virol*, 75: 5205-14.

Jin, X., Y. Chen, Y. Sun, C. Zeng, Y. Wang, J. Tao, A. Wu, X. Yu, Z. Zhang, J. Tian, and D. Guo. 2013. 'Characterization of the guanine-N7 methyltransferase activity of coronavirus nsp14 on nucleotide GTP', *Virus Res*, 176: 45-52.

Johnson, B., J. Li, J. Adhikari, M. R. Edwards, H. Zhang, T. Schwarz, D. W. Leung, C. F. Basler, M. L. Gross, and G. K. Amarasinghe. 2016. 'Dimerization Controls Marburg Virus VP24-dependent Modulation of Host Antioxidative Stress Responses', *J Mol Biol*, 428: 3483-94.

Jones, M. E., A. J. Schuh, B. R. Amman, T. K. Sealy, S. R. Zaki, S. T. Nichol, and J. S. Towner. 2015. 'Experimental Inoculation of Egyptian Rousette Bats (Rousettus aegyptiacus) with Viruses of the Ebolavirus and Marburgvirus Genera', *Viruses*, 7: 3420-42.

Jureka, A. S., J. A. Silvas, and C. F. Basler. 2020. 'Propagation, Inactivation, and Safety Testing of SARS-CoV-2', *Viruses*, 12.

Kamitani, W., K. Narayanan, C. Huang, K. Lokugamage, T. Ikegami, N. Ito, H. Kubo, and S. Makino. 2006. 'Severe acute respiratory syndrome coronavirus nsp1 protein suppresses host gene expression by promoting host mRNA degradation', *Proc Natl Acad Sci U S A*, 103: 12885-90.

Kato, H., K. Takahasi, and T. Fujita. 2011. 'RIG-I-like receptors: cytoplasmic sensors for non-self RNA', *Immunol Rev*, 243: 91-8.

Kemenesi, G., K. Kurucz, B. Dallos, B. Zana, F. Foldes, S. Boldogh, T. Gorfol, M. W. Carroll, and F. Jakab. 2018. 'Re-emergence of Lloviu virus in Miniopterus schreibersii bats, Hungary, 2016', *Emerg Microbes Infect*, 7: 66.

Kim, Y., D. George, A. M. Prior, K. Prasain, S. Hao, D. D. Le, D. H. Hua, and K. O. Chang. 2012. 'Novel triacsin C analogs as potential antivirals against rotavirus infections', *Eur J Med Chem*, 50: 311-8.

Kimberlin, C. R., Z. A. Bornholdt, S. Li, V. L. Woods, Jr., I. J. MacRae, and E. O. Saphire. 2010. 'Ebolavirus VP35 uses a bimodal strategy to bind dsRNA for innate immune suppression', *Proc Natl Acad Sci U S A*, 107: 314-9.

Kindler, E., C. Gil-Cruz, J. Spanier, Y. Li, J. Wilhelm, H. H. Rabouw, R. Zust, M. Hwang, P. V'Kovski, H. Stalder, S. Marti, M. Habjan, L. Cervantes-Barragan, R. Elliot, N. Karl, C. Gaughan, F. J. van Kuppeveld, R. H. Silverman, M. Keller, B. Ludewig, C. C. Bergmann, J. Ziebuhr, S. R. Weiss, U. Kalinke, and V. Thiel. 2017. 'Early endonuclease-mediated evasion of RNA sensing ensures efficient coronavirus replication', *PLoS Pathog*, 13: e1006195.

Kirchdoerfer, R. N., H. Wasserman, G. K. Amarasinghe, and E. O. Saphire. 2017. 'Filovirus Structural Biology: The Molecules in the Machine', *Curr Top Microbiol Immunol*, 411: 381-417.

Kirtipal, N., S. Bharadwaj, and S. G. Kang. 2020. 'From SARS to SARS-CoV-2, insights on structure, pathogenicity and immunity aspects of pandemic human coronaviruses', *Infect Genet Evol*, 85: 104502.

Klumperman, J., J. K. Locker, A. Meijer, M. C. Horzinek, H. J. Geuze, and P. J. Rottier. 1994. 'Coronavirus M proteins accumulate in the Golgi complex beyond the site of virion budding', *J Virol*, 68: 6523-34.

Knipe, David M., and Peter M. Howley. 2013. *Fields virology* (Lippincott Williams & Wilkins Health: Philadelphia, PA).

Knoops, K., M. Kikkert, S. H. Worm, J. C. Zevenhoven-Dobbe, Y. van der Meer, A. J. Koster, A. M. Mommaas, and E. J. Snijder. 2008. 'SARS-coronavirus replication is supported by a reticulovesicular network of modified endoplasmic reticulum', *PLoS Biol*, 6: e226.

Kok, K. H., P. Y. Lui, M. H. Ng, K. L. Siu, S. W. Au, and D. Y. Jin. 2011. 'The double-stranded RNA-binding protein PACT functions as a cellular activator of RIG-I to facilitate innate antiviral response', *Cell Host Microbe*, 9: 299-309.

Kolesnikova, L., S. Bamberg, B. Berghofer, and S. Becker. 2004. 'The matrix protein of Marburg virus is transported to the plasma membrane along cellular membranes: exploiting the retrograde late endosomal pathway', *J Virol*, 78: 2382-93.

Kolesnikova, L., H. Bugany, H. D. Klenk, and S. Becker. 2002. 'VP40, the matrix protein of Marburg virus, is associated with membranes of the late endosomal compartment', *J Virol*, 76: 1825-38.

Kridel, S. J., F. Axelrod, N. Rozenkrantz, and J. W. Smith. 2004. 'Orlistat is a novel inhibitor of fatty acid synthase with antitumor activity', *Cancer Res*, 64: 2070-5.

Krijnse-Locker, J., M. Ericsson, P. J. Rottier, and G. Griffiths. 1994. 'Characterization of the budding compartment of mouse hepatitis virus: evidence that transport from the RER to the Golgi complex requires only one vesicular transport step', *J Cell Biol*, 124: 55-70.

Kuhajda, F. P., E. S. Pizer, J. N. Li, N. S. Mani, G. L. Frehywot, and C. A. Townsend. 2000. 'Synthesis and antitumor activity of an inhibitor of fatty acid synthase', *Proc Natl Acad Sci U S A*, 97: 3450-4.

Kuhn, J. H., G. K. Amarasinghe, C. F. Basler, S. Bavari, A. Bukreyev, K. Chandran, I. Crozier, O. Dolnik, J. M. Dye, P. B. H. Formenty, A. Griffiths, R. Hewson, G. P. Kobinger, E. M. Leroy, E. Muhlberger, Cyrillicsmall ie Cyrillicsmall te Cyrillicsmall io Russiansmall es Cyrillicsmall o Cyrillicsmall ve Cyrillic capital E. S. Cyrillicsmall ie Cyrillicsmall er Cyrillicsmall ghe Cyrillicsmall ie Cyrillicsmall short i Cyrillic capital V. E. Cyrillicsmall i Cyrillicsmall ka Cyrillicsmall te Cyrillicsmall o Cyrillicsmall er Cyrillicsmall o Cyrillicsmall ve Cyrillicsmall i Cyrillicsmall che Cyrillic S. V. Netesov capital En, G. Palacios, B. Palyi, J. T. Paweska, S. J. Smither, A. Takada, J. S. Towner, V. Wahl, and Consortium Ictv Report. 2019. 'ICTV Virus Taxonomy Profile: Filoviridae', *J Gen Virol*, 100: 911-12.

Kuhn, J. H., S. R. Radoshitzky, A. C. Guth, K. L. Warfield, W. Li, M. J. Vincent, J. S. Towner, S. T. Nichol, S. Bavari, H. Choe, M. J. Aman, and M. Farzan. 2006. 'Conserved receptor-binding domains of Lake Victoria marburgvirus and Zaire ebolavirus bind a common receptor', *J Biol Chem*, 281: 15951-8.

Kupferschmidt, Kai. 2021. "New Ebola outbreak likely sparked by a person infected 5 years ago." In *The Scientist*. https://www.sciencemag.org/news/2021/03/new-ebola-outbreak-likely-sparked-person-infected-5-years-ago: The Scientist.

Kutateladze, T. G. 2007. 'Mechanistic similarities in docking of the FYVE and PX domains to phosphatidylinositol 3-phosphate containing membranes', *Prog Lipid Res*, 46: 315-27.

Languon, S., and O. Quaye. 2019. 'Filovirus Disease Outbreaks: A Chronological Overview', *Virology (Auckl)*, 10: 1178122X19849927.

Larson, H. E., S. E. Reed, and D. A. Tyrrell. 1980. 'Isolation of rhinoviruses and coronaviruses from 38 colds in adults', *J Med Virol*, 5: 221-9.

Lau, S. K., P. C. Woo, K. S. Li, Y. Huang, H. W. Tsoi, B. H. Wong, S. S. Wong, S. Y. Leung, K. H. Chan, and K. Y. Yuen. 2005. 'Severe acute respiratory syndrome coronavirus-like virus in Chinese horseshoe bats', *Proc Natl Acad Sci U S A*, 102: 14040-5.

Le Sage, V., A. Cinti, S. McCarthy, R. Amorim, S. Rao, G. L. Daino, E. Tramontano, D. R. Branch, and A. J. Mouland. 2017. 'Ebola virus VP35 blocks stress granule assembly', *Virology*, 502: 73-83.

Lee, J. Y., S. Bae, and J. Myoung. 2019. 'Middle East Respiratory Syndrome Coronavirus-Encoded Accessory Proteins Impair MDA5-and TBK1-Mediated Activation of NF-kappaB', *J Microbiol Biotechnol*, 29: 1316-23.

Lehmann, K. C., A. Gulyaeva, J. C. Zevenhoven-Dobbe, G. M. Janssen, M. Ruben, H. S. Overkleeft, P. A. van Veelen, D. V. Samborskiy, A. A. Kravchenko, A. M. Leontovich, I. A. Sidorov, E. J. Snijder, C. C. Posthuma, and A. E. Gorbalenya. 2015. 'Discovery of an essential nucleotidylating activity associated with a newly delineated conserved domain in the RNA polymerase-containing protein of all nidoviruses', *Nucleic Acids Res*, 43: 8416-34.

Leung, D. W., N. D. Ginder, D. B. Fulton, J. Nix, C. F. Basler, R. B. Honzatko, and G. K. Amarasinghe. 2009a. 'Structure of the Ebola VP35 interferon inhibitory domain', *Proc Natl Acad Sci U S A*, 106: 411-6.

Leung, D. W., K. C. Prins, D. M. Borek, M. Farahbakhsh, J. M. Tufariello, P. Ramanan, J. C. Nix, L. A. Helgeson, Z. Otwinowski, R. B. Honzatko, C. F. Basler, and G. K. Amarasinghe. 2010. 'Structural basis for dsRNA recognition and interferon antagonism by Ebola VP35', *Nat Struct Mol Biol*, 17: 165-72.

Leung, D. W., R. S. Shabman, M. Farahbakhsh, K. C. Prins, D. M. Borek, T. Wang, E. Mühlberger, C. F. Basler, and G. K. Amarasinghe. 2010. 'Structural and functional characterization of Reston Ebola virus VP35 interferon inhibitory domain', *J Mol Biol*, 399: 347-57.

Leung, Daisy W., Nathaniel D. Ginder, D. Bruce Fulton, Jay Nix, Christopher F. Basler, Richard B. Honzatko, and Gaya K. Amarasinghe. 2009b. 'Structure of the Ebola VP35 interferon inhibitory domain', *Proceedings of the National Academy of Sciences*, 106: 411.

Lever, A., and U. Desselberger. 2016. 'Rotavirus replication and the role of cellular lipid droplets: New therapeutic targets?', *J Formos Med Assoc*, 115: 389-94.

Li, F. 2016. 'Structure, Function, and Evolution of Coronavirus Spike Proteins', *Annu Rev Virol*, 3: 237-61.

Li, G., and E. De Clercq. 2020. 'Therapeutic options for the 2019 novel coronavirus (2019-nCoV)', *Nat Rev Drug Discov*, 19: 149-50.

Li, W., Z. Shi, M. Yu, W. Ren, C. Smith, J. H. Epstein, H. Wang, G. Crameri, Z. Hu, H. Zhang, J. Zhang, J. McEachern, H. Field, P. Daszak, B. T. Eaton, S. Zhang, and L. F. Wang. 2005. 'Bats are natural reservoirs of SARS-like coronaviruses', *Science*, 310: 676-9.

Li, X., J. Zai, Q. Zhao, Q. Nie, Y. Li, B. T. Foley, and A. Chaillon. 2020. 'Evolutionary history, potential intermediate animal host, and cross-species analyses of SARS-CoV-2', *J Med Virol*, 92: 602-11.

Licata, J. M., M. Simpson-Holley, N. T. Wright, Z. Han, J. Paragas, and R. N. Harty. 2003. 'Overlapping motifs (PTAP and PPEY) within the Ebola virus VP40 protein function independently as late budding domains: involvement of host proteins TSG101 and VPS-4', *J Virol*, 77: 1812-9.

Liefhebber, J. M., C. V. Hague, Q. Zhang, M. J. Wakelam, and J. McLauchlan. 2014. 'Modulation of triglyceride and cholesterol ester synthesis impairs assembly of infectious hepatitis C virus', *J Biol Chem*, 289: 21276-88.

Lofts, L. L., M. S. Ibrahim, D. L. Negley, M. C. Hevey, and A. L. Schmaljohn. 2007. 'Genomic differences between guinea pig lethal and nonlethal Marburg virus variants', *J Infect Dis*, 196 Suppl 2: S305-12.

Lofts, Loreen L., Jay B. Wells, Sina Bavari, and Kelly L. Warfield. 2011. 'Key Genomic Changes Necessary for an In Vivo Lethal Mouse Marburgvirus Variant Selection Process', *Journal of Virology*, 85: 3905.

Lubaki, N. M., P. Ilinykh, C. Pietzsch, B. Tigabu, A. N. Freiberg, R. A. Koup, and A. Bukreyev. 2013. 'The lack of maturation of Ebola virus-infected dendritic cells results from the cooperative effect of at least two viral domains', *J Virol*, 87: 7471-85.

Lubaki, N. M., P. Younan, R. I. Santos, M. Meyer, M. Iampietro, R. A. Koup, and A. Bukreyev. 2016. 'The Ebola Interferon Inhibiting Domains Attenuate and Dysregulate Cell-Mediated Immune Responses', *PLoS Pathog*, 12: e1006031.

Lundstrom, K. 2020. 'Coronavirus Pandemic-Therapy and Vaccines', *Biomedicines*, 8.

Lupu, R., and J. A. Menendez. 2006. 'Pharmacological inhibitors of Fatty Acid Synthase (FASN)--catalyzed endogenous fatty acid biogenesis: a new family of anti-cancer agents?', *Curr Pharm Biotechnol*, 7: 483-93.

Luthra, P., P. Ramanan, C. E. Mire, C. Weisend, Y. Tsuda, B. Yen, G. Liu, D. W. Leung, T. W. Geisbert, H. Ebihara, G. K. Amarasinghe, and C. F. Basler. 2013. 'Mutual antagonism between the Ebola virus VP35 protein and the RIG-I activator PACT determines infection outcome', *Cell Host Microbe*, 14: 74-84.

Ma, Y., W. Wang, T. Devarakonda, H. Zhou, X. Y. Wang, F. N. Salloum, S. Spiegel, and X. Fang. 2020. 'Functional analysis of molecular and pharmacological modulators of mitochondrial fatty acid oxidation', *Sci Rep*, 10: 1450.

Ma, Y., L. Wu, N. Shaw, Y. Gao, J. Wang, Y. Sun, Z. Lou, L. Yan, R. Zhang, and Z. Rao. 2015. 'Structural basis and functional analysis of the SARS coronavirus nsp14-nsp10 complex', *Proc Natl Acad Sci U S A*, 112: 9436-41.

Maes, P., G. K. Amarasinghe, M. A. Ayllon, C. F. Basler, S. Bavari, K. R. Blasdell, T. Briese, P. A. Brown, A. Bukreyev, A. Balkema-Buschmann, U. J. Buchholz, K. Chandran, I. Crozier, R. L. de Swart, R. G. Dietzgen, O. Dolnik, L. L. Domier, J. F. Drexler, R. Durrwald, W. G. Dundon, W. P. Duprex, J. M. Dye, A. J. Easton, A. R. Fooks, P. B. H. Formenty, R. A. M. Fouchier, J. Freitas-Astua, E. Ghedin, A. Griffiths, R. Hewson, M. Horie, J. L. Hurwitz, T. H. Hyndman, D. Jiang, G. P. Kobinger, H. Kondo, G. Kurath, I. V. Kuzmin, R. A. Lamb, B. Lee, E. M. Leroy, J. Li, S. L. Marzano, E. Muhlberger, S. V. Netesov, N. Nowotny, G. Palacios, B. Palyi, J. T. Paweska, S. L. Payne, B. K. Rima, P. Rota, D. Rubbenstroth, P. Simmonds, S. J. Smither, Q. Song, T. Song, K. Spann, M. D. Stenglein, D. M. Stone, A. Takada, R. B. Tesh, K. Tomonaga, N. Tordo, J. S. Towner, B. van den Hoogen, N. Vasilakis, V. Wahl, P. J. Walker, D. Wang, L. F. Wang, A. E. Whitfield, J. V. Williams, G. Ye, F. M. Zerbini, Y. Z. Zhang, and J. H. Kuhn. 2019. 'Taxonomy of the order Mononegavirales: second update 2018', *Arch Virol*, 164: 1233-44.

Majeau, N., R. Fromentin, C. Savard, M. Duval, M. J. Tremblay, and D. Leclerc. 2009. 'Palmitoylation of hepatitis C virus core protein is important for virion production', *J Biol Chem*, 284: 33915-25.

Majzoub, Karim, Florian Wrensch, and Thomas F. Baumert. 2019. 'The Innate Antiviral Response in Animals: An Evolutionary Perspective from Flagellates to Humans', *Viruses*, 11: 758.

Manicassamy, B., J. Wang, E. Rumschlag, S. Tymen, V. Volchkova, V. Volchkov, and L. Rong. 2007. 'Characterization of Marburg virus glycoprotein in viral entry', *Virology*, 358: 79-88.

Martin, B., B. Canard, and E. Decroly. 2017. 'Filovirus proteins for antiviral drug discovery: Structure/function bases of the replication cycle', *Antiviral Res*, 141: 48-61.

Martin, B., T. Hoenen, B. Canard, and E. Decroly. 2016. 'Filovirus proteins for antiviral drug discovery: A structure/function analysis of surface glycoproteins and virus entry', *Antiviral Res*, 135: 1-14.

Mateo, M., S. P. Reid, L. W. Leung, C. F. Basler, and V. E. Volchkov. 2010. 'Ebolavirus VP24 binding to karyopherins is required for inhibition of interferon signaling', *J Virol*, 84: 1169-75.

McBride, C. E., and C. E. Machamer. 2010. 'Palmitoylation of SARS-CoV S protein is necessary for partitioning into detergent-resistant membranes and cell-cell fusion but not interaction with M protein', *Virology*, 405: 139-48.

McBride, K. M., G. Banninger, C. McDonald, and N. C. Reich. 2002. 'Regulated nuclear import of the STAT1 transcription factor by direct binding of importin-alpha', *EMBO J*, 21: 1754-63.

McBride, K. M., and N. C. Reich. 2003. 'The ins and outs of STAT1 nuclear transport', *Sci STKE*, 2003: Re13.

McNab, Finlay, Katrin Mayer-Barber, Alan Sher, Andreas Wack, and Anne O'Garra. 2015. 'Type I interferons in infectious disease', *Nature Reviews Immunology*, 15: 87-103.

Memish, Z. A., N. Mishra, K. J. Olival, S. F. Fagbo, V. Kapoor, J. H. Epstein, R. Alhakeem, A. Durosinloun, M. Al Asmari, A. Islam, A. Kapoor, T. Briese, P. Daszak, A. A. Al Rabeeah, and W. I. Lipkin. 2013. 'Middle East respiratory syndrome coronavirus in bats, Saudi Arabia', *Emerg Infect Dis*, 19: 1819-23.

Menachery, V. D., B. L. Yount, Jr., L. Josset, L. E. Gralinski, T. Scobey, S. Agnihothram, M. G. Katze, and R. S. Baric. 2014. 'Attenuation and restoration of severe acute respiratory syndrome coronavirus mutant lacking 2'-o-methyltransferase activity', *J Virol*, 88: 4251-64.

Merino-Ramos, T., A. Vazquez-Calvo, J. Casas, F. Sobrino, J. C. Saiz, and M. A. Martin-Acebes. 2016. 'Modification of the Host Cell Lipid Metabolism Induced by Hypolipidemic Drugs Targeting the Acetyl Coenzyme A Carboxylase Impairs West Nile Virus Replication', *Antimicrob Agents Chemother*, 60: 307-15.

Messaoudi, I., G. K. Amarasinghe, and C. F. Basler. 2015. 'Filovirus pathogenesis and immune evasion: insights from Ebola virus and Marburg virus', *Nat Rev Microbiol*, 13: 663-76.

Michalska, A., K. Blaszczyk, J. Wesoly, and H. A. R. Bluyssen. 2018. 'A Positive Feedback Amplifier Circuit That Regulates Interferon (IFN)-Stimulated Gene Expression and Controls Type I and Type II IFN Responses', *Front Immunol*, 9: 1135.

Michel, C. J., C. Mayer, O. Poch, and J. D. Thompson. 2020. 'Characterization of accessory genes in coronavirus genomes', *Virol J*, 17: 131.

Miknis, Z. J., E. F. Donaldson, T. C. Umland, R. A. Rimmer, R. S. Baric, and L. W. Schultz. 2009. 'Severe acute respiratory syndrome coronavirus nsp9 dimerization is essential for efficient viral growth', *J Virol*, 83: 3007-18.

Minskaia, E., T. Hertzig, A. E. Gorbalenya, V. Campanacci, C. Cambillau, B. Canard, and J. Ziebuhr. 2006. 'Discovery of an RNA virus 3'->5' exoribonuclease that is critically involved in coronavirus RNA synthesis', *Proc Natl Acad Sci U S A*, 103: 5108-13.

Miyake, Tsuyoshi, Charlotte M. Farley, Benjamin E. Neubauer, Thomas P. Beddow, Thomas Hoenen, and Daniel A. Engel. 2020. 'Ebola Virus Inclusion Body Formation and RNA Synthesis Are Controlled by a Novel Domain of Nucleoprotein Interacting with VP35', *Journal of Virology*, 94: e02100-19.

Mogensen, Trine H. 2019. 'IRF and STAT Transcription Factors - From Basic Biology to Roles in Infection, Protective Immunity, and Primary Immunodeficiencies', *Frontiers in Immunology*, 9.

Mohan, G. S., W. Li, L. Ye, R. W. Compans, and C. Yang. 2012. 'Antigenic subversion: a novel mechanism of host immune evasion by Ebola virus', *PLoS Pathog*, 8: e1003065.

Mühlberger, E. 2007. 'Filovirus replication and transcription', *Future Virol*, 2: 205-15.

Mühlberger, E., M. Weik, V. E. Volchkov, H. D. Klenk, and S. Becker. 1999. 'Comparison of the transcription and replication strategies of marburg virus and Ebola virus by using artificial replication systems', *J Virol*, 73: 2333-42.

Mühlberger, Elke, Beate Lötfering, Hans-Dieter Klenk, and Stephan Becker. 1998. 'Three of the Four Nucleocapsid Proteins of Marburg Virus, NP, VP35, and L, Are Sufficient To Mediate Replication and Transcription of Marburg Virus-Specific Monocistronic Minigenomes', *Journal of Virology*, 72: 8756.

Nanbo, Asuka, Shinji Watanabe, Peter Halfmann, and Yoshihiro Kawaoka. 2013. 'The spatio-temporal distribution dynamics of Ebola virus proteins and RNA in infected cells', *Scientific Reports*, 3: 1206.

Narayanan, K., C. Huang, and S. Makino. 2008. 'SARS coronavirus accessory proteins', *Virus Res*, 133: 113-21.

Nasheri, N., M. Joyce, Y. Rouleau, P. Yang, S. Yao, D. L. Tyrrell, and J. P. Pezacki. 2013. 'Modulation of fatty acid synthase enzyme activity and expression during hepatitis C virus replication', *Chem Biol*, 20: 570-82.

Negredo, Ana, Gustavo Palacios, Sonia Vázquez-Morón, Félix González, Hernán Dopazo, Francisca Molero, Javier Juste, Juan Quetglas, Nazir Savji, Maria de la Cruz Martínez, Jesus Enrique Herrera, Manuel Pizarro, Stephen K. Hutchison, Juan E. Echevarría, W. Ian Lipkin, and Antonio Tenorio. 2011. 'Discovery of an Ebolavirus-Like Filovirus in Europe', *PLOS Pathogens*, 7: e1002304.

Nelson, E. V., K. M. Schmidt, L. R. Deflube, S. Doganay, L. Banadyga, J. Olejnik, A. J. Hume, E. Ryabchikova, H. Ebihara, N. Kedersha, T. Ha, and E. Muhlberger. 2016. 'Ebola Virus Does Not Induce Stress Granule Formation during Infection and Sequesters Stress Granule Proteins within Viral Inclusions', *J Virol*, 90: 7268-84.

Neuman, B. W. 2016. 'Bioinformatics and functional analyses of coronavirus nonstructural proteins involved in the formation of replicative organelles', *Antiviral Res*, 135: 97-107.

Nieto-Torres, J. L., M. L. DeDiego, C. Verdia-Baguena, J. M. Jimenez-Guardeno, J. A. Regla-Nava, R. Fernandez-Delgado, C. Castano-Rodriguez, A. Alcaraz, J. Torres, V. M. Aguilella, and L. Enjuanes. 2014. 'Severe acute respiratory syndrome coronavirus envelope protein ion channel activity promotes virus fitness and pathogenesis', *PLoS Pathog*, 10: e1004077.

Noda, T., K. Hagiwara, H. Sagara, and Y. Kawaoka. 2010. 'Characterization of the Ebola virus nucleoprotein-RNA complex', *J Gen Virol*, 91: 1478-83.

Noda, T., H. Sagara, E. Suzuki, A. Takada, H. Kida, and Y. Kawaoka. 2002. 'Ebola virus VP40 drives the formation of virus-like filamentous particles along with GP', *J Virol*, 76: 4855-65.

Noda, T., S. Watanabe, H. Sagara, and Y. Kawaoka. 2007a. 'Mapping of the VP40-binding regions of the nucleoprotein of Ebola virus', *J Virol*, 81: 3554-62.

Noda, Takeshi, Hideki Ebihara, Yukiko Muramoto, Ken Fujii, Ayato Takada, Hiroshi Sagara, Jin Hyun Kim, Hiroshi Kida, Heinz Feldmann, and Yoshihiro Kawaoka. 2006. 'Assembly and budding of Ebolavirus', *PLOS Pathogens*, 2: e99-e99.

Noda, Takeshi, Shinji Watanabe, Hiroshi Sagara, and Yoshihiro Kawaoka. 2007b. 'Mapping of the VP40-binding regions of the nucleoprotein of Ebola virus', *Journal of Virology*, 81: 3554-62.

Ohashi, Y., S. Tremel, G. R. Masson, L. McGinney, J. Boulanger, K. Rostislavleva, C. M. Johnson, I. Niewczas, J. Clark, and R. L. Williams. 2020. 'Membrane characteristics tune activities of endosomal and autophagic human VPS34 complexes', *Elife*, 9.

Oka, M., and Y. Yoneda. 2018. 'Importin alpha: functions as a nuclear transport factor and beyond', *Proc Jpn Acad Ser B Phys Biol Sci*, 94: 259-74.

Okamoto, M., H. Tsukamoto, T. Kouwaki, T. Seya, and H. Oshiumi. 2017. 'Recognition of Viral RNA by Pattern Recognition Receptors in the Induction of Innate Immunity and Excessive Inflammation During Respiratory Viral Infections', *Viral Immunol*, 30: 408-20.

Olejnik, J., A. J. Hume, D. W. Leung, G. K. Amarasinghe, C. F. Basler, and E. Muhlberger. 2017. 'Filovirus Strategies to Escape Antiviral Responses', *Curr Top Microbiol Immunol*, 411: 293-322.

Olejnik, J., A. J. Hume, D. W. Leung, G. K. Amarasinghe, C. F. Basler, and E. Mühlberger. 2017. 'Filovirus Strategies to Escape Antiviral Responses', *Curr Top Microbiol Immunol*, 411: 293-322.

Olejnik, J., E. Ryabchikova, R. B. Corley, and E. Muhlberger. 2011. 'Intracellular events and cell fate in filovirus infection', *Viruses*, 3: 1501-31.

Olival, K. J., and D. T. Hayman. 2014. 'Filoviruses in bats: current knowledge and future directions', *Viruses*, 6: 1759-88.

Olival, K. J., A. Islam, M. Yu, S. J. Anthony, J. H. Epstein, S. A. Khan, S. U. Khan, G. Crameri, L. F. Wang, W. I. Lipkin, S. P. Luby, and P. Daszak. 2013. 'Ebola virus antibodies in fruit bats, bangladesh', *Emerg Infect Dis*, 19: 270-3.

Orenstein, J. M., B. Banach, and S. C. Baker. 2008. 'Morphogenesis of Coronavirus HCoV-NL63 in Cell Culture: A Transmission Electron Microscopic Study', *Open Infect Dis J*, 2: 52-58.

Organization, World Health. 2019. 'Ebola situation reports: Democratic Republic of the Congo'. https://www.who.int/ebola/situation-reports/drc-2018/en/.

Oudshoorn, D., K. Rijs, Rwal Limpens, K. Groen, A. J. Koster, E. J. Snijder, M. Kikkert, and M. Barcena. 2017. 'Expression and Cleavage of Middle East Respiratory Syndrome Coronavirus nsp3-4 Polyprotein Induce the Formation of Double-Membrane Vesicles That Mimic Those Associated with Coronaviral RNA Replication', *mBio*, 8.

Oudshoorn, D., B. van der Hoeven, R. W. Limpens, C. Beugeling, E. J. Snijder, M. Barcena, and M. Kikkert. 2016. 'Antiviral Innate Immune Response Interferes with the Formation of Replication-Associated Membrane Structures Induced by a Positive-Strand RNA Virus', *mBio*, 7.

Page, A., V. A. Volchkova, S. P. Reid, M. Mateo, A. Bagnaud-Baule, K. Nemirov, A. C. Shurtleff, P. Lawrence, O. Reynard, M. Ottmann, V. Lotteau, S. S. Biswal, R. K. Thimmulappa, S. Bavari, and V. E. Volchkov. 2014. 'Marburgvirus hijacks nrf2-dependent pathway by targeting nrf2-negative regulator keap1', *Cell Rep*, 6: 1026-36.

Panne, D., T. Maniatis, and S. C. Harrison. 2007. 'An atomic model of the interferon-beta enhanceosome', *Cell*, 129: 1111-23.

Pasquier, B. 2015. 'SAR405, a PIK3C3/Vps34 inhibitor that prevents autophagy and synergizes with MTOR inhibition in tumor cells', *Autophagy*, 11: 725-6.

Pattyn, S., G. van der Groen, W. Jacob, P. Piot, and G. Courteille. 1977. 'Isolation of Marburg-like virus from a case of haemorrhagic fever in Zaire', *Lancet*, 1: 573-4.

Paweska, J. T., P. Jansen van Vuren, J. Masumu, P. A. Leman, A. A. Grobbelaar, M. Birkhead, S. Clift, R. Swanepoel, and A. Kemp. 2012. 'Virological and serological findings in Rousettus aegyptiacus experimentally inoculated with vero cells-adapted hogan strain of Marburg virus', *PLoS One*, 7: e45479.

Peeri, N. C., N. Shrestha, M. S. Rahman, R. Zaki, Z. Tan, S. Bibi, M. Baghbanzadeh, N. Aghamohammadi, W. Zhang, and U. Haque. 2020. 'The SARS, MERS and novel coronavirus (COVID-19) epidemics, the newest and biggest global health threats: what lessons have we learned?', *Int J Epidemiol*, 49: 717-26.

Pestka, S., C. D. Krause, and M. R. Walter. 2004. 'Interferons, interferon-like cytokines, and their receptors', *Immunol Rev*, 202: 8-32.

Petit, C. M., V. N. Chouljenko, A. Iyer, R. Colgrove, M. Farzan, D. M. Knipe, and K. G. Kousoulas. 2007. 'Palmitoylation of the cysteine-rich endodomain of the SARS-coronavirus spike glycoprotein is important for spike-mediated cell fusion', *Virology*, 360: 264-74.

Pichlmair, A., K. Kandasamy, G. Alvisi, O. Mulhern, R. Sacco, M. Habjan, M. Binder, A. Stefanovic, C. A. Eberle, A. Goncalves, T. Burckstummer, A. C. Muller, A. Fauster, C. Holze, K. Lindsten, S. Goodbourn, G. Kochs, F. Weber, R. Bartenschlager, A. G. Bowie, K. L. Bennett, J. Colinge, and G. Superti-Furga. 2012. 'Viral immune modulators perturb the human molecular network by common and unique strategies', *Nature*, 487: 486-90.

Piehler, Jacob, Christoph Thomas, K. Christopher Garcia, and Gideon Schreiber. 2012. 'Structural and dynamic determinants of type I interferon receptor assembly and their functional interpretation', *Immunological reviews*, 250: 317-34.

Pizzorno, A., B. Padey, O. Terrier, and M. Rosa-Calatrava. 2019. 'Drug Repurposing Approaches for the Treatment of Influenza Viral Infection: Reviving Old Drugs to Fight Against a Long-Lived Enemy', *Front Immunol*, 10: 531.

Plowright, R. K., C. R. Parrish, H. McCallum, P. J. Hudson, A. I. Ko, A. L. Graham, and J. O. Lloyd-Smith. 2017. 'Pathways to zoonotic spillover', *Nat Rev Microbiol*, 15: 502-10.

Prentice, E., W. G. Jerome, T. Yoshimori, N. Mizushima, and M. R. Denison. 2004. 'Coronavirus replication complex formation utilizes components of cellular autophagy', *J Biol Chem*, 279: 10136-41.

Prins, K. C., W. B. Cardenas, and C. F. Basler. 2009. 'Ebola virus protein VP35 impairs the function of interferon regulatory factor-activating kinases IKKepsilon and TBK-1', *J Virol*, 83: 3069-77.

Prins, K. C., S. Delpeut, D. W. Leung, O. Reynard, V. A. Volchkova, S. P. Reid, P. Ramanan, W. B. Cardenas, G. K. Amarasinghe, V. E. Volchkov, and C. F. Basler. 2010. 'Mutations abrogating VP35 interaction with double-stranded RNA render Ebola virus avirulent in guinea pigs', *J Virol*, 84: 3004-15.

Quintas-Cardama, A., K. Vaddi, P. Liu, T. Manshouri, J. Li, P. A. Scherle, E. Caulder, X. Wen, Y. Li, P. Waeltz, M. Rupar, T. Burn, Y. Lo, J. Kelley, M. Covington, S. Shepard, J. D. Rodgers, P. Haley, H. Kantarjian, J. S. Fridman, and S. Verstovsek. 2010. 'Preclinical

characterization of the selective JAK1/2 inhibitor INCB018424: therapeutic implications for the treatment of myeloproliferative neoplasms', *Blood*, 115: 3109-17.

Ramanan, P., M. R. Edwards, R. S. Shabman, D. W. Leung, A. C. Endlich-Frazier, D. M. Borek, Z. Otwinowski, G. Liu, J. Huh, C. F. Basler, and G. K. Amarasinghe. 2012. 'Structural basis for Marburg virus VP35-mediated immune evasion mechanisms', *Proc Natl Acad Sci U S A*, 109: 20661-6.

Reggiori, F., C. A. de Haan, and M. Molinari. 2011. 'Unconventional use of LC3 by coronaviruses through the alleged subversion of the ERAD tuning pathway', *Viruses*, 3: 1610-23.

Reggiori, F., I. Monastyrska, M. H. Verheije, T. Cali, M. Ulasli, S. Bianchi, R. Bernasconi, C. A. de Haan, and M. Molinari. 2010. 'Coronaviruses Hijack the LC3-I-positive EDEMosomes, ER-derived vesicles exporting short-lived ERAD regulators, for replication', *Cell Host Microbe*, 7: 500-8.

Rehwinkel, J., C. P. Tan, D. Goubau, O. Schulz, A. Pichlmair, K. Bier, N. Robb, F. Vreede, W. Barclay, E. Fodor, and C. Reis e Sousa. 2010. 'RIG-I detects viral genomic RNA during negative-strand RNA virus infection', *Cell*, 140: 397-408.

Reid, S. P., L. W. Leung, A. L. Hartman, O. Martinez, M. L. Shaw, C. Carbonnelle, V. E. Volchkov, S. T. Nichol, and C. F. Basler. 2006. 'Ebola virus VP24 binds karyopherin alpha1 and blocks STAT1 nuclear accumulation', *J Virol*, 80: 5156-67.

Reid, S. P., C. Valmas, O. Martinez, F. M. Sanchez, and C. F. Basler. 2007. 'Ebola virus VP24 proteins inhibit the interaction of NPI-1 subfamily karyopherin alpha proteins with activated STAT1', *J Virol*, 81: 13469-77.

Ren, Zhihua, Ting Ding, Zhicai Zuo, Zhiwen Xu, Junliang Deng, and Zhanyong Wei. 2020. 'Regulation of MAVS Expression and Signaling Function in the Antiviral Innate Immune Response', *Frontiers in Immunology*, 11.

Rohaim, M. A., R. F. El Naggar, E. Clayton, and M. Munir. 2021. 'Structural and functional insights into non-structural proteins of coronaviruses', *Microb Pathog*, 150: 104641.

Romero-Brey, I., A. Merz, A. Chiramel, J. Y. Lee, P. Chlanda, U. Haselman, R. Santarella-Mellwig, A. Habermann, S. Hoppe, S. Kallis, P. Walther, C. Antony, J. Krijnse-Locker, and R. Bartenschlager. 2012. 'Three-dimensional architecture and biogenesis of membrane structures associated with hepatitis C virus replication', *PLoS Pathog*, 8: e1003056.

Ronan, B., O. Flamand, L. Vescovi, C. Dureuil, L. Durand, F. Fassy, M. F. Bachelot, A. Lamberton, M. Mathieu, T. Bertrand, J. P. Marquette, Y. El-Ahmad, B. Filoche-Romme, L. Schio, C. Garcia-Echeverria, H. Goulaouic, and B. Pasquier. 2014. 'A highly potent and selective Vps34 inhibitor alters vesicle trafficking and autophagy', *Nat Chem Biol*, 10: 1013-9.

Rougeron, V., H. Feldmann, G. Grard, S. Becker, and E. M. Leroy. 2015. 'Ebola and Marburg haemorrhagic fever', *J Clin Virol*, 64: 111-9.

Saini, K. S., C. Lanza, M. Romano, E. de Azambuja, J. Cortes, B. de Las Heras, J. de Castro, M. Lamba Saini, S. Loibl, G. Curigliano, C. Twelves, M. Leone, and M. M. Patnaik. 2020. 'Repurposing anticancer drugs for COVID-19-induced inflammation, immune dysfunction, and coagulopathy', *Br J Cancer*, 123: 694-97.

Sanchez, A., M. P. Kiley, B. P. Holloway, and D. D. Auperin. 1993. 'Sequence analysis of the Ebola virus genome: organization, genetic elements, and comparison with the genome of Marburg virus', *Virus Res*, 29: 215-40.

Sanchez, A., M. P. Kiley, B. P. Holloway, J. B. McCormick, and D. D. Auperin. 1989. 'The nucleoprotein gene of Ebola virus: cloning, sequencing, and in vitro expression', *Virology*, 170: 81-91.

Sanchez, A., S. G. Trappier, B. W. Mahy, C. J. Peters, and S. T. Nichol. 1996. 'The virion glycoproteins of Ebola viruses are encoded in two reading frames and are expressed through transcriptional editing', *Proceedings of the National Academy of Sciences of the United States of America*, 93: 3602-07.

Santos, I. A., V. R. Grosche, F. R. G. Bergamini, R. Sabino-Silva, and A. C. G. Jardim. 2020. 'Antivirals Against Coronaviruses: Candidate Drugs for SARS-CoV-2 Treatment?', *Front Microbiol*, 11: 1818.

Sawicki, S. G., and D. L. Sawicki. 1995. 'Coronaviruses use discontinuous extension for synthesis of subgenome-length negative strands', *Adv Exp Med Biol*, 380: 499-506.

———. 1998. 'A new model for coronavirus transcription', *Adv Exp Med Biol*, 440: 215-9.

Sawicki, S. G., D. L. Sawicki, D. Younker, Y. Meyer, V. Thiel, H. Stokes, and S. G. Siddell. 2005. 'Functional and genetic analysis of coronavirus replicase-transcriptase proteins', *PLoS Pathog*, 1: e39.

Schneider, W. M., J. M. Luna, H. H. Hoffmann, F. J. Sanchez-Rivera, A. A. Leal, A. W. Ashbrook, J. Le Pen, I. Ricardo-Lax, E. Michailidis, A. Peace, A. F. Stenzel, S. W. Lowe, M. R. MacDonald, C. M. Rice, and J. T. Poirier. 2021. 'Genome-Scale Identification of SARS-CoV-2 and Pan-coronavirus Host Factor Networks', *Cell*, 184: 120-32 e14.

Schneider, William M., Meike Dittmann Chevillotte, and Charles M. Rice. 2014. 'Interferon-stimulated genes: a complex web of host defenses', *Annual review of immunology*, 32: 513-45.

Schoggins, J. W. 2014. 'Interferon-stimulated genes: roles in viral pathogenesis', *Curr Opin Virol*, 6: 40-6.

Schubert, K., E. D. Karousis, A. Jomaa, A. Scaiola, B. Echeverria, L. A. Gurzeler, M. Leibundgut, V. Thiel, O. Muhlemann, and N. Ban. 2020. 'SARS-CoV-2 Nsp1 binds the ribosomal mRNA channel to inhibit translation', *Nat Struct Mol Biol*, 27: 959-66.

Schuh, A. J., B. R. Amman, and J. S. Towner. 2017. 'Filoviruses and bats', *Microbiol Aust*, 38: 12-16.

Schumann, M., T. Gantke, and E. Muhlberger. 2009. 'Ebola virus VP35 antagonizes PKR activity through its C-terminal interferon inhibitory domain', *J Virol*, 83: 8993-7.

Secombes, Chris J., and Jun Zou. 2017. 'Evolution of Interferons and Interferon Receptors', *Frontiers in Immunology*, 8: 209-09.

Sekimoto, T., N. Imamoto, K. Nakajima, T. Hirano, and Y. Yoneda. 1997. 'Extracellular signal-dependent nuclear import of Stat1 is mediated by nuclear pore-targeting complex formation with NPI-1, but not Rch1', *EMBO J*, 16: 7067-77.

Sheahan, T. P., A. C. Sims, S. R. Leist, A. Schafer, J. Won, A. J. Brown, S. A. Montgomery, A. Hogg, D. Babusis, M. O. Clarke, J. E. Spahn, L. Bauer, S. Sellers, D. Porter, J. Y. Feng, T. Cihlar, R. Jordan, M. R. Denison, and R. S. Baric. 2020. 'Comparative therapeutic efficacy of remdesivir and combination lopinavir, ritonavir, and interferon beta against MERS-CoV', *Nat Commun*, 11: 222.

Shi, Mang, Xian-Dan Lin, Xiao Chen, Jun-Hua Tian, Liang-Jun Chen, Kun Li, Wen Wang, John-Sebastian Eden, Jin-Jin Shen, Li Liu, Edward C. Holmes, and Yong-Zhen Zhang. 2018. 'The evolutionary history of vertebrate RNA viruses', *Nature*, 556: 197-202.

Sims, A. C., R. S. Baric, B. Yount, S. E. Burkett, P. L. Collins, and R. J. Pickles. 2005. 'Severe acute respiratory syndrome coronavirus infection of human ciliated airway epithelia: role of ciliated cells in viral spread in the conducting airways of the lungs', *J Virol*, 79: 15511-24.

Sims, A. C., S. E. Burkett, B. Yount, and R. J. Pickles. 2008. 'SARS-CoV replication and pathogenesis in an in vitro model of the human conducting airway epithelium', *Virus Res*, 133: 33-44.

Sims, A. C., J. Ostermann, and M. R. Denison. 2000. 'Mouse hepatitis virus replicase proteins associate with two distinct populations of intracellular membranes', *J Virol*, 74: 5647-54.

Siu, Y. L., K. T. Teoh, J. Lo, C. M. Chan, F. Kien, N. Escriou, S. W. Tsao, J. M. Nicholls, R. Altmeyer, J. S. Peiris, R. Bruzzone, and B. Nal. 2008. 'The M, E, and N structural proteins of the severe acute respiratory syndrome coronavirus are required for efficient assembly, trafficking, and release of virus-like particles', *J Virol*, 82: 11318-30.

Smith, C. E., D. I. Simpson, E. T. Bowen, and I. Zlotnik. 1967. 'Fatal human disease from vervet monkeys', *Lancet*, 2: 1119-21.

Snijder, E. J., P. J. Bredenbeek, J. C. Dobbe, V. Thiel, J. Ziebuhr, L. L. Poon, Y. Guan, M. Rozanov, W. J. Spaan, and A. E. Gorbalenya. 2003. 'Unique and conserved features of genome and proteome of SARS-coronavirus, an early split-off from the coronavirus group 2 lineage', *J Mol Biol*, 331: 991-1004.

Snijder, E. J., Rwal Limpens, A. H. de Wilde, A. W. M. de Jong, J. C. Zevenhoven-Dobbe, H. J. Maier, Ffga Faas, A. J. Koster, and M. Barcena. 2020. 'A unifying structural and functional model of the coronavirus replication organelle: Tracking down RNA synthesis', *PLoS Biol*, 18: e3000715.

Snijder, E. J., Y. van der Meer, J. Zevenhoven-Dobbe, J. J. Onderwater, J. van der Meulen, H. K. Koerten, and A. M. Mommaas. 2006. 'Ultrastructure and origin of membrane vesicles associated with the severe acute respiratory syndrome coronavirus replication complex', *J Virol*, 80: 5927-40.

Sola, I., F. Almazan, S. Zuniga, and L. Enjuanes. 2015. 'Continuous and Discontinuous RNA Synthesis in Coronaviruses', *Annu Rev Virol*, 2: 265-88.

Song, H. D., C. C. Tu, G. W. Zhang, S. Y. Wang, K. Zheng, L. C. Lei, Q. X. Chen, Y. W. Gao, H. Q. Zhou, H. Xiang, H. J. Zheng, S. W. Chern, F. Cheng, C. M. Pan, H. Xuan, S. J. Chen, H. M. Luo, D. H. Zhou, Y. F. Liu, J. F. He, P. Z. Qin, L. H. Li, Y. Q. Ren, W. J. Liang, Y. D. Yu, L. Anderson, M. Wang, R. H. Xu, X. W. Wu, H. Y. Zheng, J. D. Chen, G. Liang, Y. Gao, M. Liao, L. Fang, L. Y. Jiang, H. Li, F. Chen, B. Di, L. J. He, J. Y. Lin, S. Tong, X. Kong, L. Du, P. Hao, H. Tang, A. Bernini, X. J. Yu, O. Spiga, Z. M. Guo, H. Y. Pan, W. Z. He, J. C. Manuguerra, A. Fontanet, A. Danchin, N. Niccolai, Y. X. Li, C. I. Wu, and G. P. Zhao. 2005. 'Cross-host evolution of severe acute respiratory syndrome coronavirus in palm civet and human', *Proc Natl Acad Sci U S A*, 102: 2430-5.

Stahelin, R. V. 2014. 'Membrane binding and bending in Ebola VP40 assembly and egress', *Front Microbiol*, 5: 300.

Stenvinkel, Peter, Colin J. Meyer, Geoffrey A. Block, Glenn M. Chertow, and Paul G. Shiels. 2020. 'Understanding the role of the cytoprotective transcription factor nuclear factor erythroid 2-related factor 2—lessons from evolution, the animal kingdom and rare progeroid syndromes', *Nephrology Dialysis Transplantation*, 35: 2036-45.

Stertz, S., M. Reichelt, M. Spiegel, T. Kuri, L. Martinez-Sobrido, A. Garcia-Sastre, F. Weber, and G. Kochs. 2007. 'The intracellular sites of early replication and budding of SARS-coronavirus', *Virology*, 361: 304-15.

Su, W. C., T. C. Chao, Y. L. Huang, S. C. Weng, K. S. Jeng, and M. M. Lai. 2011. 'Rab5 and class III phosphoinositide 3-kinase Vps34 are involved in hepatitis C virus NS4B-induced autophagy', *J Virol*, 85: 10561-71.

Subissi, L., C. C. Posthuma, A. Collet, J. C. Zevenhoven-Dobbe, A. E. Gorbalenya, E. Decroly, E. J. Snijder, B. Canard, and I. Imbert. 2014. 'One severe acute respiratory syndrome coronavirus protein complex integrates processive RNA polymerase and exonuclease activities', *Proc Natl Acad Sci U S A*, 111: E3900-9.

Sugita, Y., H. Matsunami, Y. Kawaoka, T. Noda, and M. Wolf. 2018. 'Cryo-EM structure of the Ebola virus nucleoprotein-RNA complex at 3.6 Å resolution', *Nature*, 563: 137-40.

Sutton, G., E. Fry, L. Carter, S. Sainsbury, T. Walter, J. Nettleship, N. Berrow, R. Owens, R. Gilbert, A. Davidson, S. Siddell, L. L. Poon, J. Diprose, D. Alderton, M. Walsh, J. M. Grimes, and D. I. Stuart. 2004. 'The nsp9 replicase protein of SARS-coronavirus, structure and functional insights', *Structure*, 12: 341-53.

Syed-Abdul, M. M., E. J. Parks, A. H. Gaballah, K. Bingham, G. M. Hammoud, G. Kemble, D. Buckley, W. McCulloch, and C. Manrique-Acevedo. 2020. 'Fatty Acid Synthase Inhibitor TVB-2640 Reduces Hepatic de Novo Lipogenesis in Males With Metabolic Abnormalities', *Hepatology*, 72: 103-18.

Takada, A., C. Robison, H. Goto, A. Sanchez, K. G. Murti, M. A. Whitt, and Y. Kawaoka. 1997. 'A system for functional analysis of Ebola virus glycoprotein', *Proc Natl Acad Sci U S A*, 94: 14764-9.

Takamatsu, Yuki, Larissa Kolesnikova, and Stephan Becker. 2018. 'Ebola virus proteins NP, VP35, and VP24 are essential and sufficient to mediate nucleocapsid transport', *Proceedings of the National Academy of Sciences*, 115: 1075.

Takeuchi, O., and S. Akira. 2010. 'Pattern recognition receptors and inflammation', *Cell*, 140: 805-20.

Team, W. H. O. Ebola Response, J. Agua-Agum, B. Allegranzi, A. Ariyarajah, R. Aylward, I. M. Blake, P. Barboza, D. Bausch, R. J. Brennan, P. Clement, P. Coffey, A. Cori, C. A. Donnelly, I. Dorigatti, P. Drury, K. Durski, C. Dye, T. Eckmanns, N. M. Ferguson, C. Fraser, E. Garcia, T. Garske, A. Gasasira, C. Gurry, E. Hamblion, W. Hinsley, R. Holden, D. Holmes, S. Hugonnet, G. Jaramillo Gutierrez, T. Jombart, E. Kelley, R. Santhana, N. Mahmoud, H. L. Mills, Y. Mohamed, E. Musa, D. Naidoo, G. Nedjati-Gilani, E. Newton, I. Norton, P. Nouvellet, D. Perkins, M. Perkins, S. Riley, D. Schumacher, A. Shah, M. Tang, O. Varsaneux, and M. D. Van Kerkhove. 2016. 'After Ebola in West Africa--Unpredictable Risks, Preventable Epidemics', *N Engl J Med*, 375: 587-96.

Thorp, E. B., J. A. Boscarino, H. L. Logan, J. T. Goletz, and T. M. Gallagher. 2006. 'Palmitoylations on murine coronavirus spike proteins are essential for virion assembly and infectivity', *J Virol*, 80: 1280-9.

Timmins, J., S. Scianimanico, G. Schoehn, and W. Weissenhorn. 2001. 'Vesicular release of ebola virus matrix protein VP40', *Virology*, 283: 1-6.

Tongluan, N., S. Ramphan, P. Wintachai, J. Jaresitthikunchai, S. Khongwichit, N. Wikan, S. Rajakam, S. Yoksan, N. Wongsiriroj, S. Roytrakul, and D. R. Smith. 2017. 'Involvement of fatty acid synthase in dengue virus infection', *Virol J*, 14: 28.

Tooze, J., S. Tooze, and G. Warren. 1984. 'Replication of coronavirus MHV-A59 in sac- cells: determination of the first site of budding of progeny virions', *Eur J Cell Biol*, 33: 281-93.

Towner, J. S., B. R. Amman, T. K. Sealy, S. A. Carroll, J. A. Comer, A. Kemp, R. Swanepoel, C. D. Paddock, S. Balinandi, M. L. Khristova, P. B. Formenty, C. G. Albarino, D. M. Miller, Z. D. Reed, J. T. Kayiwa, J. N. Mills, D. L. Cannon, P. W. Greer, E. Byaruhanga, E. C. Farnon, P. Atimnedi, S. Okware, E. Katongole-Mbidde, R. Downing, J. W. Tappero, S. R. Zaki, T. G. Ksiazek, S. T. Nichol, and P. E. Rollin. 2009. 'Isolation of genetically diverse Marburg viruses from Egyptian fruit bats', *PLoS Pathog*, 5: e1000536.

Towner, Jonathan S., Marina L. Khristova, Tara K. Sealy, Martin J. Vincent, Bobbie R. Erickson, Darcy A. Bawiec, Amy L. Hartman, James A. Comer, Sherif R. Zaki, Ute Ströher, Filomena Gomes da Silva, Fernando del Castillo, Pierre E. Rollin, Thomas G. Ksiazek, and Stuart T. Nichol. 2006. 'Marburgvirus Genomics and Association with a Large Hemorrhagic Fever Outbreak in Angola', *Journal of Virology*, 80: 6497.

Tseng, Y. T., S. M. Wang, K. J. Huang, and C. T. Wang. 2014. 'SARS-CoV envelope protein palmitoylation or nucleocapid association is not required for promoting virus-like particle production', *J Biomed Sci*, 21: 34.

Tu, C., G. Crameri, X. Kong, J. Chen, Y. Sun, M. Yu, H. Xiang, X. Xia, S. Liu, T. Ren, Y. Yu, B. T. Eaton, H. Xuan, and L. F. Wang. 2004. 'Antibodies to SARS coronavirus in civets', *Emerg Infect Dis*, 10: 2244-8.

Tyrrell, D. A., and M. L. Bynoe. 1965. 'Cultivation of a Novel Type of Common-Cold Virus in Organ Cultures', *Br Med J*, 1: 1467-70.

V'Kovski, P., A. Kratzel, S. Steiner, H. Stalder, and V. Thiel. 2021. 'Coronavirus biology and replication: implications for SARS-CoV-2', *Nat Rev Microbiol*, 19: 155-70.

Valmas, C., and C. F. Basler. 2011a. 'Marburg virus VP40 antagonizes interferon signaling in a species-specific manner', *J Virol*, 85: 4309-17.

Valmas, C., M. N. Grosch, M. Schumann, J. Olejnik, O. Martinez, S. M. Best, V. Krahling, C. F. Basler, and E. Muhlberger. 2010. 'Marburg virus evades interferon responses by a mechanism distinct from ebola virus', *PLoS Pathog*, 6: e1000721.

Valmas, Charalampos, and Christopher F. Basler. 2011b. 'Marburg virus VP40 antagonizes interferon signaling in a species-specific manner', *Journal of Virology*, 85: 4309-17.

van der Hoek, L., K. Pyrc, M. F. Jebbink, W. Vermeulen-Oost, R. J. Berkhout, K. C. Wolthers, P. M. Wertheim-van Dillen, J. Kaandorp, J. Spaargaren, and B. Berkhout. 2004. 'Identification of a new human coronavirus', *Nat Med*, 10: 368-73.

Volchkov, V. E., A. A. Chepurnov, V. A. Volchkova, V. A. Ternovoj, and H. D. Klenk. 2000. 'Molecular characterization of guinea pig-adapted variants of Ebola virus', *Virology*, 277: 147-55.

von Grotthuss, M., L. S. Wyrwicz, and L. Rychlewski. 2003. 'mRNA cap-1 methyltransferase in the SARS genome', *Cell*, 113: 701-2.

von Kobbe, C., J. M. van Deursen, J. P. Rodrigues, D. Sitterlin, A. Bachi, X. Wu, M. Wilm, M. Carmo-Fonseca, and E. Izaurralde. 2000. 'Vesicular stomatitis virus matrix protein inhibits host cell gene expression by targeting the nucleoporin Nup98', *Mol Cell*, 6: 1243-52.

Wakil, S. J., and L. A. Abu-Elheiga. 2009. 'Fatty acid metabolism: target for metabolic syndrome', *J Lipid Res*, 50 Suppl: S138-43.

Walsh, E. E., J. H. Shin, and A. R. Falsey. 2013. 'Clinical impact of human coronaviruses 229E and OC43 infection in diverse adult populations', *J Infect Dis*, 208: 1634-42.

Wan, W., L. Kolesnikova, M. Clarke, A. Koehler, T. Noda, S. Becker, and J. A. G. Briggs. 2017. 'Structure and assembly of the Ebola virus nucleocapsid', *Nature*, 551: 394-97.

Wang, C., P. W. Horby, F. G. Hayden, and G. F. Gao. 2020. 'A novel coronavirus outbreak of global health concern', *Lancet*, 395: 470-73.

Wang, L., Y. Wang, D. Ye, and Q. Liu. 2020. 'Review of the 2019 novel coronavirus (SARS-CoV-2) based on current evidence', *Int J Antimicrob Agents*, 55: 105948.

Wang, R., C. R. Simoneau, J. Kulsuptrakul, M. Bouhaddou, K. A. Travisano, J. M. Hayashi, J. Carlson-Stevermer, J. R. Zengel, C. M. Richards, P. Fozouni, J. Oki, L. Rodriguez, B. Joehnk, K. Walcott, K. Holden, A. Sil, J. E. Carette, N. J. Krogan, M. Ott, and A. S. Puschnik. 2021. 'Genetic Screens Identify Host Factors for SARS-CoV-2 and Common Cold Coronaviruses', *Cell*, 184: 106-19 e14.

Wang, Y. E., A. Park, M. Lake, M. Pentecost, B. Torres, T. E. Yun, M. C. Wolf, M. R. Holbrook, A. N. Freiberg, and B. Lee. 2010. 'Ubiquitin-regulated nuclear-cytoplasmic trafficking of the Nipah virus matrix protein is important for viral budding', *PLoS Pathog*, 6: e1001186.

Wang, Y., M. Grunewald, and S. Perlman. 2020. 'Coronaviruses: An Updated Overview of Their Replication and Pathogenesis', *Methods Mol Biol*, 2203: 1-29.

Warfield, Kelly L., Steven B. Bradfute, Jay Wells, Loreen Lofts, Meagan T. Cooper, D. Anthony Alves, Daniel K. Reed, Sean A. VanTongeren, Christine A. Mech, and Sina Bavari. 2009. 'Development and Characterization of a Mouse Model for Marburg Hemorrhagic Fever', *Journal of Virology*, 83: 6404.

Watanabe, S., T. Noda, and Y. Kawaoka. 2006. 'Functional mapping of the nucleoprotein of Ebola virus', *J Virol*, 80: 3743-51.

Wathelet, M. G., M. Orr, M. B. Frieman, and R. S. Baric. 2007. 'Severe acute respiratory syndrome coronavirus evades antiviral signaling: role of nsp1 and rational design of an attenuated strain', *J Virol*, 81: 11620-33.

Weber, F., V. Wagner, S. B. Rasmussen, R. Hartmann, and S. R. Paludan. 2006. 'Double-stranded RNA is produced by positive-strand RNA viruses and DNA viruses but not in detectable amounts by negative-strand RNA viruses', *J Virol*, 80: 5059-64.

Welsch, S., L. Kolesnikova, V. Krahling, J. D. Riches, S. Becker, and J. A. Briggs. 2010. 'Electron tomography reveals the steps in filovirus budding', *PLoS Pathog*, 6: e1000875.

Whelan, S. P., J. N. Barr, and G. W. Wertz. 2004. 'Transcription and replication of nonsegmented negative-strand RNA viruses', *Curr Top Microbiol Immunol*, 283: 61-119.

WHO. 2003. 'Cumulative Number of Reported Probable Cases of SARS'.

———. 2018. 'Marburg virus disease'. https://www.who.int/news-room/fact-sheets/detail/marburg-virus-disease.

———. 2021a. 'Ebola virus disease'. https://www.who.int/news-room/fact-sheets/detail/ebola-virus-disease.

———. 2021b. 'WHO Coronavirus (COVID-19) Dashboard'. https://covid19.who.int/.

Widagdo, W., L. Begeman, D. Schipper, P. R. V. Run, A. A. Cunningham, N. Kley, C. B. Reusken, B. L. Haagmans, and J. M. A. van den Brand. 2017. 'Tissue Distribution of the MERS-Coronavirus Receptor in Bats', *Sci Rep*, 7: 1193.

Williams, C. G., J. S. Gibbons, T. R. Keiffer, P. Luthra, M. R. Edwards, and C. F. Basler. 2020. 'Impact of Mengla Virus Proteins on Human and Bat Innate Immune Pathways', *J Virol*, 94.

Woo, P. C., S. K. Lau, C. M. Chu, K. H. Chan, H. W. Tsoi, Y. Huang, B. H. Wong, R. W. Poon, J. J. Cai, W. K. Luk, L. L. Poon, S. S. Wong, Y. Guan, J. S. Peiris, and K. Y. Yuen. 2005. 'Characterization and complete genome sequence of a novel coronavirus, coronavirus HKU1, from patients with pneumonia', *J Virol*, 79: 884-95.

Wool-Lewis, R. J., and P. Bates. 1998. 'Characterization of Ebola virus entry by using pseudotyped viruses: identification of receptor-deficient cell lines', *J Virol*, 72: 3155-60.

Woolsey, C., A. R. Menicucci, R. W. Cross, P. Luthra, K. N. Agans, V. Borisevich, J. B. Geisbert, C. E. Mire, K. A. Fenton, A. Jankeel, S. Anand, H. Ebihara, T. W. Geisbert, I. Messaoudi, and C. F. Basler. 2019. 'A VP35 Mutant Ebola Virus Lacks Virulence but Can Elicit Protective Immunity to Wild-Type Virus Challenge', *Cell Rep*, 28: 3032-46 e6.

Wu, D., T. Wu, Q. Liu, and Z. Yang. 2020. 'The SARS-CoV-2 outbreak: What we know', *Int J Infect Dis*, 94: 44-48.

Wu, J., B. Wu, and T. Lai. 2020. 'Compassionate Use of Remdesivir in Covid-19', *N Engl J Med*, 382: e101.

Wu, L., D. Jin, D. Wang, X. Jing, P. Gong, Y. Qin, and M. Chen. 2020. 'The two-stage interaction of Ebola virus VP40 with nucleoprotein results in a switch from viral RNA synthesis to virion assembly/budding', *Protein Cell*.

Xu, K., and P. D. Nagy. 2015. 'RNA virus replication depends on enrichment of phosphatidylethanolamine at replication sites in subcellular membranes', *Proc Natl Acad Sci U S A*, 112: E1782-91.

Xu, R. H., J. F. He, M. R. Evans, G. W. Peng, H. E. Field, D. W. Yu, C. K. Lee, H. M. Luo, W. S. Lin, P. Lin, L. H. Li, W. J. Liang, J. Y. Lin, and A. Schnur. 2004. 'Epidemiologic clues to SARS origin in China', *Emerg Infect Dis*, 10: 1030-7.

Xu, W., M. R. Edwards, D. M. Borek, A. R. Feagins, A. Mittal, J. B. Alinger, K. N. Berry, B. Yen, J. Hamilton, T. J. Brett, R. V. Pappu, D. W. Leung, C. F. Basler, and G. K. Amarasinghe. 2014. 'Ebola virus VP24 targets a unique NLS binding site on karyopherin alpha 5 to selectively compete with nuclear import of phosphorylated STAT1', *Cell Host Microbe*, 16: 187-200.

Xu, W., P. Luthra, C. Wu, J. Batra, D. W. Leung, C. F. Basler, and G. K. Amarasinghe. 2017. 'Ebola virus VP30 and nucleoprotein interactions modulate viral RNA synthesis', *Nat Commun*, 8: 15576.

Yan, B., H. Chu, D. Yang, K. H. Sze, P. M. Lai, S. Yuan, H. Shuai, Y. Wang, R. Y. Kao, J. F. Chan, and K. Y. Yuen. 2019. 'Characterization of the Lipidomic Profile of Human Coronavirus-Infected Cells: Implications for Lipid Metabolism Remodeling upon Coronavirus Replication', *Viruses*, 11.

Yang, X. L., C. W. Tan, D. E. Anderson, R. D. Jiang, B. Li, W. Zhang, Y. Zhu, X. F. Lim, P. Zhou, X. L. Liu, W. Guan, L. Zhang, S. Y. Li, Y. Z. Zhang, L. F. Wang, and Z. L. Shi. 2019. 'Characterization of a filovirus (Mengla virus) from Rousettus bats in China', *Nat Microbiol*, 4: 390-95.

Yasuda, J., M. Nakao, Y. Kawaoka, and H. Shida. 2003. 'Nedd4 regulates egress of Ebola virus-like particles from host cells', *J Virol*, 77: 9987-92.

Ye, Y., and B. G. Hogue. 2007. 'Role of the coronavirus E viroporin protein transmembrane domain in virus assembly', *J Virol*, 81: 3597-607.

Yen, B. C., and C. F. Basler. 2016. 'Effects of Filovirus Interferon Antagonists on Responses of Human Monocyte-Derived Dendritic Cells to RNA Virus Infection', *J Virol*, 90: 5108-18.

Yen, B., L. C. Mulder, O. Martinez, and C. F. Basler. 2014. 'Molecular basis for ebolavirus VP35 suppression of human dendritic cell maturation', *J Virol*, 88: 12500-10.

Yoshimoto, F. K. 2020. 'The Proteins of Severe Acute Respiratory Syndrome Coronavirus-2 (SARS CoV-2 or n-COV19), the Cause of COVID-19', *Protein J*, 39: 198-216.

Yu, G. Y., K. J. Lee, L. Gao, and M. M. Lai. 2006. 'Palmitoylation and polymerization of hepatitis C virus NS4B protein', *J Virol*, 80: 6013-23.

Yuan, J., Y. Zhang, J. Li, Y. Zhang, L. F. Wang, and Z. Shi. 2012. 'Serological evidence of ebolavirus infection in bats, China', *Virol J*, 9: 236.

Yuen, C. K., W. M. Wong, L. F. Mak, X. Wang, H. Chu, K. Y. Yuen, and K. H. Kok. 2021. 'Suppression of SARS-CoV-2 infection in ex-vivo human lung tissues by targeting class III phosphoinositide 3-kinase', *J Med Virol*, 93: 2076-83.

Zaki, A. M., S. van Boheemen, T. M. Bestebroer, A. D. Osterhaus, and R. A. Fouchier. 2012. 'Isolation of a novel coronavirus from a man with pneumonia in Saudi Arabia', *N Engl J Med*, 367: 1814-20.

Zang, R., J. B. Case, E. Yutuc, X. Ma, S. Shen, M. F. Gomez Castro, Z. Liu, Q. Zeng, H. Zhao, J. Son, P. W. Rothlauf, A. J. B. Kreutzberger, G. Hou, H. Zhang, S. Bose, X. Wang, M. D. Vahey, K. Mani, W. J. Griffiths, T. Kirchhausen, D. H. Fremont, H. Guo, A. Diwan, Y. Wang, M. S. Diamond, S. P. J. Whelan, and S. Ding. 2020. 'Cholesterol 25-hydroxylase suppresses SARS-CoV-2 replication by blocking membrane fusion', *Proc Natl Acad Sci U S A*, 117: 32105-13.

Zaytseva, Y. Y., P. G. Rychahou, A. T. Le, T. L. Scott, R. M. Flight, J. T. Kim, J. Harris, J. Liu, C. Wang, A. J. Morris, T. A. Sivakumaran, T. Fan, H. Moseley, T. Gao, E. Y. Lee, H. L. Weiss, T. S. Heuer, G. Kemble, and M. Evers. 2018. 'Preclinical evaluation of novel fatty acid synthase inhibitors in primary colorectal cancer cells and a patient-derived xenograft model of colorectal cancer', *Oncotarget*, 9: 24787-800.

Zhai, Y., F. Sun, X. Li, H. Pang, X. Xu, M. Bartlam, and Z. Rao. 2005. 'Insights into SARS-CoV transcription and replication from the structure of the nsp7-nsp8 hexadecamer', *Nat Struct Mol Biol*, 12: 980-6.

Zhang, A. P., Z. A. Bornholdt, D. M. Abelson, and E. O. Saphire. 2014. 'Crystal structure of Marburg virus VP24', *J Virol*, 88: 5859-63.

Zhao, G., A. J. Souers, M. Voorbach, H. D. Falls, B. Droz, S. Brodjian, Y. Y. Lau, R. R. Iyengar, J. Gao, A. S. Judd, S. H. Wagaw, M. M. Ravn, K. M. Engstrom, J. K. Lynch, M. M. Mulhern, J. Freeman, B. D. Dayton, X. Wang, N. Grihalde, D. Fry, D. W. Beno, K. C. Marsh, Z. Su, G. J. Diaz, C. A. Collins, H. Sham, R. M. Reilly, M. E. Brune, and P. R. Kym. 2008. 'Validation of diacyl glycerolacyltransferase I as a novel target for the treatment of obesity and dyslipidemia using a potent and selective small molecule inhibitor', *J Med Chem*, 51: 380-3.

Zhao, Z., L. B. Thackray, B. C. Miller, T. M. Lynn, M. M. Becker, E. Ward, N. N. Mizushima, M. R. Denison, and H. W. th Virgin. 2007. 'Coronavirus replication does not require the autophagy gene ATG5', *Autophagy*, 3: 581-5.

Zhu, N., D. Zhang, W. Wang, X. Li, B. Yang, J. Song, X. Zhao, B. Huang, W. Shi, R. Lu, P. Niu, F. Zhan, X. Ma, D. Wang, W. Xu, G. Wu, G. F. Gao, W. Tan, Investigating China Novel Coronavirus, and Team Research. 2020. 'A Novel Coronavirus from Patients with Pneumonia in China, 2019', *N Engl J Med*, 382: 727-33.

Ziebuhr, J., E. J. Snijder, and A. E. Gorbalenya. 2000. 'Virus-encoded proteinases and proteolytic processing in the Nidovirales', *J Gen Virol*, 81: 853-79.

Zust, R., L. Cervantes-Barragan, T. Kuri, G. Blakqori, F. Weber, B. Ludewig, and V. Thiel. 2007. 'Coronavirus non-structural protein 1 is a major pathogenicity factor: implications for the rational design of coronavirus vaccines', *PLoS Pathog*, 3: e109.